Investigation Of Pnictogen-Assisted Self-Assembly and Self-Sorting Design Principles Towards Preorganized Macrocycles

by

Jacob Mayhugh

A dissertation accepted and approved in partial fulfillment of the

requirements for the degree of

Doctor of Philosophy

in Chemistry

Dissertation Committee:

Michael Haley, Chair

Darren Johnson, Advisor

Ramesh Jasti, Core Member

Marian Hettiaratchi, Institutional Representative

University of Oregon

Winter 2024

DISSERTATION ABSTRACT

Jacob Mayhugh

Doctor of Philosophy in Chemistry

Title: Investigation Of Pnictogen-Assisted Self-Assembly and Self-Sorting Design Principles Towards Preorganized Macrocycles

Shape-persistent molecules have abundant chemical potential as organic functional materials. Access to these molecular cages and macrocycles, however, is nontrivial and often require long or low-yielding synthetic pathways that bottleneck their potential applications. To ameliorate this, dynamic covalent chemistry has shown to be promising in the formation of shape-persistent molecules as it marries the error-correction of self-assembly with thermodynamic control while giving the robustness of a covalent bond. The DWJ lab focuses on utilizing dynamic covalent reactions towards the facile preorganization of macrocyclic ensembles through the pnictogen-assisted self-assembly of oligothiols. This dissertation expands upon disulfide self-assembly design principles for a holistic understanding of the method's boundaries.

Chapter I introduces supramolecular concepts that are the cornerstone of this project. Specifically, self-assembly and dynamic covalent chemistry is introduced, with background information on the project's beginnings provided as well. In Chapter II, the synthetic scope of disulfide self-assembly is explored. Following, Chapter III utilizes our newfound understanding to explore efficient pathways into material formation. Specifically, Perylene Diimide-containing macrocycles are generated in an efficient and high throughput dynamic pathway with implication on tailored organic materials. Chapter IV investigates the self-assembly of multicomponent oligothiol systems (self-sorting)

towards the predictive assembly of three-dimensional architectures. Chapter V concludes the dissertation and provides potential future directions for this project.

This dissertation includes co-authored and previously published results.

ACKNOWLEDGMENTS

I would like to express my deepest gratitude to all those who have supported and guided me throughout the journey of completing this dissertation.

First and foremost, I extend my sincere appreciation to my advisor, Prof. Darren Johnson, for their invaluable guidance, patience, and unwavering support. Their expertise and insightful feedback have been instrumental in shaping the direction of this research.

I am grateful to the members of my dissertation committee, Prof. Michael Haley, Prof. Marian Hettiaratchi, and Prof. Ramesh Jasti, for their constructive feedback and thoughtful suggestions, which greatly enriched the quality of this work.

Special thanks to my colleagues and fellow researchers who provided valuable insights and encouragement. Their diverse perspectives have contributed to a more comprehensive understanding of the subject matter.

I am indebted to the library staff, research assistants, and technical support team as they have been indispensable in facilitating the smooth progress of this project.

Heartfelt thanks to my family and friends for their unwavering encouragement and understanding during the challenging phases of this journey. Their support has been a source of inspiration and motivation.

Finally, I would like to express my gratitude to all the participants who generously contributed their time and insights to this study.

This dissertation would not have been possible without the collective support of these individuals and institutions. Thank you all for being an integral part of this academic endeavor.

Jacob Tyler Mayhugh

Doctor of Philosophy in Chemistry

University of Oregon

TABLE OF CONTENTS

LIST OF FIGURES

Figure Page

LIST OF SCHEMES

Scheme Page

CHAPTER I

INVESTIGATION OF PNICTOGEN-DIRECTED SELF-ASSEMBLY AND SELF-SORTING DESIGN PRINCIPLES TOWARD PREORGANIZED CYCLOPHANES

Contributions

This dissertation describes the investigation of pnictogen-directed self-assembly and self-sorting design principles towards preorganized cyclophanes. Chapter I introduces the principles and significance of supramolecular self-assembly, self-sorting, and dynamic covalent chemistry; moreover, a general overview of pnictogen-directed self-assembly is presented. Prof. Darren W. Johnson provided intellectual input and editorial feedback for this chapter.

Introduction to Self-assembly and Self-sorting in Supramolecular Chemistry

Supramolecular chemistry, the study of molecular entities and their dynamic noncovalent interactions, stands at the intersection of chemistry, physics, and materials science. The processes of guided intramolecular associations are self-assembly and self-sorting, wherein molecules spontaneously organize into intricate structures guided by the delicate orchestration and balance of weak forces. This section overviews the historical evolution, principles, and significance of self-assembly and self-sorting in supramolecular chemistry.

The roots of supramolecular chemistry can be traced back to the late 19th century, with Emil Fischer formalizing enzyme-substrate interactions through a *lock-and-key* mechanism[1]; however, it was in the 1960s that the field began to flourish. The groundbreaking work of Jean-

Marie Lehn, Donald J. Cram, and Charles J. Pedersen, who were awarded the Nobel Prize in Chemistry in 1987 for their contributions towards the design and synthesis of cryptands, calixarenes, and crown ethers, marked a pivotal moment (**Figure 1.1**)[2]. These early pioneers laid the foundation for exploring molecular recognition and noncovalent interactions, such as hydrogen bonding and van der Waals forces, with molecular preorganization and directionality only previously performed by nature.

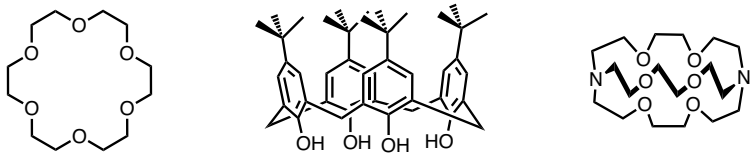

Figure 1.1: Example of a crown ethers, calixarene, and cryptand, respectively.

Self-assembly emerged as a central theme in supramolecular chemistry, describing the spontaneous organization of molecular entities into well-defined structures without external intervention. This process is inherently governed by noncovalent interactions, such as hydrogen bonding, π-π stacking, and hydrophobic interactions, which enable molecules to recognize and bind to each other selectively[3]. An example of micelle formation is provided in **Figure 1.2** to illustrate the self-assembly and self-recognition process. The advent of self-assembly as a supramolecular cornerstone opened avenues for the creation of novel materials, molecular machines, and functional nanoscale architectures[4–6]; notably, Ben Feringa, Sir Fraser Stoddart, and Jean-Pierre Sauvage were awarded the 2016 Novel Prize in Chemistry for their contributions towards molecular machines[7].

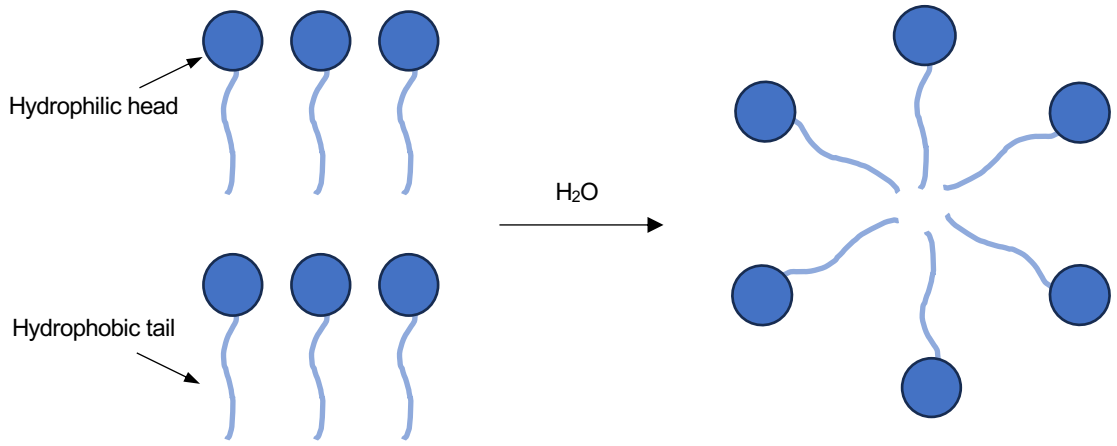

Figure 1.2: Representation of micelle self-assembly in water from a simple surfactant.

As researchers delved deeper into the intricacies of self-assembly, a complementary phenomenon known as self-sorting began to capture attention in supramolecular chemistry[8,9]. Self-sorting is the spontaneous organization of different molecular components into distinct assemblies based on their complementary interactions[10]. This selective segregation of molecules within a mixture has profound implications for designing and constructing complex supramolecular systems. Specifically, driven through self-recognition or self-discrimination, incongruent building blocks can assemble into homomeric (narcissistic self-sorting) or heteromeric (social self-sorting) ensembles; moreover, self-sorting is not limited to interactions between identical functional groups. Multicomponent systems, where each component possesses unique binding motifs, can exhibit hierarchical (integrative) self-sorting behavior or form multiple (nonintegrative) self-sorted complexes (**Figure 1.3**). Self-sorting, therefore, introduces an additional layer of complexity by considering the coexistence and selective organization of multiple molecular species. The key to self-sorting lies in the disparate affinities and specificities of noncovalent interactions exhibited by different components within a mixture; consequently, to

understand design principles in self-sorting, molecular recognition and weak interactions principles must first be explored.

The driving force behind self-assembly lies in the delicate balance of noncovalent and/or reversible interactions that dictate molecular recognition and binding. This section highlights hydrogen bonding, π-π stacking, σ-hole interactions, and metal coordination for their unparalleled

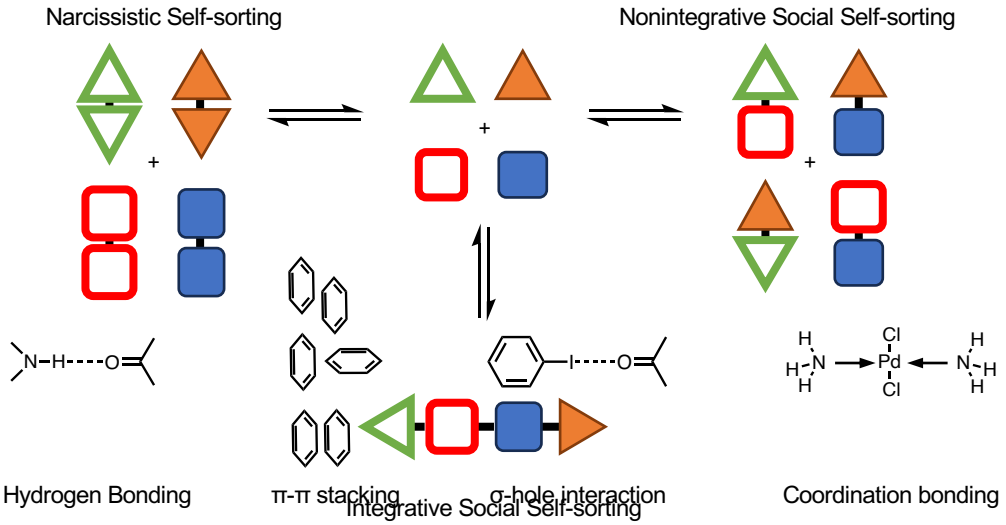

Figure 1.4: Selected examples of noncovalent interactions. Dotted bonds represent electrostatic attraction and bolded arrows represent coordination (dative) bonding. For π-π stacking, slip stacked (top), T-shaped (middle), and face-to-face (bottom) geometries are shown.

directionality in molecular self-assembly (**Figure 1.4**). Hydrogen bonding, a ubiquitous force in nature, is driven through the weak electrostatic attraction of electron-deficient protons with electron-donating atoms. While a weak interaction, hydrogen bonding can be strong in numbers and plays a crucial role in directing the assembly of many bioorganic molecules. For example, the hydrogen bond donating and accepting nature of amides guides the formation of α-helices or β-sheets in peptides[11]; moreover, DNA base pairs are joined in a double helix structure through adenine-thymine and guanine-cytosine hydrogen bond complementarity[12,13].

Due to their flat geometry and enhanced stability, aromatic π systems are pervasive scaffolds in synthetic building blocks for molecular self-assembly. As a result, their intrinsic π-π stacking, arising from intramolecular quadrupole-quadrupole attraction, is also commonplace. As electron-rich π systems are repulsive face-to-face, they preferentially form staggered or T-shaped geometries; however, electron-rich and electron-poor π systems will self-assemble into sandwich complexes, and this preorganization has been highlighted by Stoddart and coworkers in preorganized molecules for catenane formation[14].

While a newer class of noncovalent interactions, σ-hole interactions are gathering interest in supramolecular utility due to their preferential 180° binding geometries[15]. The σ-hole interaction is dubbed for low-lying σ orbitals in Lewis acids that are filled with donated electrons from a Lewis base. Since σ^* orbitals are on the backside of σ orbitals, the binding geometry is restricted without consideration of the electron donor, simplifying molecular recognition design strategies. Typical motifs for σ-hole interactions include heavy pnictogen, chalcogen, and halogen atoms. Recently, σ-hole interactions have been biased to form organic capsules through complementary building blocks towards reversible molecular transport and drug delivery[16].

Finally, coordination-driven self-assembly is directed through metal and ligand interactions. With metals having preferred binding geometries, supramolecular assemblies are predictable when paired with complimentary ligand bite angles. For example, Fujita and coworkers prepared Pd(II) molecular squares from linear, ditopic bipyridyl ligands and square planar Pd(II) precursors[17]. Metal-organic frameworks (MOFs), composed of metal ions or clusters coordinated to organic ligands, showcase the versatility of self-assembly principles in inorganic systems[18]. The coordination interactions between metal centers and ligands guide the formation of porous

three-dimensional networks with tunable properties, making MOFs promising materials for gas storage, separation, and catalysis[19,20].

Recent advancements in supramolecular chemistry have expanded the scope of self-assembly and self-sorting, introducing innovative concepts and methodologies. The development of dynamic covalent chemistry, where reversible covalent bonds are incorporated into supramolecular systems, adds an additional layer of control and adaptability to self-assembled structures. Furthermore, the integration of supramolecular chemistry with other fields, such as materials science, biology, and nanotechnology, has led to the emergence of interdisciplinary research avenues.

As we look to the future, the challenges and opportunities in self-assembly and self-sorting remain vast. Developing predictive models and computational tools for simulating and optimizing supramolecular assemblies will accelerate the design process[21,22]. Moreover, integrating self-assembly principles into the fabrication of complex nanoscale devices and exploring bioinspired systems hold the promise of transformative breakthroughs[23,24].

Introduction to Dynamic Covalent Chemistry

Dynamic covalent chemistry (DCvC) has emerged as a powerful and versatile tool within supramolecular chemistry, offering a unique approach to the design and construction of complex molecular architectures[25–27]. Unlike traditional covalent bonds, dynamic covalent bonds are reversible, enabling the continual reshaping and reconfiguring of molecular structures under the influence of external stimuli. This dynamic nature not only mirrors the adaptability observed in nature but also opens new avenues for creating responsive and programmable supramolecular

systems. This section provides an overview, principles, and significance of dynamic covalent chemistry in supramolecular chemistry highlighting recent advancements and applications.

The concept of reversibility in covalent bond formation introduced a paradigm shift in synthetic chemistry. Unlike traditional covalent bonds, which are typically forming with kinetic control, dynamic covalent bonds are constantly in flux. This inherent reversibility allows for the dynamic exchange of building blocks, leading to the continuous rearrangement of molecular structures in response to external stimuli, yielding thermodynamic control over product distribution. Thermodynamic control is advantageous in synthesizing organic macrocycles and cages because their formation is traditionally nontrivial and often requires long or low-yielding synthetic pathways that bottleneck their potential applications. To ameliorate these common synthetic challenges, dynamic covalent chemistry shows promise in the formation of shape-persistent molecules as it marries the error-correction of self-assembly with thermodynamic control while giving the robustness of a covalent bond.

Reactions that form and break covalent bonds under mild conditions are at the core of dynamic covalent chemistry. These reversible reactions are thermodynamically controlled, meaning that the equilibrium between reactants and products can be easily manipulated. Common dynamic covalent reactions include imine condensations, disulfide exchange, transesterification, and metathesis reactions (**Figure 1.5)**.

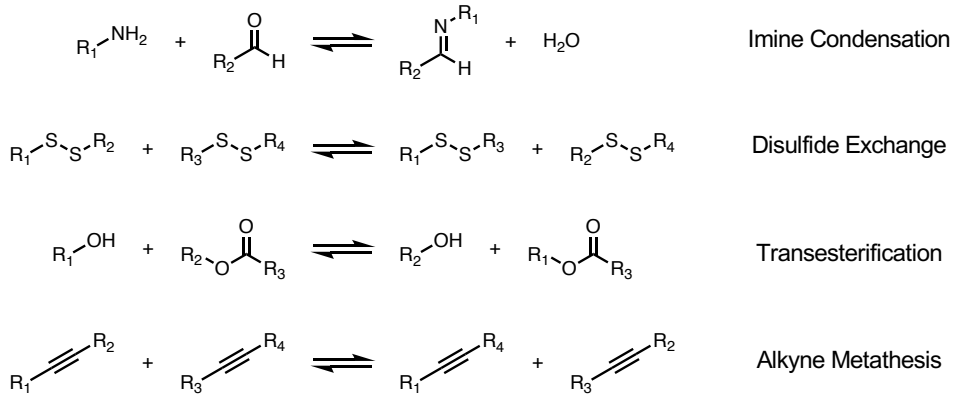

Figure 1.5: Selected examples of dynamic covalent reactions.

Imines and hydrazones, formed through the condensation of a carbonyl compound with an amine or hydrazine, exemplify the dynamic nature of covalent bonds in DCvC. These bonds can readily undergo hydrolysis and condensation reactions, resulting in the reversible formation and cleavage of covalent linkages; furthermore, the product distribution can be biased by leveraging nitrogen's affinity in metal coordination to direct the formation of entropically unfavorable complexes in high yield. An elegant example was presented recently by Nitschke and coworkers[28]. Here, the group used pentatopic amine scaffolds with pyridyl- or bipyridyl-bearing aldehydes in the presence of a zinc Lewis acid to generate a molecular dodecahedron, icosidodecahedron, rhombohedron, and octahedron. The final molecular ensemble could be biased reversibly into each shape through change in chemical stimuli.

Similarly, disulfide exchange reactions, characterized by the reversible formation and cleavage of disulfide bonds, offer a versatile platform for constructing dynamic covalent systems. Instead of adding or removing water like imine condensation, disulfide exchange or thiol-disulfide exchange is performed under oxidation or reductive conditions. For example, hair curling is dictated by disulfide bonds in keratin. To curl hair in a perm, a chemically reducing solution is

applied to break the keratin disulfide bonds, making the hair malleable. After shaping is completed, an oxidizing agent is applied to reform the disulfide bonds[29] (**Figure 1.6**).

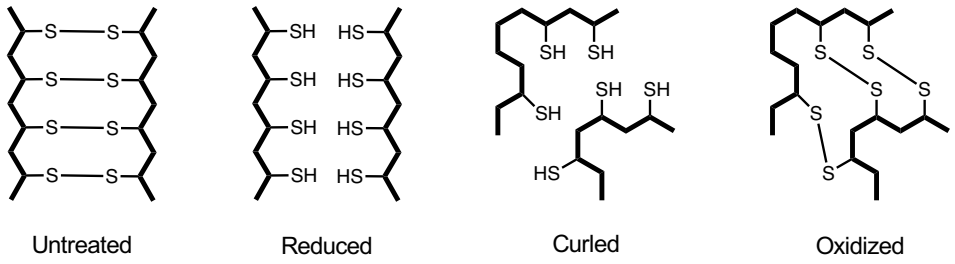

Figure 1.6. Stepwise chemical representation of hair during a perm.

One of the critical advantages of dynamic covalent chemistry in supramolecular systems is its ability to facilitate the exchange and reorganization of building blocks in response to external stimuli. This adaptability allows for facile materials creation with tunable properties, such as mechanical strength, porosity, and conductivity. For instance, the reversible nature of disulfide exchange reactions has been harnessed in the design of mechanically responsive materials, where covalent bonds break and reform in response to mechanical stress[30]. Recent advancements in dynamic covalent chemistry have expanded its scope and applicability, driving innovation in materials science, drug delivery, and nanotechnology.

In materials science, incorporating dynamic covalent bonds has led to the development of self-healing polymers with enhanced mechanical properties. These materials can repair themselves when damaged, offering potential applications in coatings, adhesives, and biomedical devices[31]. Furthermore, the introduction of dynamic covalent bonds in the design of stimuli-responsive materials has paved the way for the creation of smart materials that can adapt to environmental changes[32].

In drug delivery, the reversible nature of dynamic covalent bonds has been harnessed to design prodrugs that can release therapeutic agents in a controlled and triggered manner. The dynamic covalent linkage between the drug and its carrier allows for the release of the active compound under specific physiological conditions, improving the precision and efficiency of drug delivery systems[33].

The integration of dynamic covalent chemistry with supramolecular systems has also been explored in the design of functional nanomaterials. By combining reversible covalent bonds with noncovalent interactions, researchers have created dynamic supramolecular architectures that can adapt to changes in their surroundings. This adaptive behavior holds promise for applications in sensing, catalysis, and responsive nanodevices[23].

As the field of dynamic covalent chemistry continues to evolve, future directions may include:

- the development of new dynamic covalent reactions,
- the exploration of bioinspired systems, and
- the integration of computational tools for the rational design of dynamic materials.

The synergy between dynamic covalent chemistry and other areas of supramolecular research, such as self-assembly and self-sorting, is likely to yield novel and sophisticated functional organic materials.

Introduction of Pnictogen-Assisted Self-assembly and Self-sorting

Metalloid supramolecular chemistry represents an intriguing frontier within the broader landscape of supramolecular interactions, focusing on the unique properties of metalloid elements situated between metals and nonmetals in the periodic table. Notably, silicon, germanium, arsenic,

and other metalloids exhibit diverse coordination preferences and versatile bonding capabilities, making them distinctive players in the orchestration of molecular self-assembly[34–36]. Researchers leverage the hybrid nature of metalloids to design and construct intricate molecular architectures, ranging from supramolecular polymers to tailored nanomaterials. At the University of Oregon, the Darren W. Johnson (DWJ) lab focuses on harnessing the unique properties of pnictogen (Pn) elements—phosphorus, arsenic, antimony, and bismuth—to orchestrate the controlled self-assembly of molecular structures. This section will highlight significant topics from the DWJ lab on pnictogen self-assembly, self-sorting, and dynamic covalent chemistry.

The DWJ lab first focused on the molecular recognition of trivalent pnictogen species. As arsenic is an environmentally hazardous chemical, preliminary investigations explored fundamental design principles in the self-assembly of supramolecular pnictogen compounds toward arsenic sequestration[37]. Specifically, the DWJ lab exploited the preferred trigonal pyramidal geometry of Pn^{3+} and its intrinsically soft Lewis acidity with the chelation of multitopic benzylic thiols[38,39]. Here, thiol-containing ligands were preorganized to be unable to satisfy antimony's coordination sphere by themselves due to their separation around rigid aromatic spacers; therefore, the building blocks were biased to form $L_2As_2X_2$ or L_3As_2 metallocryptand assemblies (L = ligand, X = peripheral electron donor). Furthermore, during these preliminary

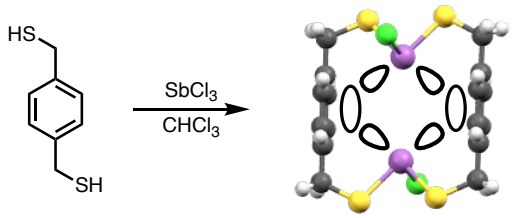

Scheme 1.1: General representation of $L_2Pn_2X_2$ metallocryptands formed through the self-assembly of trivalent pnictogens with thiol-containing ligands. Orbitals illustrate secondary π_{aryl}-σ^*_{Pn} interactions.

investigations, the arsenic self-assembly strategy was found to be general towards trivalent pnictogens, with phosphorous being a slight outlier due to its harder Lewis acidic profile[40]; moreover, besides the primary thiolate-pnictogen coordination, secondary π_{aryl}-σ^*_{Pn} interactions were also found to be a major contributor towards promoting these ensembles (**Scheme 1.1**)[41].

With the spontaneous oxidation of thiolates under atmospheric conditions, it would be expected for these thiolate-arsenic complexes to decompose over time as the chelating ligands polymerize; unexpectedly, however, the decomposition pathway had serendipitous results as the ligands oxidized quantitatively into discrete macromolecular compounds tethered by disulfide bonds. The pnictogen seemed to direct the thiol-containing ligands towards discrete cyclic oligomeric architectures instead of polymerized straight-chained composites. Following further investigation, it was found that this process could be expedited through the addition of iodine as a mild oxidant[42–44]. With these results, disulfide exchange could be paired with pnictogen-thiolate self-assembly to yield covalently linked organic macrocycles and cages in high yield and fast

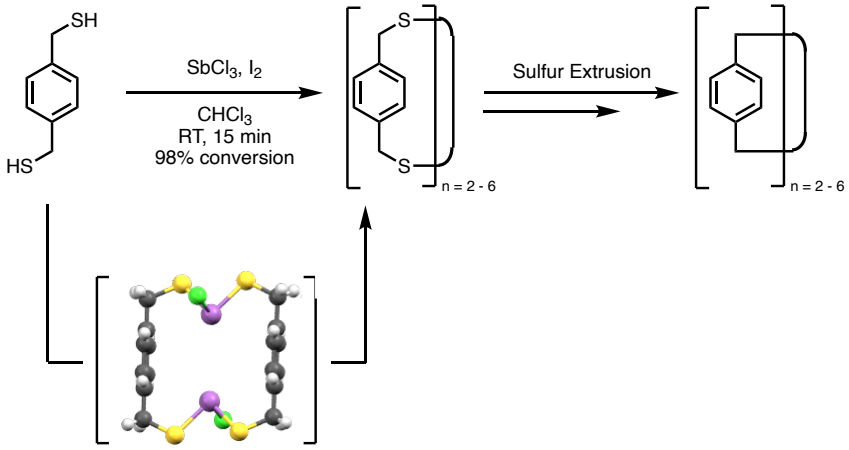

Scheme 1.2: General representation of pnictogen-directed self-assembly. Previous results suggest the thiolate-pnictogen self-assembly prevents polymerization of disulfides during the reaction.

reaction times without the high-dilution effect (**Scheme 1.2**). Moreover, the disulfide species could be sulfur extruded to the adjacent sulfide-linked derivatives before further sulfur extrusion to yield macrocycles connected by carbon-carbon bonds[45–47].

Following these initial findings, the reaction components were further explored in the DWJ lab. As arsenic trichloride is a hazardous chemical and a liquid at room temperature, alternative directing agents were trialed for this disulfide self-assembly reaction. Towards this goal, antimony and bismuth trichloride were found as alternatives in nonpolar organic solvents; alternatively, copper chloride was found to work in polar organic solvents[48]. As the reaction pathway yields multiple cyclic oligomeric disulfide products, product distribution manipulation was also investigated. Here, the DWJ lab found that product distribution could be biased utilizing the Design of Experiments (DOE) to perform nonlinear regression of initial ligand concentration, solvent composition, and oxidant equivalence[49].

With a preliminary understanding of how pnictogen-assisted self-assembly could be used in the formation of novel organic macrocycles and cages, the DWJ lab focused on utilizing this alternative thermodynamic disulfide pathway to form molecules that would be difficult to form under traditional kinetic methods. One example the lab presented was formation of an organic cage capped by a trithioorthoformate linkage[50]. Because disulfides are readily reversible under nucleophilic conditions and thiolates are an intermediate of this mechanism, the addition of bromoform as a solvent to the self-assembly of 1,3,5-tris(methylmercaptan)benzene allows the transient thiolate to undergo a thiol-based Williamson etherification . As orthoformates are formed and reacted through reversible S_N2 processes, it is believed the trithioorthoformate undergoes a similar process; therefore, a tandem dynamic sequence is believed to be responsible in the

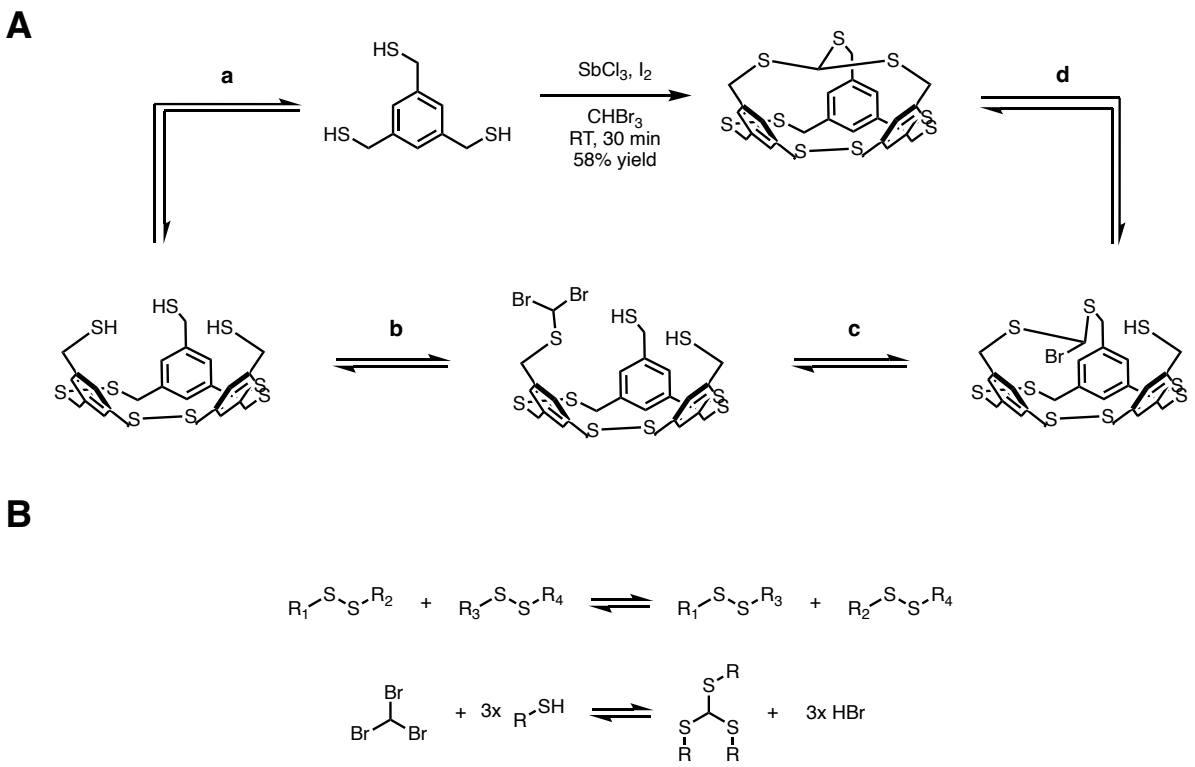

Scheme 1.3: (**A**) Synthesis of trithioorthoformate cage with 1,3,5-tris(methylmercaptan)benzene and bromoform. The self-assembly is believed to form an intermediate trimer (**a**) before sequential nucleophilic substitution between the pendant thiols and bromoform cap the cage (**b - d**). (**B**) General representation of dynamic disulfide exchange (top) and thioorthoformate formation (bottom) occurring during the self-assembly.

formation of the thermodynamically favored trithioorthoformate-capped cage (**Scheme 1.3**). While self-assembly yields macrocycles or cages composed of single ligand building blocks, the DWJ lab also explored self-sorting towards synthesizing asymmetric macrocycles. By combining dithiol biphenyl- and phenylene-spaced ligands under oxidative conditions in the presence of antimony trichloride, the ligands undergo self-recognition and self-discrimination processes in social and narcissistic self-sorted product formation[51] (**Scheme 1.4**). In Chapter VI, the design principles behind biasing this self-sorting behavior is presented.

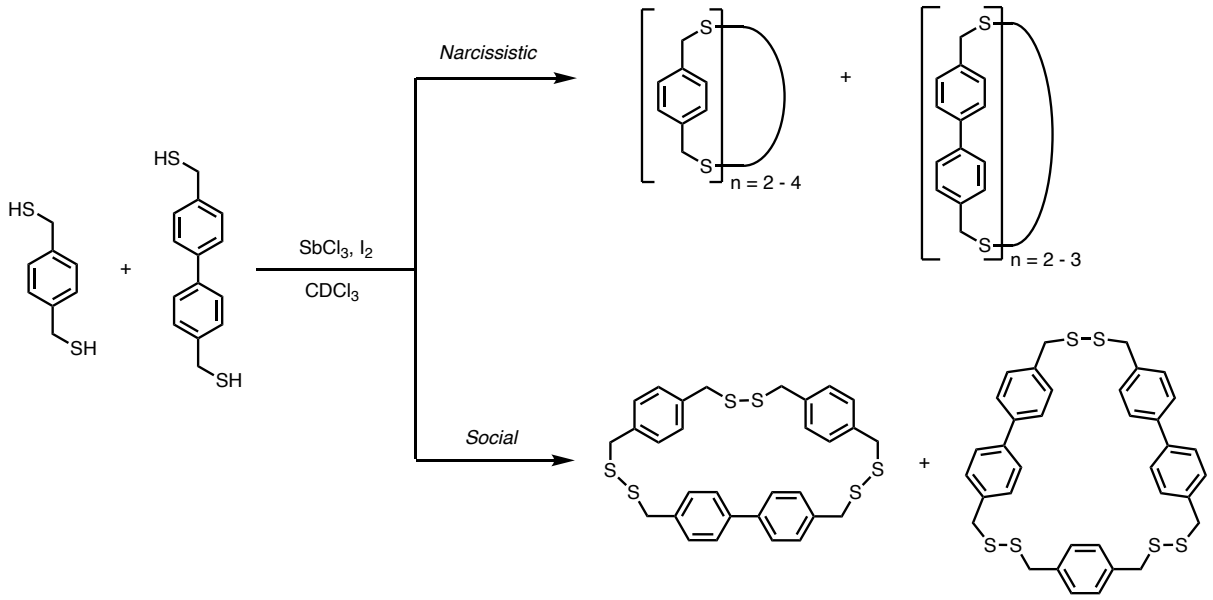

Scheme 1.4: Pnictogen-assisted self-sorting of ditopic oligothiols yields asymmetric cyclophanes *via* self-discrimination.

In conclusion, an overview of pnictogen-assisted self-assembly and self-sorting was presented to lay the foundational ideas behind the work presented in this dissertation. Chapter II presents an investigation into generalizing our methods with general oligothiol substrates. Chapter III presents an investigation into the self-assembly of perylene diimide (PDI) macrocycles toward development of efficient generation of a useful feedstock in optoelectronics. Chapter IV presents an investigation into self-sorting product distribution control with steric effects on initial oligothiols. This dissertation summarizes work in fundamental pnictogen-assisted self-assembly design strategies towards applicable and predictable pathways in designed macromolecular systems or materials in materials science, biology, and nanotechnology.

Bridge to Chapter II

Chapter I introduced supramolecular chemistry topics such as self-assembly, self-sorting, and dynamic covalent chemistry. Specifically, molecular recognition principles, such as hydrogen bonding and π-π stacking, were discussed, as well as common bonding motifs in dynamic covalent chemistry; moreover, these topics were related to applications in materials science, nanotechnology, and medicine to highlight the breadth and reach of the field. With a brief introduction, the DWJ lab research was presented to connect these topics with pnictogen-assisted self-assembly. Chapter II discusses the generalizable method for pnictogen-directed self-assembly of macrocycles, highlighting preliminary exploration into the methodologies design strategies.

CHAPTER II

EXPANDING THE SCOPE OF PNICTOGEN-ASSISTED CYCLOPHANE SELF-ASSEMBLY

Contributions

This chapter discusses the pnictogen-assisted self-assembly as a general route towards disulfide and sulfide-linked cyclophanes and macrocycles. The work described herein was published in *The European Journal of Organic Chemistry*[1]. Dr. Trevor Shear and I evenly contributed towards the final manuscript. Specifically, I wrote the introduction and provided all experimental work on the alkene, alkyne, triazine, and 1,4-bis(ethylmercaptan)benzene scaffolds. Prof. Darren. W. Johnson provided intellectual input and editorial feedback. Dr. Lev. N. Zakharov resolved all X-ray crystallography experiments. Luca J. Zocchi, Isabella S. Demachkie, and Henry J. Trubenstein assisted us in preparing and characterizing the perfluorobenzene and bis(dioxane) scaffolds.

Abstract

Cyclophanes are a fundamentally interesting class of compounds that host a wide range of unique and emergent properties. However, synthesis of complex and/or functionalized cyclophanes can often suffer from harsh reaction conditions, long reaction times, and sometimes low yields using stepwise methods. We have previously reported an efficient, high-yielding, metalloid-directed self-assembly method to prepare disulfide, thioether, and hydrocarbon

cyclophanes and cages that feature mercaptomethyl-arenes as starting materials. Herein, we report the synthesis of 21 new disulfide and thioether assemblies that expand this high yielding self-assembly method to a wide breadth of macrocycles and cages with diverse structures. Remarkably, the high-yielding, efficient syntheses still proceed under dynamic covalent control using electron-deficient, heteroaryl, cycloalkyl, spiro, and even short alkenyl/alkynyl substrates.

Introduction

By exploiting weak noncovalent interactions, supramolecular chemistry has transformed the bottom-up preparation of discrete macrocycles and cages with efficient synthetic methods.[2] Specifically, self-assembly yields thermodynamic control over reaction pathways in the synthesis of discrete structures while deterring the formation of undesirable side products that result from kinetic pathways.[3] By using reversible covalent reactions, dynamic covalent chemistry (DCC) combines the error-correction and directionality of self-assembly with the robustness of a covalent bond.[2-6] DCC is shown to be applicable in tailor-made molecules for use in various applications, including plastics, host-guest chemistry, and organic electronics, among others.[7-17]

Recently, we have shown that this strategy can be applied to the formation of cyclophanes from benzylic di- and trithiol precursors by manipulating dynamic disulfide exchange with the inclusion of a pnictogen (Pn) directing agent coupled with a mild oxidant.[18-20] Our approach complements related disulfide exchange and self-assembly methods that proceed via aerobic oxidation and/or macrocyclization pathways, and it enables quick (as fast as 5 minutes) and

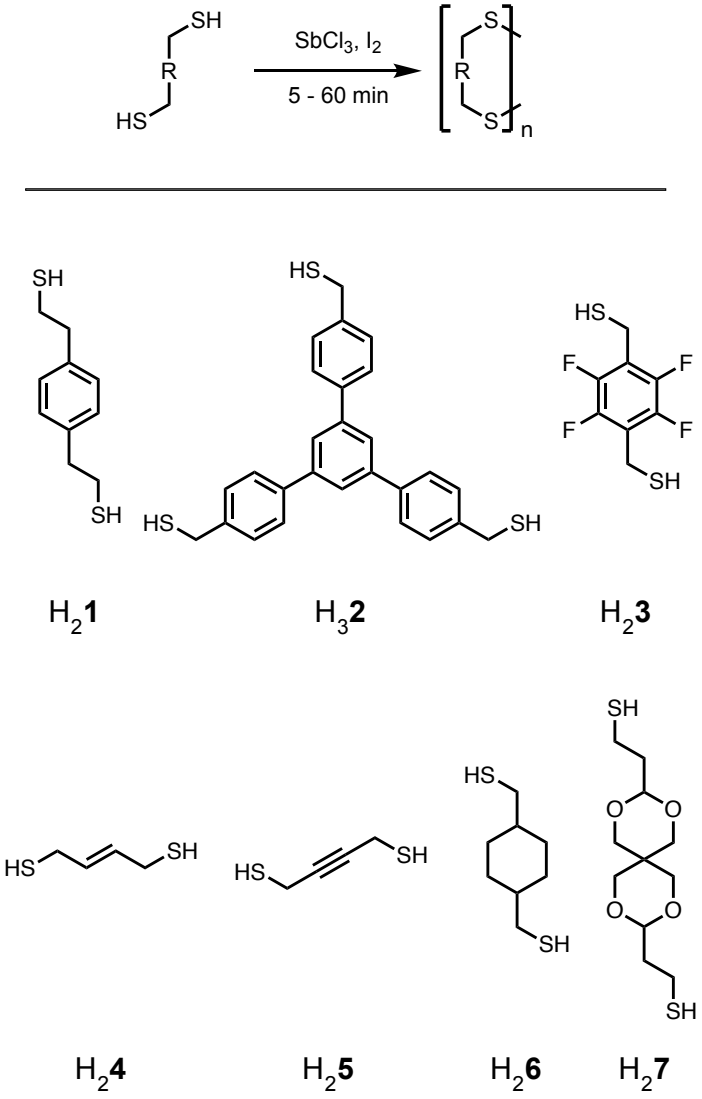

Figure 2.1: Top: General reaction scheme for the pnictogen-assisted self-assembly (R = bridging group between thiols). Bottom: Di- and trithiols used to assess the efficacy and generality of pnictogen-assisted disulfide macrocyclization in this report.

quantitative formation of discrete disulfide-bridged macrocycles and cages over extended oligomers using a variety of simple di- and/or trithiols.[18, 21-24]

Moreover, using design of experiments (DOE), we have shown we can easily bias the self-assembly reaction mixture to optimize specific multimeric products and, using self-sorting methods, readily form asymmetric disulfide macrocycles.[24-25] However, thus far our methods have

been limited to utilizing benzylic thiol precursors as we believed the Pn-π interaction to be of importance in the pnictogen's directing ability, greatly limiting the scope of suitable precursors.[26-27]

In this work, we show the Pn-directed self-assembly method is, in fact, capable of forming a wider array of discrete disulfide macrocycles and cages than we previously realized using a variety of starting multi-thiol substrates (**Figure 2.1**, **$H_2$1**-**$H_2$7**). Specifically, we vary the spacer size, shape, and electronics in a series of di- and trithiols to showcase the scope and utility of this reaction in the formation of disulfide-linked macrocycles before kinetically trapping them as thioether-linked macrocycles utilizing sulfur extrusion methods.

Results and Discussion

To probe the extent of this method, we began to assess the necessity of the Pn-π interaction, which was previously thought to be required for proper alignment of the Pn-directing agent ($AsCl_3$, $SbCl_3$, or $BiCl_3$) via metalloid-π secondary bonding interactions.[28] Our investigation started with testing extended benzylic linking arms, such as those seen in 1,4-bis(2-mercaptoethyl)benzene (**$H_2$1**) and the extended triazine system 2,4,6-tris(4-mercaptomethyl)-1,3,5-triazine (**$H_3$2**), and reducing the electron density of the arene system using 2,3,5,6-tetrafluoro-1,4-bis(mercaptomethyl)benzene (**$H_2$3**). The extended arm systems were chosen primarily because of their added flexibility, and to investigate if having a heterocyclic substrate would affect the synthetic method. Substrate **$H_2$3** was chosen to explore highly electron deficient cores and the resulting effects on macrocyclization. All substrates easily underwent Pn-directed self-assembly to form discrete disulfides, including the dimer through tetramer (79% combined yield) for **$H_2$1** and dimer and trimer (72% combined yield) for **$H_2$3**. Low quality crystals of the resulting trimer

(3D3) were grown, providing insight into the connectivity of the molecule. Substrate H32 only forms the dimer (93% yield), although a more complex tetrahedron should be theoretically possible and has been seen in simpler trithiols.[10] It is likely this tetrahedron species is only formed in trace amounts, as the inner cavity would be expected to collapse unless a suitable guest were introduced to provide further stabilization.[29-31]

X-ray quality crystals of the 1,4-bis(mercaptoethyl)phenyl dimer ($\mathbf{1_{D2}}$) were grown from vapor diffusion of hexanes into CHCl3 and crystallized in the P21/n space group (**Figure 2.2a**). The C-S-S-C dihedral angles (∢: 84.1°, 84.1°) are close to ideality (90°) and the arene rings adopt a parallel displacement conformation with an interplanar distance of 4.81 Å.[32] The triazine dimer ($\mathbf{2_{D2}}$) crystallized in the P2/n space group upon layering benzene on a solution of the dimer in $CHCl_3$ (**Figure 2.2b**). The C-S-S-C dihedral bond angle of all three disulfide bridges deviate considerably from ideality (∢: 104.2°, 111.1°, 112.7°). The distance between the three benzene ring pairs (3.58 Å, 3.64 Å, 3.71 Å) and the two triazine cores (3.58 Å) suggest that there may be slightly favorable transannular π-π stabilization which allows such strained disulfide bonds to readily form. All adjacent ring systems within $\mathbf{2_{D2}}$ adopt a parallel-displacement conformation. Sulfur extrusion using hexamethylphosphorous triamide (HMPT) with $\mathbf{2_{D2}}$ (95% yield) resulted in the respective thiacyclophane and was purified via recirculating gel permeation chromatography (GPC). Crystals of the triazine thioether ($\mathbf{2_{T2}}$) were grown from slow evaporation in chloroform

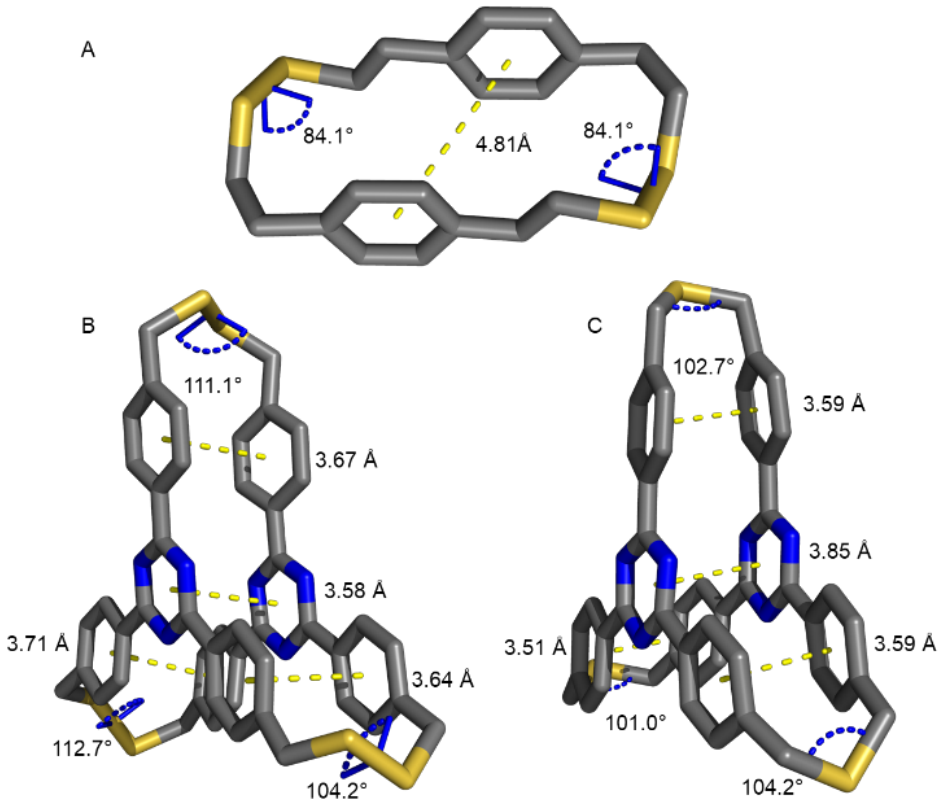

Figure 2.2: Single-crystal X-ray structures of 1_{D2} (A), 2_{D2} (B) and 2_{T2} (C). Disulfide dihedral angles are shown in blue, arene-arene distances are shown in yellow. Hydrogens have been omitted for clarity.

and crystallize in the P-1 space group (**Figure 2.3c**). The associated C-S-C bond angles (∡: 99.0°, 102.7°, and 104.2°) all align closely with ideality (103°). The interplanar distance between the three benzene rings decrease further compared to the disulfide $\mathbf{2_{D2}}$ (3.51 Å, 3.53 Å, 3.59 Å), while the C_3N_3-C_3N_3 distance increased (3.85 Å) and the overall π-π stacking adopted more of a sandwich stacking conformation.

Continuing our investigation, we began to deviate from the standard substrate motif of di- or trithiols that featured an arene ring spacer. Instead, the hypothesis that aromatic interactions were required for this method to function was tested in the context of two dithiols with nonaromatic π-systems: E-2-butene-1,4-dithiol ($\mathbf{H_24}$) and 2-butyne-1,4-dithiol ($\mathbf{H_25}$).[26] These substrates readily

undergo discrete disulfide macrocycle formation using our self-assembly methods, with alkene **$H_2$4** generating the dimer through pentamer (95% combined yield). The dimer has been previously reported, although in lower yields in comparison to using our method (5.6% vs 32%).[27] Moreover, previous work by Whitesides showcases that polymerization readily occurs without the inclusion of a trivalent pnictogen for both substrates, suggesting some level of preorganization is still provided by the pnictogen additive (presumably via secondary bonding interactions with the thiols) to enable efficient macrocyclization.[34-35]

Alkyne substrate **$H_2$5** underwent an unexpected transformation and formed the thioether directly (36% yield) along with a smaller amount of disulfide (13% yield). This was quite surprising since this was the first time our pnictogen-assisted self-assembly method had not produced exclusively disulfides and, to our knowledge, the only reported example of disulfide sulfur auto extrusion. This is thought to occur because of the alkyne's heightened nucleophilicity towards the polarized disulfide bond. Following nucleophilic displacement of the disulfide bond by the alkyne, the generated sulfide can readily attack the other sulfur's α-carbon to yield a neutral thioether species. Further evidence in support of this transformation is the combined 51% loss of alkyne disulfide and thioether products following purification, suggesting that half of the alkyne is consumed in this transformation to facilitate sulfur extrusion to the thioether. This reactivity has been previously observed utilizing trisulfide antimonate salts to form thiirenium ions selectively from alkyne substrates.[36-37]

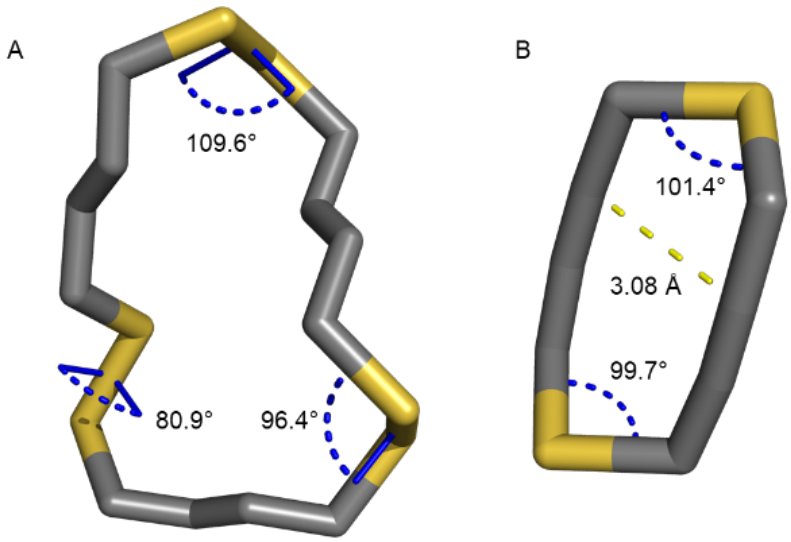

Figure 2.3: Single-crystal X-ray crystal structure of 4_{D3} (A) and 5_{T2} (B). Disulfide dihedral and thioether bond angles are shown in blue, alkyne-alkyne distance is shown in yellow. Hydrogens have been omitted for clarity.

X-ray quality crystals of the alkene disulfide trimer (**4_{D3}**) and alkyne thioether dimer (5T2) were both grown from vapor diffusion of hexanes into CHCl3 (**Figure 2.3**). 4D3 crystallizes in the P21/c space group with two of the three disulfide dihedral angles diverging from ideality substantially (C-S-S-C ∢: 80.9°, 96.4°, 109.6°). **5_{T2}** has been reported in the literature previously, however, we have crystallized a new polymorph of this structure which crystallized in the P21 space group with thioether bond angles close to ideality (C-S-C ∢: 99.7°, 101.4°).[38-39] The alkyne cores are slightly bent out of linearity, varying between 5-8° from linearity, with parallel alkyne units lying 3.08 Å from each other. Sulfur extrusion on **4_{D3}** was attempted using HMPT and hexaethylphosphorous triamide (HEPT) but proved to be unsuccessful due to the reactivity of the alkene core, resulting in polymer and/or oligomer formation. However, these two examples showcase that pnictogen-directed disulfide macrocyclization is not limited only to substrates that

possess aromatic π-systems, as previously thought, and can be extended into simple nonaromatic π-systems as well; moreover, current work in our lab is focusing on the utility of the alkynyl disulfide macrocycles as sulfur extrusion reagents themselves.

Next, we sought to assess if any π-system is even necessary for this method to function effectively. For this, we chose to use trans-1,4-bis(mercaptomethyl)cyclohexane (**$H_2$6**). To our surprise, this method produced discrete disulfide macrocycles, including the dimer through heptamer (89% combined yield), with the tetramer and pentamer being the dominant products (31% and 23%, respectively). Additionally, since previous studies had shown that aryl systems predominantly form oligomers/polymers without the presence of the pnictogen additive, we sought to understand if the pnictogen additive was necessary in these non-aryl systems as well. Indeed, oxidation of **$H_2$6** without the pnictogen present yielded mostly oligomer/polymer formation with almost no discrete cyclophane produced, again highlighting a critical role for the pnictogen additive in these self-assembly reactions.

The trimer (**6_{D3}**) crystallizes from vapor diffusion of hexanes into CHCl3, the tetramer (**6_{D4}**) crystallizes from slow evaporation in $CHCl_3$, and the pentamer (**6_{D5}**) crystallizes from slow evaporation in DCM (**Figure 2.4**). Trimer **6_{D3}** crystallizes in the P21/c space group with the disulfide bridges showing slight strain (C-S-S-C ∡: 80.0°, 85.3°, 100.5°). **6_{D4}** crystallizes in the P2/c space group with disulfide bridges adopting a slightly more strained conformation (C-S-S-C ∡: 79.8°, 79.8°, 81.49°, 81.49°). Pentamer **6_{D5}** crystallizes in the Iba2 space group with three of the five disulfide bridges deviating from ideality by a considerable amount (C-S-S-C ∡: 78.1°, 79.6°, 84.7°, 92.9°, 133.3°). All crystals showed only the chair conformation of the cyclohexane core to be present with no considerable deviation from ideal cyclohexane bond angles (**Figure**

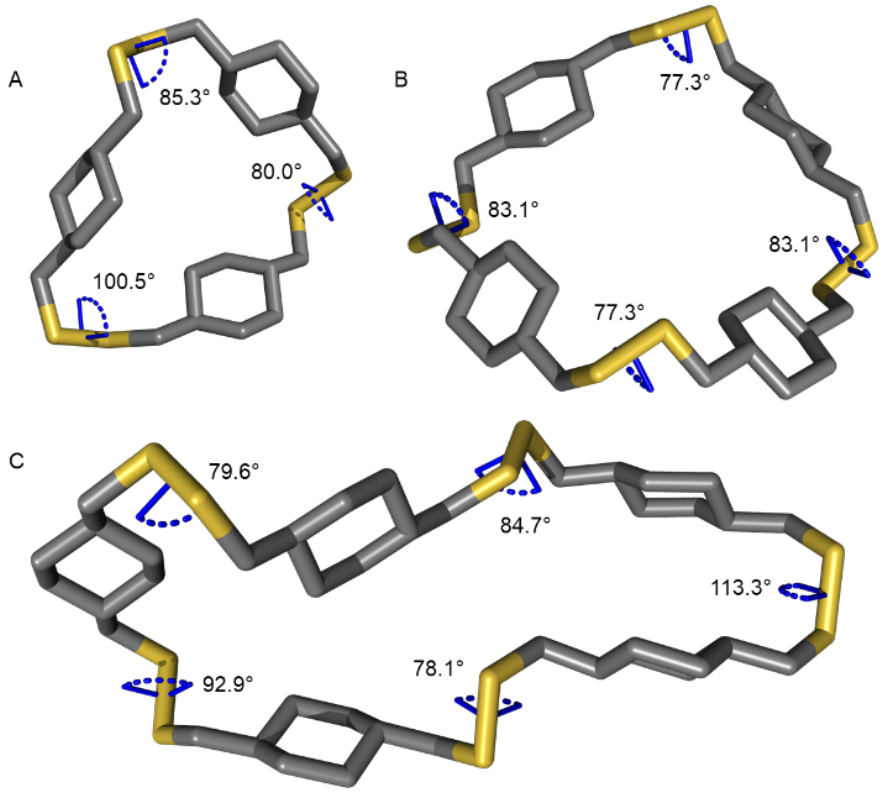

Figure 2.4: Single-crystal X-ray crystal structure of 6_{D3} (A) 6_{D4} (B), and 6_{D5} (C). Disulfide dihedral angles are shown in blue. Hydrogens have been omitted for clarity.

2.4). Tetramer $\mathbf{6_{D4}}$ was then treated with HMPT, generating the thioether ($\mathbf{6_{T4}}$) in quantitative yield (see ESI).

To fully explore the viability of this method to make what we believe to be unusual disulfide macrocycles, we chose a substrate that lacks a π-system, contains heteroatoms we have not used previously (oxygen), and possesses an inherently unique spatial arrangement. To accomplish this, we used 3,9-ethanedithiol-2,4,8,10-tetraoxaspiro[5.5]undecane ($\mathbf{H_2 7}$), which to our pleasant surprise formed the disulfide dimer ($\mathbf{7_D 2}$) with relative ease in 50% yield, with higher ordered species forming only in trace yields. Crystals of $\mathbf{7_D 2}$ were grown from vapor diffusion of hexanes into CHCl3 and crystallized in the P21/c space group (**Figure 2.5**). The disulfide bridges

adopt a rather strained conformation, likely due to the unique structural twist of the spiro center (C-S-S-C ∢: 73.7°, 73.7°). This helical twisting also leads to complex ^{1}H and ^{13}C NMR spectra. Assignment of all associated peaks were confirmed using ^{1}H COSY and ^{13}C HSQC 2D NMR experiments and further validated using ^{13}C DEPT 45, 90, and 135 NMR experiments, which confirms that the crystallized dimeric structure also persists in solution (see Supporting Information for further details). Facile generation of this dimer highlights the ability of this method to form disulfide macrocycles, even with substrates containing unique heterocyclic geometries and without any π-system involvement whatsoever.

Conclusion

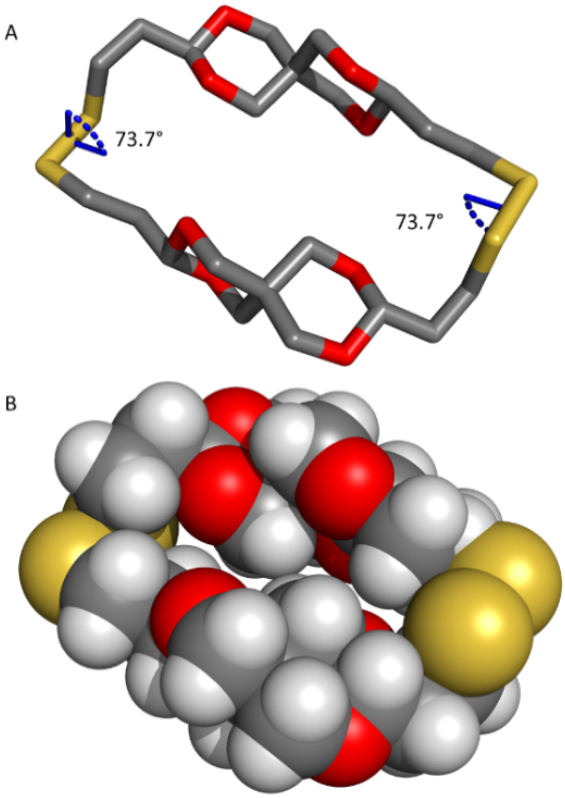

Figure 2.5: A) Stick and B) space-filling representation of single-crystal X-ray crystal structure of 7_{D2}. Disulfide dihedral angles are shown in blue. Hydrogens have been omitted from stick representation for clarity.

In conclusion, we have successfully synthesized 21 new disulfide and thioether macrocycles/cages containing a wide breadth of structural and electronic variations, including extended linker arms (**$H_2$1**), expanded π-systems (**$H_3$2**), electron deficient arene rings (**$H_2$3**), and alkene (**$H_2$4**), alkyne (**$H_2$5**), cyclohexane (**$H_2$6**), and twisted heterocyclic spiro motifs (**$H_2$7**). Of these 21 total structures, 9 crystal structures have been obtained, elucidating many interesting structural features for future study. We have shown that an aromatic system is not required for this metalloid-assisted self-assembly method to proceed, which makes this reaction amenable to a wide range of di- and trithiol substrates (and perhaps even more complex thiols). This discovery allows for a generalized method for the facile formation of discrete disulfide and thioether macrocycles in moderate to high overall yields with excellent efficiency, and we are exploring the nature of the secondary bonding interactions at play (e.g., pnictogen-π, pnictogen-sulfur, etc.) in enabling discrete disulfide formation over oligomeric products. We hope these new insights lead us and others to several new and exciting disulfide, thioether, and hydrocarbon macrocycles which have not been previously reported.

Bridge to Chapter III

Chapter II showcases pnictogen-assisted self-assembly is not substrate-dependant and the reaction conditions are suitable for general macrocyclization pathways. Biasing this new information, as will be discussed in Chapter III, I investigated our pnictogen-assisted self-assembly as a facile pathway into macromolecular materials. Specifically, design methods in PDI-containing macrocycle formation were investigated.

Experimental

General Considerations

Unless otherwise stated, reactions were conducted under atmospheric conditions. All commercially obtained reagents were used as received unless otherwise stated. Purification and separation of disulfide and thioether products were performed by using Japan Analytical Instruments Inc. LC-9101 recycling preparative high-performance liquid chromatography with gel permeation chromatography columns JAIGEL-1H and JAIGEL-2H. ^{1}H, ^{13}C NMR and 2D-COSY and HSQC spectra were recorded with a Bruker AVANCE 500, Bruker AVANCE 600 or Varian INOVA 500 in $CDCl_3$. Spectra were referenced using the residual solvent resonances as internal standards and reported in ppm. High resolution mass spectrometry was obtained with a Xevo G2-XS TOF system from Waters using an atmospheric solids analysis probe.

General Disulfide Macrocycle Synthesis

To a dilute solution of a di- or trithiol, a separate solution of I_2 (2-4 equivalents) and $SbCl_3$ (2-4 equivalents) are added slowly under ambient conditions with stirring. The reaction is then allowed to stir briefly (15-60 minutes), then quenched with saturated Na_2SO_3 solution until the reaction is no longer purple. The reaction was then added to a separatory funnel and washed with H_2O, dried with $MgSO_4$, and condensed. The discrete disulfide macrocycle species were then separated using a prep-HPLC. Equivalents of I_2 and $SbCl_3$ to be used is substrate dependent. Solvents are generally $CHCl_3$, CH_2Cl_2, or benzene.

Synthetic Procedures

Synthesis of thiols

The preparation of 1,4-bis(2-mercaptoethyl)benzene (**$H_2$1**),[40] 2,3,5,6-tetrafluoro-1,4-bis(mercaptomethyl)benzene (**$H_2$3**)[41], *trans*-2-butene-1,4-dithiol (**$H_2$4**)[42], 2-butyne-1,4-dithiol

(**$H_2$5**)[42], and *trans*-1,4-bis(mercaptomethyl)cyclohexane (**$H_2$6**)[43] were previously reported and characterized. Synthesis of precursors to *trans*-1,4-bis(mercaptomethyl)cyclohexane (**$H_2$6**)[44] and 2,4,6-tris(4-bromomethyl)-1,3,5-triazine (**$H_3$2**)[45] were previously reported. Synthesis of 3-9,ethanedithiol-2,4,8,10-tetaoxaspiro[5.5]undecane **($H_2$7)** was accomplished using a slightly modified literature procedure.[44] ^{1}H-NMR spectral data and mass spectrometry data matched those reported in the literature.

Synthesis of 2,4,6-tris[4-(mercaptomethyl)phenyl]-1,3,5-triazine ($H_3$2)

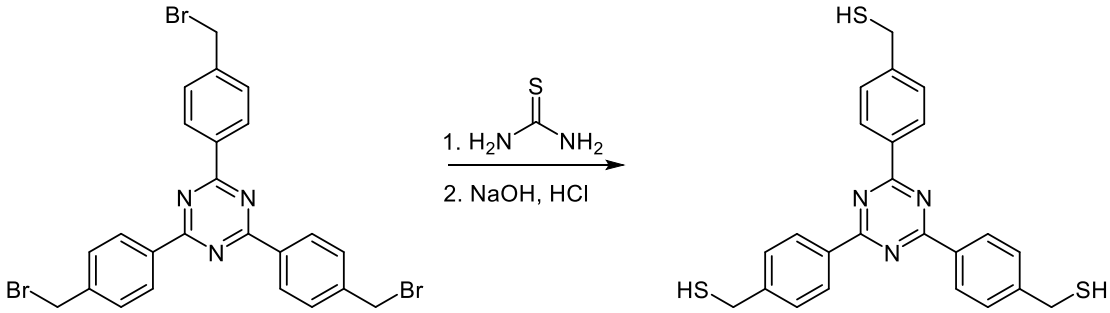

To a 250 mL round bottom flask, 2,4,6-tris[4-(bromomethyl)phenyl]-1,3,5-triazine (0.988 g, 1.68 mmol) was dissolved in 60 mL $CHCl_3$. In a flask, thiourea (0.766 g, 10.1 mmol) was added to 50 mL acetone and sonicated. The thiourea solution was added to the RBF and left to stir for 16 hours at reflux. The resulting thiouronium salt was then vacuum filtered and washed with acetone. The solid was collected and used without further purification. The thiouronium triazine salt was added to a 500 mL RBF and 150 mL of NaOH (3M) and heated to 80 °C for 16 hours. The reaction was then cooled and put on ice then 9M HCl was added until the solution turned acidic, and a white precipitate formed. The solid was vacuum filtered, washed with water, and used without further purification (95% yield). ^{1}H-NMR (500 MHz, CD_2Cl_2) δ: 8.73 – 8.72 ppm (d, 6H), 7.56 – 7.55 ppm (d, 6H), 3.87 – 3.86 ppm (d, 6H), 1.93 ppm (t, 3H); ^{13}C-NMR (125 MHz, $CDCl_3$) δ:

170.33, 146.47, 129.31, 128.29 ppm; HRMS-ASAP [M+H]+ $C_{24}H_{22}N_3S_3$ predicted: 448.0976, found: 448.1002.

Modified synthesis of 3-9,ethanedithiol-2,4,8,10-tetaoxaspiro[5.5]undecane ($H_2$7)

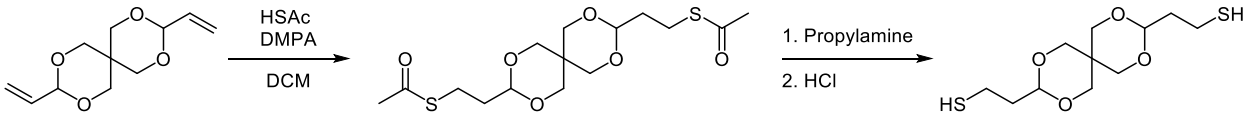

To a 100 mL round bottom flask, 3,9-divinyl-2,4,8,10-tetraoxaspiro[5.5]undecane (1 g, 47 mmol), thioacetic acid (7.4 mL, 104 mmol) and DMPA (0.24 g, 0.90 mmol) were added in 25 mL THF. The reaction was sparged with N_2 and irradiated with LED-UV (λ = 370 nm) for 3 hours. The solvent was then evaporated and product was recrystallized from hexane/ethyl acetate (9:1). The product was filtered and washed with hexane to yield the dithioacetate as white crystals (76% yield). Deprotection of the thioacetate followed literature procedures and matched previously reported characterization data (50% yield).[44]

Synthesis of 1,4-bis(2-mercaptoethyl)benzene (1_{D2-4}) associated disulfide macrocycles

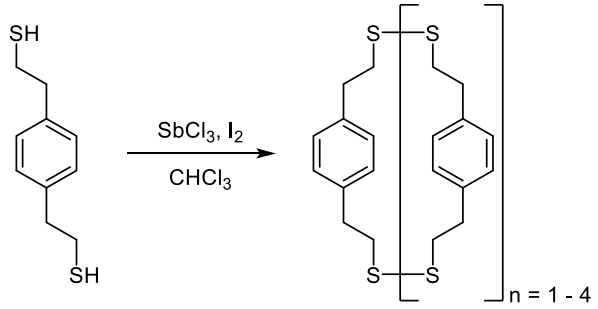

To a 50 mL solution of **$H_2$1** (164 mg, 0.83 mmol) in $CHCl_3$, a 50 mL solution of $SbCl_3$ (340 mg, 1.5 mmol) and I_2 (380 mg, 2 mmol) was added slowly through a cotton-stuffed funnel. The reaction was allowed to stir for 15 minutes under ambient conditions. The reaction was then quenched with Na_2SO_3 until the reaction mixture turns from purple to white. The organic layer was collected and washed with 100 mL of H_2O (3x), dried with $MgSO_4$, and condensed to yield 159 mg of a white powder (79% combined yield: 57% dimer, 14% trimer, 13% tetramer). Dimer: ^{1}H-NMR (500 MHz, $CDCl_3$) δ: 7.07 (s, 8H), 2.66 (t, 8H), 2.50 (t, 8H) ppm; ^{13}C-NMR (125 MHz, $CDCl_3$) δ: 138.19, 129.12, 43.18, 35.79 ppm; HRMS-ASAP [M+H]+ $C_{20}H_{25}S_4$ predicted: 393.0839, found: 393.0814. Trimer: ^{1}H-NMR (500 MHz, $CDCl_3$) δ: 7.15 (q, 2H), 3.84 (t, 6H), 2.99 – 2.86 (m, 12H), 2.84 (t, 6H) ppm; ^{13}C-NMR (125 MHz, $CDCl_3$) δ: 138.34, 136.74, 129.35, 129.01, 63.79, 40.44, 38.93, 35.45 ppm; HRMS-ASAP [M+H]+ $C_{30}H_{37}S_6$ predicted: 589.1220, found: 589.1200. Tetramer: ^{1}H-NMR (500 MHz, $CDCl_3$) δ: 7.10 ppm (s, 16H), 2.90 ppm (m, 32H); ^{13}C-NMR (125 MHz, $CDCl_3$) δ: 138.30, 128.90, 40.60, 35.51 ppm; HRMS-ASAP [M+H]+ $C_{40}H_{49}S_8$ predicted: 785.1600, found: 785.4924.

Synthesis of 12,4,6-tris(4-mercaptomethyl)-1,3,5-triazine (2_{D2}) associated disulfide macrocycles

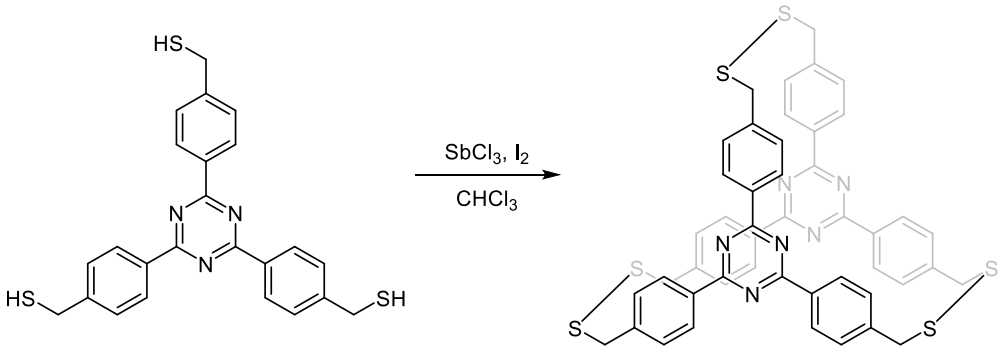

To a 200 mL solution of **$H_3$2** (297 mg, 0.66 mmol) in benzene, a 100 mL solution of I_2 (1.02 g, 4.01 mmol) and $SbCl_3$ (611 mg, 2.68 mmol) was added slowly. The reaction was allowed to stir for 30 minutes under ambient conditions. The reaction was then quenched with Na_2SO_3 until the reaction mixture turns from purple to clear. The organic layer was collected and washed with 100 mL of H_2O (3x), dried with $MgSO_4$, and condensed to yield an off-white powder (92% yield). ^{1}H-NMR (500 MHz, $CDCl_3$) δ: 8.31 – 8.29 ppm (d, 6H), 7.12 – 7.11 ppm (d, 6H), 3.78 (s, 6H); ^{13}C-NMR (125 MHz, $CDCl_3$) δ: 170.65, 143.47, 134.86, 129.05, 128.91 ppm; HRMS-ASAP [M+H]+ $C_{48}H_{37}N_6S_6$ predicted: 888.1326, found: 888.1453.

Synthesis of 2,3,5,6-tetrafluoro-1,4-bis(mercaptomethyl)benzene (3) associated disulfide macrocycles

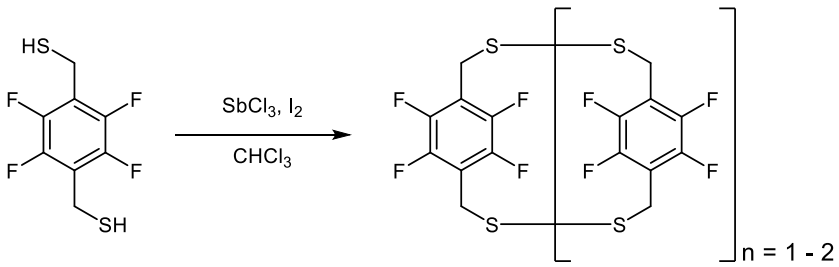

To a 50 mL solution of **$H_2$3** (220 mg, 0.91 mmol) in $CHCl_3$, a 100 mL solution of I_2 (412.9 mg, 1.81 mmol) and $SbCl_3$ (460.2 mg, 1.81 mmol) was added slowly. The reaction was allowed to stir for 30 minutes under ambient conditions. The reaction was then quenched with Na_2SO_3 until the reaction turned from purple to clear. The organic layer was collected and washed with H_2O (3x), dried with $MgSO_4$, and condensed to give an off-white solid (70% combined yield: 20% dimer, 50% trimer). Dimer: ^{1}H-NMR (500 MHz, $CDCl_3$) δ: 3.98 ppm - 3.92 ppm (dt, 4H), 3.66 – 3.61 ppm (dt, 4H). HRMS (ASAP) (m/z), calculated for $C_{16}H_8F_8S_4$ (M+H) predicted: 480.9072, found: 480.9036. Trimer: ^{1}H-NMR (500 MHz, $CDCl_3$) δ: 3.97 ppm (s, 8H). ^{19}F-NMR (500 MHz,

$CDCl_3$) δ: -142 ppm. HRMS (ASAP) (m/z), calculated for $C_{24}H_{12}F_{12}S_6$ (M+H) predicted: 719.9072, found: 719.9072.

Synthesis of *trans*-2-butene-1,4-dithiol (4_{D2-4}) associated disulfide macrocycles

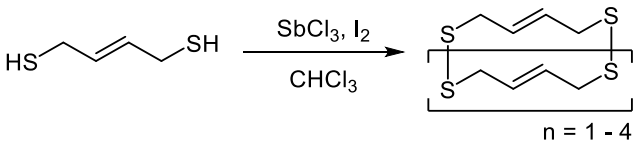

To a 50 mL solution of **$H_2$4** (60 mg, 0.5 mmol) in $CHCl_3$, a 50 mL solution of I_2 (254 mg, 1 mmol) and $SbCl_3$ (228 mg, 1 mmol) was added slowly through a cotton-stuffed funnel. The reaction was allowed to stir for 15 minutes under ambient conditions. The reaction was then quenched with Na_2SO_3 until the reaction mixture turns from purple to white. The organic layer was collected and washed with 100 mL of H_2O (3x), dried with $MgSO_4$, and condensed to yield an orange oil (94% combined yield: 32% dimer, 29% trimer, 25% tetramer, 8% pentamer). Dimer: ^{1}H-NMR (500 MHz, $CDCl_3$) δ: 5.67 (m, 4H), 3.36 – 3.35 (m, 8H) ppm; ^{13}C-NMR (125 MHz, $CDCl_3$) δ: 129.52, 42.15 ppm; HRMS-ASAP [M+H]+ $C_8H_{13}S_4$ predicted: 236.9900, found: 236.9937. Trimer: ^{1}H-NMR (500 MHz, $CDCl_3$) δ: δ 5.70 (m, 6H), 3.41 – 3.40 (m, 12H) ppm; ^{13}C-NMR (125 MHz, $CDCl_3$) δ: 129.69, 41.68 ppm; HRMS-ASAP [M+H]+ $C_{12}H_{19}S_6$ predicted: 354.9811, found: 354.9891. Tetramer: ^{1}H-NMR (500 MHz, $CDCl_3$) δ: 5.72 – 5.64 (m, 8H), 3.43 – 3.33 (m, 16H) ppm; ^{13}C-NMR (125 MHz, $CDCl_3$) δ: 129.59, 41.76 ppm; HRMS-ASAP [M+H]+ $C_{16}H_{25}S_8$ predicted: 472.9722, found: 472.9787. Pentamer: ^{1}H-NMR (500 MHz, $CDCl_3$) δ: 5.72 – 5.68 (m, 10H), 3.40 – 3.36 (m, 20H) ppm; ^{13}C-NMR (125 MHz, $CDCl_3$) δ: 129.56, 41.59 ppm; HRMS-ASAP [M+H]+ $C_{20}H_{31}S_{10}$ predicted: 590.9633, found: 590.9696.

Synthesis of 2-butyne-1,4-dithiol associated disulfide (5_{D2}) and thioether (5_{T2}) macrocycles

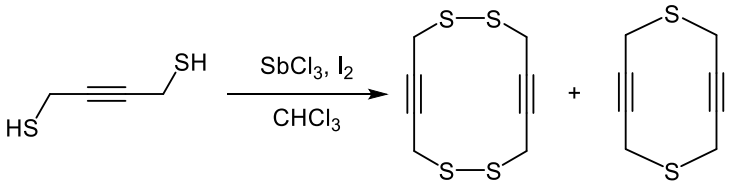

To a 100 mL solution of **$H_2$5** (230 mg, 1.9 mmol) in $CHCl_3$, a 150 mL solution of I_2 (533 mg, 2.1 mmol) and $SbCl_3$ (866 mg, 3.8 mmol) in $CHCl_3$ was added slowly through a cotton-stuffed funnel. The reaction was allowed to stir for 15 minutes under ambient conditions. The reaction was then quenched with Na_2SO_3 until the reaction mixture turns from purple to white. The organic layer was collected and washed with 100 mL of H_2O (3x), dried with $MgSO_4$, and condensed to yield a dark orange oil (49% combined yield: 36% thioether dimer, 13% disulfide dimer). Thioether dimer: ^{1}H-NMR (500 MHz, $CDCl_3$) δ: 3.48 ppm (s, 8H); ^{13}C-NMR (125 MHz, $CDCl_3$) δ: 80.71, 22.87 ppm. Disulfide dimer: ^{1}H-NMR (500 MHz, $CDCl_3$) δ: 3.47 ppm (s, 8H); ^{13}C-NMR (125 MHz, $CDCl_3$) δ: 81.65, 80.71, 29.17, 22.22 ppm; HRMS-ASAP [M+H]+ $C_8H_9S_4$ predicted: 232.9587, found: 233.0991.

Synthesis of trans-1,4-bis(mercaptomethyl)cyclohexane (6_{D2-7}) associated disulfide macrocycles

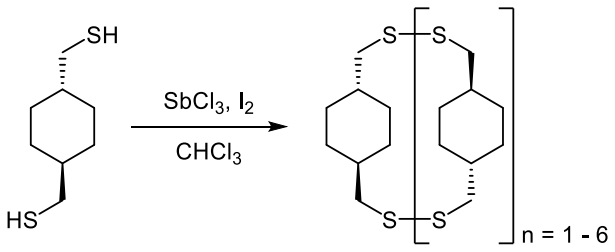

To a 100 mL solution of **$H_2$6** (385 mg, 2.18 mmol) in $CHCl_3$, a 150 mL solution of I_2 (2.2 g, 8.67 mmol) and $SbCl_3$ (1.07 g, 4.41 mmol) in $CHCl_3$ was added slowly. The reaction is allowed to stir for 30 minutes under ambient conditions. The reaction was then quenched with Na_2SO_3 until the reaction mixture turns from purple to clear. The organic layer was collected and washed with 100 mL of H_2O (3x), dried with $MgSO_4$, and condensed to yield a brown powder (76% combined yield: 3% dimer, 17% trimer, 24% tetramer, 17% pentamer, 10% hexamer, 5% heptamer). Dimer: ^{1}H-NMR (500 MHz, $CDCl_3$) δ: 2.61 – 2.60 (d, 8H), 2.00 – 1.80 (m, 8H), 1.63 – 1.41 (m, 4H), 1.03 – 0.94 (m, 8H); ^{13}C-NMR (125 MHz, $CDCl_3$) δ: 46.90, 37.74, 32.01 ppm; HRMS-ASAP [M+H]+ $C_{16}H_{29}S_4$ predicted: 349.1152, found: 349.1146. Trimer: ^{1}H-NMR (500 MHz, $CDCl_3$) δ: 2.66 – 2.65 ppm (d, 12H), 2.05 – 1.98 ppm (m, 12H), 1.63 – 1.50 (m, 6H), 1.04 – 0.95 (m, 12H); ^{13}C-NMR (125 MHz, $CDCl_3$) δ: 48.06, 37.57, 32.45 ppm; HRMS-ASAP [M+H]+ $C_{24}H_{43}S_6$ predicted: 523.1689, found: 523.1693. Tetramer: ^{1}H-NMR (500 MHz, $CDCl_3$) δ: 2.64 – 2.63 ppm (d, 16H), 2.03 – 1.87 ppm (m, 16H), 1.67 – 1.50 ppm (m, 8H), 1.05 – 0.96 ppm (m, 16H); ^{13}C-NMR (125 MHz, $CDCl_3$) δ: 47.35, 37.71, 32.31 ppm; HRMS-ASAP [M+H]+ $C_{32}H_{57}S_8$ predicted: 697.2226, found: 697.4011. Pentamer: ^{1}H-NMR (500 MHz, $CDCl_3$) δ: 2.63 – 2.62 ppm (d, 20H), 1.98 – 1.92 ppm (m, 20H), 1.63 – 1.51 ppm (m, 10H), 1.04 – 0.95 ppm (m, 20H); ^{13}C-NMR (125 MHz, $CDCl_3$) δ: 47.34, 37.69, 32.28 ppm; HRMS-ASAP [M+H]+ $C_{40}H_{71}S_{10}$ predicted: 871.2763, found:871.6844. Hexamer: ^{1}H-NMR (500 MHz, $CDCl_3$) δ: 2.62 – 2.61 ppm (d, 24H), 1.98 – 1.92 (m, 24H), 1.65 – 1.51 ppm (m, 12H), 1.03 – 0.95 ppm (m, 24H); ^{13}C-NMR (125 MHz, $CDCl_3$) δ: 47.08, 37.63, 32.27 ppm; HRMS-ASAP [M+H]+ $C_{48}H_{85}S_{12}$ predicted: 1045.3300, found: 1045.5718. Heptamer: ^{1}H-NMR (500 MHz, $CDCl_3$) δ: 2.62 – 2.60 ppm (d, 28H), 1.98 – 1.91 ppm (m, 28H), 1.63 – 1.51 ppm (m, 14H), 1.03 – 0.95 ppm (m, 28H); ^{13}C-NMR (125 MHz, $CDCl_3$) δ:

46.99, 37.60, 32.26 ppm; HRMS-ASAP [M+H]+ $C_{56}H_{99}S_{14}$ predicted: 1219.3837, found: 1219.2675.

Synthesis of 3-9,ethanedithiol-2,4,8,10-tetaoxaspiro[5.5]undecane (7_{D2}) associated disulfide macrocycles

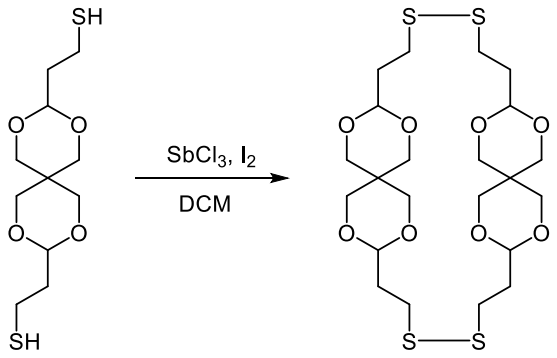

To a 250 mL solution of **$H_2$7** (200 mg, 12 mmol) in CH_2Cl_2, a 100 mL solution of I_2 (0.536 g, 23 mmol) and $SbCl_3$ (0.594 g, 23 mmol) in CH_2Cl_2 was added slowly. The reaction was allowed to stir for 30 minutes under ambient conditions. The reaction was then quenched with Na_2SO_3 until the reaction mixture turns from purple to clear. The organic layer was collected and washed with 100 mL of H_2O (3x), dried with $MgSO_4$, and condensed to yield an off-white powder (50% dimer). ^{1}H-NMR (500 MHz, $CDCl_3$) δ: 4.66 (q, 2H), 4.56 (t, 2H), 3.62 – 3.51 (m, 4H), 3.39 – 3.36 (dd, 2H), 2.86 – 2.81 (dm, 2H), 2.08 – 1.93 (m, 4H); ^{13}C-NMR (125 MHz, $CDCl_3$) δ: 100.98, 100.93, 70.58, 70.56, 70.20, 70.16, 33.77, 32.65, 32.50, 32.42, 32.00 ppm; HRMS-ASAP [M+H]+ $C_{22}H_{37}O_8S_4$ predicted: 557.1293, found: 557.2857.

Synthesis of triazine thioether (2_{T2})

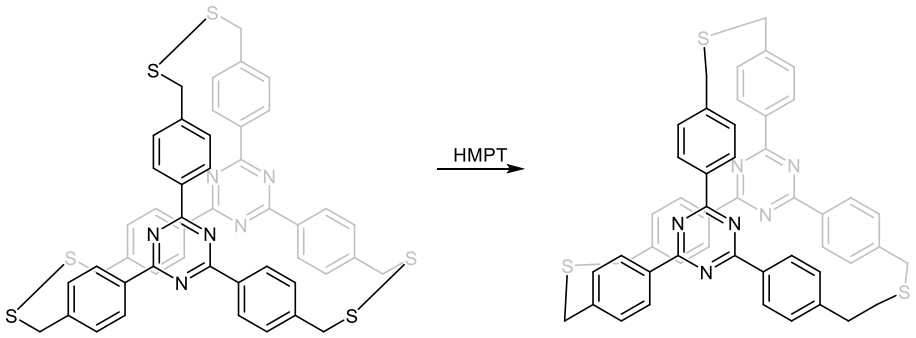

To a 40 mL solution of $\mathbf{2_{D2}}$ (50 mg, 0.06 mmol) in N_2 sparged $CHCl_3$, hexamethylphosphorous triamide (50 µL, 0.28 mmol) was added via glass syringe and allowed to react for 16 hours. The reaction was then opened to atmosphere, condensed to dryness, and purified using a prep-HPLC (91% yield). ^{1}H-NMR (500 MHz, $CDCl_3$) δ: 8.21 – 8.20 ppm (d, 6H), 7.19 – 7.18 ppm (d, 6H), 3.97 ppm (s, 6H); ^{13}C-NMR (125 MHz, $CDCl_3$) δ: 170.78, 143.28, 134.37, 129.30, 128.74 ppm; HRMS-ASAP [M+Na]+ $C_{48}H_{37}N_6S_3Na$ predicted: 815.2061, found: 815.2087.

Synthesis of 5,8,14,17,23,24,30,31-tetrathia[3.3.3.3]paracyclohexane ($\mathbf{6_{T4}}$)

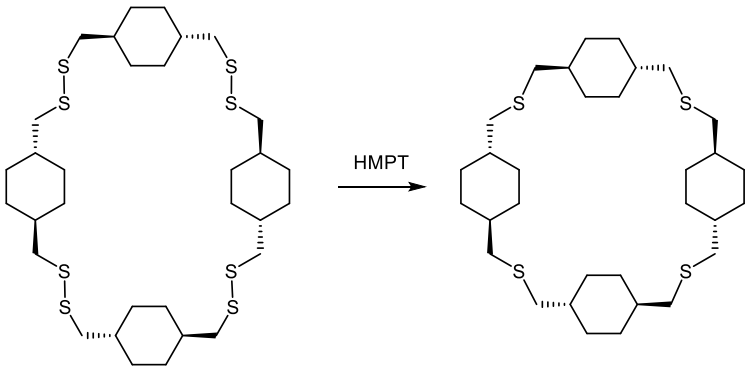

To a 15 mL solution of $\mathbf{6_{T4}}$ (46 mg, 0.066 mmol) in N_2 sparged $CHCl_3$, hexamethylphosphorous triamide (70 µL, 0.39 mmol) was added via glass syringe and allowed to

react for 16 hours. The reaction was then opened to atmosphere, condensed to dryness, and purified using a prep-HPLC (87% yield). ^{1}H-NMR (500 MHz, $CDCl_3$) δ: 2.66 – 2.65 ppm (d, 4H), 2.04 – 1.98 ppm (m, 4H), 1.67 – 1.51 (m, 2H), 1.04 – 0.95 (m, 4H) ^{13}C-NMR (125 MHz, $CDCl_3$) δ: 48.07, 37.57, 32.46 ppm; HRMS-ASAP [M+Na]+ $C_{32}H_{56}S_4Na$ predicted: 591.3163, found: 591.7262.

Supplemental Characterization Data

For additional information pertaining to NMR experimental data, please see Supplemental Information of article "*Expanding the Scope of Pnictogen-Assisted Cyclophane Self-Assembly.*"[1]

X-ray Crystallography

Diffraction intensities for $\mathbf{2_{D2}}$, $\mathbf{2_{T2}}$, $\mathbf{1_{D2}}$, $\mathbf{4_{D3}}$, $\mathbf{6_{D4}}$, $\mathbf{6_{D5}}$, $\mathbf{6_{D3}}$, $\mathbf{5_{T2}}$ and $\mathbf{7_{D2}}$ were collected at 100 K ($\mathbf{2_{D2}}$), 200 K ($\mathbf{4_{D3}}$), 223 K ($\mathbf{5_{T2}}$) and 173 K on a Bruker Apex2 CCD diffractometer using CuKα and MoKα ($\mathbf{2_{D2}}$, $\mathbf{1_{D2}}$) radiation, λ = 1.54178 and 0.71073 Å, respectively. Space groups were determined based on systematic absences and intensity statistics ($\mathbf{2_{T2}}$). Absorption corrections were applied by SADABS. Structures were solved by direct methods and Fourier techniques and refined on F^2 using full matrix least-squares procedures. All non-H atoms were refined with anisotropic thermal parameters. H atoms in all structures were refined in calculated positions in a rigid group model. One S atom in $\mathbf{7_{D2}}$, two S atoms in $\mathbf{2_{T2}}$ and one S atom in $\mathbf{2_{D2}}$ are disordered over two positions in ratio 1:1. Crystals of $\mathbf{2_{D2}}$ were very thin strips and it was possible collect diffraction data only up to $2\theta_{max}$ = 46.65° using a Mo-radiation source. However, it provides appropriate number of reflections per number of refined parameters, 6271/588. The structure of $\mathbf{6_{D5}}$ was solved as a racemic twin consisting of two domains, the Flack is 0.15(3). The structure of $\mathbf{5_{T2}}$ was solved having two symmetrically independent molecules in

chiral space group of symmetry $P2_1$. The found Flack parameter, 0.47(4), indicates on a possible centro-symmetrical space group, but all our efforts to get the structure in centro-symmetrical space groups were failed. The structure of $\mathbf{5_{T2}}$ seems having a pseudo-symmetry. It also should be mentioned that we could not get convergence in the refinement of the structure of $\mathbf{5_{T2}}$ even with applying some geometrical restrictions. The structure of this compound was determined in several possible space groups and it was found that in all of them refinement of the structure can't get converged. We think it could be related to the flat minimum of energy for the molecule of $\mathbf{5_{T2}}$ or them packing in the crystal structure. Crystal structures of $\mathbf{2_{D2}}$, $\mathbf{2_{T2}}$ and $\mathbf{6_{D4}}$ include solvent molecules C_6H_6 and $CHCl_3$, respectively. Three solvent molecules $CHCl_3$, 58 electrons, in the full unit cell of $\mathbf{2_{T2}}$, and four solvent molecules $CHCl_3$ in $\mathbf{6_{D4}}$ are highly disordered and have been treated by SQUEEZE. The corrections of the X-ray data by SQUEEZE are 170 and 240 electron/cell, respectively for $\mathbf{2_{T2}}$ and $\mathbf{6_{D4}}$. All calculations were performed by the Bruker SHELXL-2014 package.

Crystallographic data for $\mathbf{1_{D2}}$

$C_{20}H_{24}S_4$, M = 392.63, 0.18 x 0.16 x 0.14 mm, T = 173(2) K, Monoclinic, space group $P2_1/n$, a = 8.2013(9) Å, b = 6.5677(7) Å, c = 18.298(2) Å, β = 101.160(2)°, V = 966.93(18) Å^3, Z = 2, D_c = 1.349 Mg/m^3, μ(Mo) = 0.491 mm^{-1}, F(000) = 416, $2\theta_{max}$ = 58.17°, 11469 reflections, 2707 independent reflections [R_{int} = 0.0442], R1 = 0.0479, wR2 = 0.1380 and GOF = 1.033 for 2707 reflections (110 parameters) with I>2σ(I), R1 = 0.0540, wR2 = 0.1434 and GOF = 1.033 for all reflections, max/min residual electron density +1.574/-0.371 eÅ^{-3}.

Crystallographic data for $\mathbf{2_{D2}}$

$C_{51}H_{45}N_6S_6$, M = 934.29, 0.330 x 0.03 x 0.02 mm, T = 100(2) K, Monoclinic, space group *P*2/*n*, *a* = 18.647(3) Å, *b* = 8.0678(14) Å, *c* = 30.375(5) Å, β = 107.510(3)°, *V* = 4357.8(13) Å^3, *Z* = 4, D_c = 1.424 Mg/m^3, μ(Mo) = 0.360 mm^{-1}, *F*(000) = 1956, $2\theta_{max}$ = 46.65°, 24289 reflections, 6271 independent reflections [R_{int} = 0.1125], R1 = 0.0629, wR2 = 0.1380 and GOF = 1.038 for 6271 reflections (588 parameters) with I>2σ(I), R1 = 0.1409, wR2 = 0.1738 and GOF = 1.038 for all reflections, max/min residual electron density +0.447/-0.447 eÅ^{-3}.

Crystallographic data for 2_{T2}

$C_{49}H_{37}Cl_3N_6S_3$, M = 912.37, 0.07 x 0.04 x 0.02 mm, T = 173(2) K, Triclinic, space group *P*-1, *a* = 8.7460(2) Å, *b* = 13.2094(2) Å, *c* = 20.2583(3) Å, α = 107.517(2)°, β = 93.520(1)°, γ = 90.456(1)°, *V* = 2226.84(7) Å^3, *Z* = 2, D_c = 1.361 Mg/m^3, μ(Cu) = 3.511 mm^{-1}, *F*(000) = 944, $2\theta_{max}$ = 152.14°, 28159 reflections, 8900 independent reflections [R_{int} = 0.0251], R1 = 0.0536, wR2 = 0.1618 and GOF = 1.069 for 8900 reflections (534 parameters) with I>2σ(I), R1 = 0.0604, wR2 = 0.1682 and GOF = 1.093 for all reflections, max/min residual electron density +0.473/-0.230 eÅ^{-3}.

Crystallographic data for 3_{D3}

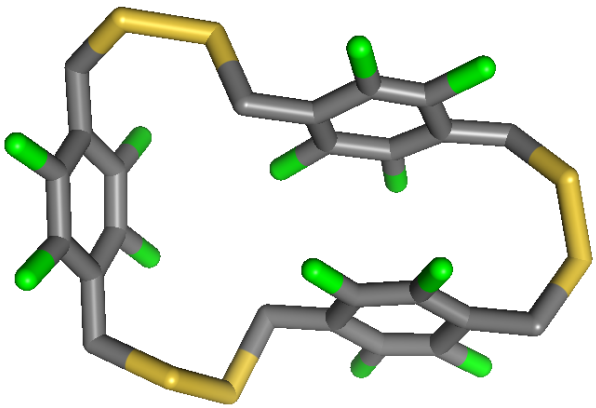

Crystals of $\mathbf{3_{D3}}$ were grown in dichloromethane utilizing vapor diffusion with pentanes, however, a full data set could not be collected due to low angle of diffraction. A low-res collection was possible and is shown above for connectivity purposes.

Crystallographic data for $\mathbf{4_{D3}}$

$C_{12}H_{18}S_6$, M = 354.62, 0.21 x 0.08 x 0.07 mm, T = 200(2) K, Monoclinic, space group $P2_1/c$, a = 5.3348(1) Å, b = 30.1158(9) Å, c = 10.7618(3) Å, β = 101.617(1)°, V = 1693.59(8) Å^3, Z = 4, D_c = 1.391 Mg/m^3, μ(Cu) = 7.301 mm^{-1}, F(000) = 744, $2\theta_{max}$ = 136.53°, 15587 reflections, 3097 independent reflections [R_{int} = 0.0717], R1 = 0.0687, wR2 = 0.1804 and GOF = 1.049 for 3097 reflections (163 parameters) with I>2σ(I), R1 = 0.0708, wR2 = 0.1823 and GOF = 1.049 for all reflections, max/min residual electron density +0.909/-0.526 eÅ^{-3}.

Crystallographic data for $\mathbf{5_{T2}}$

$C_8H_8S_2$, M = 168.26, 0.16 x 0.14 x 0.09 mm, T = 223(2) K, Monoclinic, space group $P2_1$, a = 4.3260(8) Å, b = 11.792(2) Å, c = 15.762(3) Å, β = 95.731(9)°, V = 800.1(3) Å^3, Z = 4, D_c = 1.397 Mg/m^3, μ(Cu) = 5.332 mm^{-1}, F(000) = 352, $2\theta_{max}$ = 136.70°, 6094 reflections, 2779 independent reflections [R_{int} = 0.0446], R1 = 0.0472, wR2 = 0.1495 and GOF = 1.005 for 2779 reflections (182 parameters) with I>2σ(I), R1 = 0.0561, wR2 = 0.1697 and GOF = 1.005 for all reflections, the Flack = 0.47(4), max/min residual electron density +0.374/-0.250 eÅ^{-3}.

Crystallographic data for $\mathbf{6_{D3}}$

$C_{24}H_{42}S_6$, M = 522.93, 0.23 x 0.09 x 0.02 mm, T = 173(2) K, Monoclinic, space group $P2_1/c$, a = 5.6958(2) Å, b = 22.7213(6) Å, c = 21.1880(5) Å, β = 91.957(2)°, V = 2740.47(14) Å^3,

$Z = 4$, $D_c = 1.267$ Mg/m^3, μ(Cu) = 4.671 mm^{-1}, $F(000) = 1128$, $2\theta_{max} = 132.95°$, 14297 reflections, 4787 independent reflections [$R_{int} = 0.0394$], R1 = 0.0386, wR2 = 0.0990 and GOF = 1.041 for 4787 reflections (271 parameters) with I>2σ(I), R1 = 0.0457, wR2 = 0.1034 and GOF = 1.041 for all reflections, max/min residual electron density +0.408/-0.237 eÅ^{-3}.

Crystallographic data for 6_{D4}

$C_{33}H_{57}Cl_3S_8$, M = 816.61, 0.16 x 0.14 x 0.09 mm, T = 173(2) K, Monoclinic, space group *P*2/*c*, $a = 30.3668(17)$ Å, $b = 5.2860(4)$ Å, $c = 29.9122(16)$ Å, $\beta = 119.248(4)°$, $V = 4189.3(5)$ Å^3, $Z = 4$, $D_c = 1.295$ Mg/m^3, μ(Cu) = 5.871 mm^{-1}, $F(000) = 1736$, $2\theta_{max} = 133.80°$, 26763 reflections, 7348 independent reflections [$R_{int} = 0.0926$], R1 = 0.0866, wR2 = 0.2107 and GOF = 1.098 for 7348 reflections (361 parameters) with I>2σ(I), R1 = 0.0994, wR2 = 0.2178 and GOF = 1.098 for all reflections, max/min residual electron density +1.036/-0.697 eÅ^{-3}.

Crystallographic data for 6_{D5}

$C_{40}H_{70}S_{10}$, M = 871.56, 0.14 x 0.06 x 0.01 mm, T = 173(2) K, Orthorhombic, space group *Iba*2, $a = 10.9400(8)$ Å, $b = 78.496(7)$ Å, $c = 10.7608(9)$ Å, $V = 9240.7(13)$ Å^3, $Z = 8$, $D_c = 1.253$ Mg/m^3, μ(Cu) = 4.618 mm^{-1}, $F(000) = 3760$, $2\theta_{max} = 134.37°$, 18659 reflections, 6953 independent reflections [$R_{int} = 0.0974$], R1 = 0.0686, wR2 = 0.1702 and GOF = 1.005 for 6953 reflections (451 parameters) with I>2σ(I), R1 = 0.1038, wR2 = 0.1906 and GOF = 1.005 for all reflections, the Flack = 0.15(3), max/min residual electron density +0.550/-0.437 eÅ^{-3}.

Crystallographic data for 7_{D2}

$C_{22}H_{36}O_8S_4$, M = 556.75, 0.18 x 0.11 x 0.02 mm, T = 173(2) K, Monoclinic, space group $P2_1/c$, a = 11.6003(5) Å, b = 5.5764(2) Å, c = 20.1918(8) Å, β = 97.537(3)°, V = 1294.88(9) Å^3, Z = 2, Z' = 0.5, D_c = 1.428 Mg/m^3, μ(Cu) = 3.755 mm^{-1}, F(000) = 592, $2\theta_{max}$ = 133.11°, 8561 reflections, 2287 independent reflections [R_{int} = 0.0452], R1 = 0.0793, wR2 = 0.2018 and GOF = 1.088 for 2287 reflections (158 parameters) with I>2σ(I), R1 = 0.0875, wR2 = 0.2078 and GOF = 1.088 for all reflections, max/min residual electron density +1.135/-0.403 eÅ^{-3}.

CHAPTER III

SELF-ASSEMBLY ROUTE TO PERYLENE DIIMIDE(PDI)-BRIDGED CYCLOPHANES

Contributions

This chapter discusses pnictogen-assisted self-assembly as a general route towards disulfide and sulfide-linked macrocycles for optoelectronic and other material applications. The work described herein was accepted with revision in *Advanced Functional Materials*. I wrote the manuscript and performed all synthetic procedure and data analysis. Prof. Darren. W. Johnson provided intellectual input and editorial feedback. Willow A. Davis performed UV-Vis experiments and Dr. Shiva Moaven performed cyclic voltammetry experiments.

Abstract

Herein we report the synthesis and self-assembly of perylene diimide (PDI)-containing macrocycles designed for facile and high-throughput production of shape-persistent, macrocyclic organic electronic materials. Specifically, utilizing dynamic covalent chemistry (DCvC), we showcase ditopic thiols can be utilized as building blocks towards 3D materials with defined porosity, low-lying unoccupied molecular orbitals, and intrinsic fluorescence. The PDI disulfide-linked macrocycles were generated in a single step from the thiolic building block to yield dimeric through pentameric assemblies in overall 95% combined yield; moreover, following self-assembly, the disulfide ensemble was sulfur extruded to the more kinetically stable thioether in 79% combined yield. The modular design suggests these methods can be used to easily self-

assemble other electronically active precursors for utility in porous macrocyclic materials where stepwise pathways may be laborious and/or low yielding.

Introduction

Cyclophanes are a historically significant class of macrocycles characterized by non-adjacent tethering across a benzene core. The distinctive geometry and rigidity of cyclophanes bestow them with remarkable properties, making them valuable building blocks in the design of functional materials. For example, due to their intrinsic strain energy, cyclophanes are the precursors in Parylene production due to their affinity to undergo living polymerization at low temperature[1–3]. Moreover, the unique electronic properties and shape-persistent geometry of cyclophanes renders them highly useful in the construction of organic solid-state materials[4,5]. For instance, conjugated macrocycles with low-lying unoccupied molecular orbitals have garnered recent interest because of their complementarity with fullerenes as n-type electron transport vessels[6,7]. While possessing similar function, conjugated macrocycles differ from fullerenes with other advantageous auxiliary characteristics, such as: (1) intrinsic porosity allowing tunability with host-guest inclusion, (2) conjugated and fully delocalized π systems for interior and exterior π accessibility for tailored electron transport, and (3) circular geometry removing deleterious end groups that can hinder electron transport in linear polymers. Moreover, when compared to their acyclic analogues, macrocycles are found to absorb more visible light, act as more efficient electron transporting materials in organic photovoltaics, and have greater synergy with p-type donors[8–13].

The synthesis of macrocyclic molecules, however, is often limited by burdensome bottom-up pathways. Due to a macrocycle's unfavorable entropic driving force or strain energy, kinetic ring-closing reactions often lead to undesirable side products, lowering overall yield and an increase in

complexity during purification. In addition, linear oligomers and polymers are often favored kinetically over discrete, cyclic self-assembled products. As ring closing is often the final step in such a reaction sequence, multistep approaches that are not high yielding and efficient can lead to large waste in fine materials during buildup. To ameliorate the time and resource sink of generating useful macrocyclic materials, dynamic covalent chemistry (DCvC) can be used as a thermodynamically-driven alternative during bottom-up preparation and design[14,15]. By using reversible bonds in the macrocyclization step, molecules can 'error correct' themselves by breaking and reforming covalent bonds until a thermodynamic sink is reached (i.e. the discreet, self-assembled macrocycle, which is favored thermodynamically over larger acyclic oligomers). DCvC has also proven applicable in the efficient preparation of plastics, organic electronics, and stimuli-responsive materials, among other uses, making it an amenable approach to cyclophane self-assembly for organic materials applications[16–18].

In our lab, we have shown that this strategy can be applied with oligothiols in the formation of disulfide-linked cyclophanes by utilizing a pnictogen directing agent in tandem with a mild oxidant (**Scheme 3.1**)[19–21]. Our pnictogen-directed self-assembly approach allows the generation of disulfide macrocycles in high overall yields and fast reaction times and seems to avoid, in all cases studied so far, the formation of oligomers

Previous Work

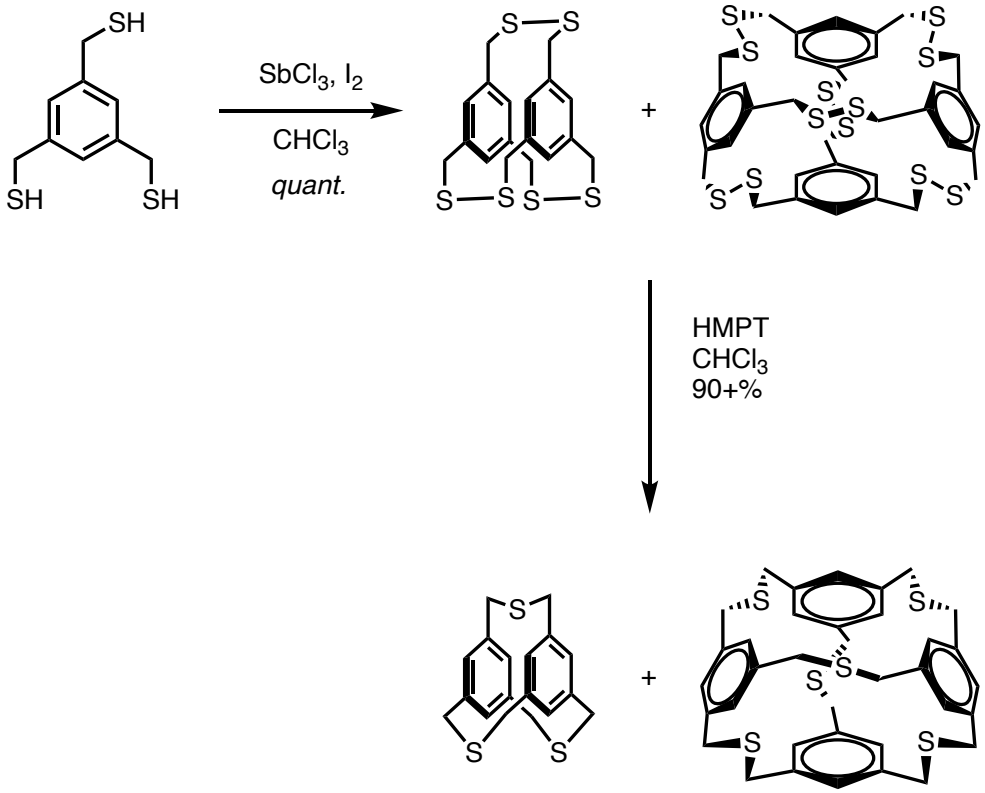

This Work

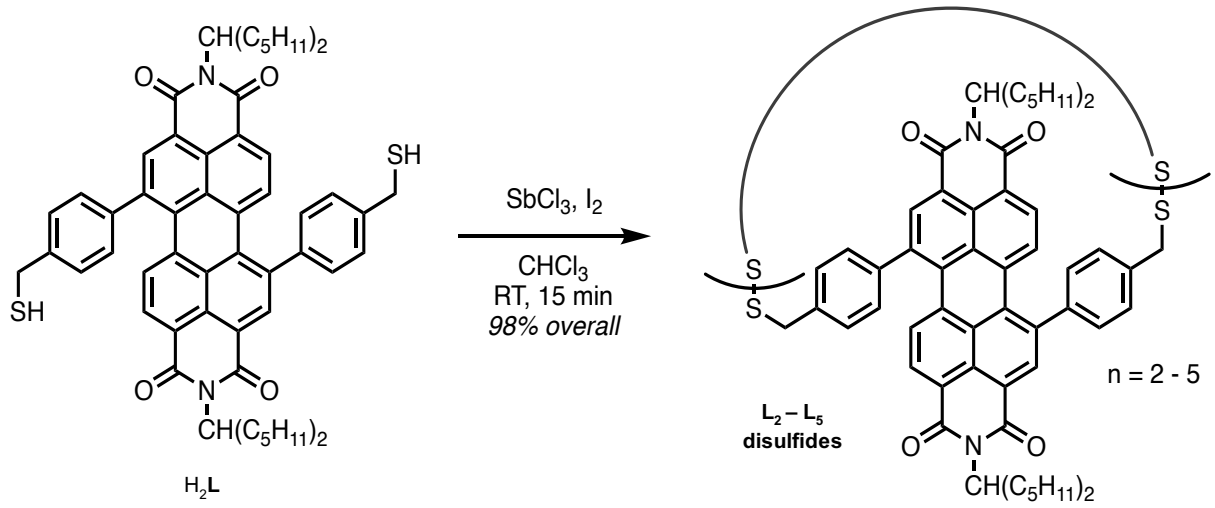

Scheme 3.1. Top: Pnictogen-assisted self-assembly of ditopic and tritopic oligothiols yield quantitative formation of discrete disulfide cyclophanes. Bottom: Self-assembly approach yields almost quantitative formation of PDI-containing macrocycles.

or polymers. Therefore, we thought this method might be particularly well-suited for the formation of macrocycles for organic electronics studies, where discrete macrocycles often show superior properties to their linear congeners[22,23]. For example, previous work has suggested that PDI-containing macrocycles outperform their linear congener as organic photovoltaics due to their enhanced energy alignment and increased efficacy in electron transport[13]. In addition, the synthesis of these self-assembled macrocyclic species can be optimized utilizing Design of Experiments (DOE) to bias individual ensembles by varying starting conditions of the equilibrating reaction mixtures[24]; furthermore, purification is simplified using size-exclusion chromatographic techniques due to the stepwise increase in macrocyclic molecular weight. Finally, the disulfide macrocycles can be sulfur extruded to yield robust sulfide (thioether) bridges in place of the labile disulfide linkages.

Recently, the Nuckolls group has investigated perylene diimide(PDI)-containing macrocycles as key targets in developing alternative n-type organic electronic materials[25,26]. The PDI core has accessible low-lying molecular orbitals, efficient electron transport, and ease of functionality, allowing handles for us to append thiolic linkages for macrocyclization[27–31]. With increased interest in the optoelectronic properties of macrocyclic PDIs, the scaffold was ideal for testing our macrocyclization for facile generation of functional materials. In this work, we utilize a PDI core as a general proof of concept in pnictogen-directed self-assembly for the modular generation of porous organic electronic materials (**Scheme 3.1**).

Results and Discussion

Dynamic Covalent Design Strategy

The PDI core has two primary handles for appending auxiliary groups: (1) the imide nitrogen and (2) the *bay* positions (**Figure 1**). Dynamic covalent reactions have been used in elegant PDI systems from the imide position. For example, the Stoddart group used the thermodynamic imidation reaction to generate molecular triangles from Perylene dianhydride and 1,2-diaminocyclohexane[28]. Moreover, in similar systems, Stefankiewiscz and coworkers generated a dynamic covalent library through disulfide exchange by appending L-cysteine onto the imide position of biphenyl diimide scaffolds[32], whereas Sanders and colleagues used naphthalene diimides to generate elegant catenanes[33,34]; however, for tailoring the PDI scaffold's optoelectronic properties towards specific applications, the bay position has more tunability through additional π overlap of appended aryl subunits. With this in mind, and with recent advances in the preparation of regioselective *bay*-substituted PDI precursors for cross coupling reactions[35], we hypothesized that benzylic thiols could be appended onto the scaffold and undergo self-assembly to readily form functional macrocycles in high yield and fast reaction times. Furthermore, this pathway suggests a simple process towards accessing many other PDI

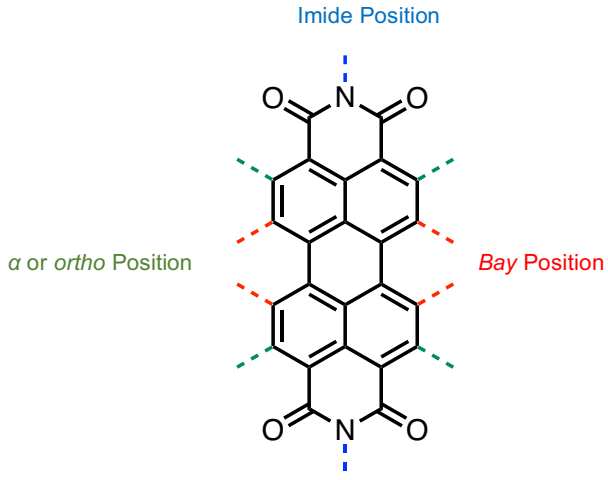

Figure 3.1. Functionalization positions on PDI scaffold.

derivatives by simply changing the aryl cross coupling partner. Additionally, with DOE

optimization or potentially template syntheses, host-guest interactions can be tailored *via* modular molecular porosity contingent on the number/size/shape of building blocks that comprise the macrocycle.

Preparation of PDI-containing Cyclophanes via Pnictogen-directed DCvC

To create a simple pathway towards generating functionalized thiolic building blocks, we sought a simple protected thiol precursor that could be coupled onto a scaffold before self-assembly (**Scheme 3.2**). Towards this goal, Suzuki-Miyaura cross coupling seemed ideal due to the reaction's robustness and stability of boronic ester precursors; moreover, using synthetic pathways that generated an arene-arene bond would increase the efficacy in chaining complementary π systems together for modular materials. Compound **1** was generated from 4-bromomethylphenyl bromide following thiolation, s-tetrahydropyran (THP) protection, and borylation in overall 65% yield on a decagram scale (see Supporting Information). The thiol was protected to prevent oxidation from prolonged storage and prevent palladium chelation during coupling. Compound **1** was subsequently cross coupled to Br-PDI-OTf under typical Suzuki-Miyaura conditions before deprotection to yield H_2**L** in 86% yield. Using our pnictogen-assisted self-assembly pathway, discrete disulfide macrocycles were isolated in overall 98% yield at 6 mM concentration of initial ligand. The macrocycles were purified with gel permeation

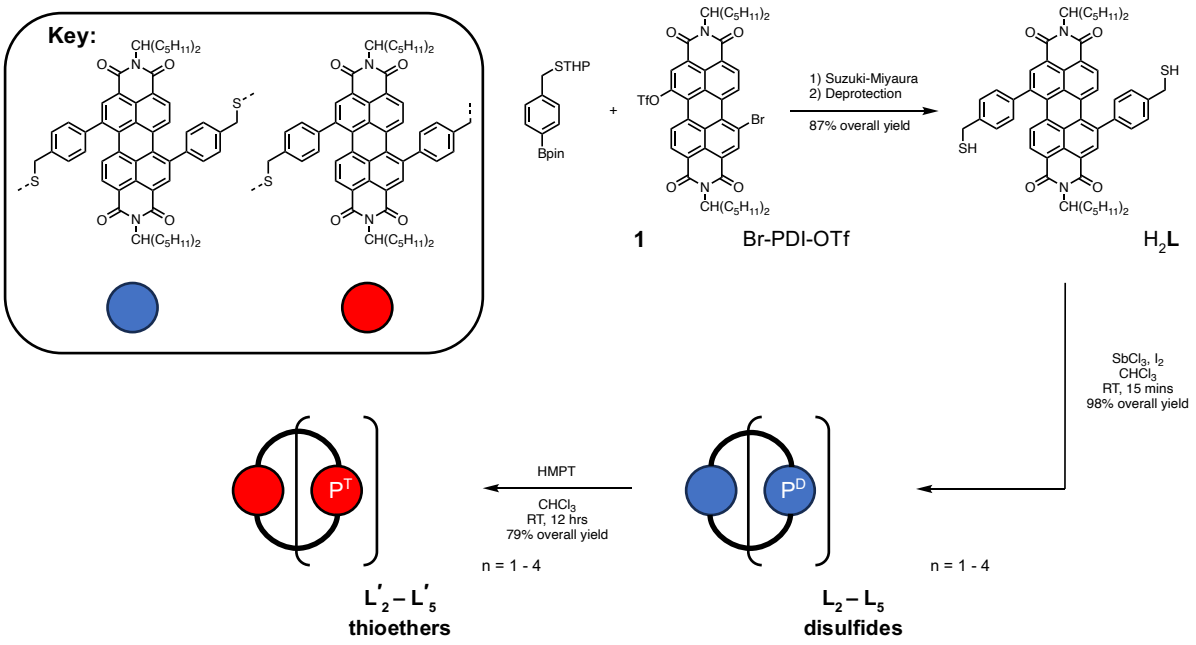

Scheme 3.2. Overview of dynamic synthetic pathway of PDI-containing macrocycles. P^D denotes an aromatic core contained within a disulfide macrocycle, and P^T denotes a thioether bridge.

chromatography (GPC) to yield dimer through pentamer (isolated yields from 200 mg crude material: 31 mg, 16% $\mathbf{L}_2$; 53 mg, 27% $\mathbf{L}_3$; 41 mg, 21% $\mathbf{L}_4$; 39 mg, 20% $\mathbf{L}_5$). High resolution mass spectrometry confirms individual fractions obtained from GPC purification correspond to each stoichiometry of macrocycle, dimer through pentamer, which each also provide distinct NMR spectra (see ESI).

Finally, following self-assembly, the unpurified disulfide ensemble was sulfur extruded to yield sulfide-linked macrocycles in overall 79% yield. The sulfide-linked macrocycles were purified with GPC to yield dimer through pentamer (isolated yields from 100 mg crude material: 13 mg, 13% $\mathbf{L'}_2$; 35 mg, 35% $\mathbf{L'}_3$; 22 mg, 22% $\mathbf{L'}_4$; 19 mg, 19% $\mathbf{L'}_5$). During GPC purification of the disulfide- and sulfide-linked assemblies, macrocycles that diffused into each other were wasted to ensure purify in subsequent characterization; moreover, GPC traces corresponding to hexamer

and septamer were detected but were unable to be isolated due to size exclusion limits of the HPLC columns. The DFT minimized structures, HOMO/LUMO, and ESP maps for $\mathbf{L}_2$ and $\mathbf{L'}_2$ are shown in **Figure 3.2.**

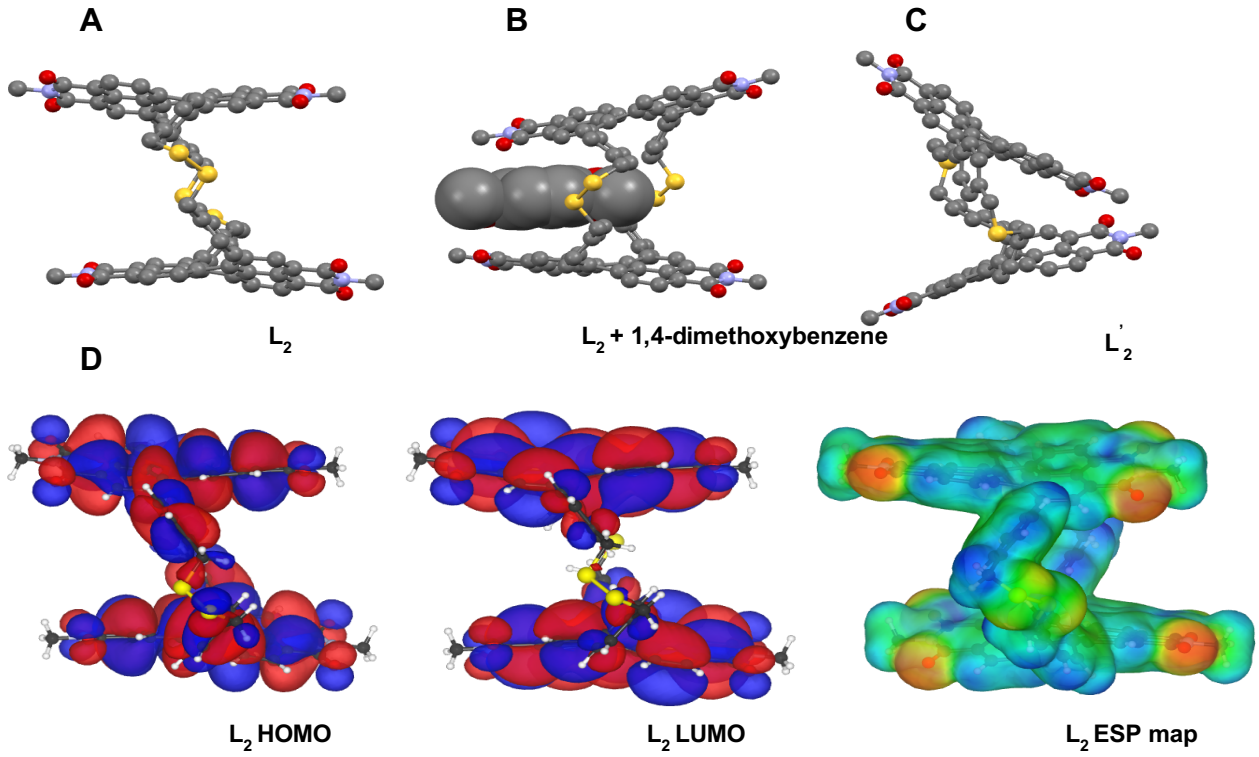

Figure 3.2. DFT energy minimized structures of (A) L_2, (B) L_2 + 1,4-dimethoxybenzene, and (C) L'_2,. (A) – (C) Side-on view of labelled macrocycle. L_2 is suggested to minimize into a cylindrical conformation and adopt a vase conformation upon host-guest interactions. L'_2 minimizes into a vase conformation due to the increased strain of the sulfide tether. (D) Side-on view of L_2 and its calculated HOMO, LUMO, and ESP map. DFT calculations showcase orbital overlap of the pendant aryl π system with the PDI core. Orbitals and electrostatic potential are shown at an isosurface level of 0.005 $e^-/Å^3$.

Absorption and Emission Properties

For insight into the frontier molecular orbitals and electronic properties of the PDI-containing macrocycles, UV-Vis absorption spectroscopy was performed and is summarized in **Figure 3A**. Of note, all macrocycles feature a prominent optical π-π^* transition at 560 nm. The macrocycles have slight bathochromic shifts as the number of building blocks in the system increases, suggesting the optical band gap is slightly affected by the strain of contorting smaller subunits. This trend is most evident in red shifted $\mathbf{L}_2$ with a $\Delta\lambda_{max}$ of 19 nm. The optical band gap (E_g) was

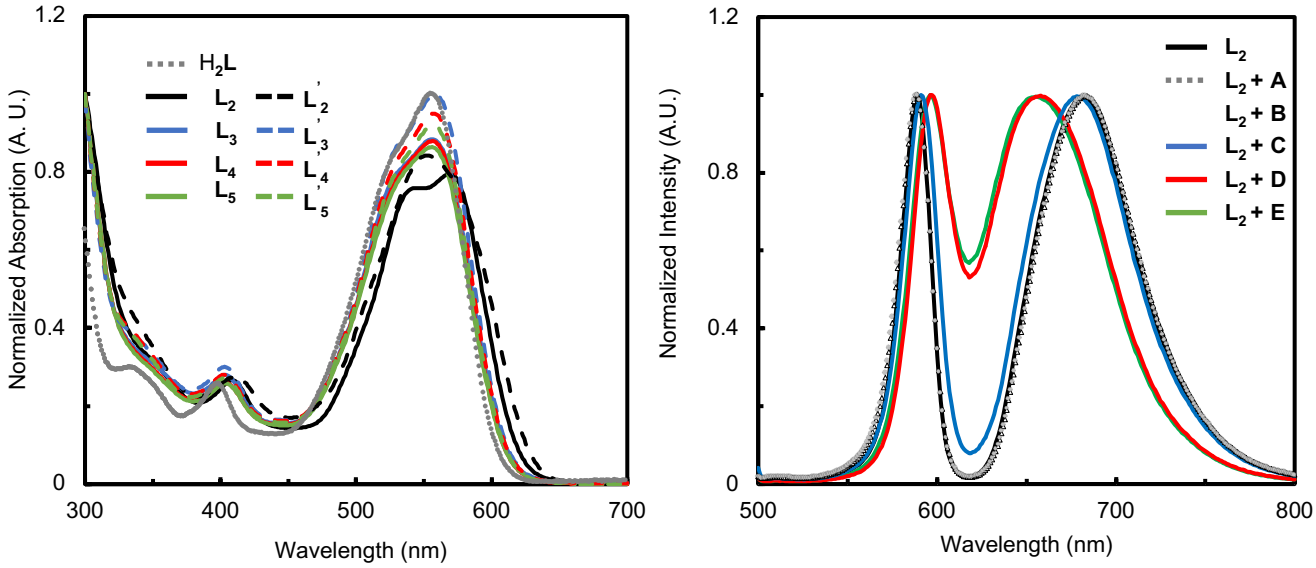

Figure 3.3. (A) UV-Vis absorption spectra of PDI-containing macrocycles. Spectra were recorded in $CHCl_3$ and normalized to the highest intensity. (B) Fluorescence emission spectra of PDI-containing disulfide dimer (L_2) with *p*-xylene (A), 1,3,5-trimethoxybenzene (B), fullerene C60 (C), 1,4-diethoxybenzene (D), and 1,4-dimethoxybenzene (E). Spectra were recorded in $CHCl_3$ and normalized to the highest intensity. Concentrations were normalized to 10 μMol with respect to the PDI species. Samples in fluorescence measurements were excited at λ_{ex} = 495 nm with 5 eq of guest.

estimated via the onset of the longest wavelength transition (λ_{onset})[36].Compounds $\mathbf{L}_3$/$\mathbf{L}'_3$ – $\mathbf{L}_5$/$\mathbf{L}'_5$ were found to have an approximate E_g of 1.98 eV, whereas $\mathbf{L}_2$ and $\mathbf{L}'_2$ were approximated to 1.92 and 1.90 eV, respectfully. All macrocycles showcase tighter band gaps relative to the acyclic analogue ($H_2\mathbf{L}$), which was approximated to be 2.05 E_g and agrees with results reported by Nuckolls and coworkers on a similar PDI scaffold[13]. The proximity of the macrocycles λ_{onset} suggest that the preorganization of macrocyclization is the key factor in increasing organic photovoltaic efficacy with respect to the acyclic building block, with $\mathbf{L}_2$ and $\mathbf{L}'_3$ being the main outliers in optical band gap due to the increased strain inherent in [2,2]-paracyclophane derivatives[37].

Notably, these results suggest our self-assembly pathway could be used to tailor preorganized systems used in host-guest materials without a drastic shift in OPV performance for larger self-assembled systems. During our investigation, we found preliminary evidence of exciplex formation between electron-poor $\mathbf{L}_2$ and electron-rich 1,4-dimethoxybenzene (**Figure 3.4**) with a blue-shifted emission. To probe this interaction further, fluorescence spectroscopy was performed and is summarized in **Figure 3B**. Similar to previously reported work on PDI assemblies, compound $\mathbf{L}_2$ emission showcases sharp and resolved S_0-S_0 relaxations and S_0-S_1 transitions[38–40]. Large PDI aggregates driven through π stacking yield broad and unresolved vibrational-electronic transitions due to overlapping orbital interactions with neighboring aromatic rings; however, when tethered together, intense red-shifted S_0-S_1 transitions are associated with discrete PDI assemblies because of J-type π stacking that can occur from relaxing chromophores distorting with respect to one another. Interestingly, the addition of *p*-dimethylbenzene, *p*-diethylbenzene, and fullerene C60

Figure 3.4. Screening of host-guest interactions of L_2 with aromatic small molecules. a – e are L_2 with 1,4-dimethoxybenzene, 1,3,5-trimethoxybenzene, xylenes, toluene, and benzene. (A) without UV radiation and (B) with UV radiation.

show stabilized/red-shifting of the S_0-S_0 relaxation and destabilized/blue-shifting of the S_0-S_1 transition without affecting emission intensity relative to the free host solution. This information supports exciplex formation with intercalation breaking up J-type π interactions of the PDI cores as evident from the broadening emission spectra of the host-guest systems. For further support, 1,3,5-trimethyoxybenzene was also tested and did not showcase an effect on the fluorescence of $\mathbf{L}_2$. This suggests intercalation is a necessary driving force for exciplex formation and is not driven through peripheral interactions. Current work in our lab is focused on investigating these potential donor-acceptor properties, and DFT studies (**Figure 2B**) suggest that macrocycle $\mathbf{L_2}$ has a suitable cavity for electron-rich, planar guests, such as *para*-substituted benzenes.

Electrochemistry

To probe preliminary electronic characteristics of the PDI macrocycles, $H_2\mathbf{L}$, $\mathbf{L}_2$, and $\mathbf{L'}_2$ were investigated for variations in frontier orbital energies using cyclic voltammetry (CV). Here, we used the onset of the oxidation and reduction peaks as estimates for highest occupied molecular orbital (HOMO) and lowest unoccupied molecular orbital (LUMO) energy levels, respectively (**Figure 3.5**)[41]. These results parallel those reported by the Nuckolls group for related

macrocycles synthesized by stepwise methods, suggesting this self-assembly pathway is a facile method for generating species of this type. Our self-assembled macrocycles have less negative first reduction potentials relative to the thiolic building block; therefore, the LUMO is higher in H_2**L** (-3.46 eV) than $\mathbf{L}_2$ (-3.56 eV) or $\mathbf{L'}_2$ (-3.52 eV) macrocycles. Moreover, as expected in a strained system, the HOMOs of the cyclic analogues are higher in the macrocycles (-5.76 eV and -5.78 eV for $\mathbf{L}_2$ and $\mathbf{L'}_2$, respectfully) compared to untethered H_2**L** (-5.85 eV). Our approximated CV band gaps for H_2**L** (2.39 eV), $\mathbf{L}_2$ (2.20 eV), and $\mathbf{L'}_2$ (2.26 eV) agree with those found from UV-Vis experiments. These preliminary results suggest our macrocycles are better suited for electron transport than the acyclic congener with more closely aligned LUMOs preventing exciton recombination and increasing mobility[42,43].

Conclusion

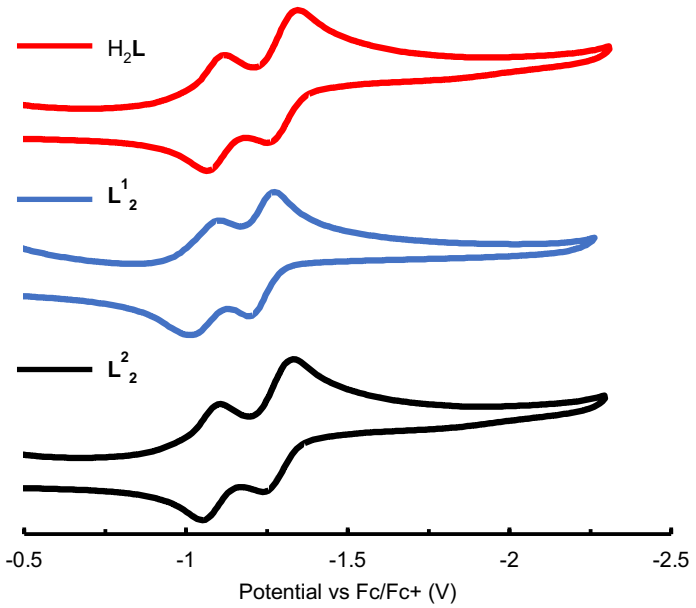

Figure 3.5. Cyclic voltammograms for H_2L, L_2, and L'_2. CVs were run in DCM at 0.1 M with NBu_4PF_6 as the supporting electrolyte and referenced with respect to ferrocene.

In conclusion, we have successfully synthesized novel PDI-containing cyclophanes utilizing pnictogen-directed self-assembly. With this approach, macrocyclization was conducted in an efficient and high yielding sequence that can be biased for the facile formation of novel materials for applied materials chemistry purposes. Our PDI-containing cyclophanes showcase similar optoelectronic properties reported from macrocycles formed utilizing kinetic pathways, and the preorganization gained from self-assembly agrees with other reported work on macrocyclization biasing favorable optical band gaps for electron transport; moreover, our systems showcase potential excited-state tunability for light gathering application with donor-acceptor interactions. The methods of synthesis reported herein are modular, enabling a great diversity of macrocyclic PDIs to be prepared in gram scale, efficient syntheses, which we hope is useful to the organic materials community. Current work in the lab is focused on utilizing this design strategy to tether disparate aryl appendages onto the PDI core before self-assembly to explore new properties in these extended macrocyclic systems and to utilize design of experiments for dynamic synthetic optimization of individual macrocycles.

Bridge to Chapter IV

Chapter III reported the self-assembly of PDI-containing macrocycles for facile pathways into designer organic materials. The dynamic pathway is modular and increases the efficacy in reaching oligothiol precursors required for macrocyclization. After showcasing our pnictogen-direct self-assembly pathway is a fruitful pathway into macrocycles composed of a single building block, I investigated our approaches towards self-sorting. Specifically, in Chapter IV, I examined pnictogen-directed self-sorting design strategies towards asymmetric multicomponent ensemble formation.

Experimental

General Procedures

Unless otherwise stated, reactions were conducted under atmospheric conditions with flame-dried reactions flasks. Flasks were fitted with rubber septa when conducted under ambient conditions; when at elevated temperature, flasks were fitted with a condenser and drying tube with Drierite ($CaSO_4$) as the drying agent. Reaction monitoring by thin layer chromatography (TLC) was performed on Merck TLC silica gel 60 F_{254} (5 x 10 cm) plates. TLC visualization was conducted with visual observation with PDI substrates or under short-wave irradiation from a UV lamp otherwise.

Reagents

All commercially obtained reagents were used as received unless otherwise noted from TCI America. Solvents used were dried over 3 Å molecular sieves and degassed under nitrogen prior to use unless stated otherwise. Br-PDI-OTf and 4-bromobenzylthiol were prepared according to previously reported procedures[44,45].

Purification

Purification and separation of disulfide and thioether products were performed by using Japan Analytical Instruments Inc. LC-9101 recycling preparative high-performance liquid chromatography with gel permeation chromatography columns JAIGEL-1H and JAIGEL-2H with $CHCl_3$ as the eluent. GPC separation was monitored with internal UV-Vis detector UV-4ch 800 LA. Flash Column Chromatography was performed with dry packed Macron Silica Gel 60 (230-

400 Mesh) under 4-6 PSI of nitrogen. Pressure was regulated to maintain 2 inches of mobile phase through the column per minute. Crude reaction mixtures were adsorbed onto celite before column loading. Column separation was monitored with TLC or visual observation with PDI reaction mixtures.

Spectrometry

^{1}H, ^{13}C NMR, and 2D-COSY spectra were recorded with a Bruker AVANCE 500, Bruker AVANCE 600, or Varian INOVA 500. Spectra were referenced using the residual solvent resonances as internal standards and reported in ppm. Data are represented as follows: chemical shift, multiplicity (s = singlet, d = doublet, dd = doublet of doublets, t = triplet, m = multiplet, b = broad).

High-resolution mass spectrometry (HRMS) and low-resolution mass spectrometry (LRMS) data were obtained via Dr. Furong Sun's mass spectroscopy lab at the University of Chicago: Urbana-Champaign with Bruker Autoflex Speed LRF MALDI, Bruker Daltonics UltrafleXtreme MALDI TOFTOF, or Waters GCT Premier EI/CI/FD/FI.

UV-Vis absorption spectra were recorded with an Agilent Technologies Cary 60 UV-Vis spectrometer and Cary WinUV Scan application. Fluorescence emission spectra were recorded with a Horiba Jobin Yvon FluoroMax-4 fluorimeter. All spectra were collected using a 1 cm quartz cuvette with concentrations in the range of 4 μM – 10 μM in $CHCl_3$. IR spectroscopy was performed on Thermo Nicolet 6700 FT-IR spectrometer with diamond ATR attachment. IR data is averaged across 64 scans.

Cyclic Voltammetry

Cyclic voltammetry experiments were performed using a BioLogic potentiostat model SP50. All experiments were conducted under inert dinitrogen gas using standard Schlenk line techniques in a 25 mL three-necked flask equipped with a glassy-carbon electrode (3 mm diameter) as the working electrode, a platinum coil as the auxiliary electrode, and a silver wire as the pseudo-reference electrode. All measurements were performed in a 0.1 M $TBAPF_6$ dichloromethane (DCM) solution. The ferrocene/ferrocenium (Fc/Fc^+) couple was used as an internal standard for each experiment. Potentials were re-referenced to SCE using the value of 0.46 V (*vs*. SCE) for the Fc/Fc^+ in DCM. LUMO and HOMO levels were approximated using $Fc/Fc^+ = -4.8$ eV *vs*. vacuum. Voltammograms were recorded at a sweep rate of 50 $mV \cdot s^{-1}$, at 22 °C. The $E_{½}$ values were calculated assuming $E_{½} \approx E_0' = (E_{anodic} + E_{cathodic})$. Concentrations for **$H_2$L**, **$L_2$,** and **$L_2$'** were 0.42, 0.30, and 0.27 mM respectively.

Synthetic Procedures

4-bromobenzylSTHP

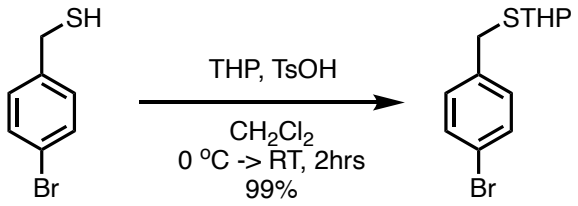

To a stirred 0 °C 250 mL solution of 4-bromobenzylthiol (16.26 g, 80.0 mmol) and dihydropyran (8.08 g, 9 mL, 96.1 mmol) in CH_2Cl_2, TsOH (1.52 g, 8.00 mmol) was added in a single portion and washed in with 50 mL of CH_2Cl_2. The reaction was allowed to stir for 2 hours and warm to room temperature. The reaction was quenched with 2.5 mL of triethylamine and taken to a concentrate under reduced pressure to yield a crude oil. 4-bromobenzylSTHP was purified via

flash column chromatography (isocratic 1:1 CH_2Cl_2/hexanes (v/v)) to yield a clear oil (22.8 g, 79.4 mmol, 99% yield). ^{1}H NMR (500 MHz, $CDCl_3$) δ 7.42 (d, *J* = 8.0 Hz, 2H), 7.19 (d, *J* = 8.1 Hz, 2H), 4.67 (dd, *J* = 6.2, 3.7 Hz, 1H), 4.08 (m, 1H), 3.79 (d, *J* = 13.4 Hz, 1H), 3.64 (d, *J* = 13.5 Hz, 1H), 3.48 (m, 1H), 1.81 (m, 2H), 1.59 (m, 4H). ^{13}C NMR (126 MHz, $CDCl_3$) δ 137.75, 131.59, 130.79, 120.76, 80.48, 64.33, 33.36, 30.81, 25.69, 21.63. HRMS-EI+ [M]+ $C_{12}H_{15}OBrS$ predicted: 286.00270, found: 286.00193.

4-B(pin)benzylSTHP.

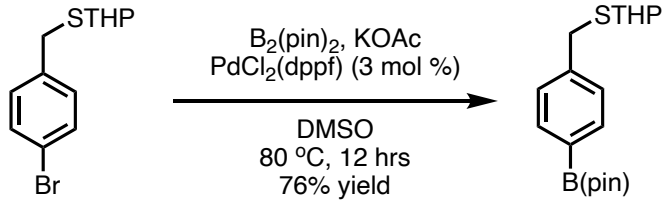

To a stirred vessel of 4-bromobenzylSTHP (14.4 g, 50 mmol), $B_2(pin)_2$ (13.5 g, 53 mmol), and KOAc (14.7 g, 150 mmol), 300 mL of DMSO was added in a single portion. The solution was homogenized and degassed via sonication under vacuum and backfilled with nitrogen. Following completion, $PdCl_2$(dppf) (1.22 g, 1.5 mmol) was added in a single portion under a stream of nitrogen. The solution was heated to 80 °C and monitored via TLC. After 12 hours, the reaction was cooled to room temperature and quenched onto an ice bath (~150 mL). The aqueous suspension was extracted with 3x with pentane (~100 mL each) and the combined organics were dried over magnesium sulfate. The solution was taken to dryness under reduced pressure to yield a pale green oil as a mixture of homocoupled product and borylated product. 4-B(pin)benzylSTHP was purified via flash column chromatography (isocratic 4% EtOAc in hexanes) to yield a white crystalline solid (13.0 g, 39 mmol, 78% yield). ^{1}H NMR (500 MHz, Chloroform-*d*) δ 7.75 (d, *J* = 7.6 Hz, 2H), 7.32 (d, *J* = 7.7 Hz, 2H), 4.65 (dd, *J* = 6.5, 3.3 Hz, 1H), 4.09 (m, 1H), 3.85 (d, *J* =

13.3 Hz, 1H), 3.70 (d, J = 13.3 Hz, 1H), 3.48 (m, 1H), 1.79 (m, 2H), 1.67 – 1.44 (m, 4H), 1.33 (s, 12H). ^{13}C NMR (126 MHz, $CDCl_3$) δ 141.91, 135.00, 128.47, 83.82, 80.42, 64.49, 53.54, 34.00, 30.87, 25.70, 24.95, 24.93, 21.75. HRMS-EI+ [M+H]+ [$C_{18}H_{28}O_3SB$]+ predicted: 335.1852, found: 335.1848.

SI-1.

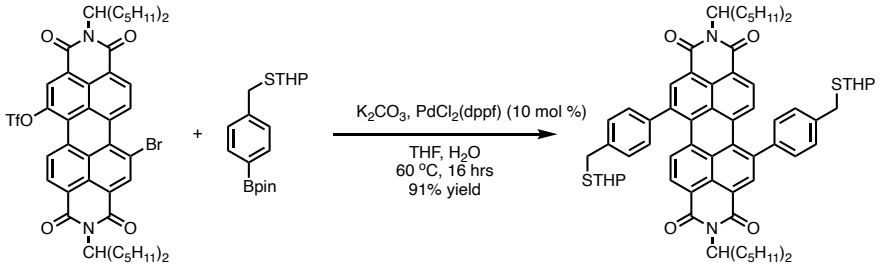

SI-1

Br-PDI-OTf (1.165 g, 1.26 mmol), 4-B(pin)benzylSTHP (1.26 g, 3.78 mmol), K_2CO_3 (4.14 g, 30 mmol), THF (35 mL), and water (7 mL) was added to a vessel equipped with a stir bar. The reaction flask was capped and sparged with nitrogen for 20 minutes. While under nitrogen, $PdCl_2$(dppf) (106 mg, 0.13 mmol) was added in a single portion. The reaction flask was sparged for 10 additional minutes. The reaction flask was heated at reflux for 16 hours. After the allotted time, the THF was removed under reduced pressure and the organics were extracted with $CHCl_3$ (~100 mL). The extract was washed 1x with water (~50 mL) and 2x with sat. sodium bicarbonate solution (~50 mL each). The organics were then washed with brine, dried over magnesium sulfate, and filtered. The organics were taken to dryness under reduced pressure to yield a purple solid. **SI-1** was purified with flash column chromatography (gradient 1:1 CH_2Cl_2/Hexanes -> 1% EtOAc in CH_2Cl_2) to yield a violet crystalline powder (1.272 g, 91% yield). ^{1}H NMR (500 MHz, $CDCl_3$) δ 8.61 (d, J = 16.1 Hz, 2H), 8.10 (d, J = 18.1 Hz, 2H), 7.84 (d, J = 8.1 Hz, 2H), 7.57 – 7.43 (m, 8H),

5.17 (d, *J* = 19.2 Hz, 2H), 4.79 (m, 2H), 4.14 (m, 2H), 3.96 (d, *J* = 13.3 Hz, 2H), 3.82 (d, *J* = 13.2 Hz, 2H), 3.53 (m, 2H), 2.22 (m, 4H), 1.99 – 1.52 (m, 22H), 1.33 – 1.20 (m, 28H). ^{13}C NMR (126 MHz, $CDCl_3$) δ 140.90, 139.49, 135.08, 132.65, 130.95, 130.26, 129.42, 129.30, 128.53, 128.06, 80.88, 64.56, 54.79, 33.89, 32.47, 31.90, 31.02, 26.73, 25.80, 22.70, 21.80. HRMS-MALDI- $[C_{70}H_{82}N_2O_6S_2]^-$ predicted: 1,110.5609, found: 1,110.5595.

H_2L.

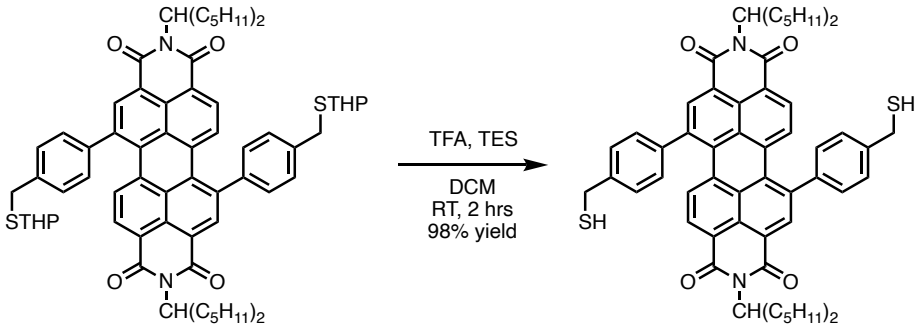

To a 120 mL degassed solution of **SI-1** (1.11 g, 1 mmol) and triethylsilane (2.3 g, 20 mmol) in CH_2Cl_2, 18 mL of degassed TFA was added in a single portion. After 2 hours, the reaction was taken to a concentrate under reduced pressure and triturated with methanol to yield H_2**L** as a purple crystalline powder (924 mg, 98%). ^{1}H NMR (500 MHz, $CDCl_3$) δ 8.67 – 8.55 (m, 2H), 8.12 (d, *J* = 18.6 Hz, 2H), 7.84 (d, *J* = 8.2 Hz, 2H), 7.57 – 7.44 (m, 8H), 5.17 (m, 2H), 3.86 (d, *J* = 7.7 Hz, 4H), 2.22 (m, 4H), 1.88 (t, *J* = 7.7 Hz, 2H), 1.83 (d, *J* = 6.2 Hz, 4H), 1.35 – 1.18 (m, 28H), 0.83 (t, *J* = 6.5 Hz, 12H). ^{13}C NMR (126 MHz, $CDCl_3$) δ 164.80, 164.09, 142.01, 141.09, 140.79, 136.11, 135.44, 134.94, 132.65, 130.67, 130.01, 129.55, 129.40, 129.02, 128.07, 32.47, 31.90, 28.82, 26.73, 22.70, 12.38, 8.30. HRMS-MALDI- $[C_{60}H_{66}N_2O_4S_2]^-$ predicted: 942.4459, found: 942.4479. λ_{max} = 553 nm. ν_{max}/cm^{-1} 2953, 2916 and 2857 (C_{aryl}-H), 2555br (S-H), 1695, 1656 and 1589 (C=O), 1322 (C-N), 813 (C-S).

PDI Disulfides L_2 – L_5.

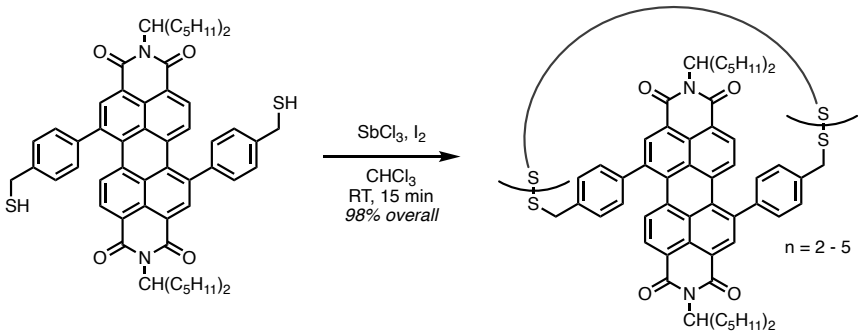

To a 25 mL solution of H_2**L** (283 mg, 0.3 mmol) and $SbCl_3$ (137 mg, 0.6 mmol), a 25 mL solution of I_2 (228 mg, 0.9 mmol) in $CHCl_3$ was added slowly (~5 mL per minute) with an addition funnel. After 15 minutes, the solution was washed with sat. sodium sulfite solution (~50 mL), 2x with water (~50 mL each), and brine (~50 mL). The organic layer was separated, and the aqueous layers were combined and extracted 3x with $CHCl_3$ (~50 mL each). The combined organics were dried over magnesium sulfate, filtered, and taken to dryness under reduced pressure to yield crude disulfide macrocycles as a purple waxy solid (277 mg, 98% overall). 200 mg of the macrocycle was dissolved in 10 mL of $CHCl_3$ purified with GPC to yield dimer through pentamer PDI macrocycle (**L**$_2$: 31 mg, 16%, **L**$_3$: 53 mg, 27%, **L**$_4$: 41 mg, 21%, **L**$_5$: 39 mg, 20%).

L$_2$: H NMR (500 MHz, $CDCl_3$) δ 8.68 – 8.37 (m, 4H), 8.08 (m, J = 18.5 Hz, 4H), 7.92 – 7.81 (m, 4H), 7.85 – 6.51 (b, 16H), 5.06 (m, 4H), 3.75 (m, 8H), 2.33 – 1.65 (m, 18H), 1.28 – 1.09 (m, 48H), 0.78 (m, 24H). ^{13}C NMR (126 MHz, $CDCl_3$) δ 164.43, 163.80, 140.99, 140.41, 137.24, 134.74, 132.66, 131.76, 131.15, 130.33, 130.15, 129.39, 127.75, 123.85, 123.40, 54.68, 42.29, 32.29, 29.84, 26.62, 22.58, 14.15.. LRMS-MALDI- $[C_{120}H_{128}N_4O_8S_4]^-$ predicted: 1880.86, found:

1880.601. λ_{max} = 544, 572 nm. ν_{max}/cm^{-1} 3018, 2958, 2859 and 2801 (C_{aryl}-H), 1693, 1653 and 1584 (C=O), 1214 (C-N), 751 (C-S).

L$_3$: H NMR (500 MHz, $CDCl_3$) δ 8.54 (m, 6H), 8.14 – 7.98 (m, 5H), 7.82 (m, 6H), 7.59 – 7.32 (m, 24H), 5.22 – 5.00 (m, 6H), 3.83 (m, 12H), 2.24 – 1.97 (m, 12H), 1.83 – 1.69 (m, 12H), 1.40 – 0.94 (m, 82H), 0.83 – 0.64 (m, 36H).^{13}C NMR (126 MHz, $CDCl_3$) δ 164.68, 163.55, 141.57, 140.60, 138.24, 135.86, 134.82, 132.54, 131.33, 130.26, 129.32, 128.04, 122.74, 122.03, 121.52, 119.90, 54.64, 42.97, 32.35, 31.77, 26.61, 22.67, 14.09. LRMS-MALDI- $[C_{180}H_{191}N_6O_{12}S_6]^-$ predicted: 2820.29, found: 2820.257. λ_{max} = 558 nm. ν_{max}/cm^{-1} 3013, 2956, 2924 and 2858 (C_{aryl}-H), 1693, 1652 and 1586 (C=O), 1430 and 1301 (C-N), 812 and 745 (C-S).

L$_4$: H NMR (500 MHz, $CDCl_3$) δ 8.58 (m, 8H), 8.19 – 7.95 (m, 8H), 7.95 – 7.71 (m, 8H), 7.74 – 7.26 (m, 32H), 5.27 – 4.96 (m, 8H), 3.88 (m, 12H), 2.32 – 2.03 (m, 16H), 1.80 (m, 16H), 1.46 – 0.97 (m, 96H), 0.87 – 0.63 (m, 48H). ^{13}C NMR (126 MHz, $CDCl_3$) δ 164.88, 163.60, 141.63, 140.64, 138.23, 138.04, 134.61, 134.29, 132.59, 131.37, 130.35, 129.46, 128.08, 123.12, 122.24, 119.25, 54.72, 43.16, 32.37, 31.80, 26.71, 26.64, 22.61, 14.11. LRMS-MALDI+ $[C_{240}H_{256}N_8O_{16}S_8Na]$ predicted: 3784.71, found: 3783.753. λ_{max} = 558 nm.

L$_5$: ^{1}H NMR (500 MHz, Chloroform-*d*) δ 8.75 – 8.54 (m, 10H), 8.06 (m, 10H), 7.97 – 7.76 (m, 10H), 7.69 – 7.34 (m, 40H), 5.10 (m, 10H), 3.88 (m, 18H), 2.28 – 2.04 (m, 20H), 1.82 (s, 20H), 1.20 (m, 120H), 0.77 (m, 60H). ^{13}C NMR (126 MHz, $CDCl_3$) δ 164.50, 163.85, 141.65, 140.69, 138.23, 135.70, 135.00, 133.52, 133.18, 131.39, 130.42, 129.50, 128.10, 123.37, 122.95, 54.74, 43.05, 32.41, 31.86, 26.70, 22.67, 14.15.LRMS-MALDI- $[C_{300}H_{320}N_{10}O_{20}S_{10}]^-$ predicted: 4702.15, found: 4702.5. λ_{max} = 558 nm.

PDI Thioether Macrocycles L'$_2$ – L'$_5$.

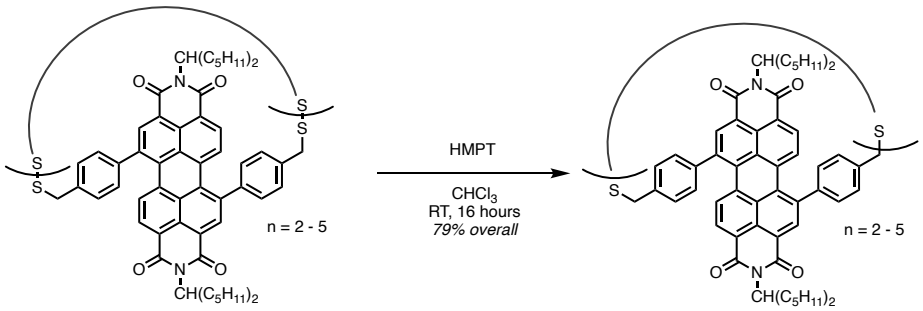

To a degassed 50 mL solution of PDI disulfide macrocycles (237 mg, 126 μmol) in $CHCl_3$, degassed HMPT (82 mg, 504 μmol) was added in a single portion. The solution was stirred overnight (~16 hours) and taken to a concentrate under reduced pressure. The products were isolated via vacuum filtration following trituration with methanol to yield crude thioether macrocycles (182 mg, 79% overall yield). 100 mg of thioether macrocycle was dissolved in 10 mL of $CHCl_3$ and purified with GPC to yield dimer – pentamer thioether PDI macrocycles (**L**'$_2$: 13 mg, 13%, **L**'$_3$: 35 mg, 35 %, **L**'$_4$: 22 mg, 22%, **L**'$_5$: 19 mg, 19%). Mass spectrometry studies on the larger tetramer and pentamer thioether macrocycles were unsuccessful due to fragmentation to PDI monomers, but the GPC traces and NMR spectra are consistent with their formation from the corresponding disulfides. Broadening in the NMR is likely due to slow conformational effects within these larger systems.

L'$_2$: ^{1}H NMR (500 MHz, $CDCl_3$) δ 8.66 (m, 4H), 8.52 – 6.71 (m, 24H), 5.17 (s, 2H), 5.14 – 2.59 (b, 4H), 2.39 – 2.09 (m, 6H), 1.84 (m, 12H), 1.40 – 1.19 (m, 48H), 0.92 – 0.72 (m, 24H). HRMS-MALDI- $[C_{120}H_{128}N_4O_8S_2]^-$ predicted: 1816.9168, found: 1816.9146. λ_{max} = 552 nm. ν_{max}/cm^{-1} 2986, 2961 and 2901 (C_{aryl}-H), 1692, 1650 and 1543 (C=O), 1323 (C-N), 813, 738, and 556 (C-S).

L'$_3$: ^{1}H NMR (500 MHz, $CDCl_3$) δ 8.63 (m, 6H), 8.37 – 7.29 (m, 36H), 5.14 (m, 6H), 5.02 – 2.61 (b, 12H), 2.32 – 2.10 (m, 12H), 1.91 – 1.74 (m, 12H), 1.38 – 1.14 (m, 72H), 0.90 – 0.70 (m, 36H). ^{13}C NMR (126 MHz, $CDCl_3$) δ 164.59, 163.49, 141.18, 140.41, 134.29, 132.51, 131.42, 130.91, 130.73, 130.03, 129.27, 128.20, 127.98, 127.85, 123.32, 122.72, 54.76, 32.30, 32.23, 31.66, 26.58, 26.50, 22.56, 14.05. HRMS-MALDI- $[C_{180}H_{192}N_6O_{12}S_3]^-$ predicted: 2,725.3755, found: 2,725.3863. λ_{max} = 560 nm. ν_{max}/cm^{-1} 2939, 2913 and 2850 (C_{aryl}-H), 1686, 1641 and 1573 (C=O), 1429 and 1301 (C-N), 805, 770 and 553 (C-S).

L'$_4$: ^{1}H NMR (500 MHz, $CDCl_3$) δ 8.68 (m, 8H), 8.29 – 7.45 (m, 48H), 5.17 (m, 8H), 4.93 – 2.47 (b, 12H), 2.24 (m, 12H), 1.84 (m, 20H), 1.47 – 1.17 (m, 96H), 0.97 – 0.62 (m, 48H). ^{13}C NMR (126 MHz, $CDCl_3$) δ 164.70, 162.73, 137.43, 135.74, 134.23, 131.42, 130.38, 130.01, 129.31, 128.94, 127.99, 124.10, 123.27, 120.61, 105.33, 54.76, 35.98, 32.30, 31.74, 29.71, 26.58, 22.56, 14.04. λ_{max} = 558 nm.

L'$_5$: ^{1}H NMR (500 MHz, $CDCl_3$) δ 8.67 (m, 10H), 8.52 – 7.31 (m, 59H), 5.17 (s, 10H), 5.07 – 2.40 (b, 20H), 2.28 – 2.20 (m, 14H), 1.85 (m, 26H), 1.37 – 1.21 (m, 119H), 0.85 (dd, *J* = 15.9, 9.2 Hz, 61H). ^{13}C NMR (126 MHz, $CDCl_3$) δ 164.54, 160.60, 144.63, 140.78, 140.06, 139.44, 131.44, 130.01, 129.28, 128.20, 127.96, 123.91, 123.52, 121.68, 100.00, 54.77, 32.30, 31.73, 29.72, 26.58, 22.56, 14.04. λ_{max} = 557 nm.

Supplemental Characterization Data

For additional information pertaining towards the NMR, Mass spectrometry, IR spectroscopy, or HPLC traces, see the Appendix A.

Density Functional Theory (DFT) Calculations

All quantum chemical calculations were performed with Gaussian 09 (See Gaussian 09, Revision ***A.1***, M. J. Frisch, G. W. Trucks, H. B. Schlegel, G. E. Scuseria, M. A. Robb, J. R. Cheeseman, G. Scalmani, V. Barone, B. Mennucci, G. A. Petersson, H. Nakatsuji, M. Caricato, X. Li, H. P. Hratchian, A. F. Izmaylov, J. Bloino, G. Zheng, J. L. Sonnenberg, M. Hada, M. Ehara, K. Toyota, R. Fukuda, J. Hasegawa, M. Ishida, T. Nakajima, Y. Honda, O. Kitao, H. Nakai, T. Vreven, J. A. Montgomery, Jr., J. E. Peralta, F. Ogliaro, M. Bearpark, J. J. Heyd, E. Brothers, K. N. Kudin, V. N. Staroverov, R. Kobayashi, J. Normand, K. Raghavachari, A. Rendell, J. C. Burant, S. S. Iyengar, J. Tomasi, M. Cossi, N. Rega, J. M. Millam, M. Klene, J. E. Knox, J. B. Cross, V. Bakken, C. Adamo, J. Jaramillo, R. Gomperts, R. E. Stratmann, O. Yazyev, A. J. Austin, R. Cammi, C. Pomelli, J. W. Ochterski, R. L. Martin, K. Morokuma, V. G. Zakrzewski, G. A. Voth, P. Salvador, J. J. Dannenberg, S. Dapprich, A. D. Daniels, O. Farkas, J. B. Foresman, J. V. Ortiz, J. Cioslowski, and D. J. Fox, Gaussian, Inc., Wallingford CT, 2009.) on *Talapas* HPC clusters at the University of Oregon. All geometries were optimized using wB97x functional and cc-pVDZ basis set. Undecane on imides were replaced with methyl groups to reduce computational run time. ESP and HOMO/LUMO images were made with Cubegen function in Gaussian.

For cartesian coordinates of the PDI models, please see Appendix B.

CHAPTER IV

USING STERIC GEARING IN DISPARATE OLIGOTHIOLS TO DRIVE SORTING IN SELF-ASSEMBLED CYCLOPHANES

Contributions

This chapter discusses investigations into pnictogen-assisted self-sorting for preorganized multicomponent ensembles. This chapter is a manuscript in preparation for *Angewandte Chemie International Edition*. I prepared the entire manuscript and performed most experimental contributions and analysis. Prof. Darren. W. Johnson provided intellectual input and editorial feedback. Dr. Lev. N. Zakharov resolved all X-ray crystallography experiments. Willow A. Davis, Luka J. Zocchi, and Henry J. Trubenstein assisted with oligothiol preparation and crystal growing.

Abstract

Herein, we report the synthesis of small organic cages with oligothiols using pnictogen-assisted self-sorting. By including antimony trichloride, benzylic di- and tritopic thiol-containing ligands yield disulfides as social cages or narcissistic macrocycles in overall quantitative yield via dynamic covalent chemistry. With the inclusion of peripheral methyl substituents, social self-sorting is biased over narcissistic self-sorting. Using steric gearing, the pnictogen-assisted self-sorting pathway enables social A_2B_2 and A_2B_3 cage formation (A = trithiol; B = dithiol). These results suggest that subtle steric interactions can augment complex self-assembly pathways followed in DCvC.

Introduction

The organization of chemical building blocks through molecular self-assembly, guided by weak and reversible interactions, has emerged as an effective strategy in fabricating desirable nanostructures[1–21]. Moreover, incorporating dynamic covalent chemistry (DCvC) into self-assembly methodologies has further empowered the generation of complex covalently bound supramolecular architectures, augmenting the stability and tunability of these ensembles[22–31]. Despite its unparalleled ability to produce symmetric molecular aggregates, self-assembly can encounter challenges in generating multicomponent and/unsymmetrical systems. To overcome this limitation, the concept of 'self-sorting' has been explored, enabling the selective assembly of complementary building blocks to yield intricate multicomponent ensembles[32–34]. Self-sorting operates through the chemical components' ability to *self-discriminate* and construct heteromeric (social self-sorting) assemblies or *self-associate* and construct homomeric (narcissistic self-sorting) assemblies. Steric effects have been investigated in self-sorting events related to noncovalent or reversible interactions[35–38]; however, steric gearing has been overlooked in dynamic covalent small molecule design. Specifically, steric gearing is only reported in augmenting intra- and intermolecular interactions of synthetic oligopeptides for preorganizing macromolecular ensembles [39–41].

Using dynamic disulfide bonds and an additive, we have shown that thermodynamic distributions of oligothiols into cyclic disulfide macrocycles are favored over linear disulfide polymers/oligomers which are presumably preferred kinetically (Scheme 1, top). This process is done by mildly oxidizing thiol substrates in the presence of a thiophilic Lewis acid (Sb^{3+}, As^{3+}, or Cu^{2+})[42–44]; moreover, we have also demonstrated that product distribution can be influenced by tuning its environmental parameters and optimized using nonlinear regression methods with Design of Experiments[45]. In a previous study, we reported the successful formation of asymmetric

disulfide-, sulfide-, and methylene-linked macrocycles achieved through pnictogen-directed self-sorting of linear benzylic dithiols[46]. Building on these results, our objective in this investigation was to explore alternative pnictogen-directed disulfide self-sorting strategies for the targeted synthesis of organic cages. Specifically, we targeted self-association in disparate oligothiols exhibiting C_2- and C_3-symmetry and probed subtle steric effects on the resulting self-sorting. Here, we aimed to expand the range of accessible discrete organic cages through DCvC as an alternative to traditional stepwise methods (**Scheme 4.1**). In addition, this work would yield further insight into guided small molecule design strategies for the supramolecular community. Herein, we report the assembly of disulphide-linked organic cages through self-sorting and provide insight into steric gearing towards their selective formation.

Results and Discussion

By combining both two-fold and three-fold symmetric di- and tri-thiols, this approach might also showcase the utility of self-sorting coupled DCvC to yield heteromeric cages comprising each ligand if the factors controlling narcissistic or social self-sorting could be controlled. Such unsymmetrical cages would be quite difficult to synthesize with traditional stepwise chemistry. To begin this investigation, we first attempted self-sorting of biphenyl-bridged and benzene-spaced oligothiols **A** and **B**, respectfully (**Scheme 4.2**). These ligands were ideal candidates because their (homomeric) self-assembly was well

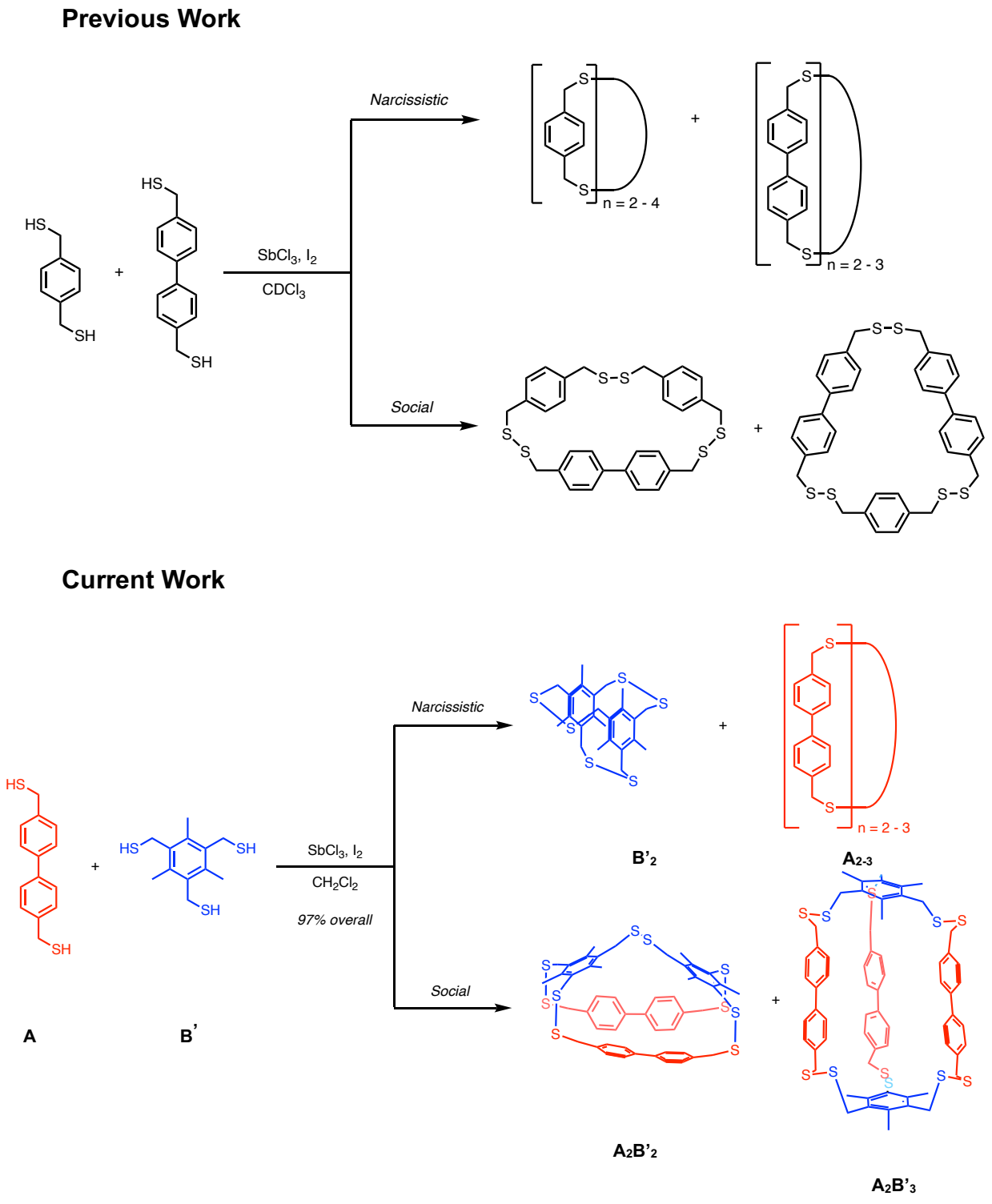

Scheme 4.1. Pnictogen-directed self-sorting of oligothiols. (Top) Previous work on C_2-symmetric scaffolds in the formation of asymmetric macrocycles; (bottom) Current work combining C_2- and C_3-symmetric scaffolds for organic cage formation.

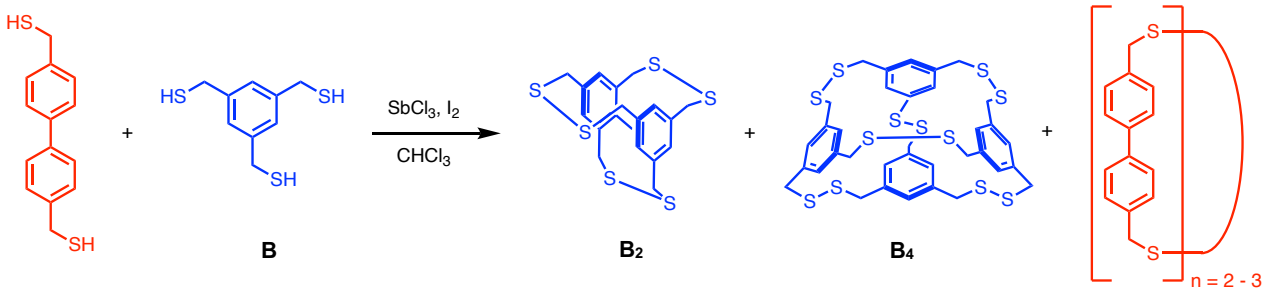

Scheme 4.2. Self-sorting of phenyl- and biphenyl-spaced oligothiols **A** and **B** yield only narcissistic products.

characterized previously in our group as individual building blocks, and social self-sorting would lead to heteromeric, unsymmetrical products. To our surprise, the building blocks showcased complete self-association, forming only discrete narcissistic products $\mathbf{A_{2\text{-}3}}$, $\mathbf{B_2}$, and $\mathbf{B_4}$. As statistical self-sorting would lead to 40% social product formation in a 1:1 mixture, there was an unknown thermodynamic bias precluding heteromeric association. This result suggested two theories that we could explore: (1) pnictogen-directed self-sorting of oligothiols favors higher symmetry/homomeric product formation, or (2) social species have a higher entropic cost than previously anticipated, leading to favored narcissistic product formation.

Following these results, we explored alternative building blocks for self-sorting feasibility. Here, **B'**, a mesitylene-spaced scaffold, was tried as an alternative for the C_3 building block as we believed the bulkier methyl groups could be used to disfavor narcissistic self-sorting. The self-assembly of **B'** alone was found to form only discrete disulfide dimer $\mathbf{B'_2}$ in 13% yield. Compared to ligand **B**, this building block was not found to form a tetrahedral ensemble during self-assembly, and disulfide polymer was observed as the dominant product from the reaction. The dimer was crystallized with vapour diffusion of hexanes into chloroform. Disulfide dimer $\mathbf{B'_2}$ was found to have average disulfide dihedral angles of 109°, deviating significantly from the typical 90° found in unstrained disulfides (**Figure 4.1**); moreover, the pendant methylene groups on the mesitylene

core feature significant steric strain as observed from the 7° average deviation from planarity of the methyl groups with respect to the aromatic plane. This solid-state evidence is corroborated with solution-state evidence as two symmetrically inequivalent **B'$_2$** conformations are observed with slow rotation on the NMR timescale (see ESI), one possessing three-fold symmetry and the other lacking the C_3 axis. These results suggest the bulkier mesitylene scaffold resists self-recognition to lower the enthalpic energy of the disulfide system.

With evidence suggesting we had inhibited narcissistic self-assembly using this approach with **A** and **B**, the ligands **A** and **B'** were subjected to pnictogen-directed self-sorting in a 1:1 ratio. Here, nonintegrative self-sorting is observed with the formation of **A$_2$** (25% isolated yield), **A$_3$**

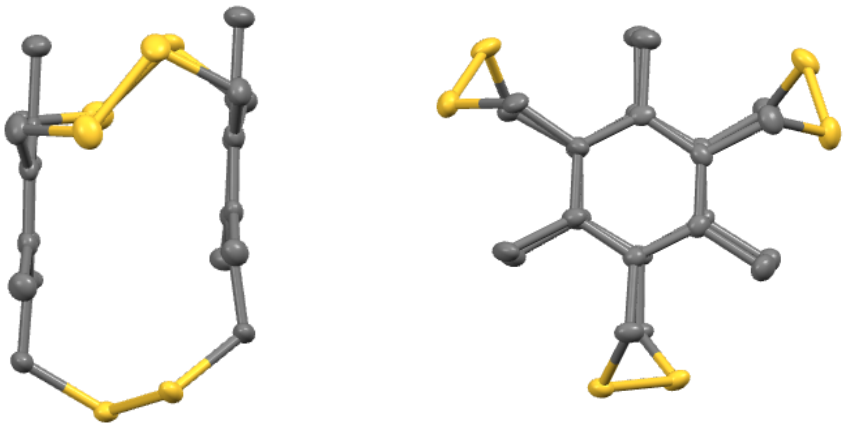

Figure 4.1. Crystal structure of B'$_2$ from side-on (left) and front (right) perspectives.

(13% isolated yield), **A$_2$B'$_2$** (22% isolated yield), **A$_2$B'$_3$** (18% isolated yield), and **B'$_2$** (15% isolated yield) disulfide macrocycles and cages (93% overall yield of discrete products). **A$_2$B'$_2$** was recrystallized by slow diffusion of n-hexane into chloroform to yield crystals suitable for x-ray diffraction (**Figure 4.2**). In the solid state, **A$_2$B'$_2$** is found to have dihedral disulfide angles of 86° and suggests the heteromeric assembly results in less steric strain relative to the homomeric **B'$_2$**. Interestingly, the sterically encumbered **B'$_2$** was formed in higher yield during self-sorting than by

performing self-assembly with only **B'**, with a 230% increase in product formation relative to the initial concentration of **B'**. With these results, we hypothesized that steric gearing of the mesitylene scaffold was biasing the formation of social self-sorted products to minimize repulsive interactions in the system; moreover, we believed the favorable **A**/**B'** equilibrium was preventing **B'** from polymerization, augmenting an increase in narcissistic **B'$_2$** formation.

To further explore this steric bias, oligothiol **A'** was synthesized as an additional C_2-symmetric scaffold to query the observed steric gearing bias in self-sorting (**Figure 3a**). Here, ^{1}H NMR experiments were conducted to probe their self-recognition and self-discriminating tendencies (**Figure 3b**). Remarkably, NMR experiments suggested the building blocks exhibit

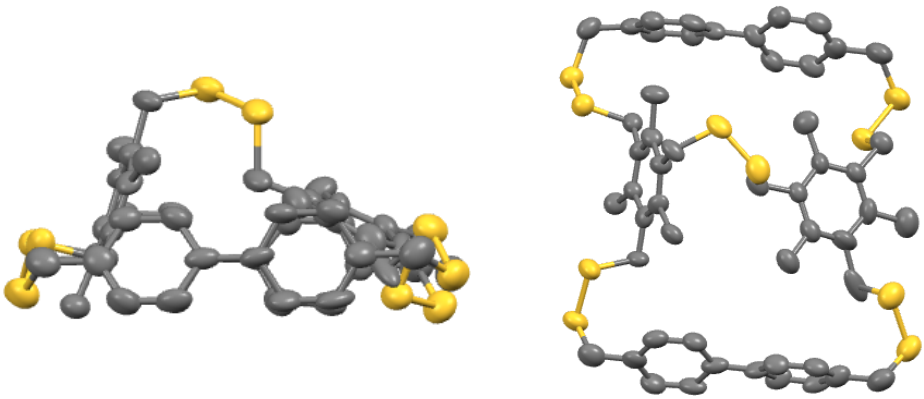

Figure 4.2. Crystal Structure of $A_2B'_2$ from side-on (left) and top-down (right) perspectives.

complete self-discrimination, forming *only* social products – no evidence of the homomeric/narcissistic sorted products was observed.

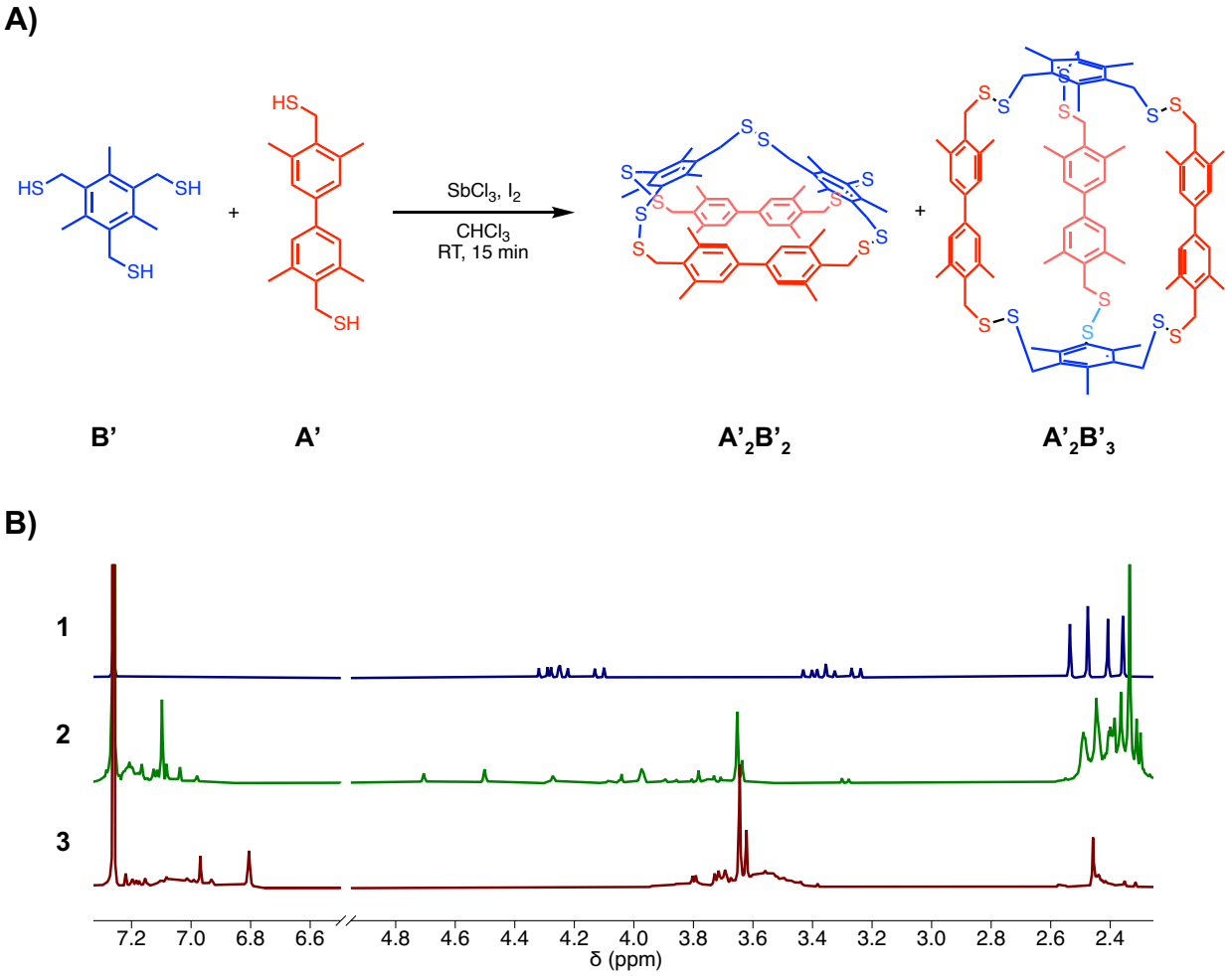

Figure 4.3. (**A**) Self-sorting of **A'** and **B'** yields only social products. (**B**) NMRs of self-assemblies **B'** (**1**), **A'** (**2**), and self-sorting of equimolar **A'** + **B'** (**3**). Self-sorting does not exhibit narcissistic B'$_2$ formation with exclusion of its characteristic methylene and tolyl protons.

To further probe this observation, the self-sorted products were separated with size exclusion chromatography to yield 3 major products **A'$_2$B'**, **A'$_2$B'$_2$**, and **A'$_2$B'$_3$**, with minor formation of **A'$_2$**

and **A'$_3$**. Most notable, **B'$_2$** was not observed during the reaction and suggests the building blocks were augmented to form social products to avoid the steric penalty in its formation (i.e., less strained heteromeric products form instead). Current work in the lab is focused on growing crystals of social and narcissistic **A'** products to compare their solid-state disulfide dihedral angle. This information will solidify the steric gearing argument and is necessary for publication.

Conclusion

In conclusion, utilizing simple oligothiols, we have showcased steric gearing is a subtle yet powerful directing force in the self-discrimination of self-sorting building blocks; furthermore, we believe this insight can be useful to the supramolecular community in designing novel ensembles with engineered building blocks.

Bridge to Chapter V

Chapter IV showcases pnictogen-assisted self-sorting can be biased towards social self-sorting *via* steric gearing. Through subtle changes of the oligiothiol substrates, self-recognition and self-discrimination is observed to be biased during the self-sorting event. Chapter V provides concluding remarks to this dissertation and yields insight into future directions for this project.

Experimental

General Considerations

Unless otherwise stated, reactions were conducted under atmospheric conditions with flame-dried reactions flasks. Flasks were fitted with rubber septa when conducted under ambient conditions; when at elevated temperature, flasks were fitted with a condenser and drying tube with

Drierite ($CaSO_4$) as the drying agent. Reaction monitoring by thin layer chromatography (TLC) was performed on Merck TLC silica gel 60 F_{254} (5 x 10 cm) plates. TLC visualization was conducted under short-wave irradiation from a UV lamp otherwise.

Reagents

All commercially obtained reagents were used as received unless otherwise noted from TCI America. Solvents used were dried over 3 Å molecular sieves and degassed under nitrogen prior to use unless stated otherwise. 4,4'-bis(methylmercaptan)biphenyl, 1,4-bis(bromomethyl)-2,3,4,5-tetramethylbenzene, and 1,3,5-tris(methylmercaptan)benzene were prepared according to a previously reported procedure[47–49].

Purification

Purification and separation of disulfide and thioether products were performed by using Japan Analytical Instruments Inc. LC-9101 recycling preparative high-performance liquid chromatography with gel permeation chromatography columns JAIGEL-1H and JAIGEL-2H with $CHCl_3$ as the eluent. GPC separation was monitored with internal UV-Vis detector UV-4ch 800 LA. Flash Column Chromatography was performed with dry packed Macron Silica Gel 60 (230-400 Mesh) under 4-6 PSI of nitrogen. Pressure was regulated to maintain 2 inches of mobile phase through the column per minute. Crude reaction mixtures were adsorbed onto celite before column loading. Column separation was monitored with TLC.

Spectrometers

^{1}H, ^{13}C NMR, and 2D-COSY spectra were recorded with a Bruker AVANCE 500, Bruker AVANCE 600, or Varian INOVA 500. Spectra were referenced using the residual solvent resonances as internal standards and reported in ppm. Data are represented as follows: chemical shift, multiplicity (s = singlet, d = doublet, dd = doublet of doublets, t = triplet, m = multiplet, b = broad).

High-resolution mass spectrometry (HRMS) and low-resolution mass spectrometry (LRMS) data were obtained via Dr. Furong Sun's mass spectroscopy lab at the University of Chicago: Urbana-Champaign with Bruker Autoflex Speed LRF MALDI, Bruker Daltonics UltrafleXtreme MALDI TOFTOF, or Waters GCT Premier EI/CI/FD/FI.

Synthetic Procedures

Preperation of B'

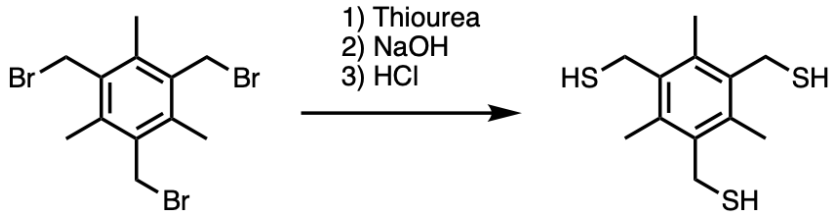

A solution of 2,4,6-tris(bromomethyl)mesitylene (1.2 g, 3 mmol) and thiourea (708 mg, 9.3 mmol) in acetone/chloroform (2:3 v/v) was heated to reflux and stirred vigorously overnight. Following the allotted time, the reaction mixture was cooled to room temperature to yield a white precipitate. The precipitate was collected via vacuum filtration and added to a degassed 150 mL 3M solution of NaOH. The reaction mixture was allowed to stir for 2 hours under nitrogen at room temperature. The product was precipitated with 4 M HCl to yield a white powder (755 mg, 97%). H NMR (500 MHz, $CDCl_3$) δ 3.79 (d, 6H), 2.44 (s, 9H), 1.58 (t, 3H) ^{13}C NMR (126 MHz, $CDCl_3$)

δ 136.19, 133.24, 77.28, 77.03, 76.78, 24.11, 15.60. HRMS-ASAP [M]+ $C_{12}H_{18}S_3$ predicted: 258.4589, found: 258.4603.

Preperation of A'

Bromomethylation

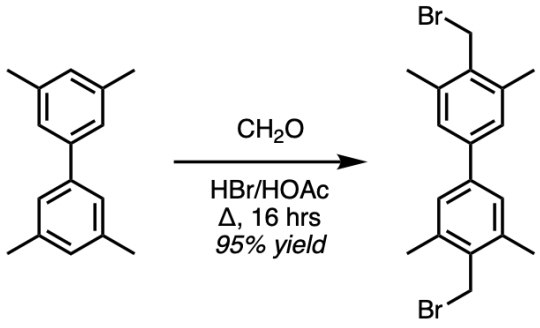

To a 5 mL solution of 3,3',5,5'-tetramethylbiphenyl (2.1 g, 10 mmol) and paraformaldehyde (616 mg, 20.5 mmol) in HOAc, 4 mL of 31% HBr in HOAc was added at once. The reaction was heated to reflux and allowed to stir overnight. Following the allotted time, the reaction mixture was quenched in 100 mL of ice water to yield an off white precipitate. The precipitate was dissolved in chloroform and purified over activated charcoal. The mixture was filtered and taken to dryness under reduced pressure to yield the product (**S1)** as a white precipitate (3.8 g, 95% yield). The product was used without further purification.

Thiolation

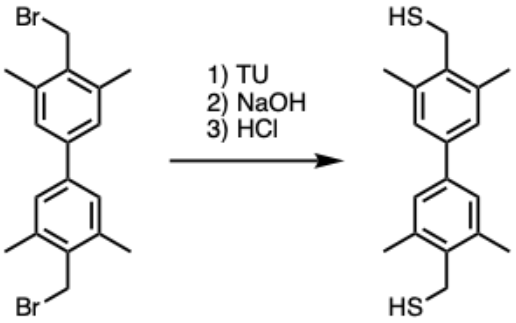

To a 150 mL solution of **S1** (3.5 g, 8.8 mmol) in acetone/chloroform (1:2 v/v), thiourea was added in a single portion (1.42 g, 18.6 mmol). The reaction mixture was heated to reflux overnight. After the allotted time, ther eaction was decanted to yield a brown solid. To the reaction vessel, degassed 10 mL of 2.5 M NaOH was added at once and allowed to stir under nitrogen at room temperature. After 16 hours, the reaction mixture was quenched with 6 M HCl and a precipitate was formed. The solid was isolated via vacuum filtration and washed 3x with 100 mL of water. The solid was purified via column chromatography (1% EtOAc/Hex (v/v) -> 6% EtOAc/ Hex (v/v)) to yield the product as an off-white powder (1.6 g, 62% yield). ^{1}H NMR (500 MHz, $CDCl_3$) δ 7.22 (s, 4H), 3.80 (d, J = 6.8 Hz, 4H), 2.46 (s, 12H), 1.61 (t, J = 6.7 Hz, 2H).

Self-sorting of A + B

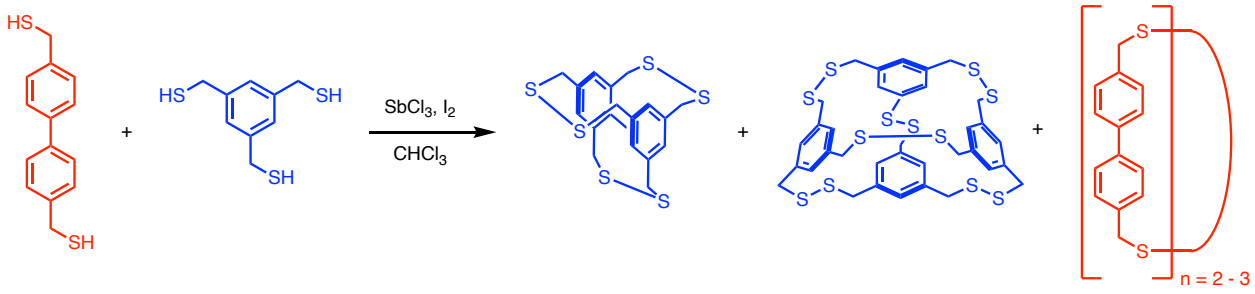

To a 75 mL solution of **A** (123 mg, 0.5 mmol) and **B** (108 mg, 0.5 mmol) in chloroform, a 25 mL solution of $SbCl_3$ (456 mg, 2 mmol) and iodine (381 mg, 1.5 mmol) is added dropwise. Following complete addition, the reaction was allowed to stir for 15 minutes before being quenched with 100 mL of saturated sodium sulfite solution and washed 3x with 100 mL of water. The organics were collected and taken to dryness under reduced pressure to yield composite narcissistic disulfide cyclophanes. NMR matches previously reported products.[47-48]

Self-sorting of A + B'

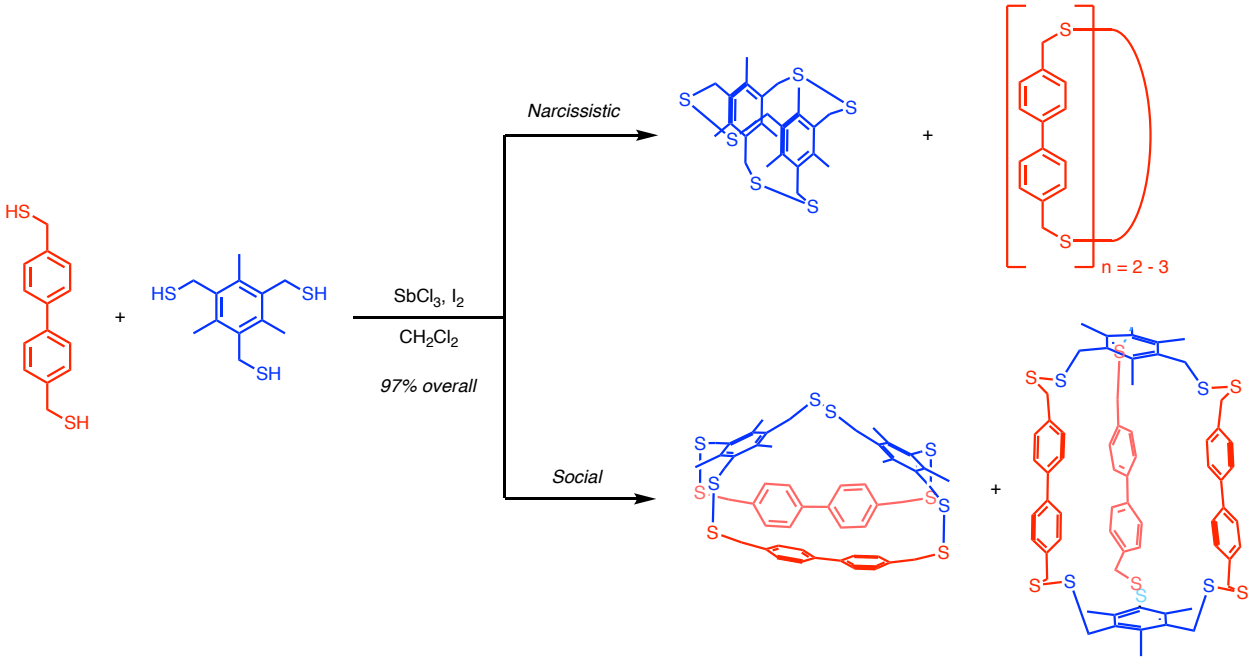

To a 75 mL solution of **A** (123 mg, 0.5 mmol) and **B'** (129 mg, 0.5 mmol) in chloroform, a 25 mL solution of $SbCl_3$ (456 mg, 2 mmol) and iodine (381 mg, 1.5 mmol) is added dropwise. Following complete addition, the reaction was allowed to stir for 15 minutes before being quenched with 100 mL of saturated sodium sulfite solution and washed 3x with 100 mL of water. The organics were collected and taken to dryness under reduced pressure to yield composite

disulfide cyclophanes. The disulfides were purified via size exclusion chromatography to yield **A_2-$_3$**, **B'_2**, **A_2B_2**, and **A_2B_3**.

B'_2: ^{1}H NMR (500 MHz, $CDCl_3$) δ 4.37 – 4.05 (m, 6H), 3.46 – 3.22 (m, 6H), 2.58 – 2.34 (m, 18H).

A'_2B_2': ^{1}H NMR (500 MHz, Tetrachloroethane-d_2) δ 7.69 (d, J = 7.8 Hz, 8H), 7.50 (d, J = 7.7 Hz, 9H), 3.98 (s, 10H), 3.41 (s, 12H), 2.30 (s, 8H), 1.93 (s, 12H). ^{13}C NMR (126 MHz, CD_2Cl_2) δ 138.04, 137.04, 136.67, 135.33, 132.84, 130.94, 129.93, 129.78, 125.86, 98.85, 60.22, 59.95, 42.07, 40.26, 29.20, 19.64, 16.26, 15.54, 14.97, 13.78.

A'_2B_3': ^{1}H NMR (500 MHz, Chloroform-d) δ 7.55 (m, 24H), 3.70 (m, 24H), 2.24 (m, 18H) ^{13}C NMR (126 MHz, CD_2Cl_2) δ 139.90, 139.80, 137.04, 136.84, 136.70, 136.11, 132.06, 130.80, 130.33, 130.25, 130.15, 127.36, 127.31, 127.15, 58.77, 43.19, 43.13, 42.51, 32.22, 31.41, 30.02, 29.67, 23.04, 18.86, 16.93, 16.50, 14.57.

Self-sorting of A' + B'

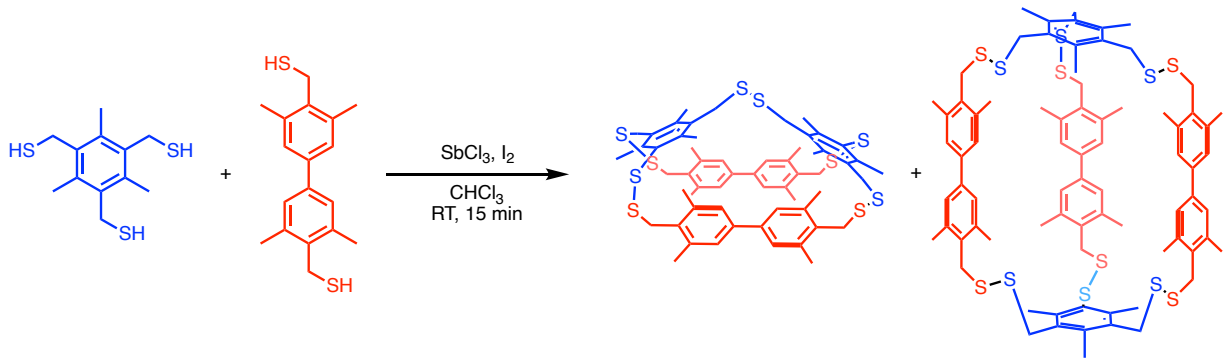

General NMR Experiment

To a 0.8 mL solution of 2.5 mM **A'** and 2.5 mM **B'** in $CDCl_3$, 0.1 mLs of 100 mMol $SbCl_3$ and 100 mMol I_2 in $CDCl_3$ were added sequentially to an NMR tube. The iodine was added as to not break the meniscus of the reaction solution to allow slow diffusion. After complete diffusion of the iodine solution, the reaction mixture was allowed to sit unperturbed for 15 minutes and ^1H NMR was performed to analyze self-sorting behavior.

Analysis of Self-sorting Oligothiol Equivalence Dependance

The above setup was performed for 1:0, 1:2, 2:2, 3:2, 4:2, and 0:1 equivalents of **A'**:**B'**. The ratios were normalized to 5 mMol of total substrate concentration.

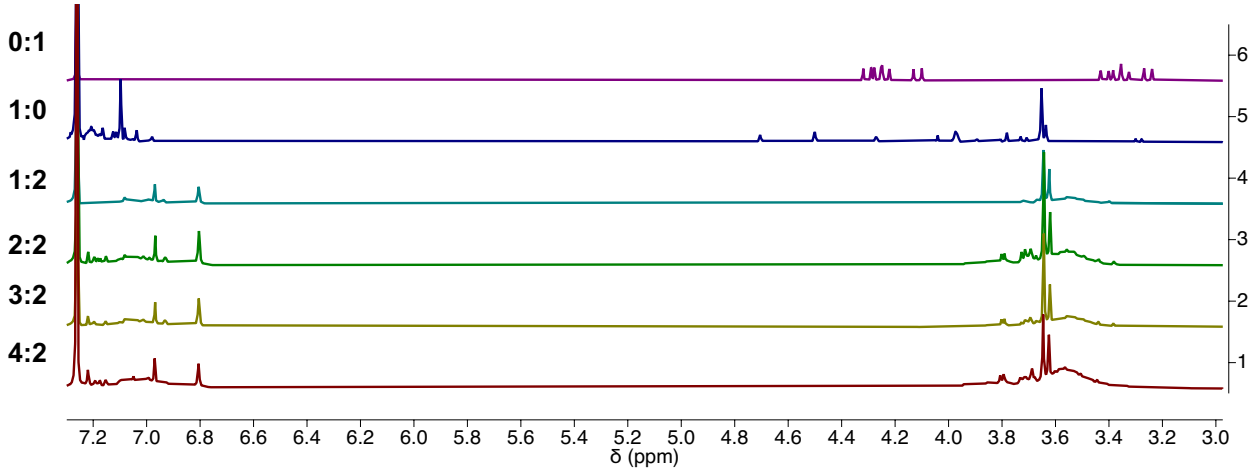

CHAPTER V

CONCLUSIONS AND FUTURE OUTLOOK

CONTRIBUTIONS

This final chapter discusses current and future work towards investigating pnictogen-directed self-assembly and self-sorting design principles in preorganized macrocycles and cages. This chapter includes unpublished work by my rotation student, Leif Lindberg, and myself. Professor Darren W. Johnson and Dr. Shiva Moaven provided intellectual support.

INTRODUCTION

This body of work investigated supramolecular design strategies in pnictogen-directed self-assembly and self-sorting. Chapter II describes the start of this journey through the investigation of the macrocyclization substrate scope. To our delight, the thermodynamic pathway was tolerant to a wide array of scaffolds and provided a basis for planning more intricate synthetic targets. Following that work, Chapter III investigated PDI-containing scaffolds toward the facile assembly of optoelectronic materials; moreover, this work showcased that self-assembly precursors could be prepared in high yield and throughput with Suzuki cross-coupling reactions. Finally, Chapter IV discussed the steric effects of biasing pnictogen-directed self-sorting of oligothiols. This final chapter will discuss unpublished results and future endeavors that can be developed on this project.

FUTURE DIRECTIONS

High throughput self-assembly of unsaturated cyclophanes and catenanes

Catenanes are a class of mechanically interlocked molecules (MIMs) defined by two macrocycles threaded together[1] (Figure 5.1). Catenation is complex because of the preorganization required during the ring-closing process. For our chemistry, it has proved to be a challenge to both intertwine two ligands and perform the disulfide self-assembly as orthogonal supramolecular processes are complex to find with competing Lewis acids and bases. Because of this intrinsic bottleneck, we were inspired by work in the Itami group that used spirosilation to fuse two scaffolds before macrocyclization and desilation to yield the first all hydrocarbon catenane[2]; moreover, Chapter III showcased Suzuki cross-coupling can be a valuable tool in the synthesis of self-assembly precursors in our chemistry.

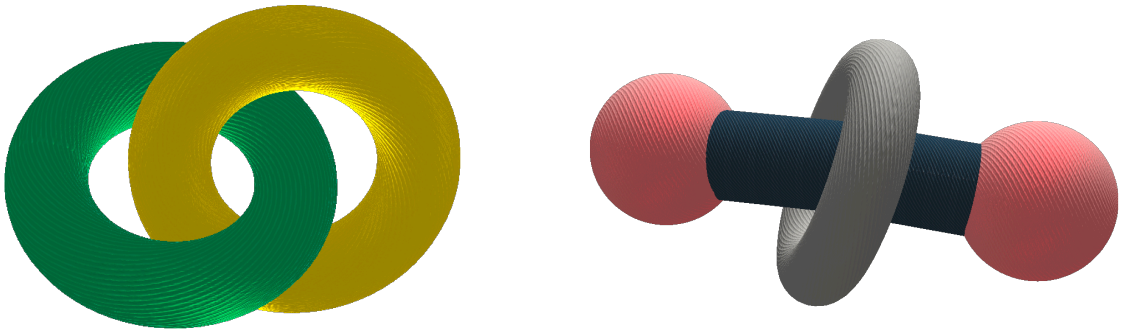

[2]Catenane **[2]Rotaxane**

Figure 5.1: Representation of select MIMs: (left) catenane and (right) rotaxane.

With this knowledge, a spirosilated self-assembly precursor was devised for catenane formation (Scheme 5.1). The unbound ligand was synthesized, and disulfide-linked macrocycles were self-assembled in excellent yield. Following this success, sulfur extrusion conditions of the untethered macrocycle were optimized. The sulfur extrusion to the thioether macrocycles also occurs in excellent yield and attempts were made to find reaction conditions for unsaturated cyclophane formation. Here, a benzyne-induced Steven's rearrangement, followed by sulfoxide

formation from sulfide oxidation, and a cope elimination seemed to result in the intended product (**Scheme 5.2**). While yield was minimal, preliminary evidence suggests the formation of unsaturated macrocycles, with fluorescent emission following the reaction (Figure 5.2); however, the products are not exceptionally air-stable and seem to degrade upon long-standing to air.

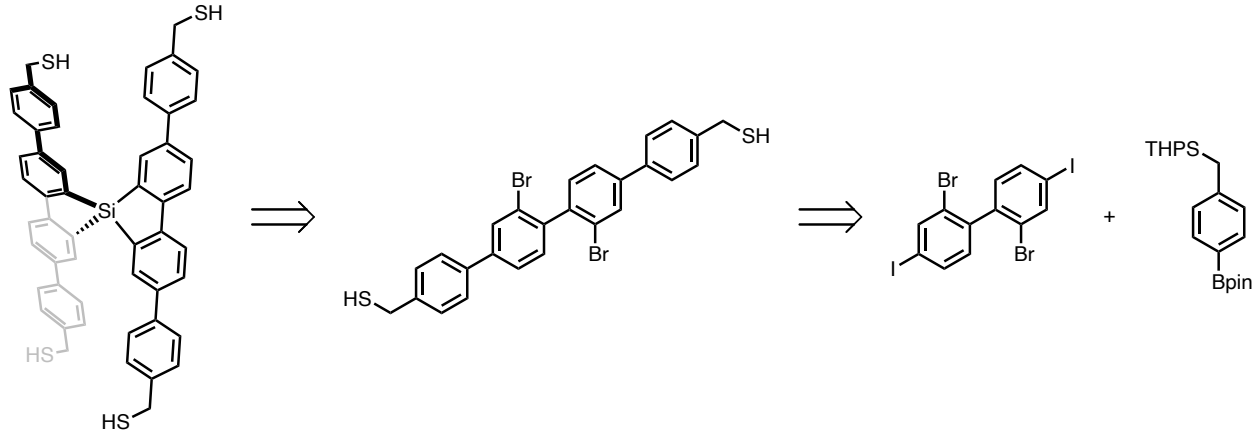

Scheme 5.1: Retrosynthetic pathway for spirosilated thiol-containing ligand preorganized for catenane formation. The untethered species was successfully synthesized.

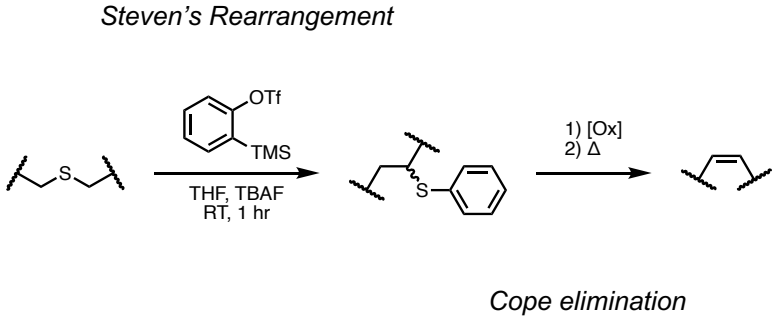

Scheme 5.2: General Reaction pathway for unsaturated carbon-carbon formation following sulfur extrusion. Cope elimination results in *cis* alkene due to *syn* elimination.

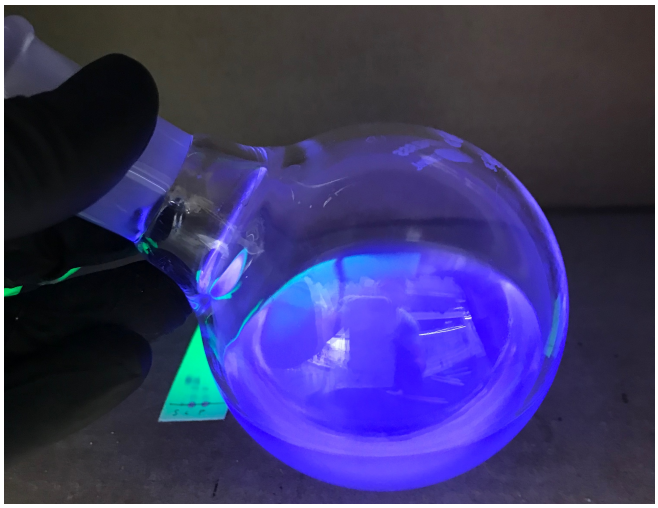

Figure 5.2: Cope elimination reaction mixture under 254 and 366 nm UV light following work up.

Following the success of the reaction pathway for unsaturated cyclophanes, biphenyl-linked disulfide macrocycles were used to optimize the unsaturated cyclophane reaction pathway. The purpose of this was two-fold: (1) the ligand is more accessible and hastens optimization, and (2) this pathway could lead to a novel route towards the self-assembly of unsaturated cyclophanes. Furthermore, work from the Lee group at LSU suggests unsaturated cyclophanes can act as preliminary building blocks in the formation of CPPA carbon nanohoops[3]. During this endeavor,

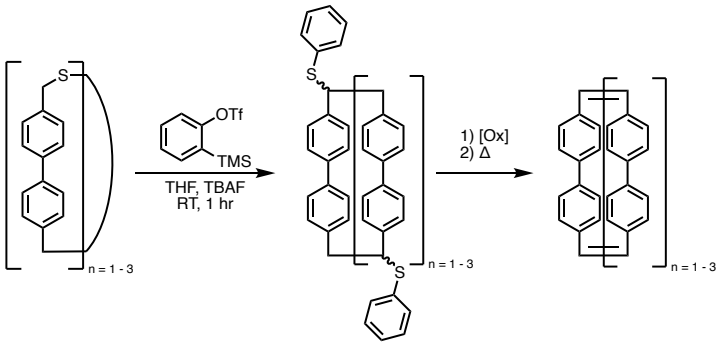

Scheme 5.3: Reaction pathway for unsaturated cyclophanes with biphenyl spacer.

we optimized the reaction pathway to the next-to-last step before the Cope elimination (**Scheme 5.3**).

Future work on this project could elucidate pathways for catenane formation from simple self-assembly pathways; moreover, with accessible pathways in alkene-linked macrocycle formation, through-bond conjugation of resulting macrocycles could be explored for variable optoelectronic properties. Specifically, HOMO-LUMO gaps could be tailored for specificity in guest transport, electron transport, or as responsive small molecules.

Anion recognition and templation of PDI macrocycles

Anion-π recognition is a thematic noncovalent interaction in electron-withdrawn π systems[4]. Specifically, due to a vacancy of electron density, electrostatic attraction draws these aromatic scaffolds and anions together. This motif has been used with PDI scaffolds for the fluorescent detection of anions[5,6]. During the investigation of PDI macrocycles discussed in Chapter III, we believed our systems could have similar effects as described; moreover, we could bias the macrocyclic effect in our endeavors. Specifically, the entropic cost of preorganizing PDI scaffolds was paid in the self-assembly. To test our hypothesis, a preliminary fluorescence experiment was conducted with tetrabutylammonium iodide (**Figure 5.3**). As expected, the fluorescence emission of our PDI macrocycle was shifted like a π-π interaction with an electron-rich aromatic small molecule. Assuming this trend upholds with other anionic guests, self-assembled PDI macrocycles can act as fluorescent probes in anion detection; furthermore, this noncovalent interaction may pair with the pnictogen-directed self-assembly and allow us to

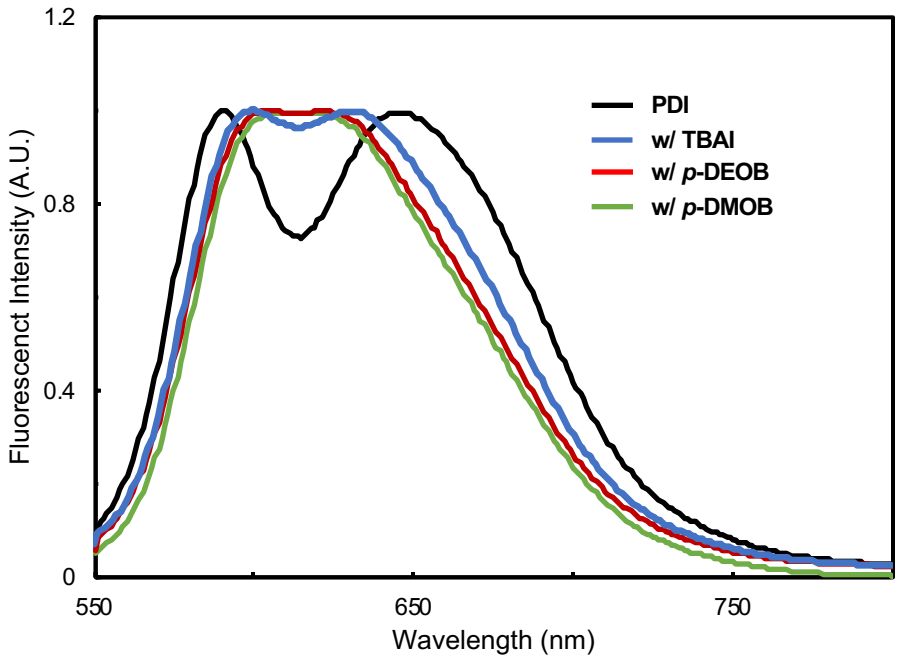

Figure 5.3. Fluorescence emission spectra of PDI macrocycle with guests: (blue) tetrabutylammonium iodide, (red) *p*-diethoxybenzene, and (blue) *p*-dimethoxybenzene. Emission spectra was recorded at 10 μMol PDI with 10 eq guests, λ_{ex} = 525 nm.

template variably sized PDI macrocycles with different anionic guests, like Pederson's work with crown ethers.

As a follow-up to the host-guest interactions observed in the PDI macrocycles, the preorganization of aromatic π systems could be used in pnictogen-directed catenane formation (Scheme 5.4). Once an avenue for mechanical bond formation is elucidated, these pathways could be expanded to mechanically interlocked polymer formation towards the elusive class of poly[n]catenanes.

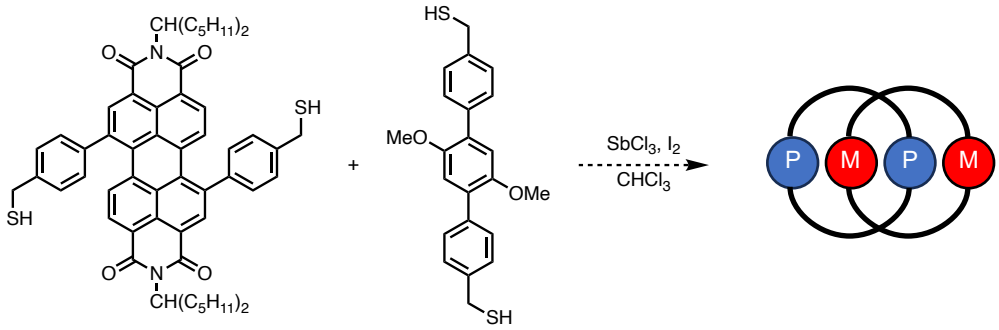

Scheme 5.4: Proposed pathway towards catenated species through pnictogen-assisted self-assembly. P = PDI scaffold; M = dimethoxybenzene scaffold.

Synthesis of macrocycles for materials application

Macrocycles are ubiquitous in supramolecular materials chemistry due to their affinity in host-guest chemistry; however, their utility in industrial applications is bottlenecked because of low-yielding or laborious synthetic pathways. With the Suzuki cross-coupling route yielding promising results in self-assembly precursor formation, future endeavors can utilize this pathway towards the facile production of tailor-made macrocycles. As a simple example, recent advancements in chemotherapy show synergistic effects in drug combinations, which is an effective method in antitumor response[7]. To accomplish this feat, albumin can be modified with calixarene hosts to transport chemotherapeutic drugs in specific stoichiometric quantities[8]. To release the drug, hypoxia-responsive azo linkages were appended onto the macrocyclic host. This mechanism could be tested with our chemistry for drug delivery or other targeted-release applications (Scheme 5.5).

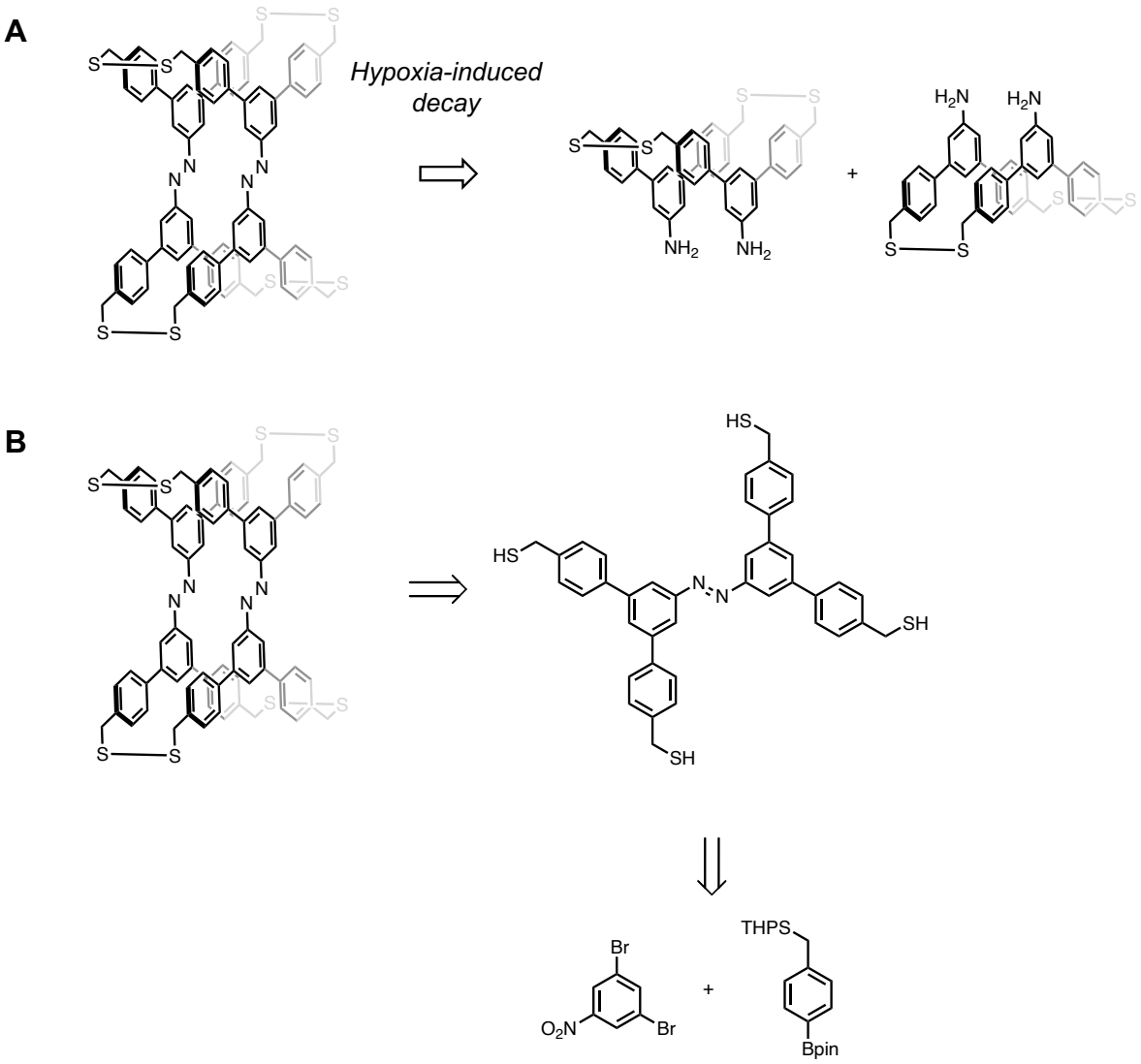

Scheme 5.5: (**A**) hypoxia-induced decay of aza-linked disulfide cyclophanes. (**B**) Proposed retrosynthetic pathway to target molecule.

Appendix A

CHARACTERIZATION DATA FOR SELF-ASSEMBLY ROUTE TO PERYLENE DIIMIDE(PDI)-BRIDGED CYCLOPHANES

I. ^{1}H NMR and ^{13}C NMR Spectra

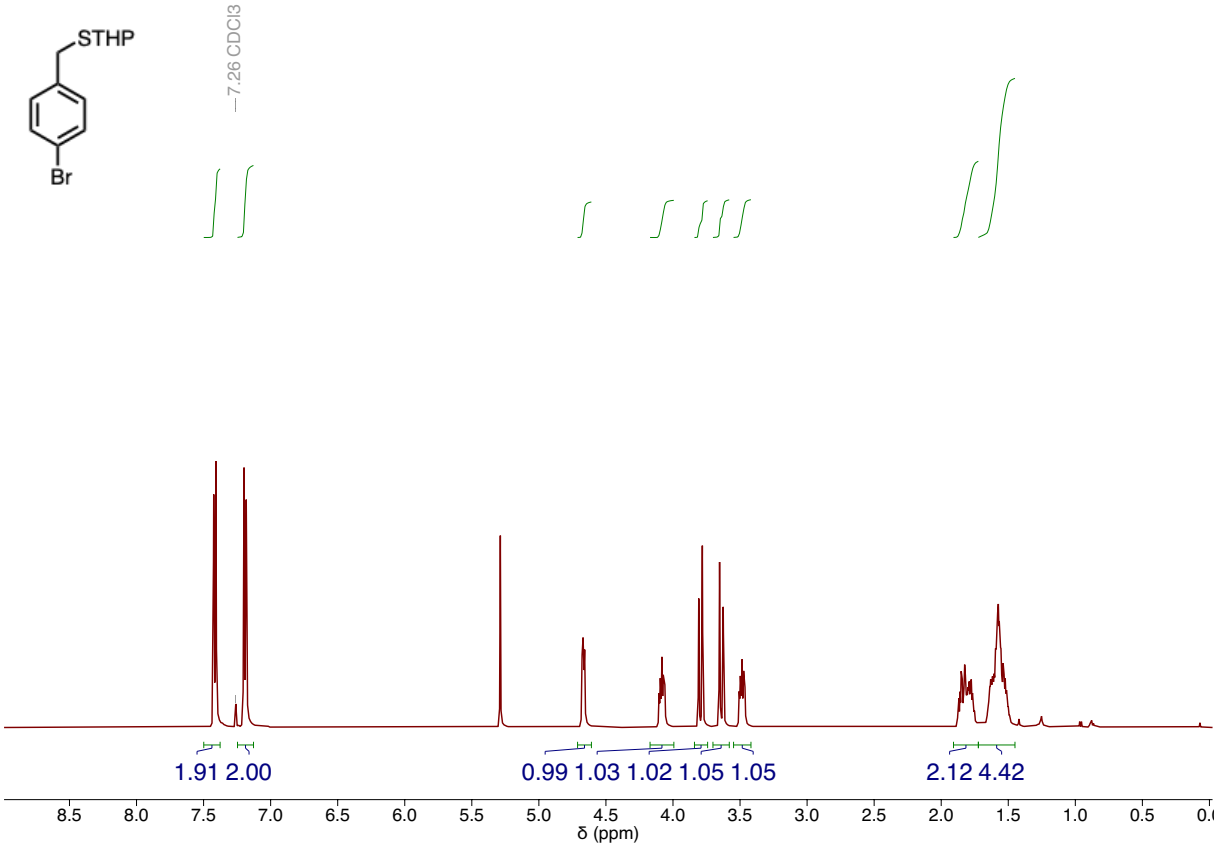

Figure S1. ^{1}H NMR spectrum of 4-bromobenzylSTHP in $CDCl_3$.

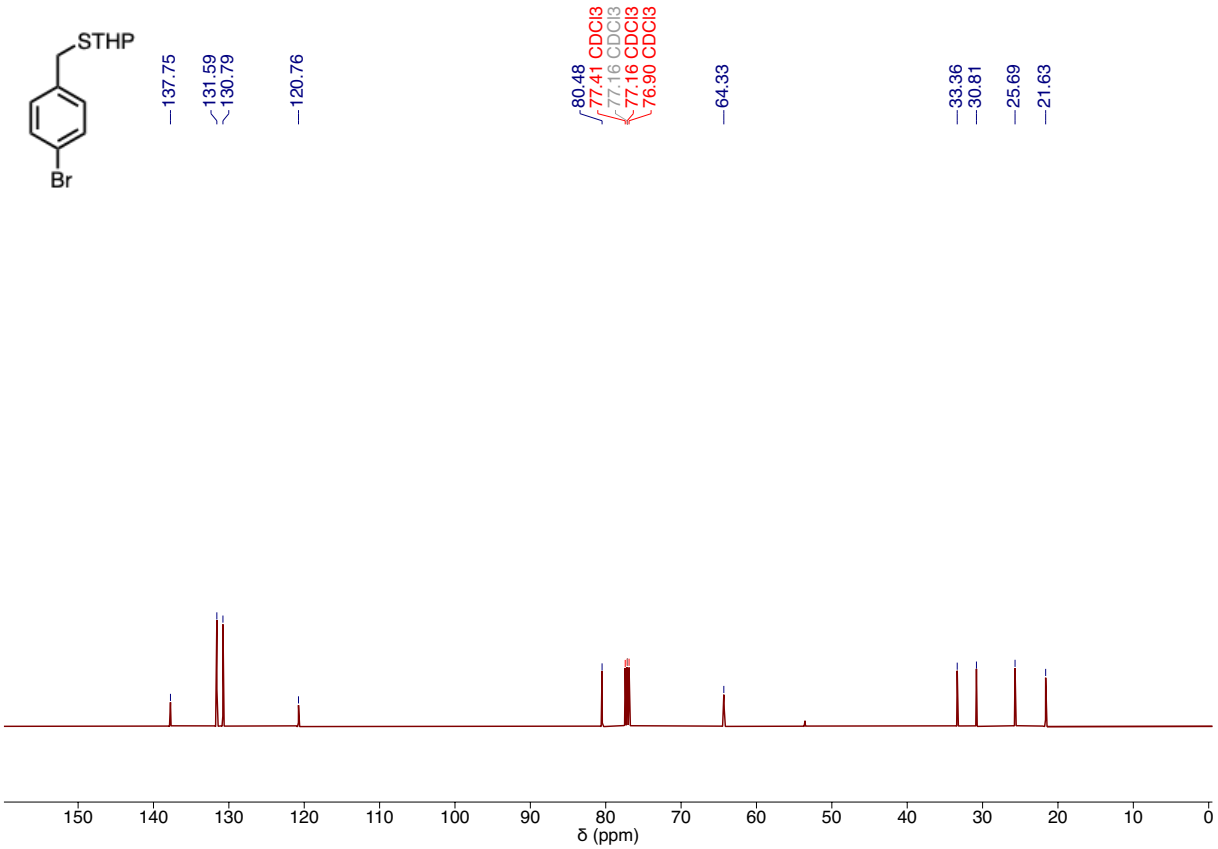

Figure S2. ^{13}C NMR spectrum of 4-bromobenzylSTHP in $CDCl_3$.

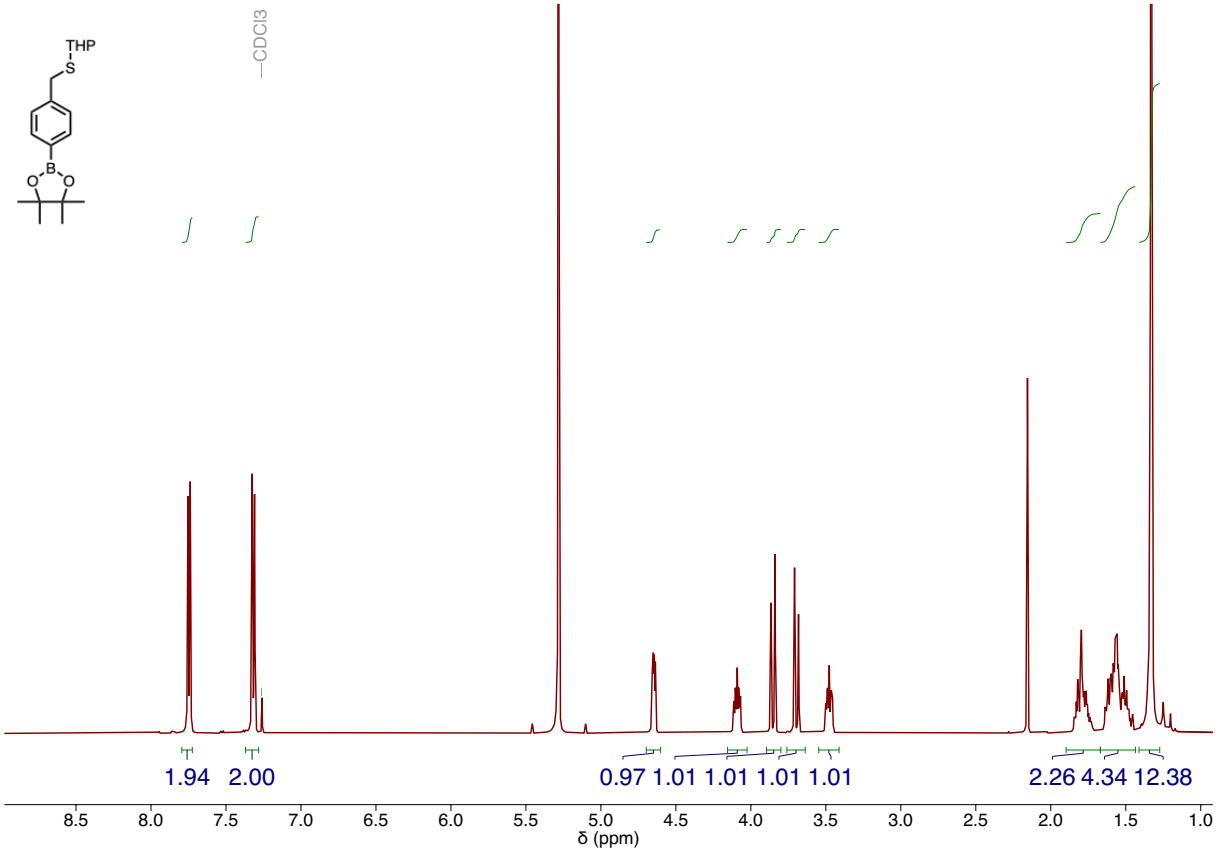

Figure S3. ^{1}H NMR spectrum of 4-B(pin)benzylSTHP in $CDCl_3$.

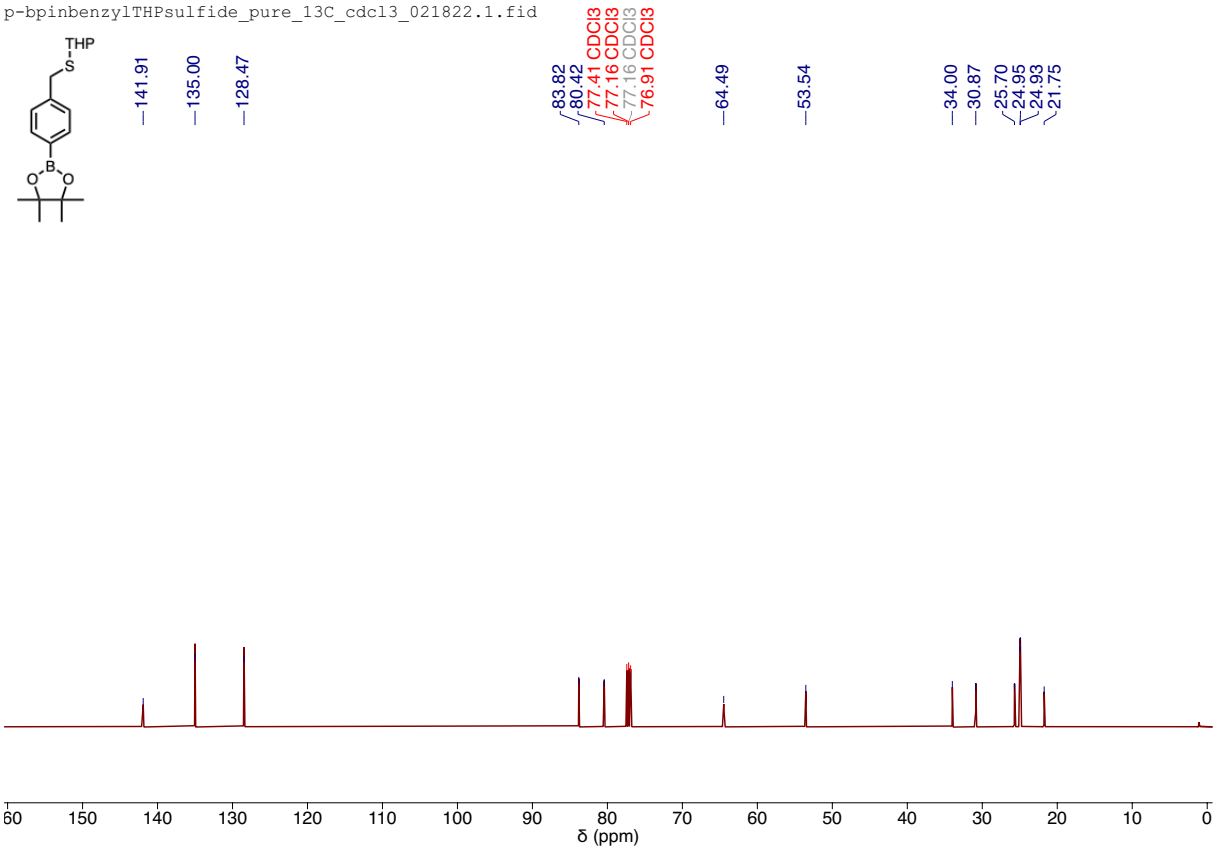

Figure S4. ^{13}C NMR spectrum of 4-B(pin)benzylSTHP in $CDCl_3$.

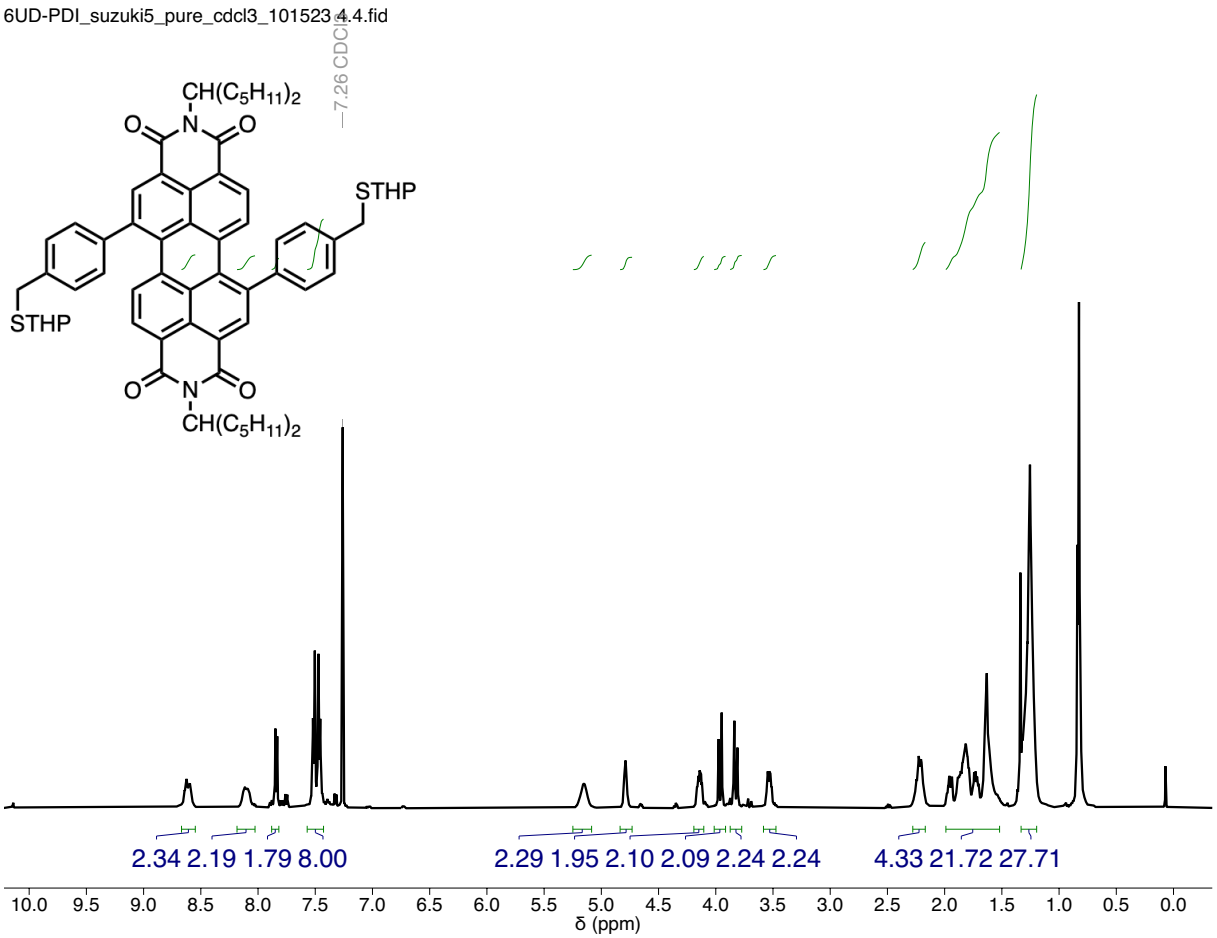

Figure S5. ^{1}H NMR spectrum of SI-1 in $CDCl_3$.

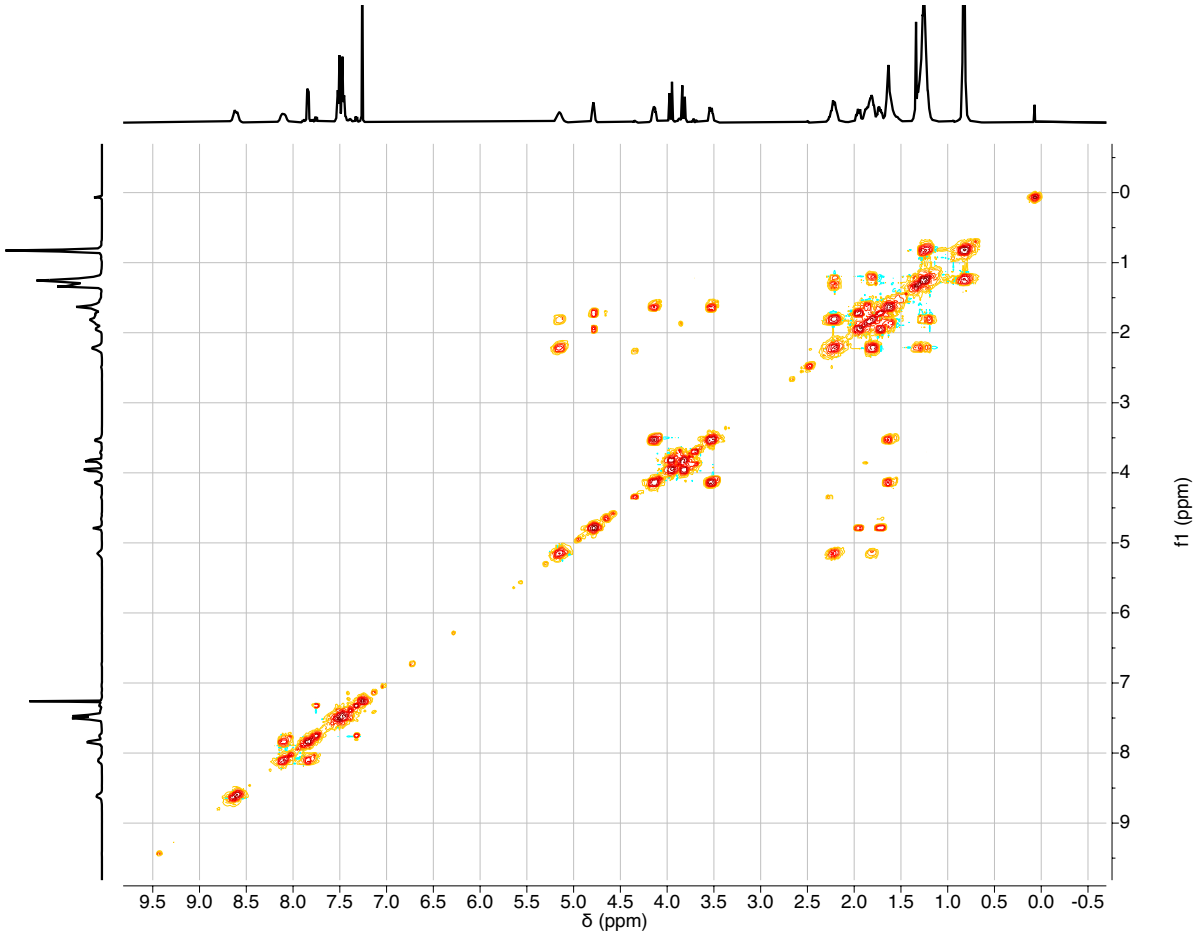

Figure S6. *COSY* NMR spectrum of SI-1 in $CDCl_3$.

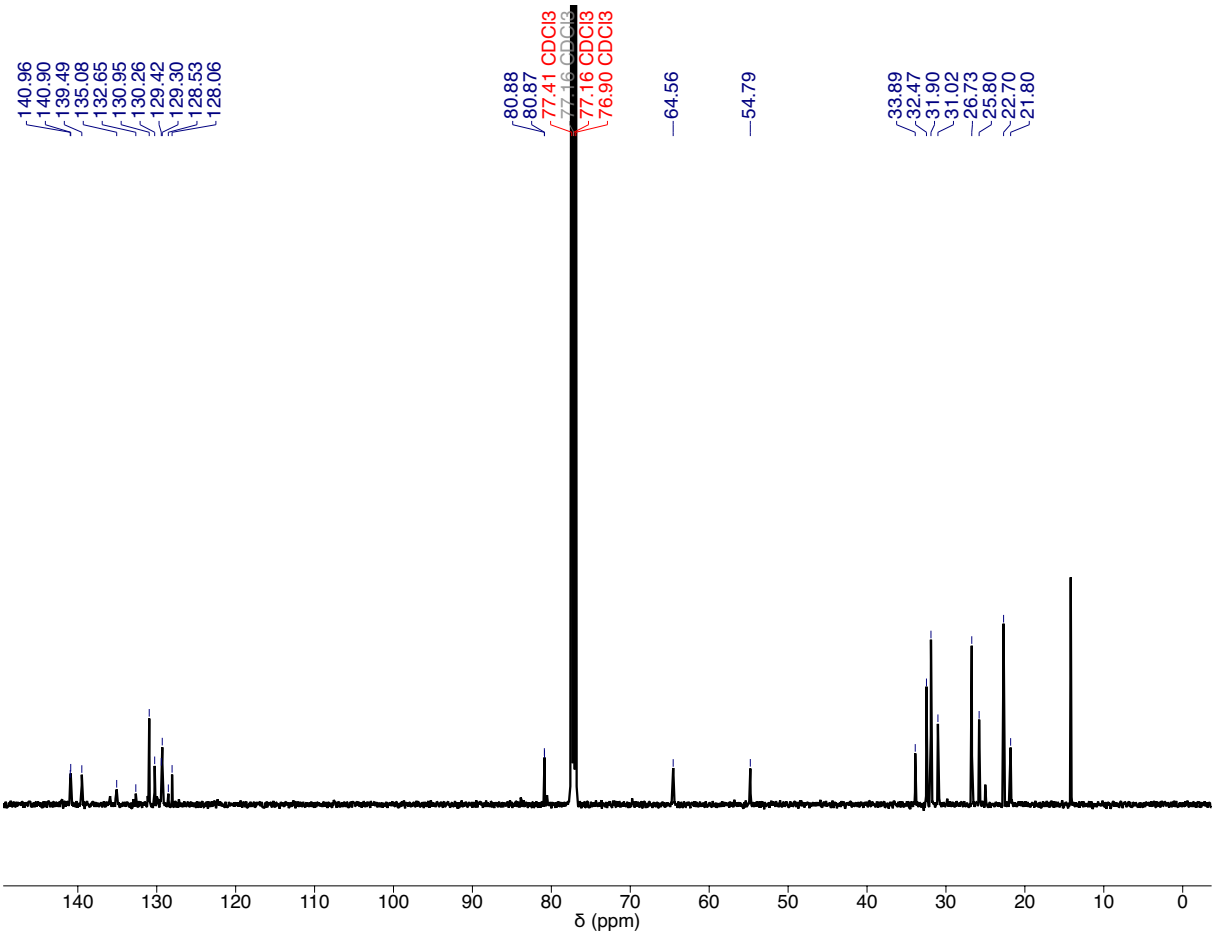

Figure S7. ^{13}C NMR spectrum of SI-1 in $CDCl_3$.

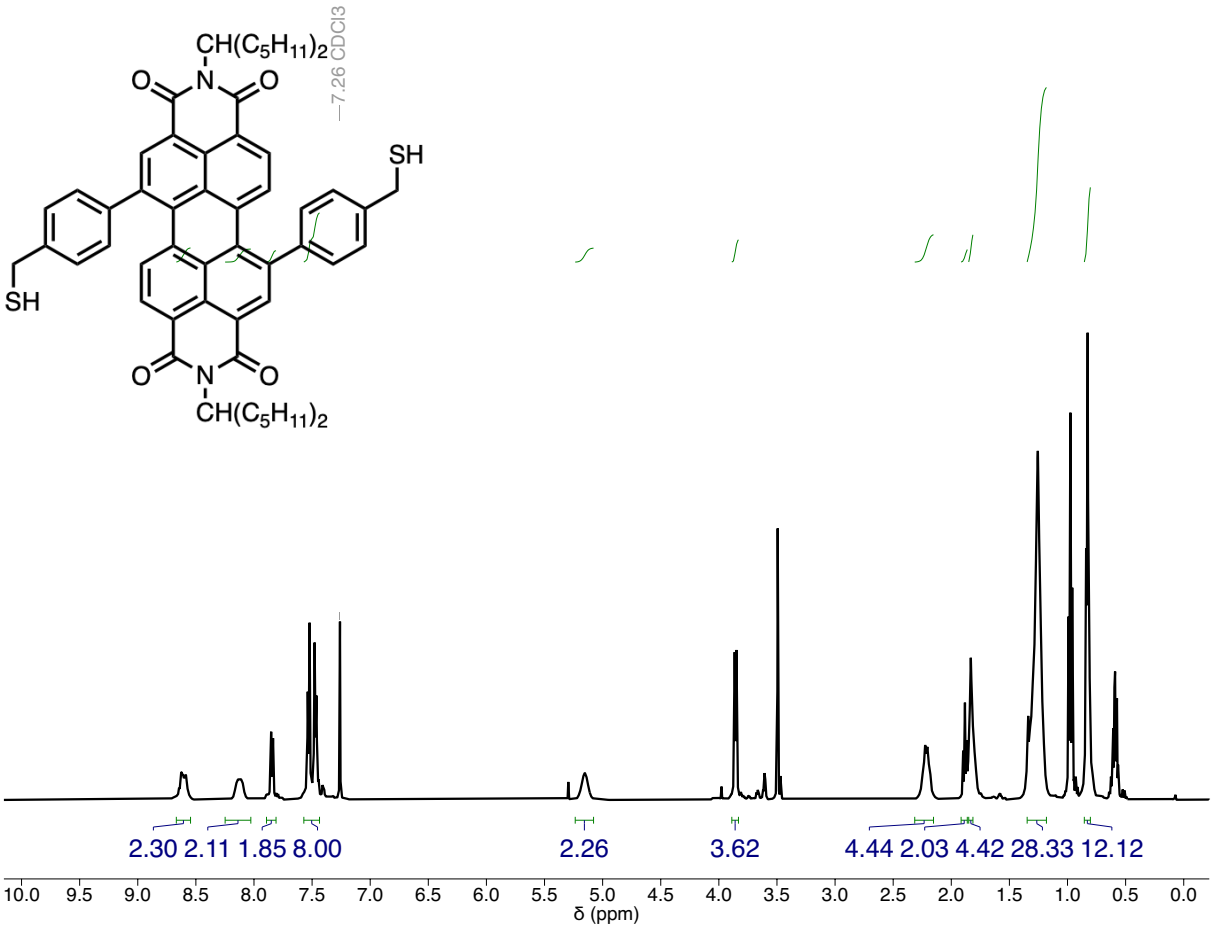

Figure S8. ^{1}**H NMR spectrum of** H_2L $CDCl_3$.

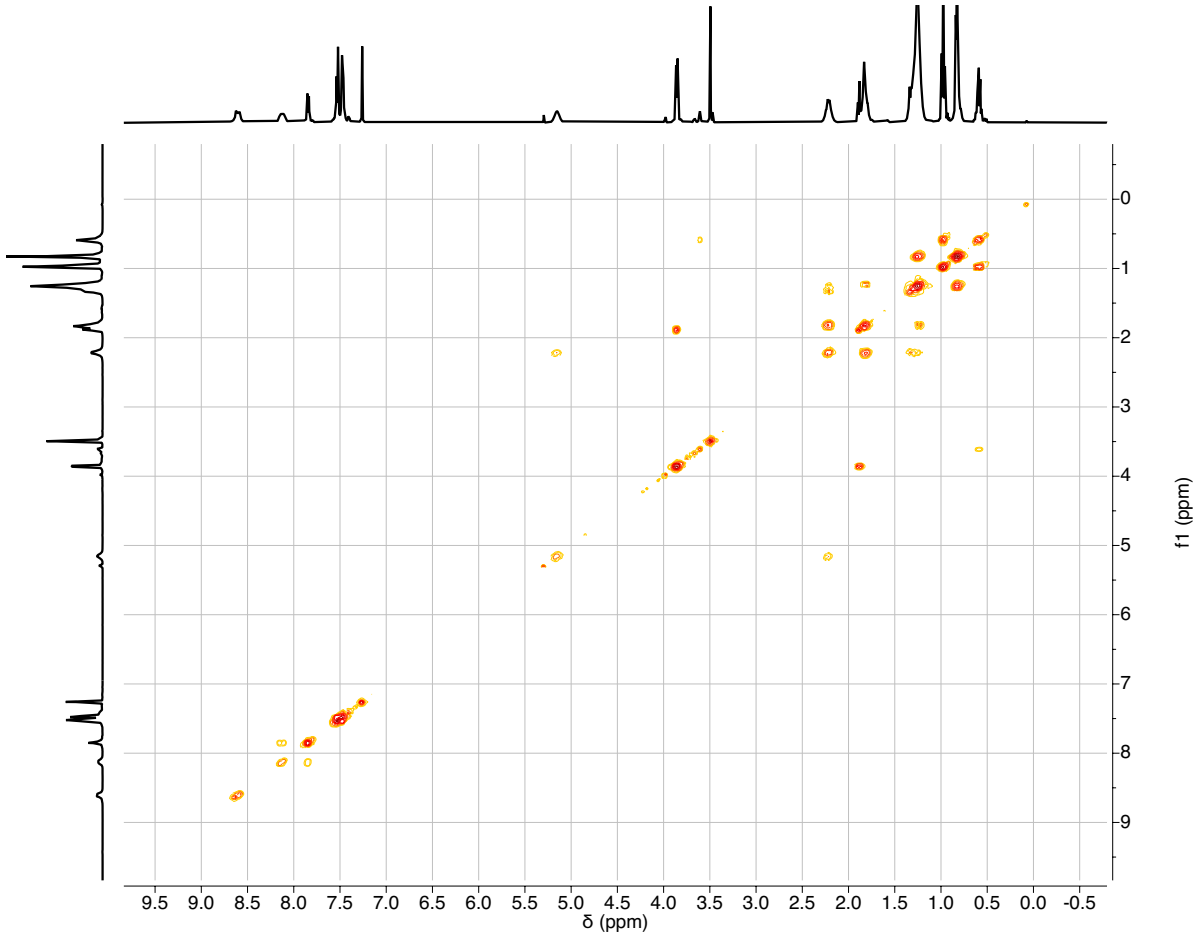

Figure S9. COSY NMR spectrum of H_2L $CDCl_3$.

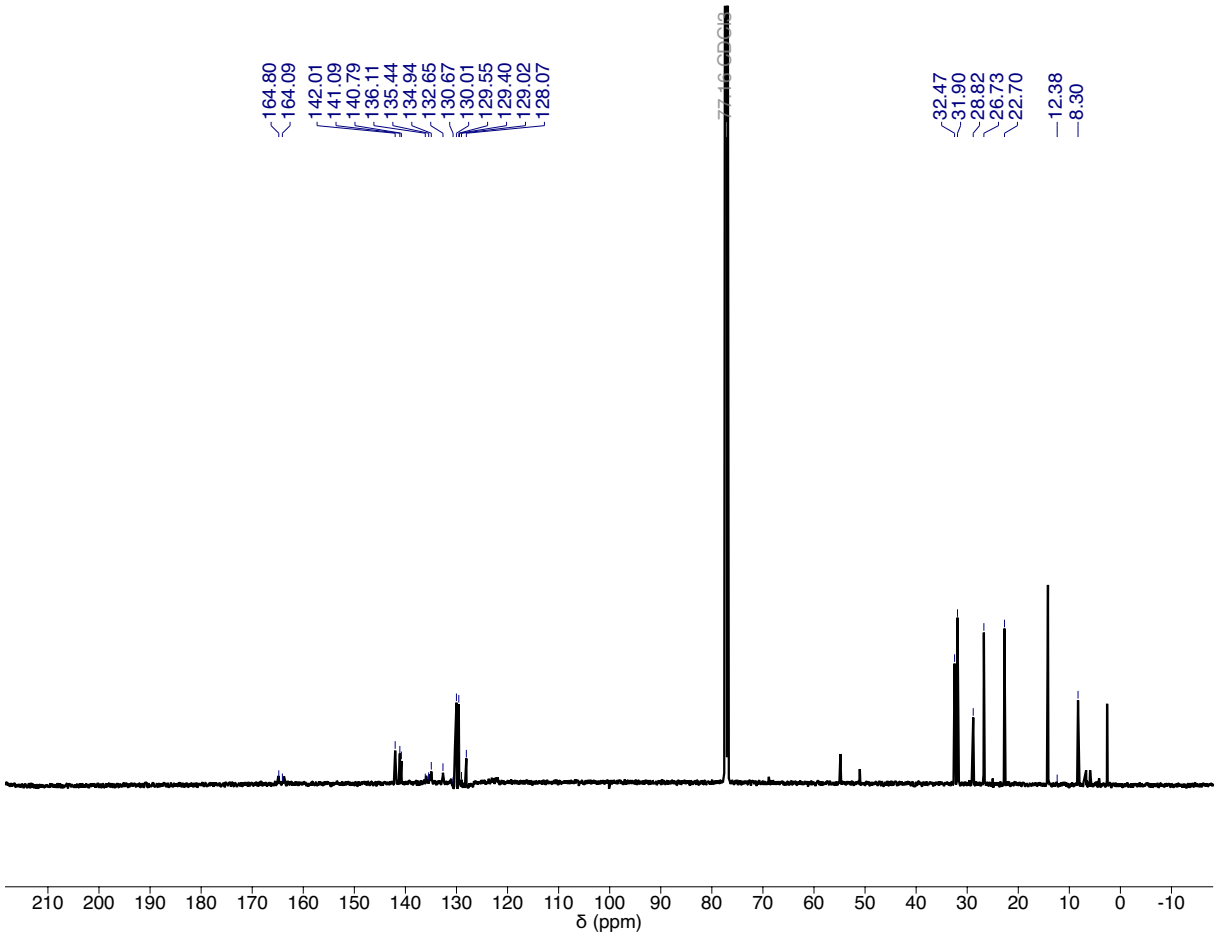

Figure S10. ^{13}C NMR spectrum of H_2L $CDCl_3$.

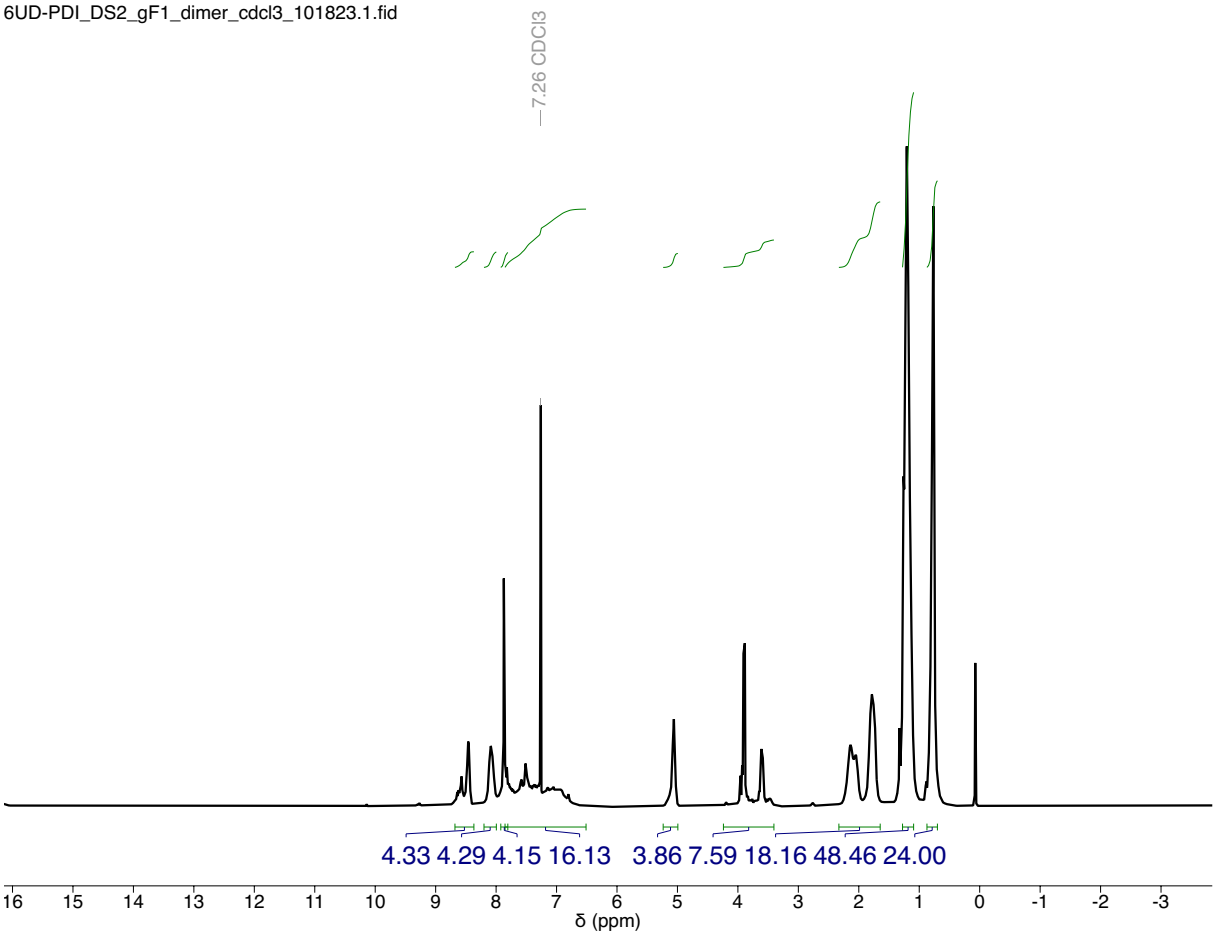

Figure S11. ^{1}H NMR spectrum of L_2 in $CDCl_3$.

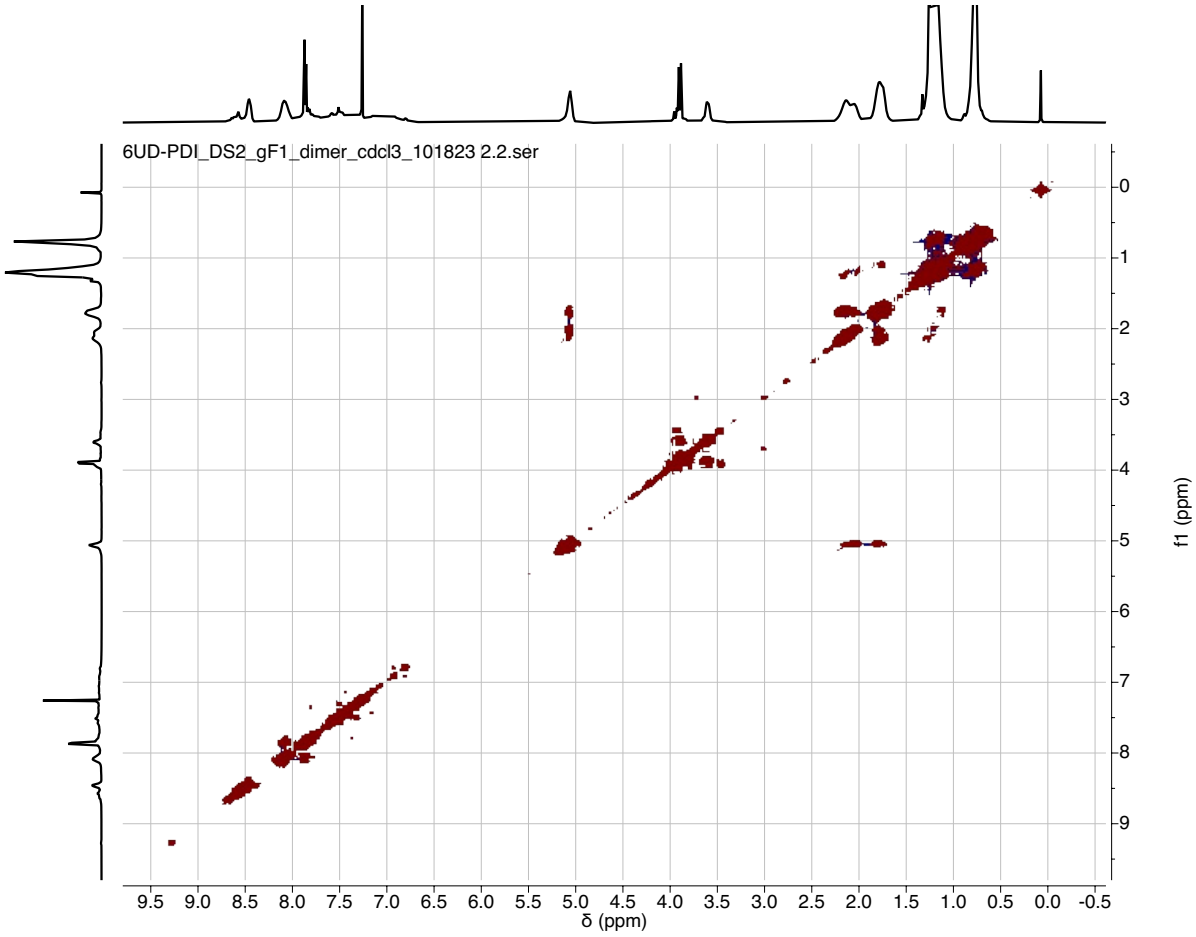

Figure S12. COSY NMR spectrum of L_2 in $CDCl_3$.

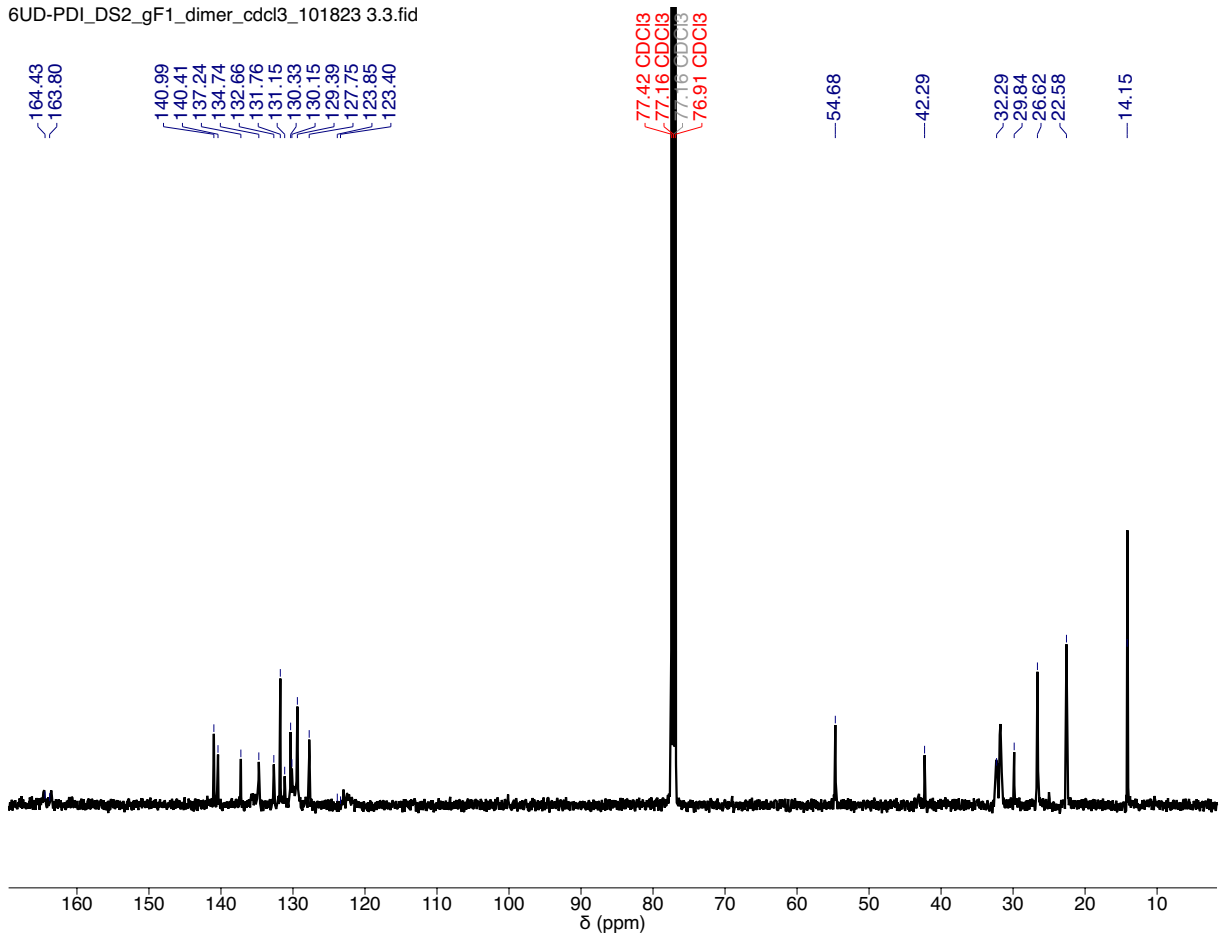

Figure S13. ^{13}C NMR spectrum of L_2 in $CDCl_3$.

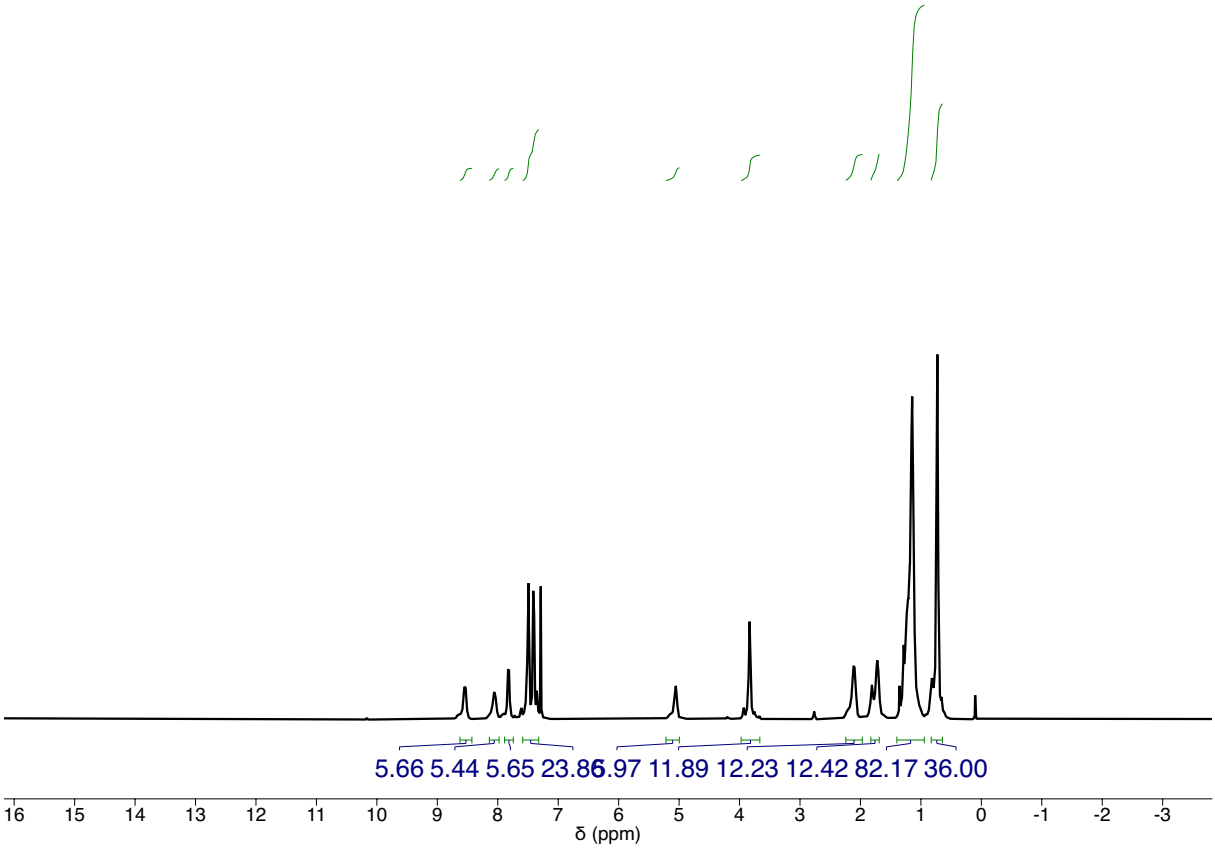

Figure S14. ^{1}H NMR spectrum of L_3 in $CDCl_3$.

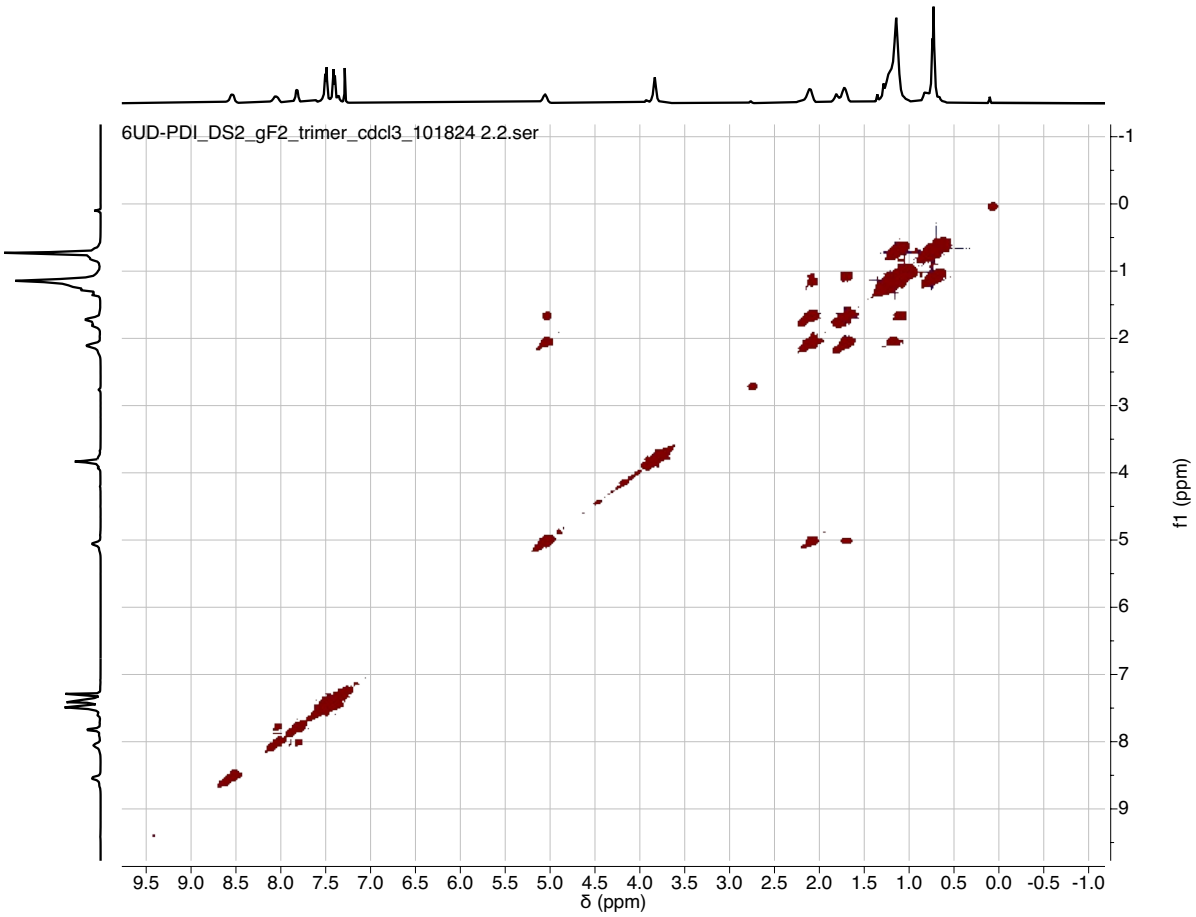

Figure S15. COSY NMR spectrum of L_3 in $CDCl_3$.

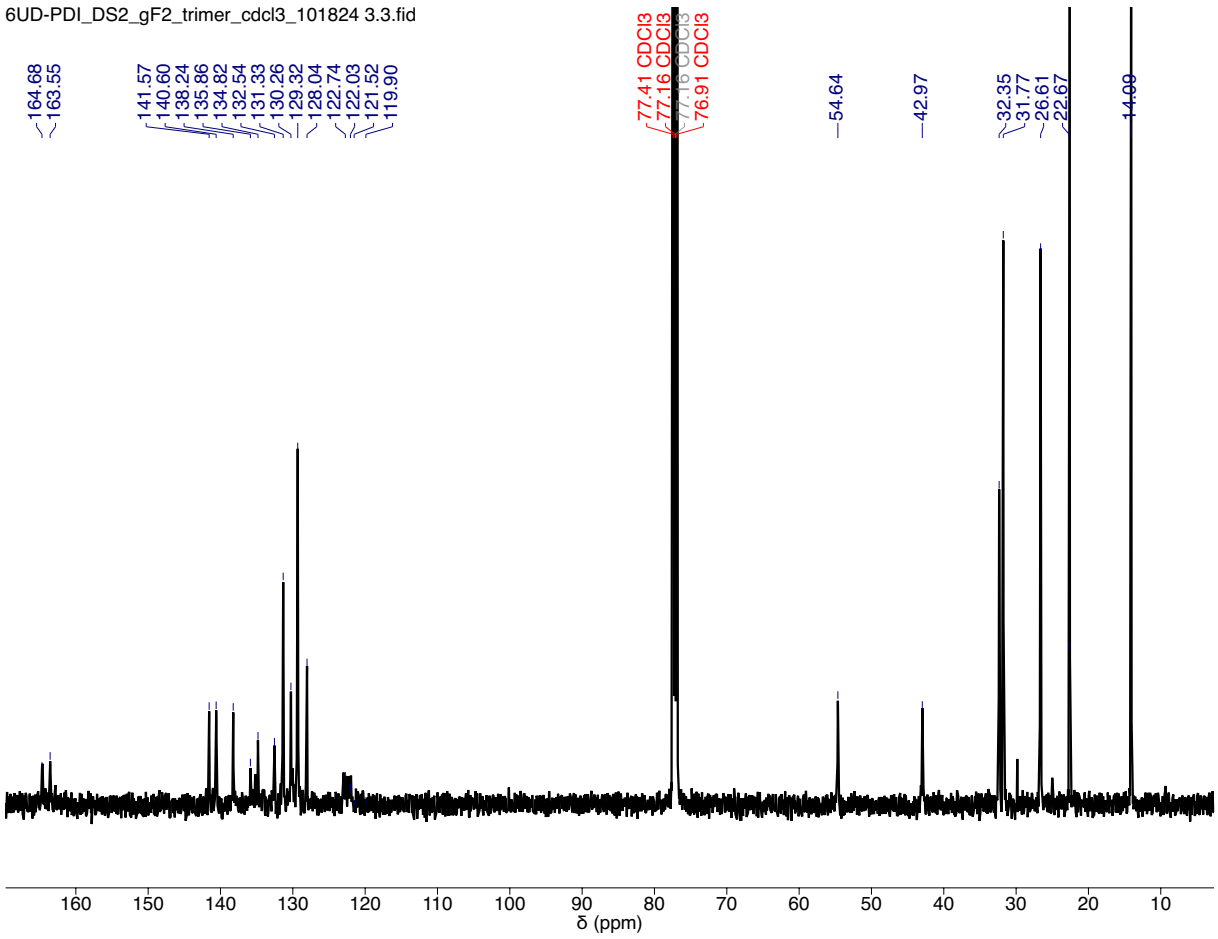

Figure S16. ^{13}C NMR spectrum of L_3 in $CDCl_3$.

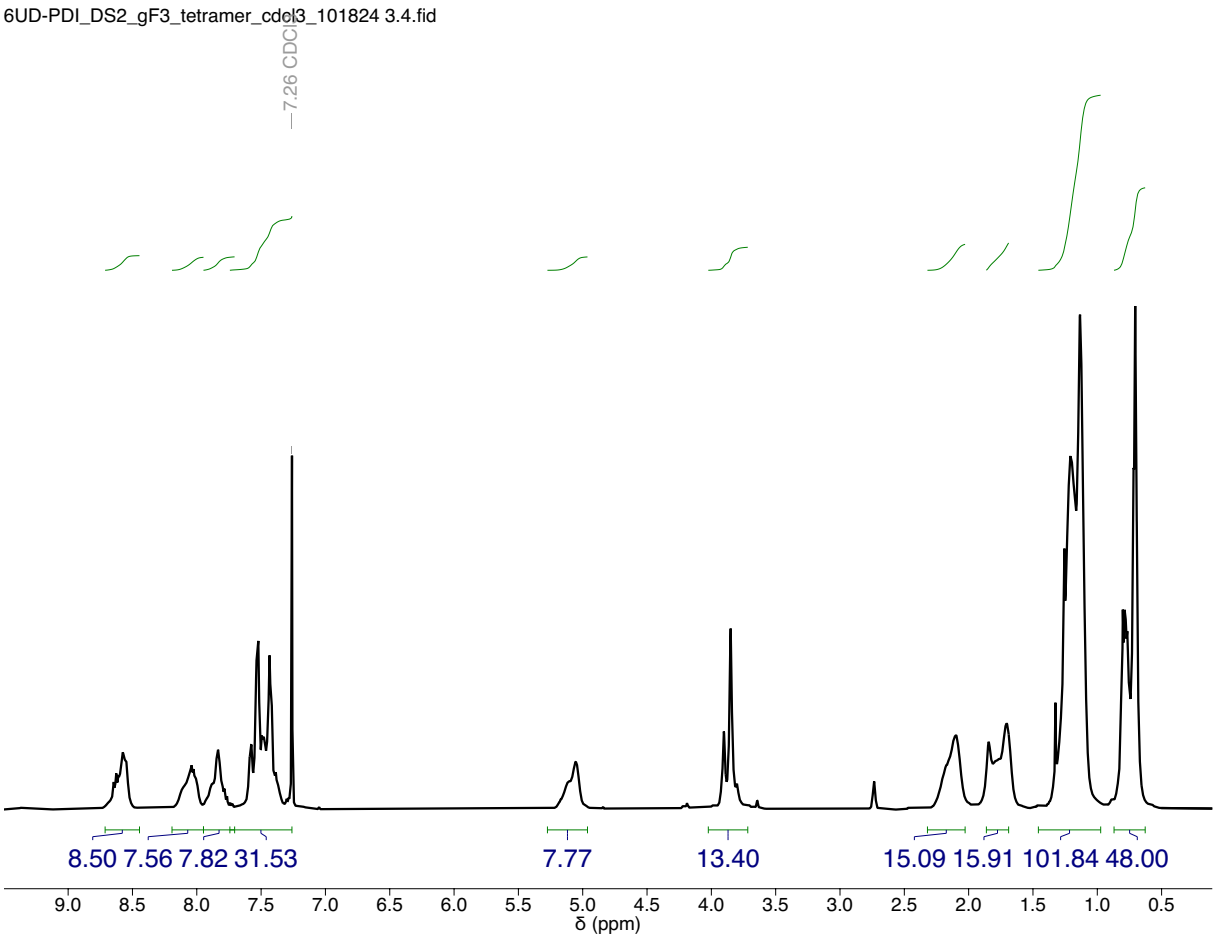

Figure S17. ^{1}H NMR spectrum of L_4 in $CDCl_3$.

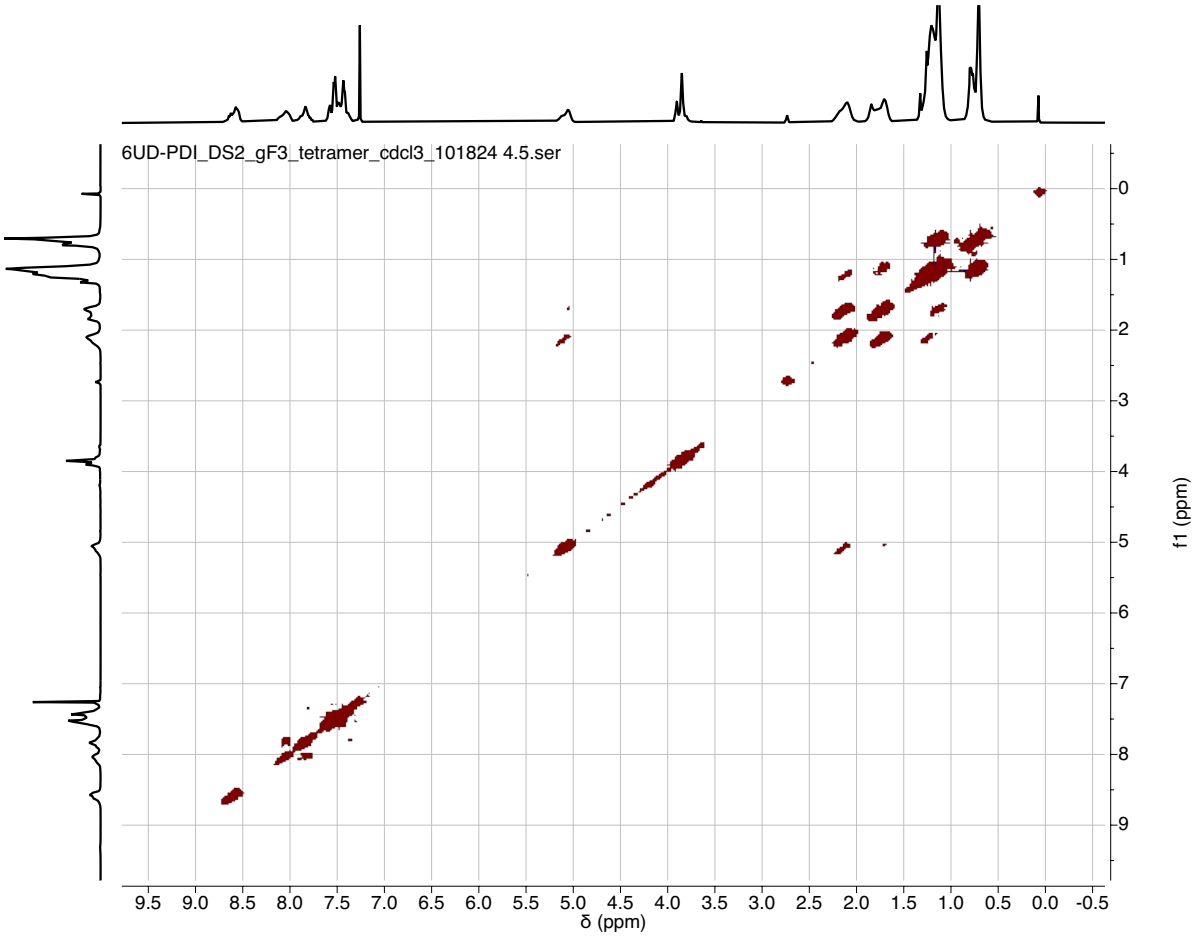

Figure S18. COSY NMR spectrum of L_4 in $CDCl_3$.

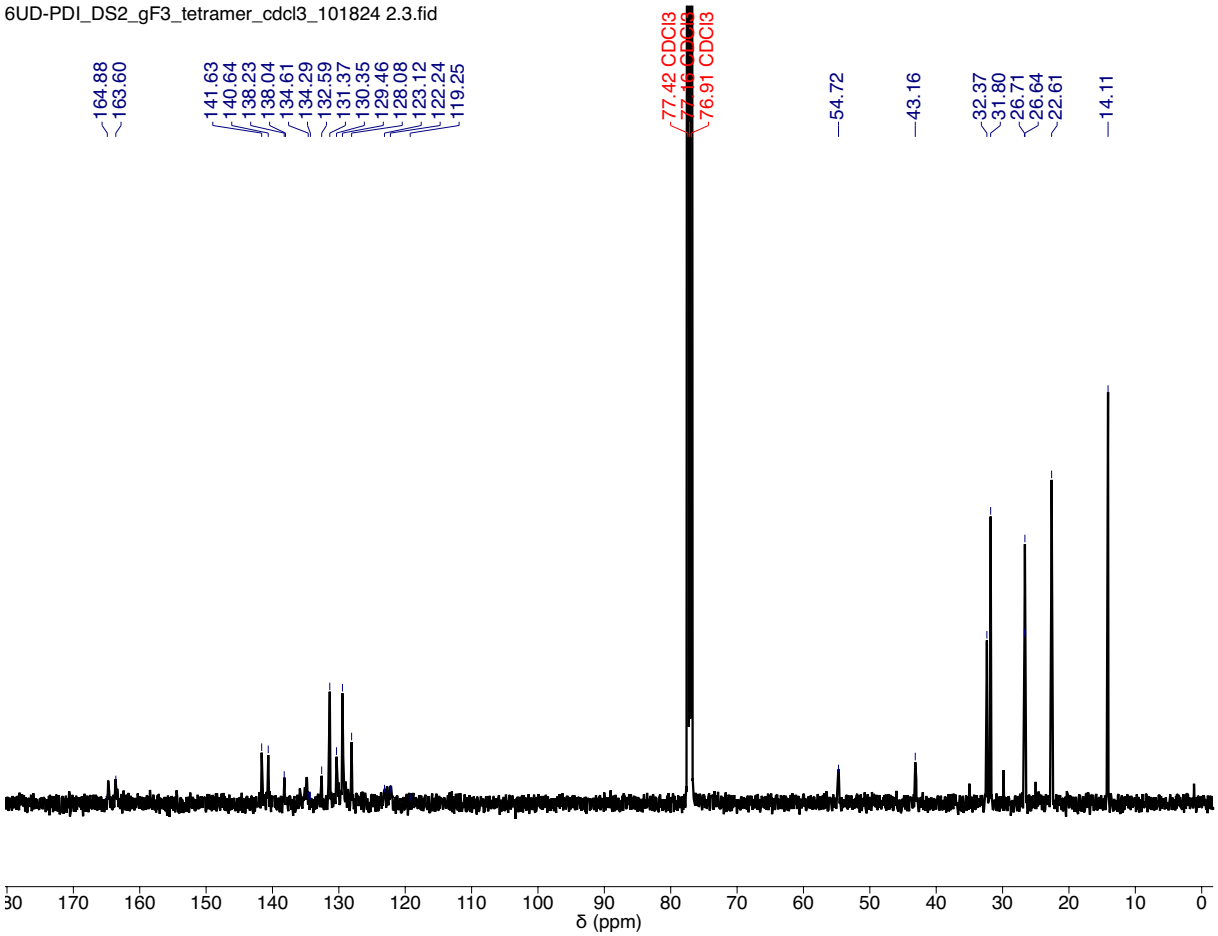

Figure S19. ^{13}C NMR spectrum of L_4 in $CDCl_3$.

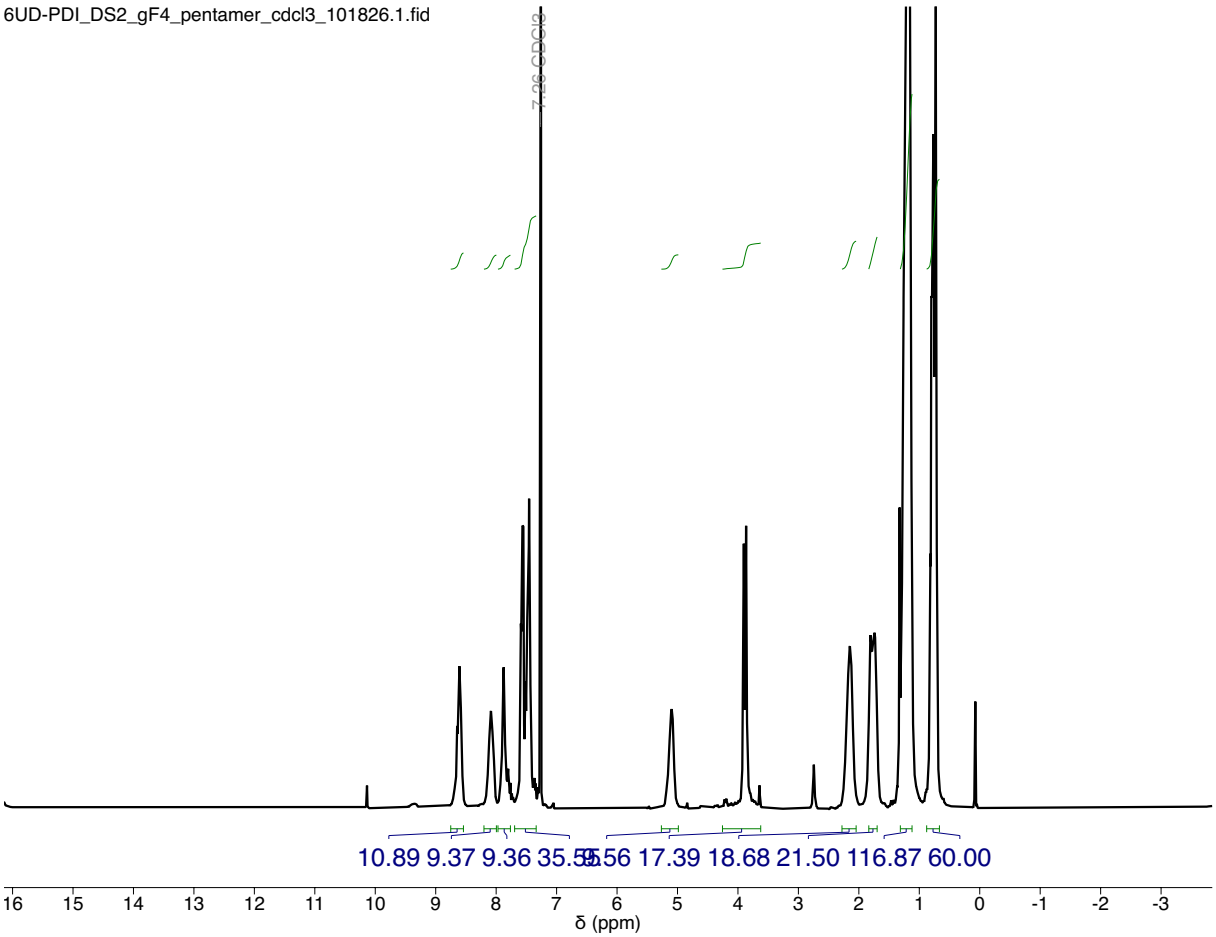

Figure S20. ^{1}H NMR spectrum of L_5 in $CDCl_3$.

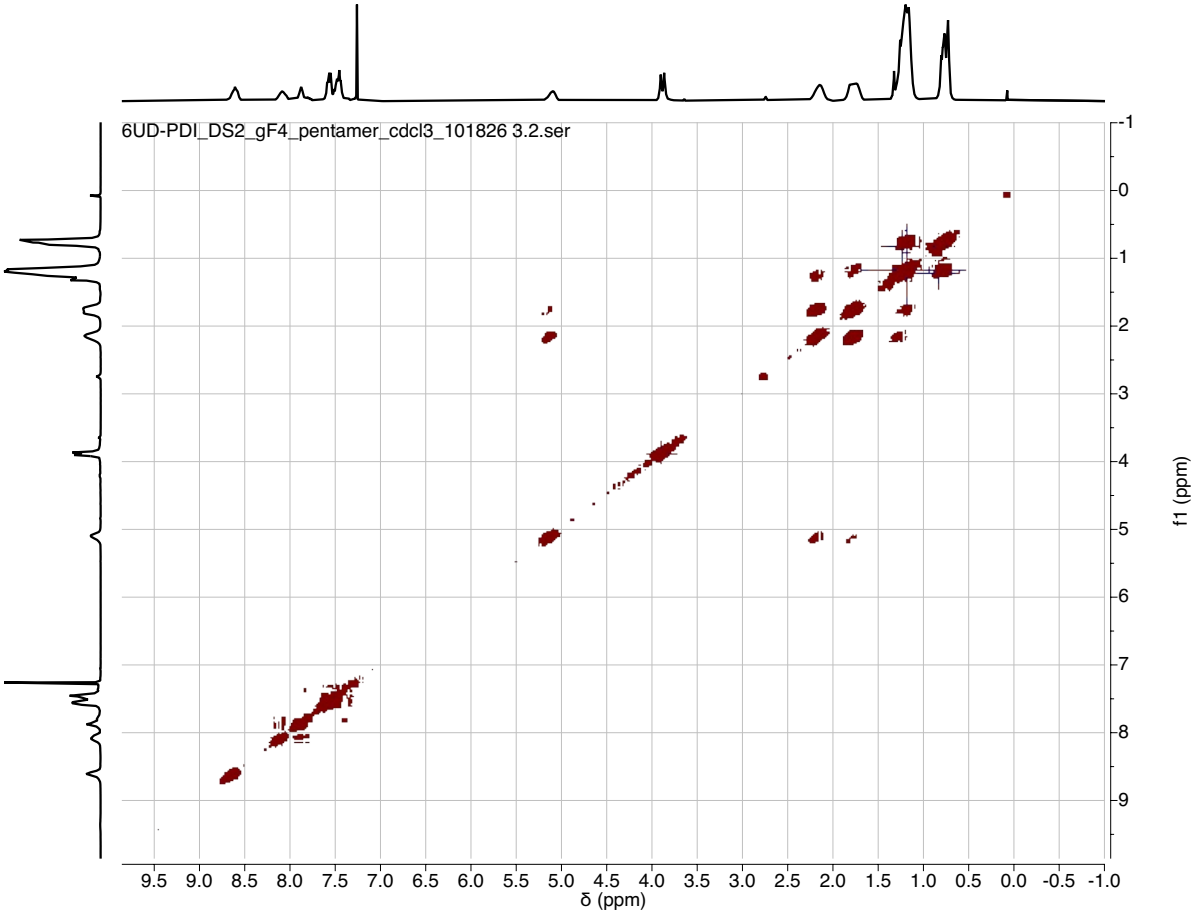

Figure S21. COSY NMR spectrum of L_5 in $CDCl_3$.

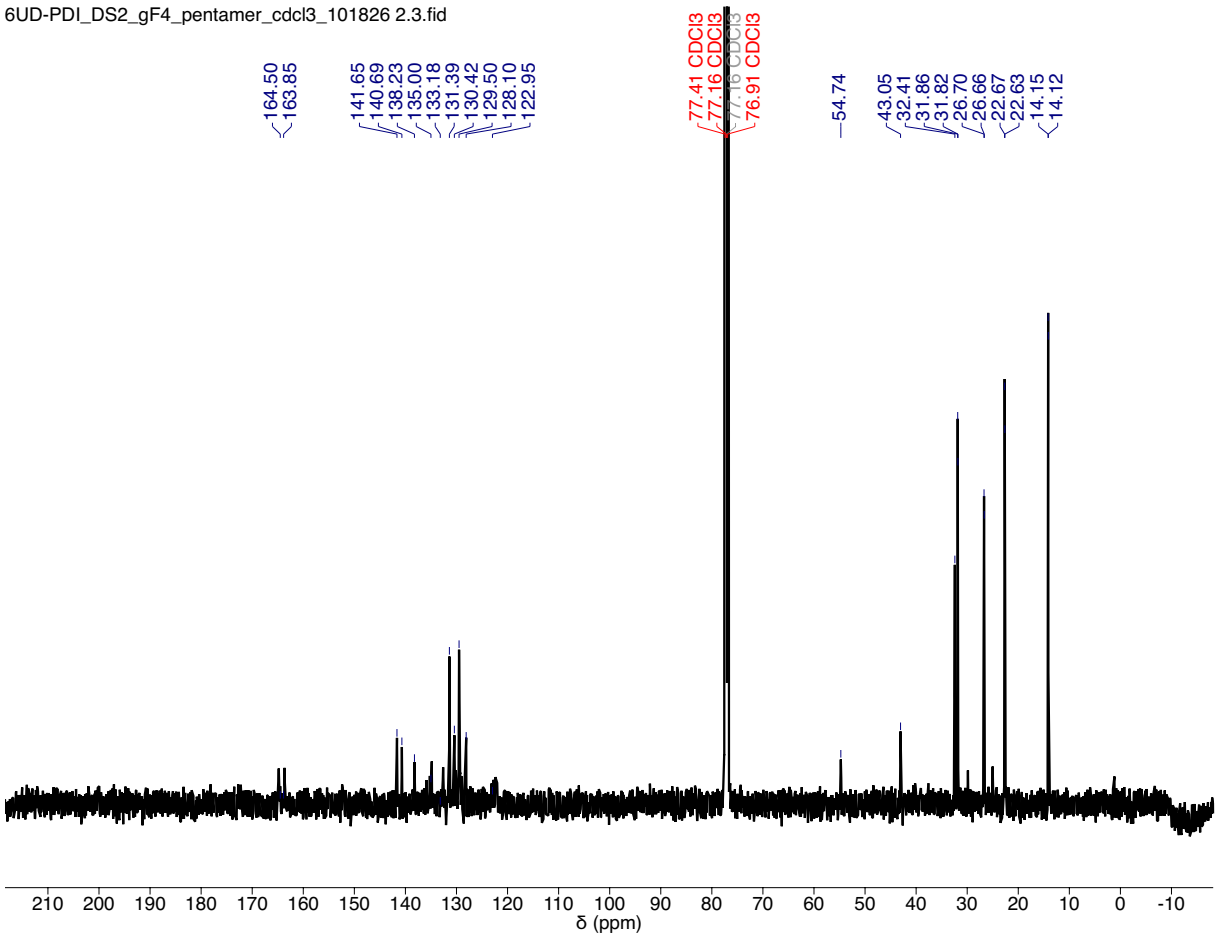

Figure S22. ^{13}C NMR spectrum of L_5 in $CDCl_3$.

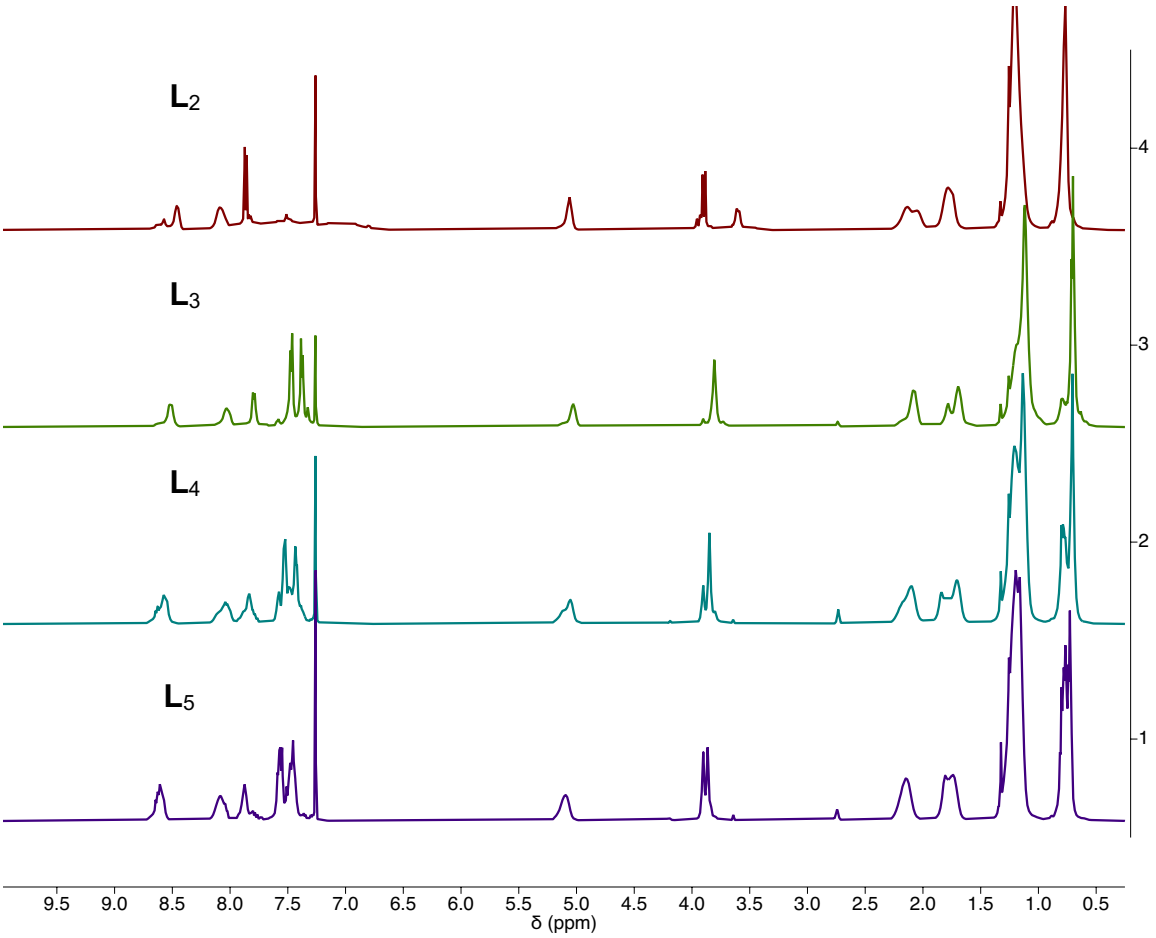

Figure S23. ^{1}H NMR spectra of L_2-L_5 in $CDCl_3$.

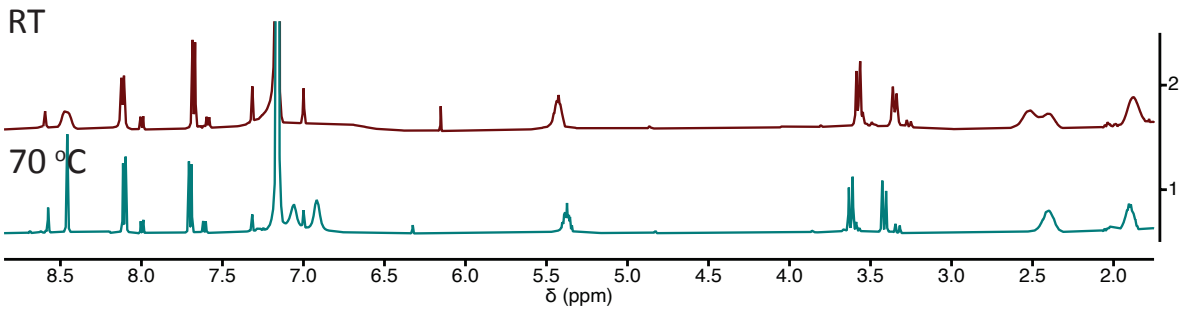

Figure S24. ^{1}H VT-NMR spectra of L_2 in C_6H_6 at room temperature and 70 ^{0}C. Broadened aryl peaks at 7 ppm sharpen at elevated temperature.

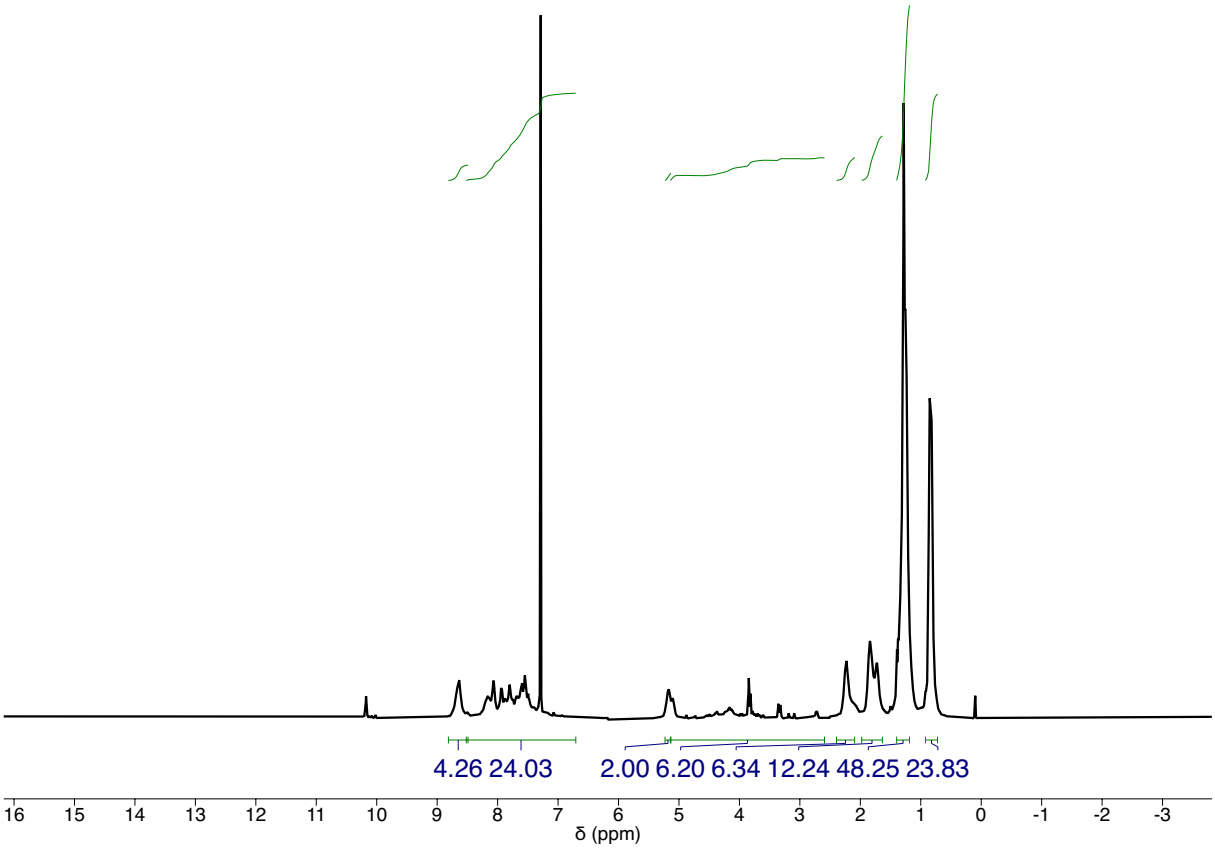

Figure S25. ^{1}H NMR spectrum of L'$_2$ in $CDCl_3$.

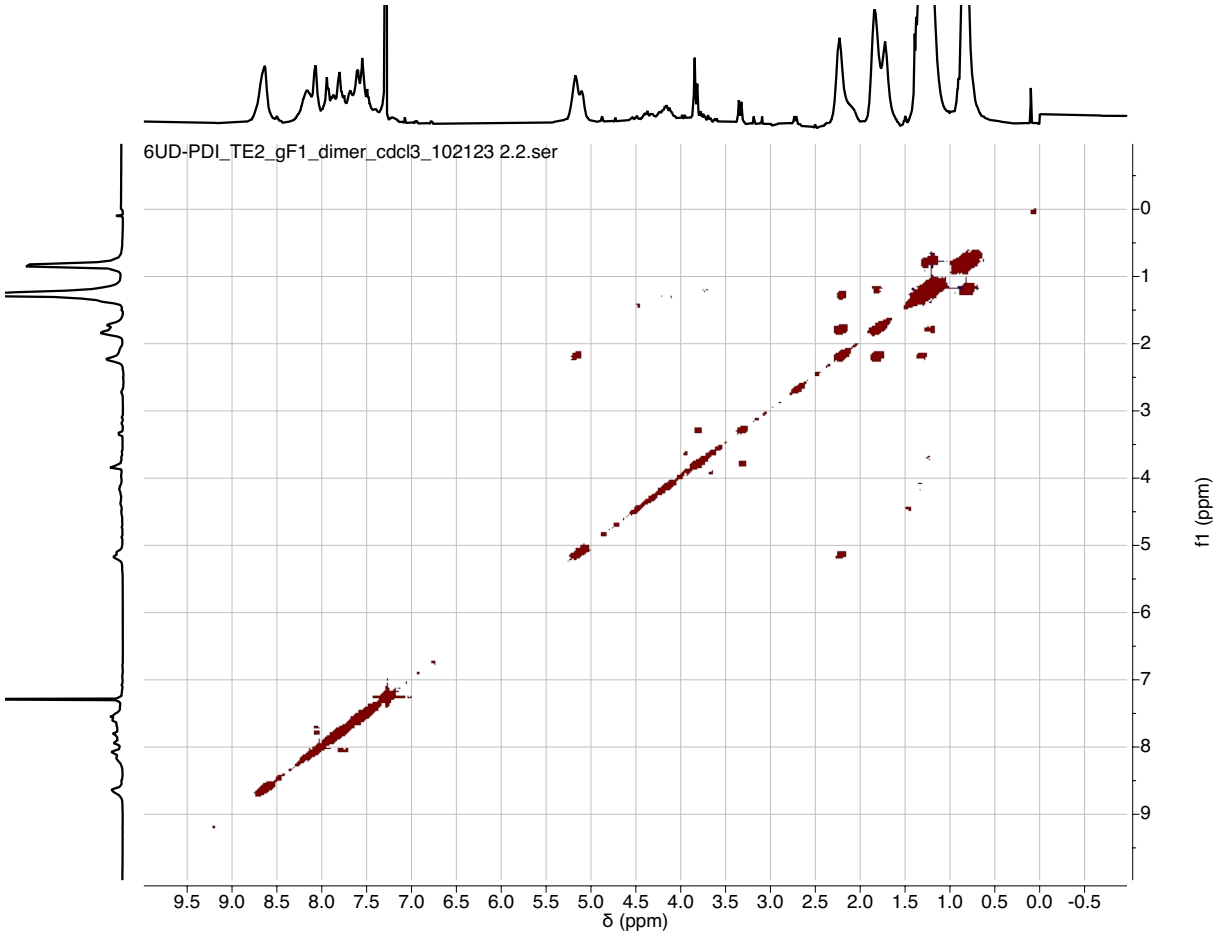

Figure S26. COSY NMR spectrum of L'_2 in $CDCl_3$.

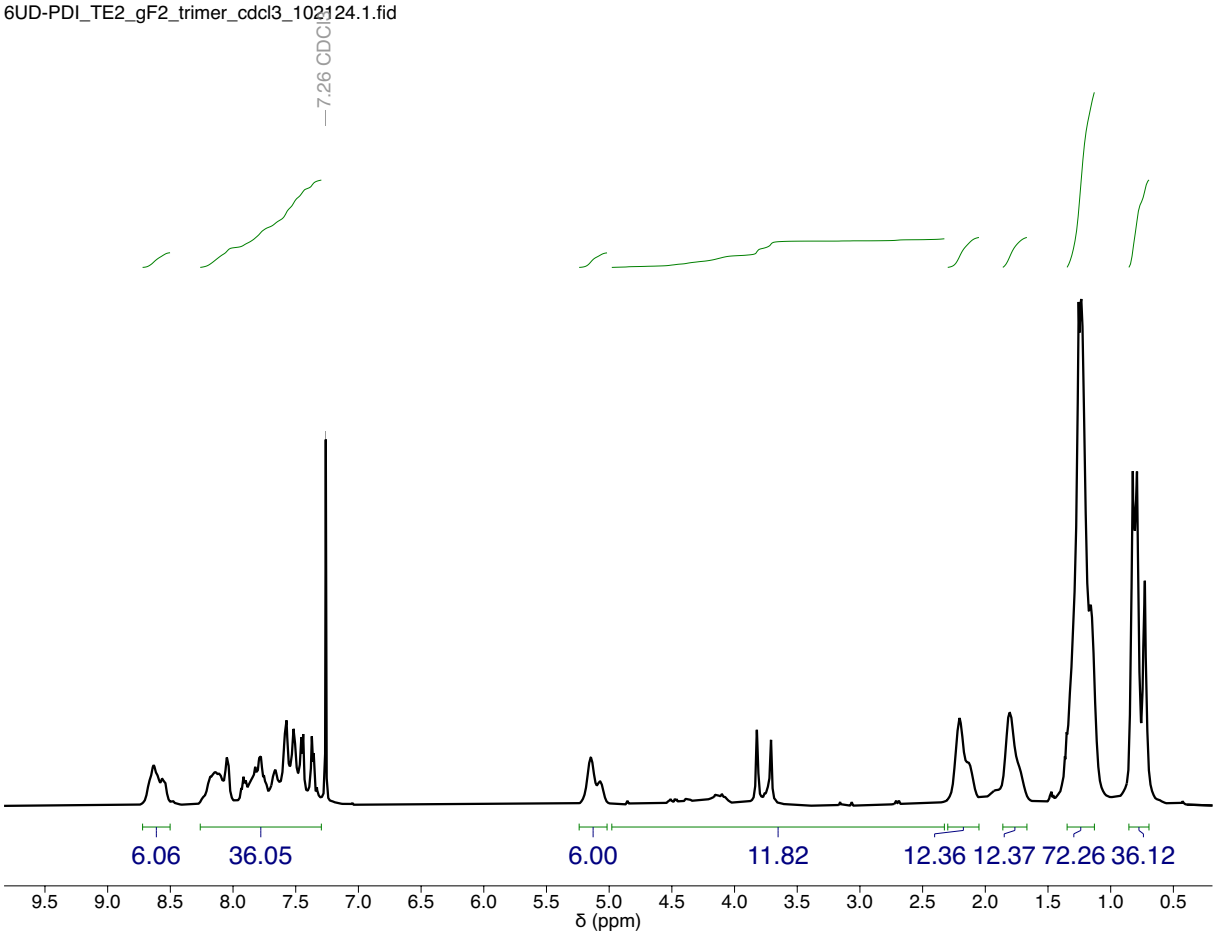

Figure S27. ^{1}H NMR spectrum of L'$_3$ in CDCl$_3$.

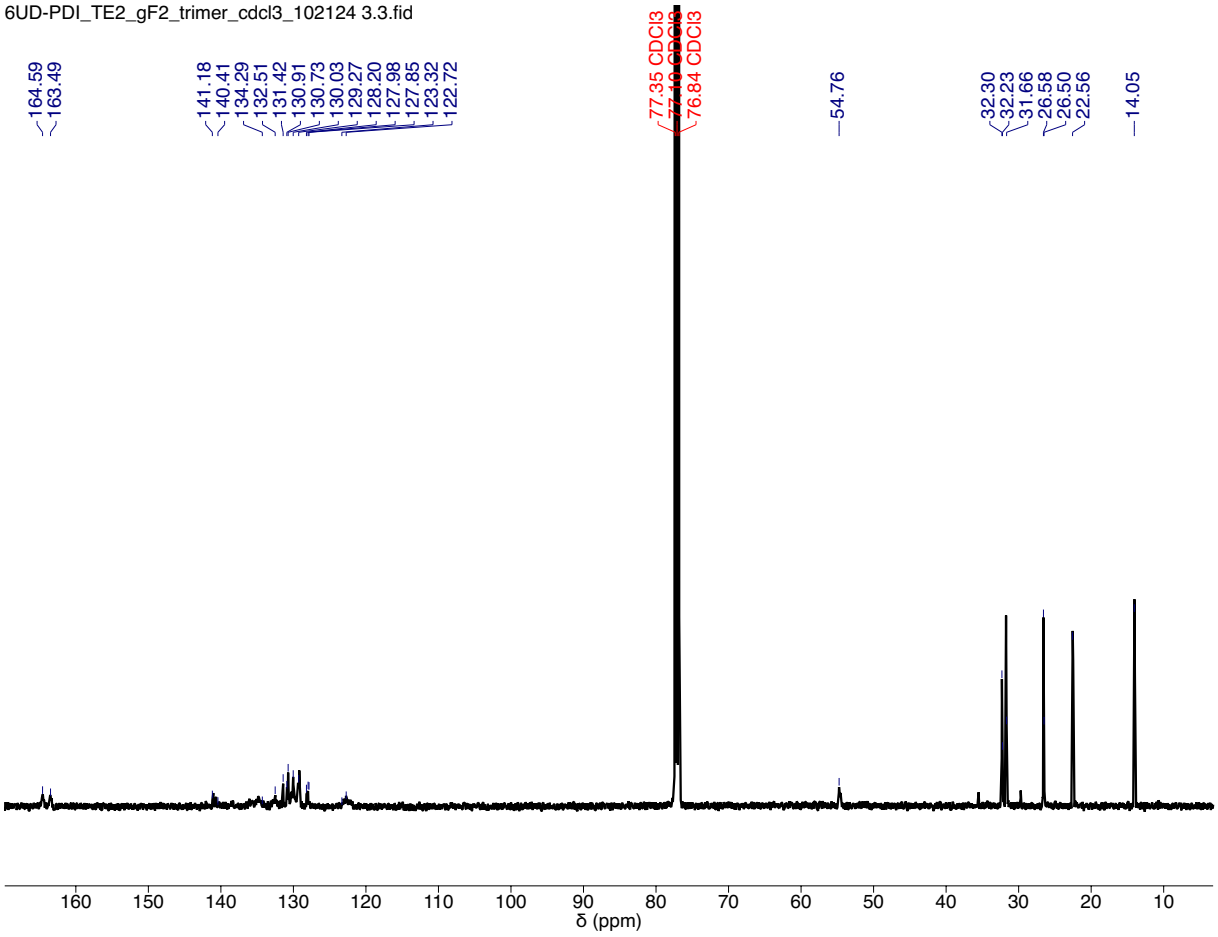

Figure S28. ^{13}C NMR spectrum of L'$_3$ in CDCl$_3$.

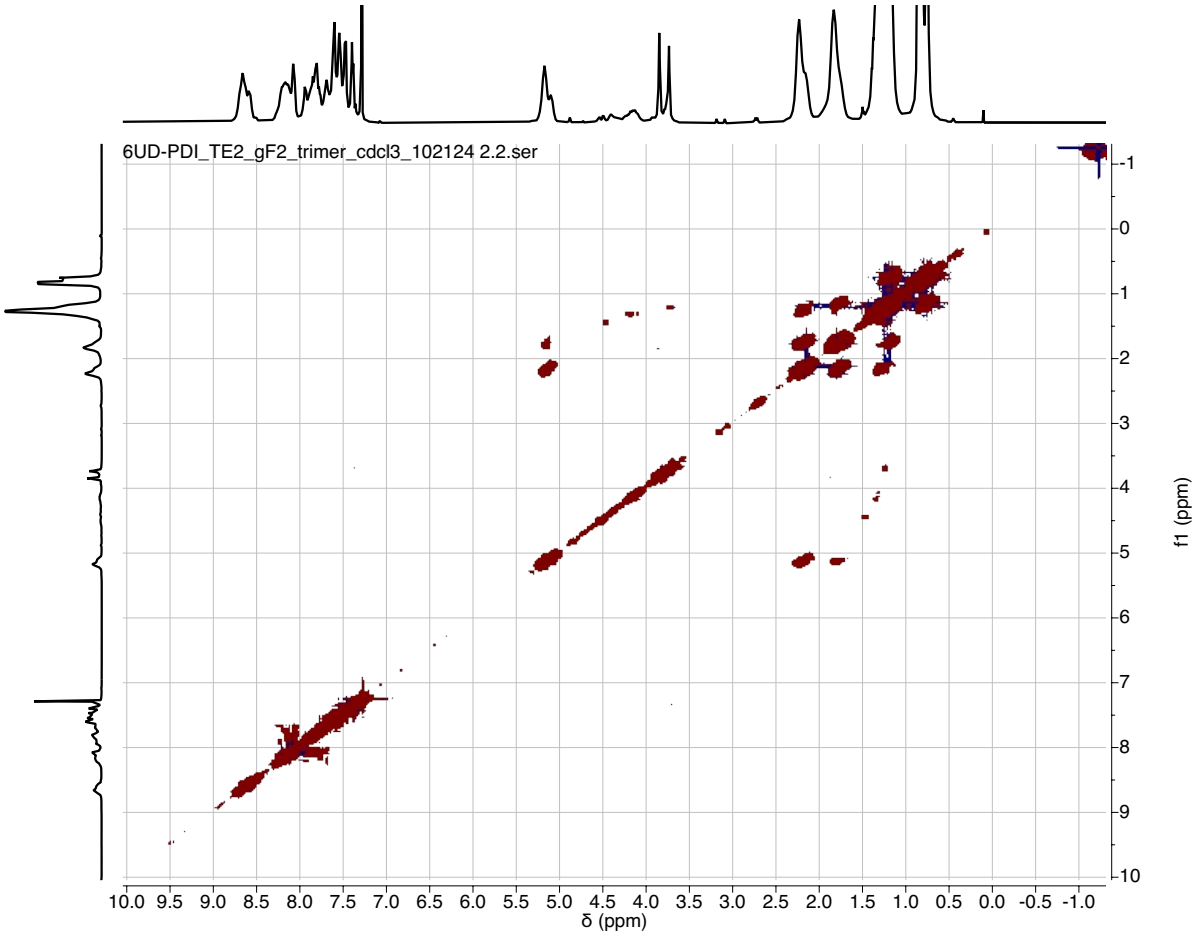

Figure S29. ^{13}C NMR spectrum of L'$_3$ in $CDCl_3$.

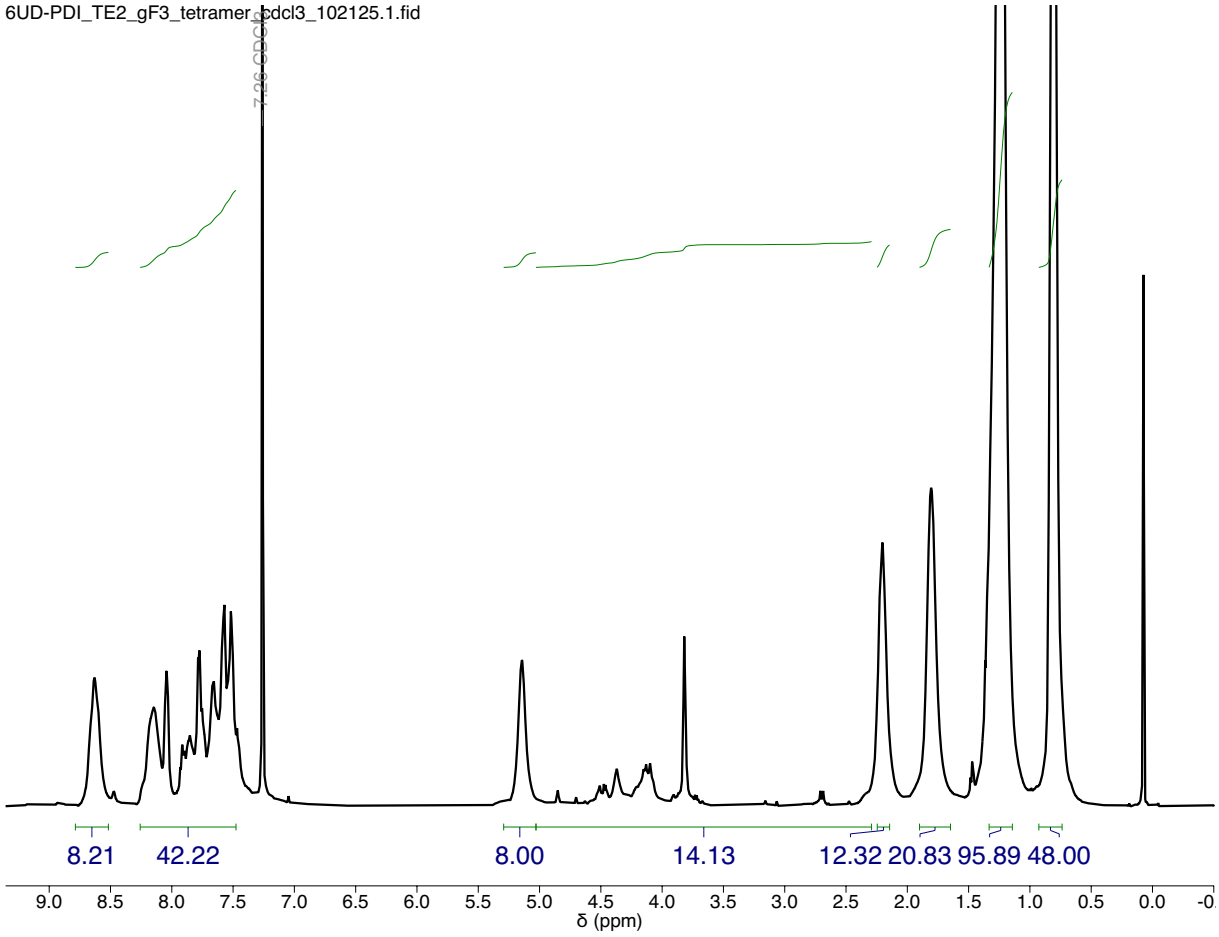

Figure S30. ^{1}H NMR spectrum of L'$_4$ in $CDCl_3$.

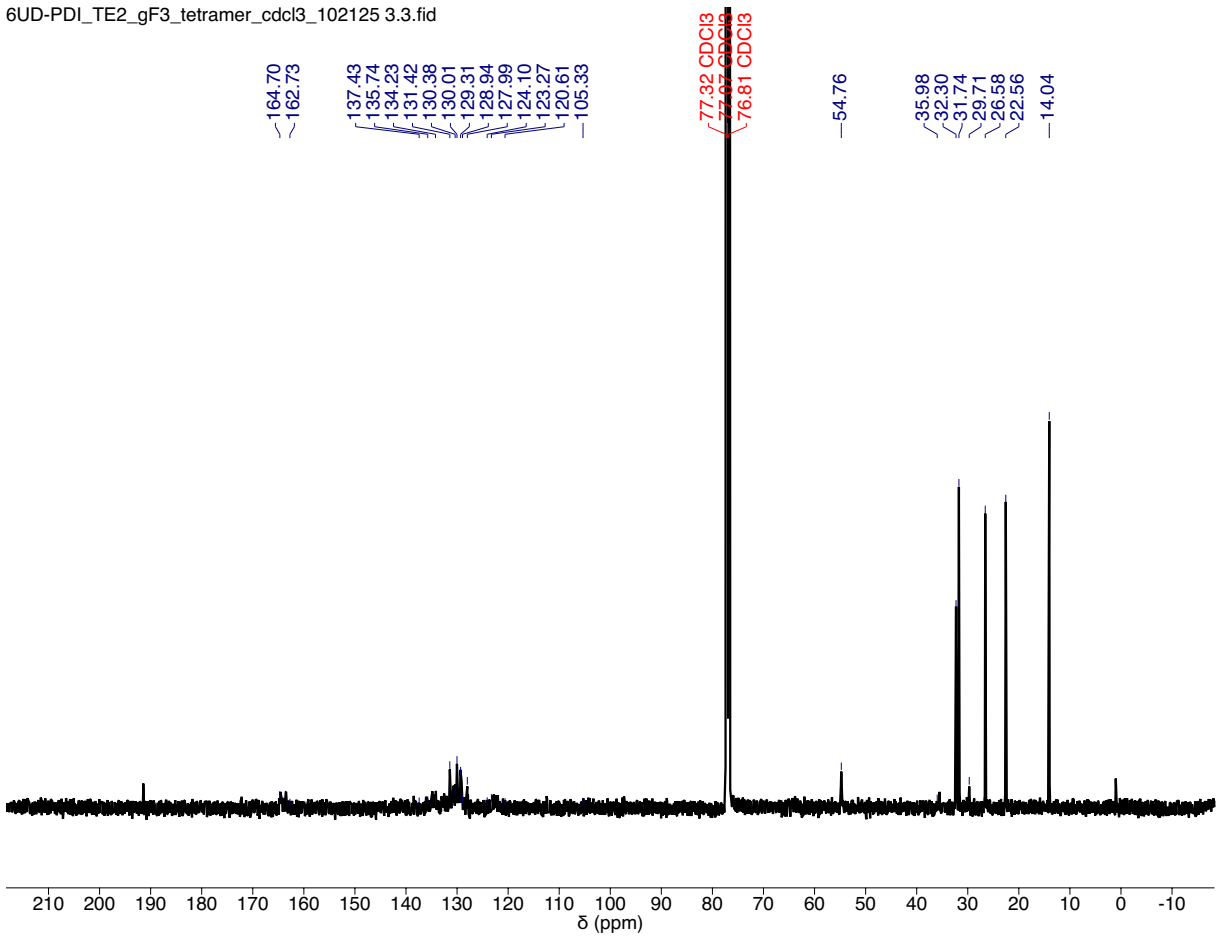

Figure S31. ^{13}C NMR spectra of L'_4 in $CDCl_3$.

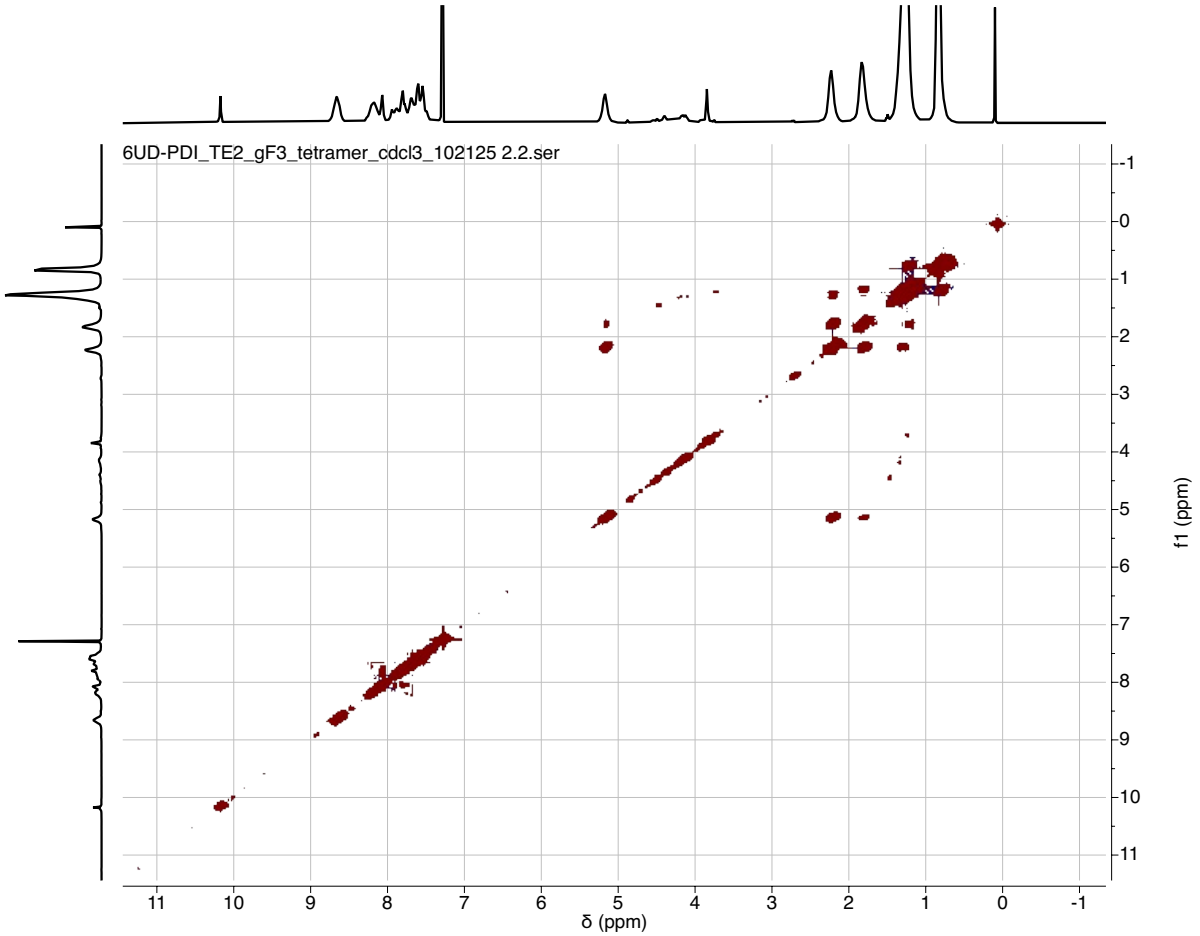

Figure S32. COSY NMR spectrum of L'_4 in $CDCl_3$.

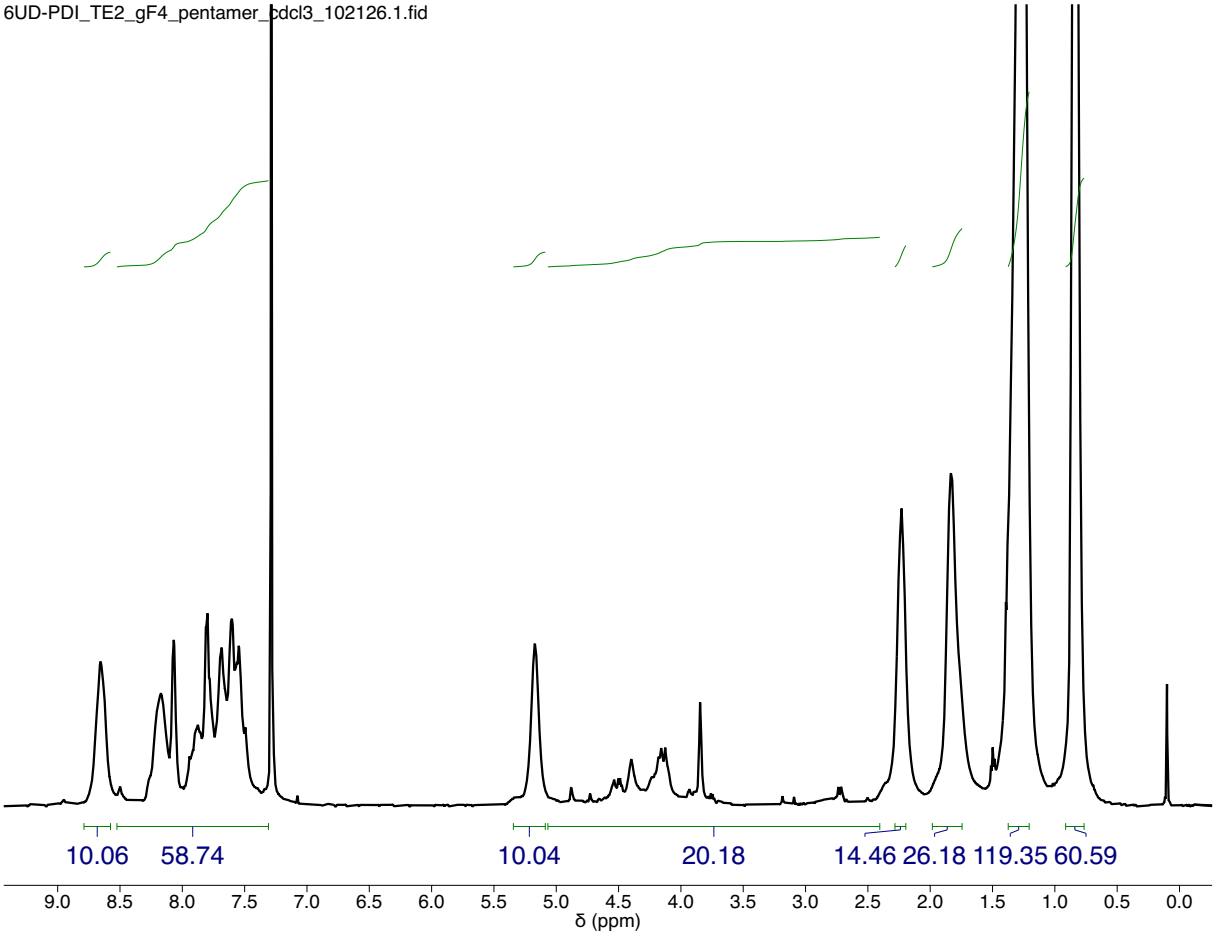

Figure S33. ^{1}H NMR spectrum of L'$_5$ in $CDCl_3$.

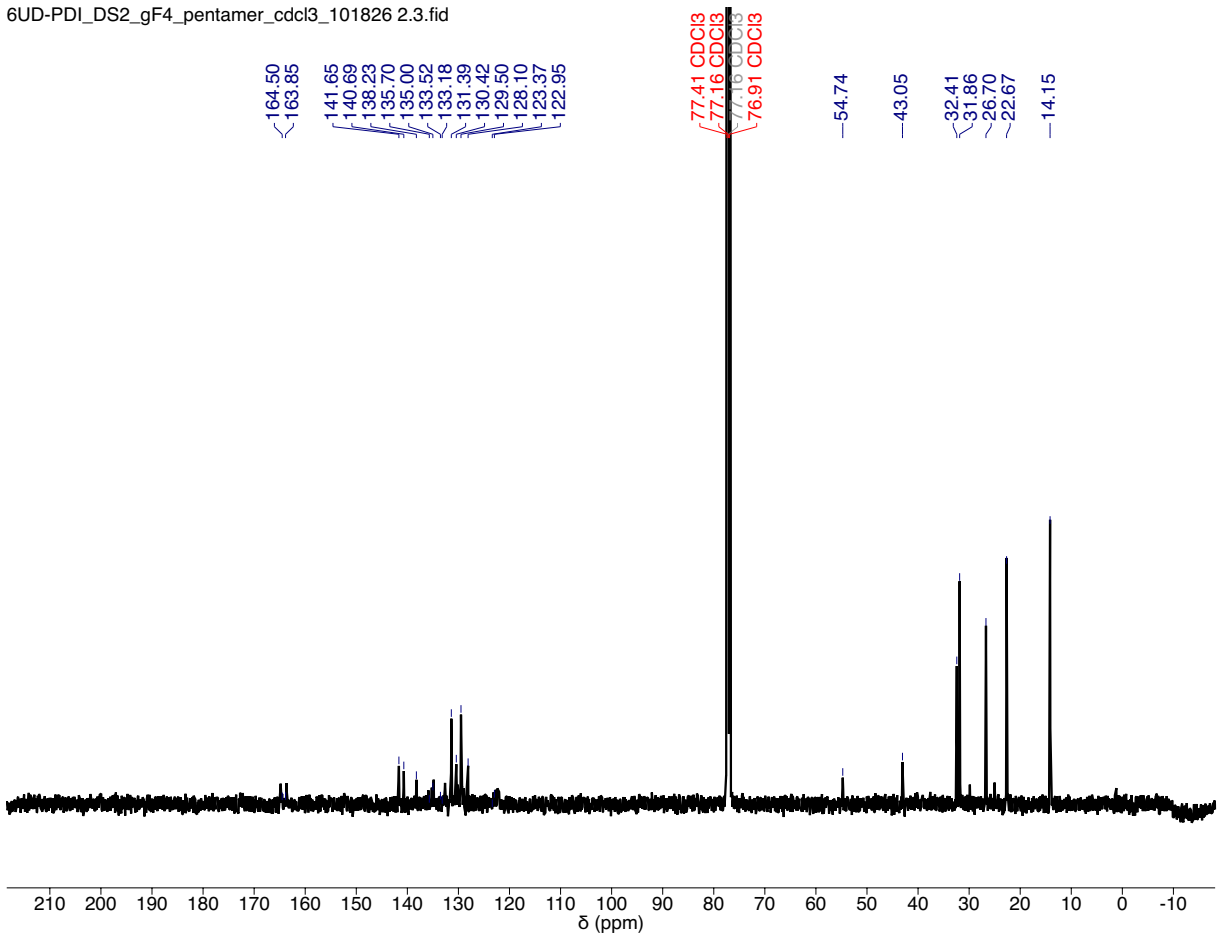

Figure S34. ^{13}C NMR spectra of L'$_5$ in $CDCl_3$.

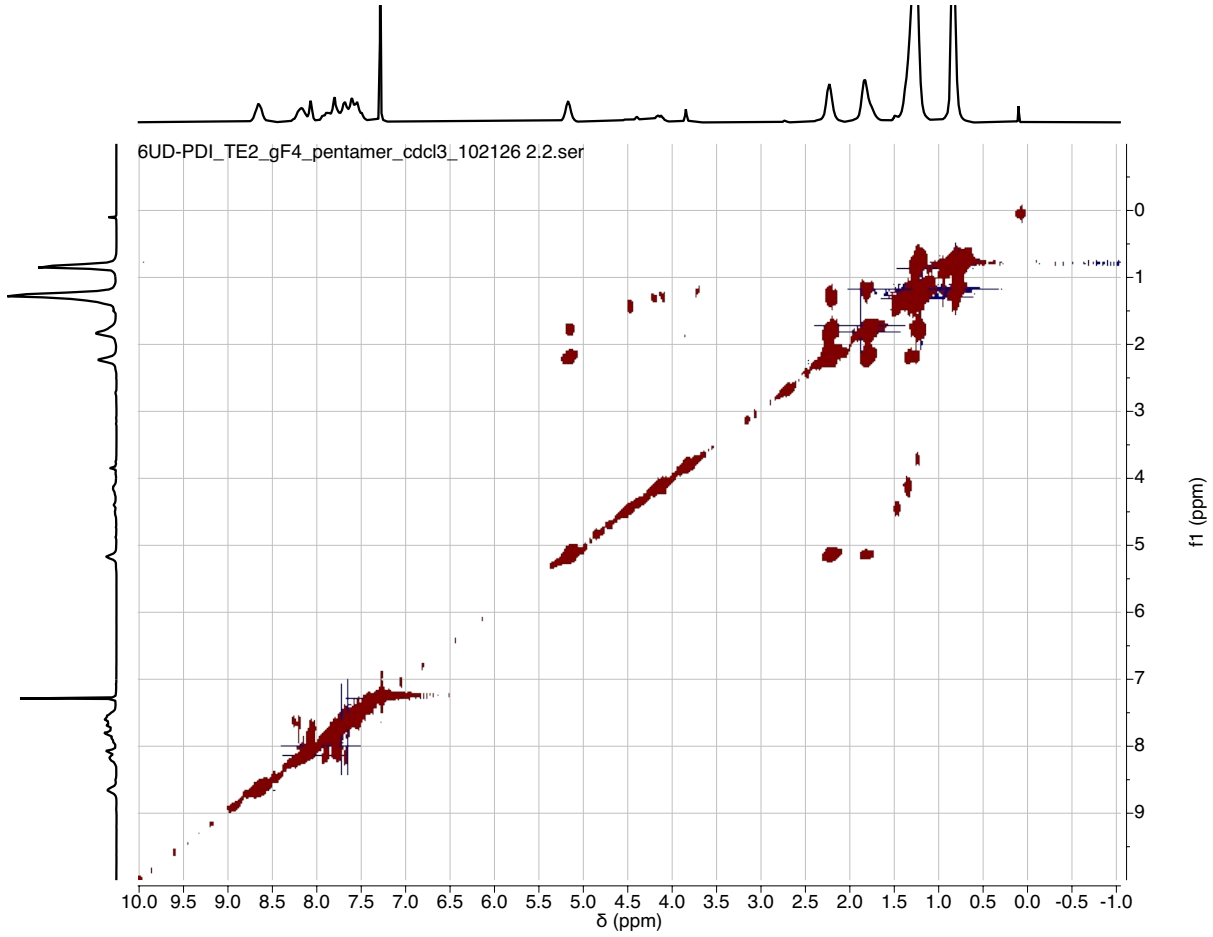

Figure S35. COSY NMR spectra of L'$_5$ in $CDCl_3$.

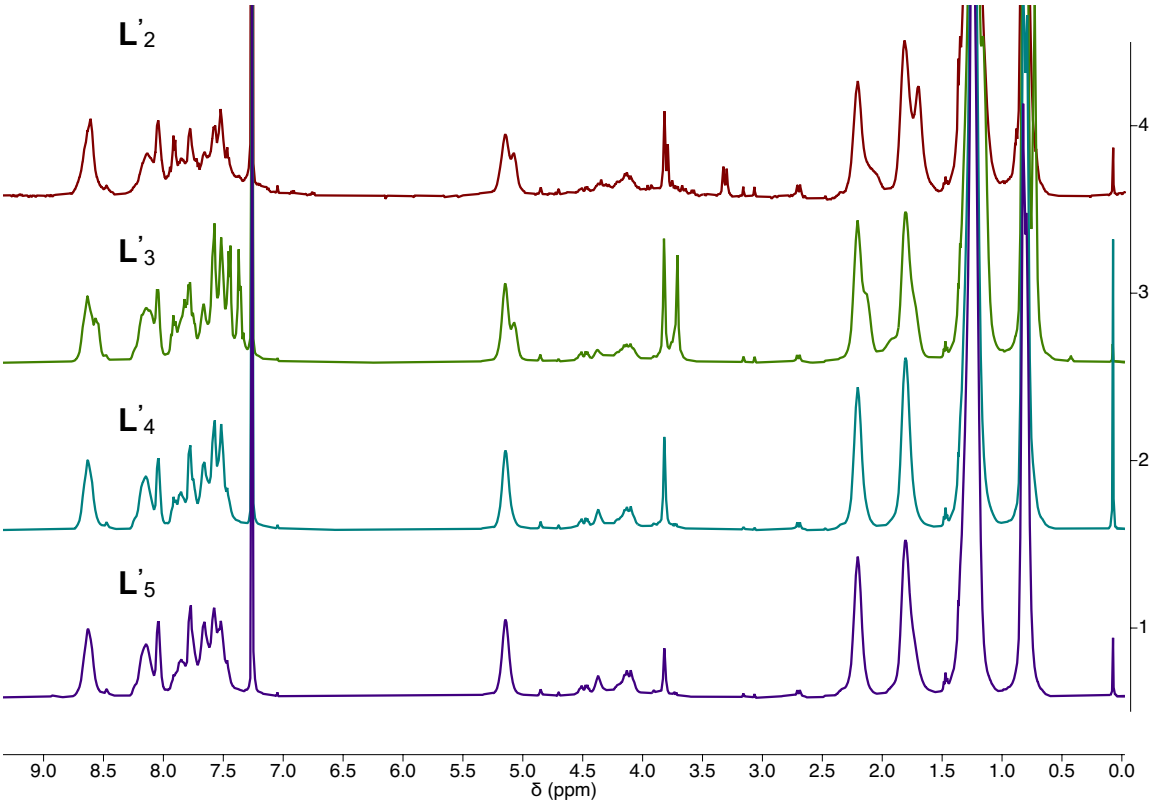

Figure S 36. ^{1}H NMR spectra of L'$_5$- L'$_2$

II. Mass Spectrometry Data

University of Illinois SCS Mass Spectrometry Laboratory

File: P-brombenylSTHP-HR
Sample:

Date Run: 10-31-2023 (Time Run: 09:48:58)

Ionization mode: EI+
Instrument: VG 70-VSE(A)

Scan: 12-18

Base: m/z 281; 12.2%FS

Selected Isotopes : C H O_{0-1} N_{0-1} Br_{0-1} S_{0-1}

Error Limit : 5 ppm

Unsaturation Limits : -.5 to 50

Measured Mass	*% Base*	*Formula*	*Calculated Mass*	*Error*	*Unsaturation*
286.00193	57.0%	$C_{12}H_{15}OBrS$	286.00270	-2.7	5.0

Figure S37. Mass spectrometry data of 4-bromobenzylSTHP.

Elemental Composition Report **Page 1**

Single Mass Analysis
Tolerance = 5.0 PPM / DBE: min = -1.5, max = 200.0
Element prediction: Off
Number of isotope peaks used for i-FIT = 9

Monoisotopic Mass, Even Electron Ions
25 formula(e) evaluated with 1 results within limits (up to 50 closest results for each mass)
Elements Used:
C: 0-50 H: 0-60 O: 0-5 S: 1-1 B: 1-1

Order#- Jacob Mayhugh p-b(pin)THPsulfide
Synapt2_17887a 19 (0.397) Cm (17:22-3:7)

MSL, SCS, UIUC

SYNAPTG2-Si#UGA354
1: TOF MS ES+
3.63e+004

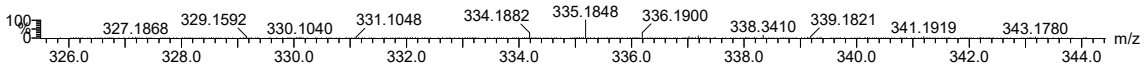

Minimum:				-1.5				
Maximum:		5.0	5.0	200.0				
Mass	Calc. Mass	mDa	PPM	DBE	i-FIT	Norm	Conf(%)	Formula
335.1848	335.1852	-0.4	-1.2	5.5	1552.7	n/a	n/a	C18 H28 O3 S B

Figure S38. Mass spectrometry data of 4-B(pin)benzylSTHP.

D:\All User Data\Mass Spec Users\Data_2023\Order13144_PDI_Suzuki_HR\0_P23\1\1Ref

Comment 1 Mayhugh, Jacob
Comment 2 DCTB

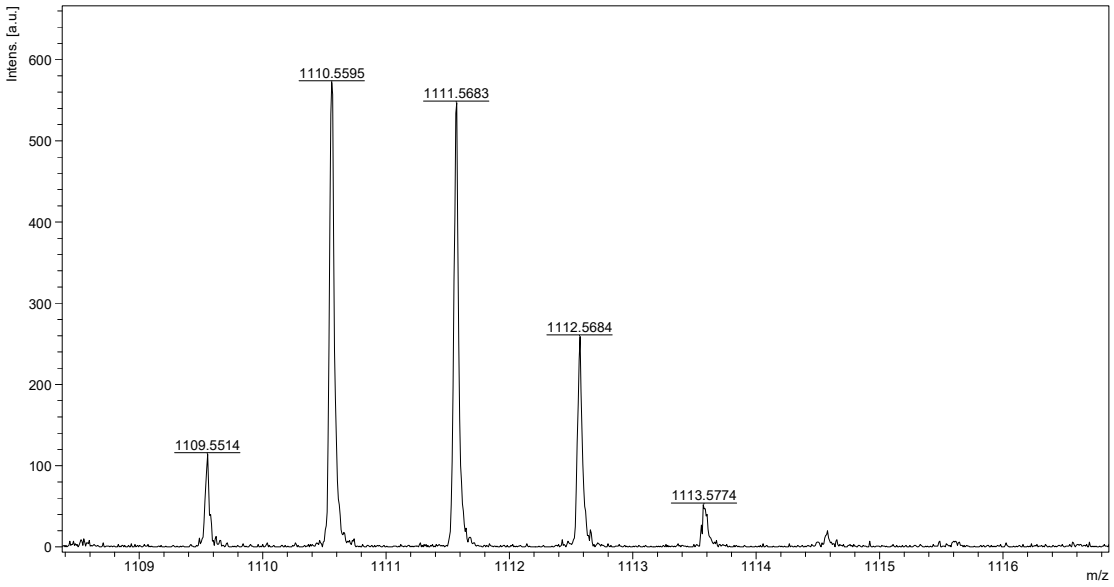

printed: 10/30/2023 11:34:36

Figure S39. Mass spectrometry data of SI-1.

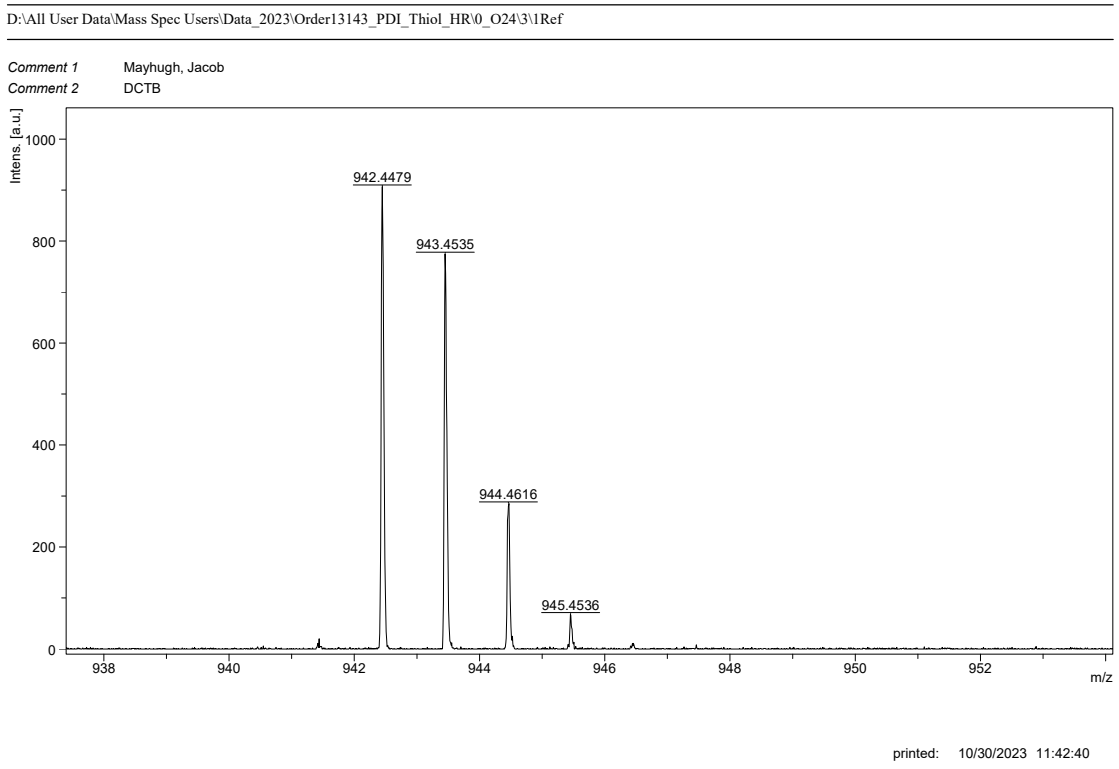

Figure S40. Mass spectrometry data of H_2L.

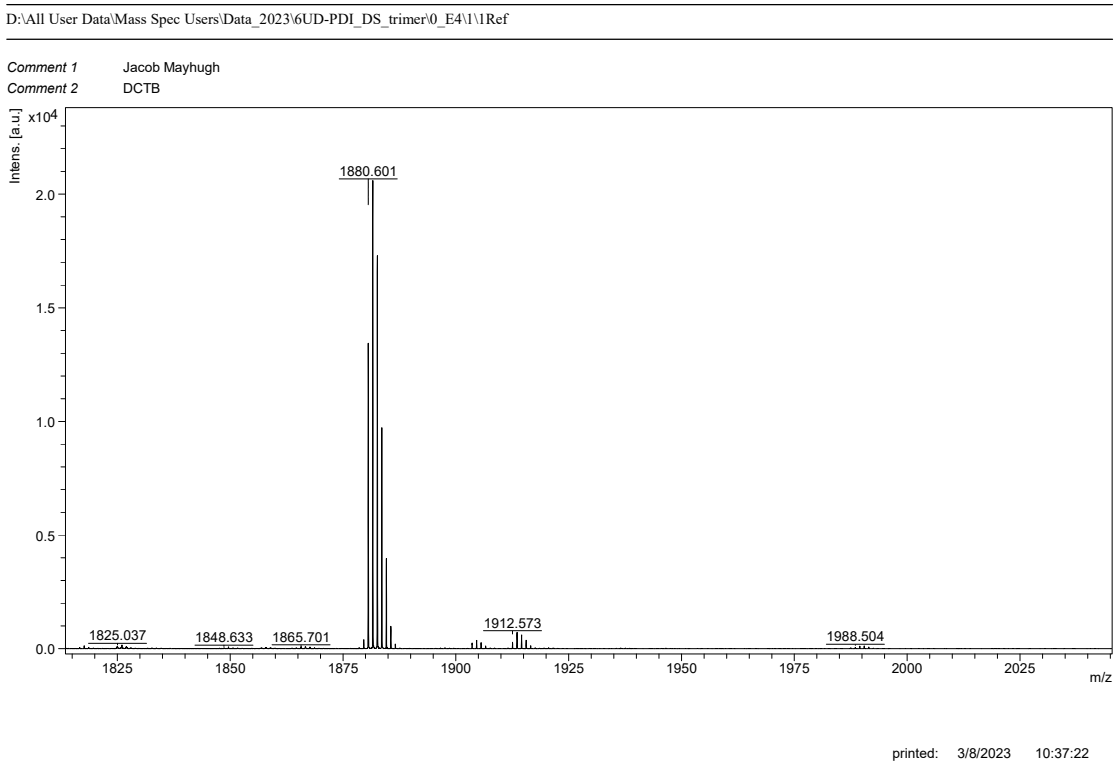

Figure S41. Mass spectrometry data of L_2.

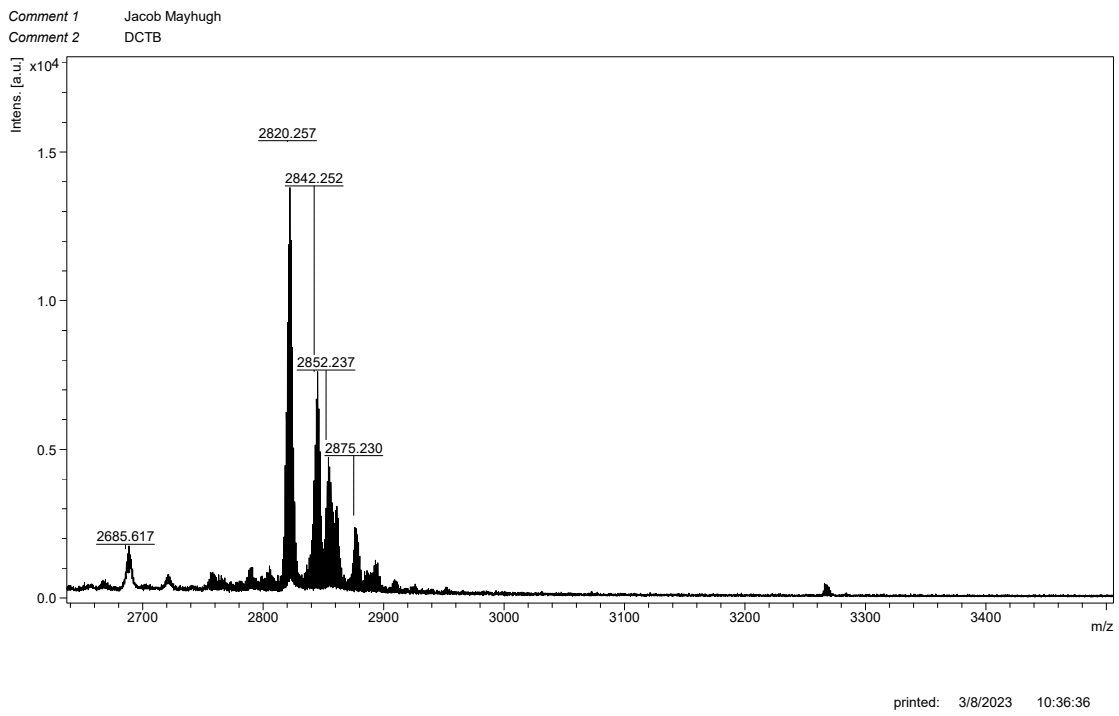

Figure S42. Mass spectrometry data of L_3.

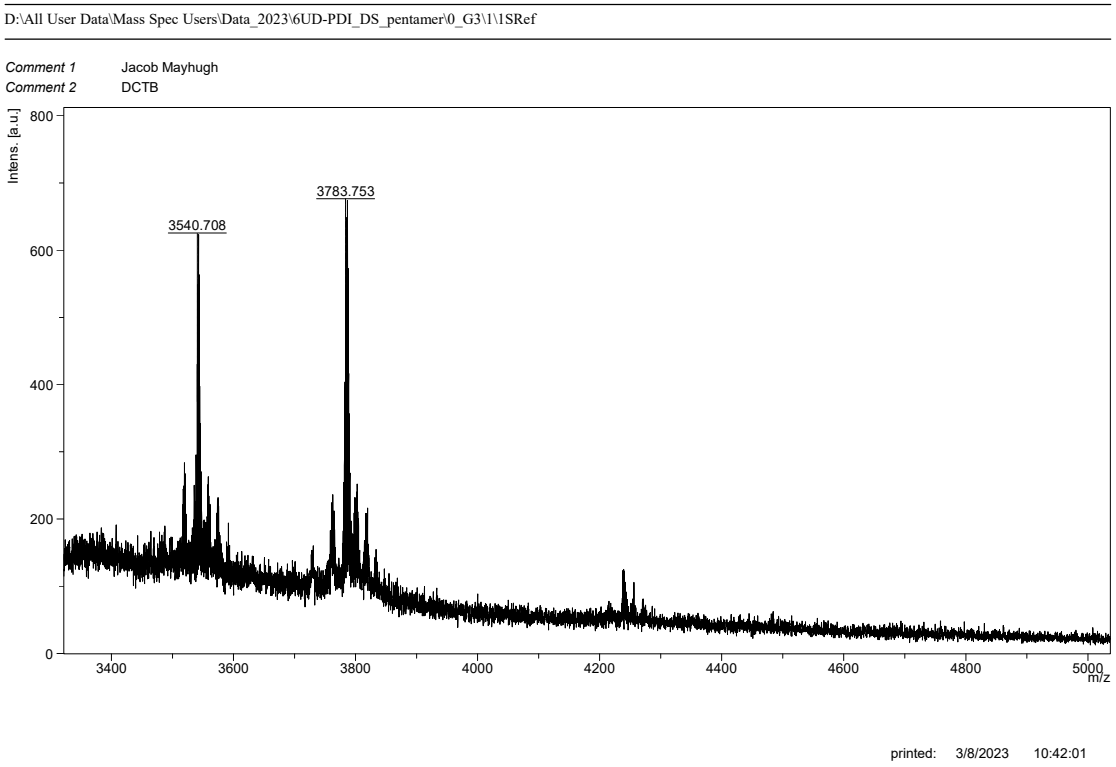

Figure S43. Mass spectrometry data of L_4.

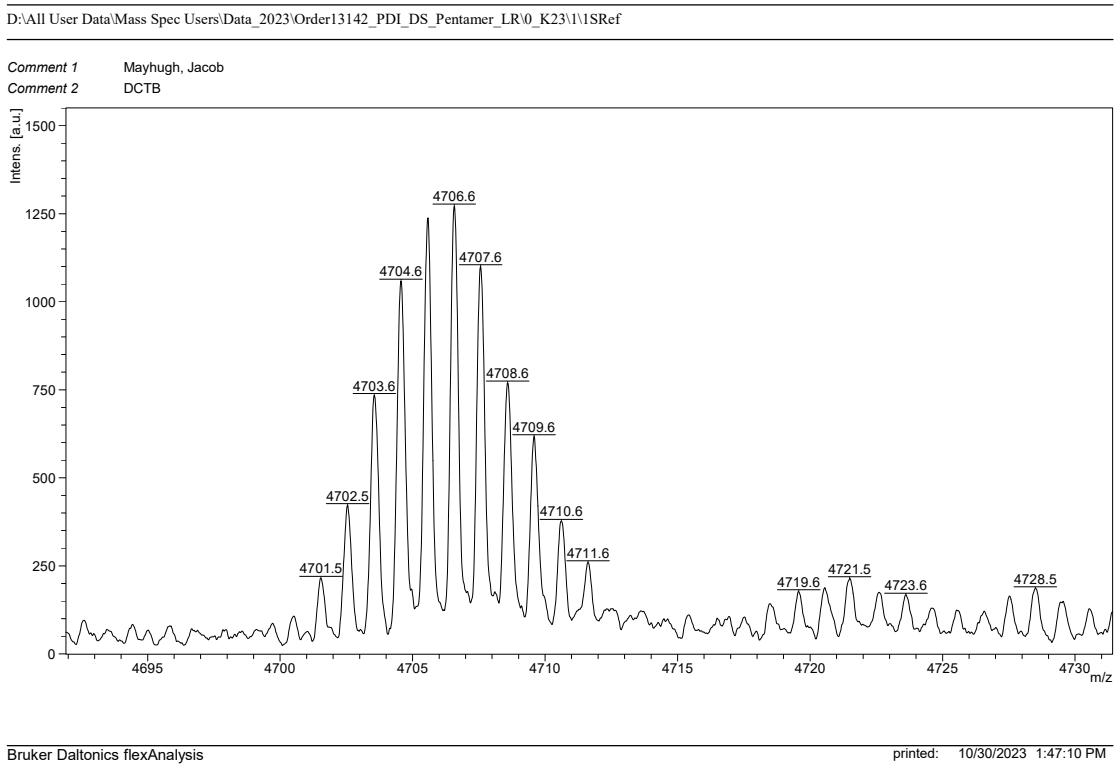

Figure S44. Mass spectrometry data of L_5.

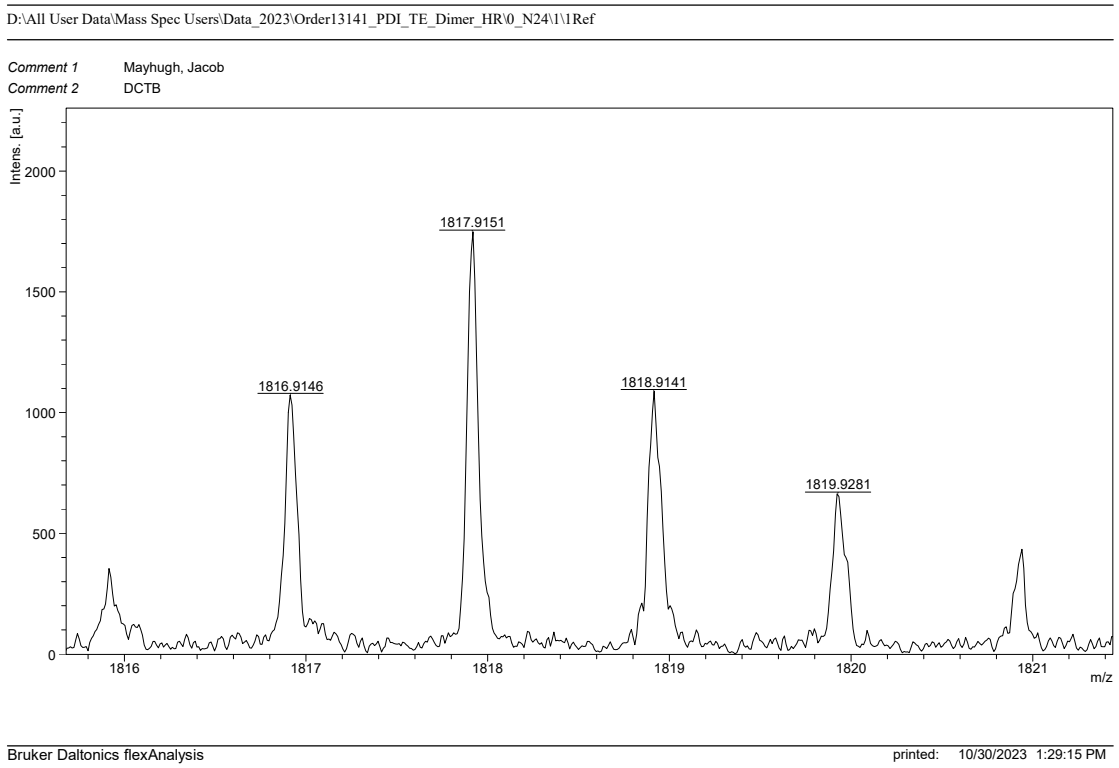

Figure S45. Mass spectrometry data of L'$_2$.

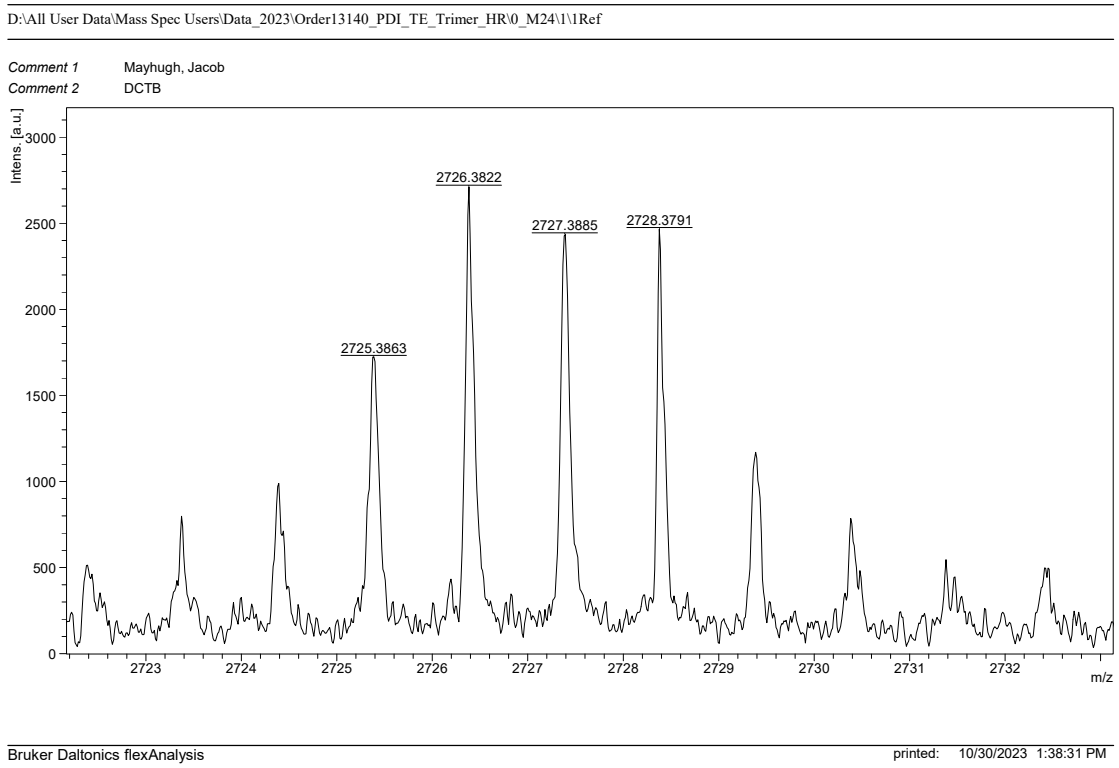

Figure S46. Mass spectrometry data of L'$_3$.

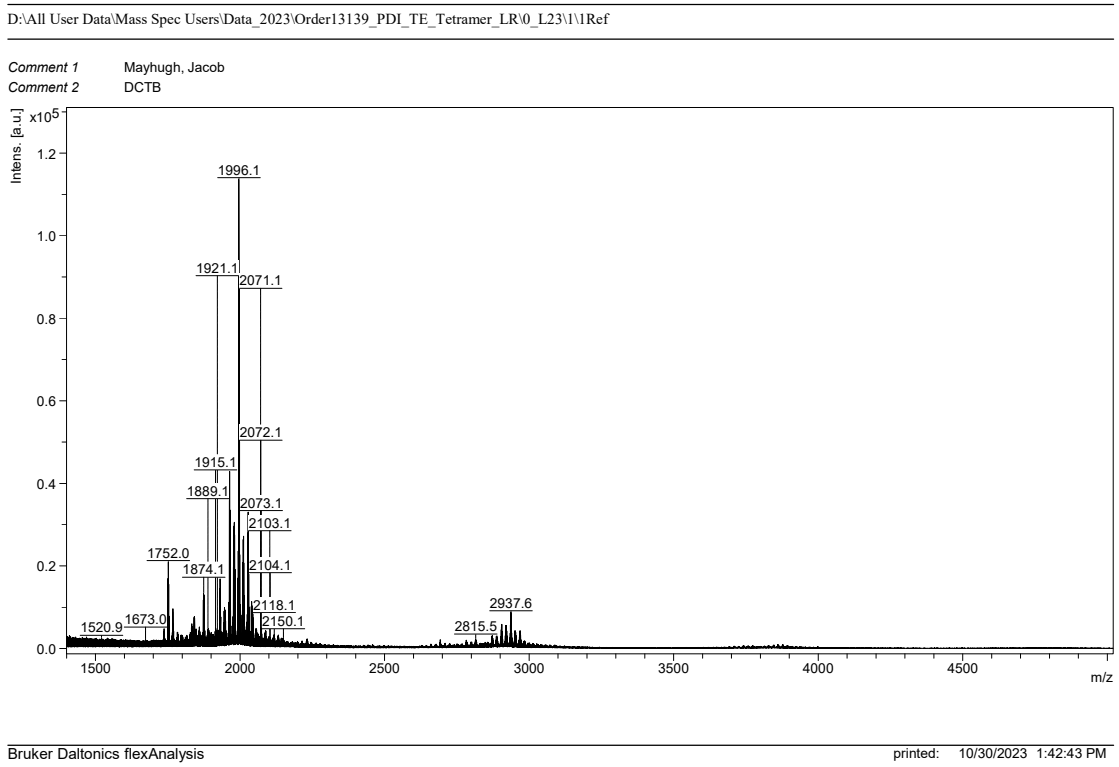

Figure S47. Mass spectrometry data of L'$_4$.

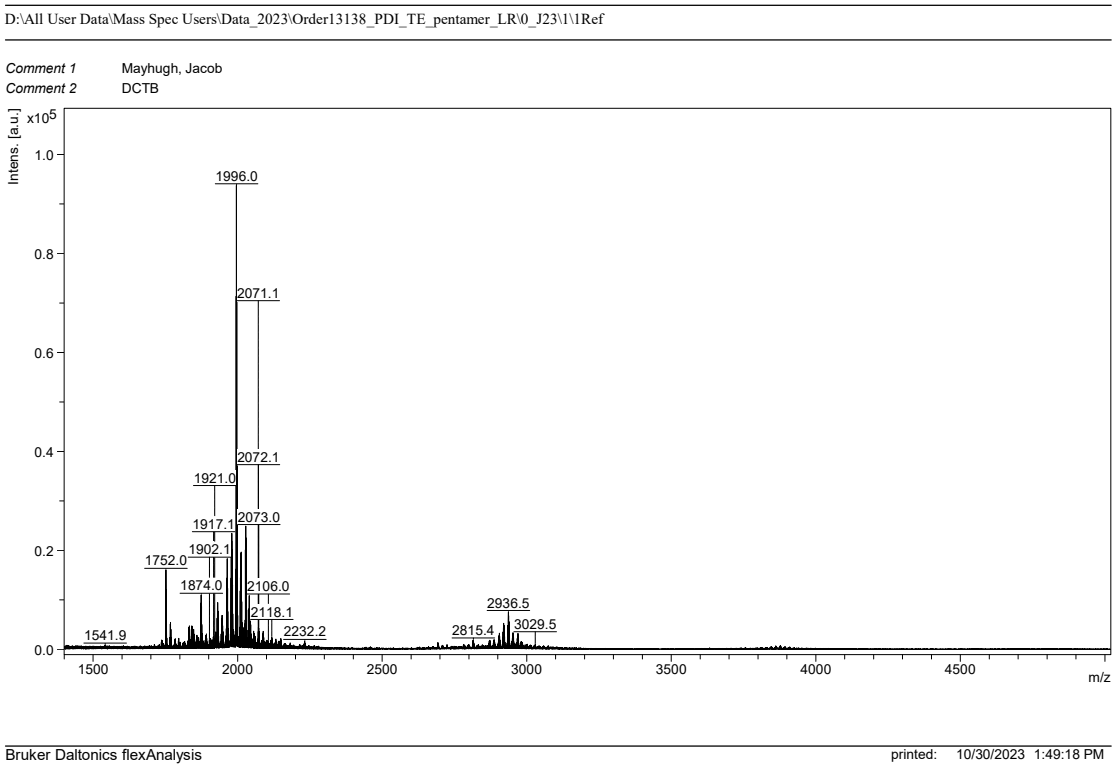

Figure S48. Mass spectrometry data of L'$_5$.

III. GPC Traces of Disulfide- and Sulfide-linked PDI macrocycles

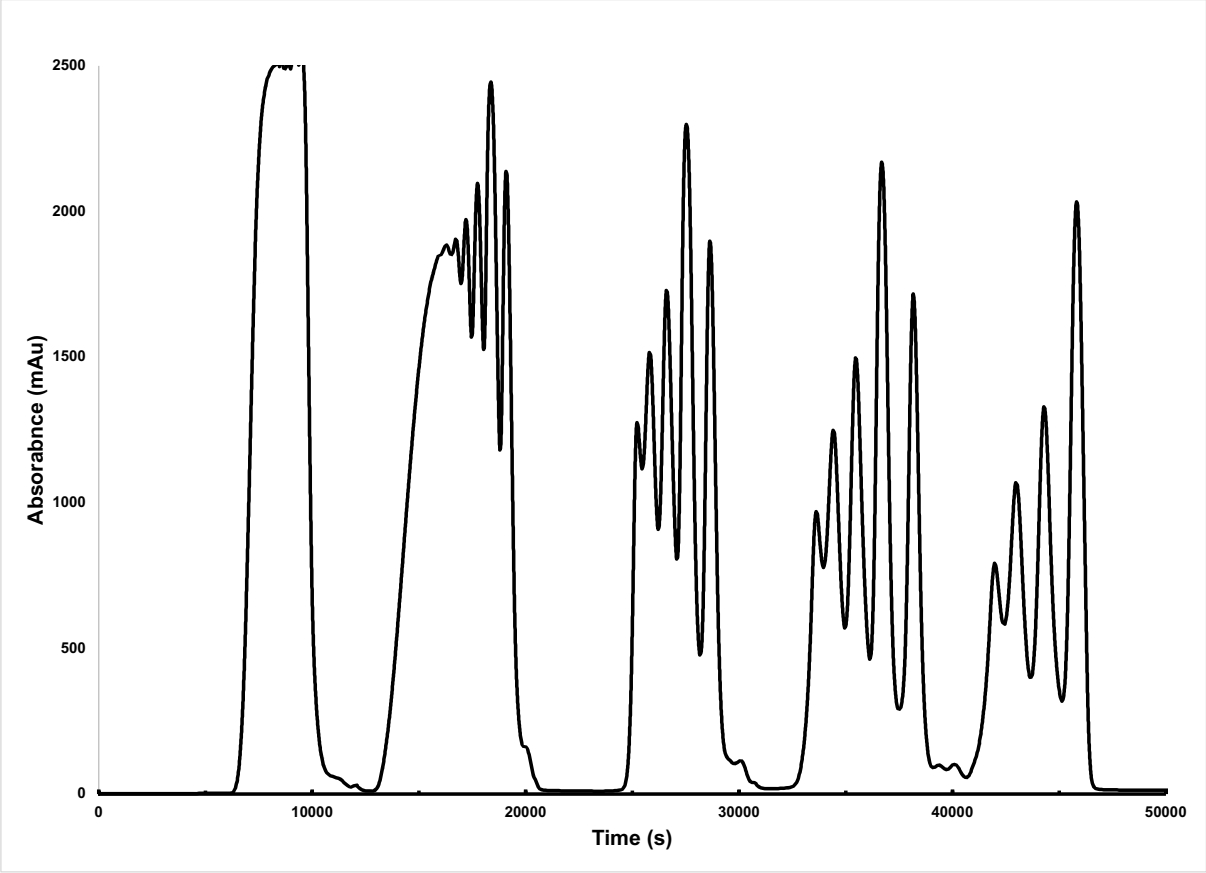

Figure S49. GPC Chromatogram of L_2-L_5.

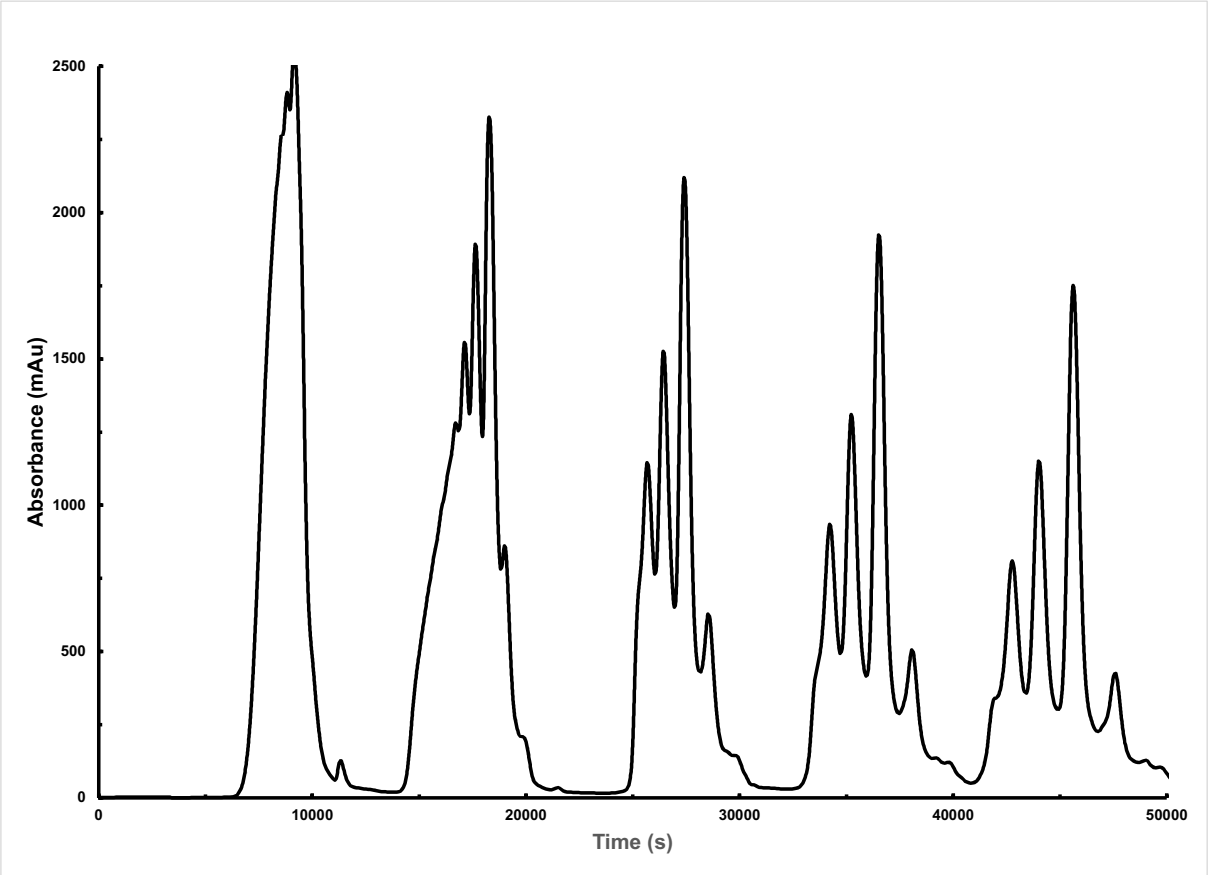

Figure S50. GPC Chromatogram of L'$_2$-L'$_5$.

IR Spectra of select PDI compounds

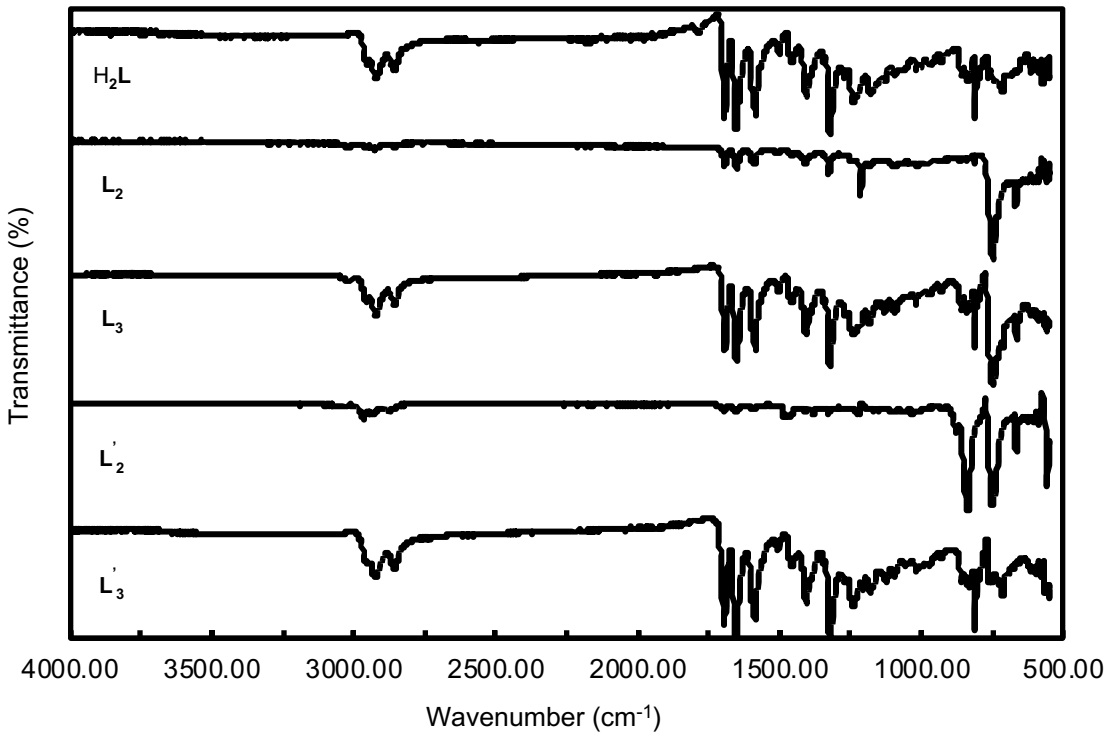

Figure A 51. Full IR spectra of select PDI compounds.

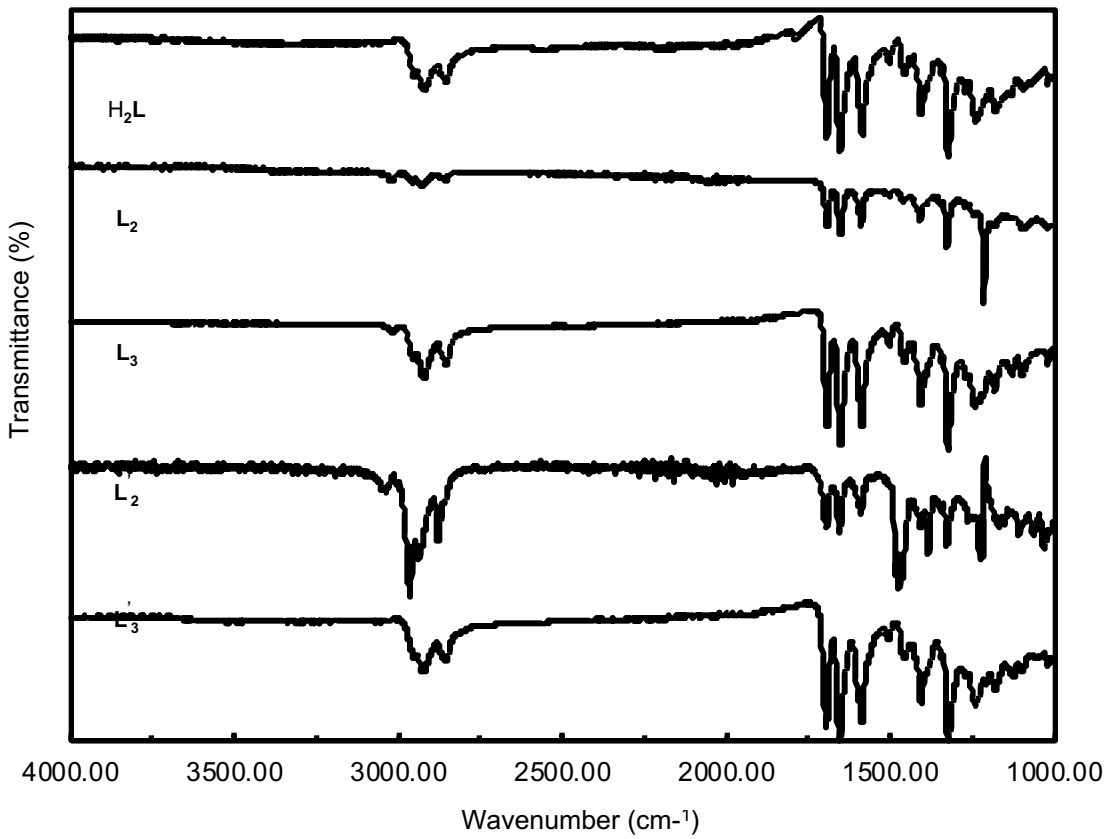

Figure A52. Partial IR spectra of select PDI compounds. Highlights IR stretching and bending modes hidden from intense C-S bending from 500-1000 cm^{-1}.

Appendix B

CARTESIAN COORDINATES FOR MODELING IN SELF-ASSEMBLY ROUTE TO PERYLENE DIIMIDE(PDI)-BRIDGED CYCLOPHANES

Optimized Geometry for L_2

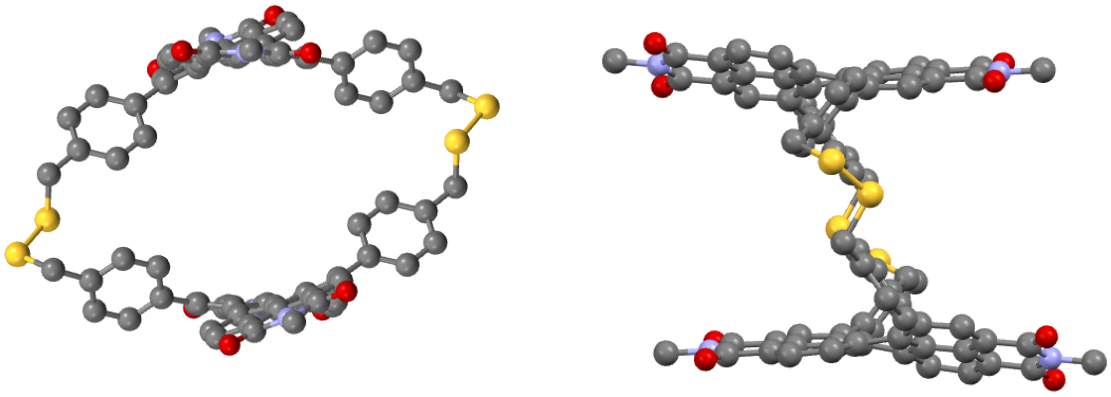

Atom, angstroms (x, y, z)

C	3.53799	1.63724	3.33585
C	2.95231	0.79854	4.24899
C	2.81372	-0.57626	3.95095
C	4.10752	1.14958	2.13249
C	4.09802	-0.22616	1.87998
C	3.32793	-1.08325	2.73344
C	2.16052	-1.43102	4.86837
C	2.01829	-2.76624	4.57077
C	3.05320	-2.44485	2.38460

C	2.45043	-3.26360	3.32903
C	4.88745	-0.89165	0.81525
C	4.49904	-2.20169	0.38553
C	3.45860	-2.93428	1.04500
C	6.01038	-0.31160	0.24283
C	6.70944	-0.93303	-0.80700
C	6.27117	-2.13368	-1.31529
C	5.15883	-2.77791	-0.72635
C	4.69863	-4.00680	-1.25249
C	2.93887	-4.07762	0.42922
C	3.58791	-4.60544	-0.71441
C	2.42123	1.35432	5.52206
N	1.80535	0.45961	6.39821
C	1.63747	-0.90822	6.15991
O	2.51009	2.53158	5.80927
O	1.08945	-1.63006	6.96962
C	1.30125	1.02271	7.64746
H	0.85591	0.20764	8.22481
H	0.55373	1.79814	7.43290
H	2.12473	1.48722	8.20605
C	6.98496	-2.74610	-2.46883
N	6.48257	-3.96171	-2.94493
C	5.37701	-4.63125	-2.41919

H	7.58910	-0.46367	-1.25058
H	6.36456	0.65458	0.59822
H	3.20546	-5.51241	-1.18791
O	7.95568	-2.21952	-2.97583
O	5.00437	-5.67931	-2.90846
C	7.14199	-4.59776	-4.08175
H	7.48887	-5.60034	-3.79818
H	7.98591	-3.96657	-4.37388
H	6.43273	-4.70401	-4.91350
H	1.54200	-3.42078	5.30259
H	2.29168	-4.31857	3.11308
H	3.56065	2.70716	3.55440
C	4.59124	2.18904	1.17510
C	4.08674	2.22926	-0.12859
C	4.44120	3.26020	-0.99279
C	5.30291	4.27977	-0.58151
C	5.81685	4.23358	0.71683
C	5.46395	3.20491	1.58457
H	5.87045	3.19114	2.59948
H	6.48141	5.02993	1.06291
H	3.39777	1.44975	-0.46449
H	4.02906	3.27873	-2.00649
C	5.61862	5.42087	-1.50850

S	5.01004	7.06114	-0.94174
H	5.22768	5.21884	-2.51658
H	6.70557	5.57755	-1.60238
C	1.66701	-4.74641	0.83581
C	0.48250	-3.99934	0.89993
C	1.60369	-6.12116	1.07426
C	-0.72305	-4.60961	1.21062
C	0.38989	-6.73156	1.39393
C	-0.78509	-5.98425	1.47428
H	0.51266	-2.92640	0.69420
H	-1.64242	-4.01758	1.22992
H	2.51464	-6.72349	1.02076
H	0.36037	-7.80818	1.58231
C	-2.10933	-6.62906	1.79430
S	-3.11320	-6.66782	0.25854
H	-2.65616	-6.04020	2.54567
H	-1.97974	-7.65097	2.17645
C	-5.37671	4.63115	2.41943
O	-5.00403	5.67918	2.90872
N	-6.48226	3.96162	2.94521
C	-7.14160	4.59764	4.08209
H	-6.43235	4.70367	4.91388
H	-7.48830	5.60031	3.79862

H	-7.98563	3.96655	4.37413
C	-6.98470	2.74603	2.46910
O	-7.95539	2.21944	2.97615
C	-6.27099	2.13364	1.31550
C	-6.70932	0.93301	0.80719
H	-7.58895	0.46365	1.25081
C	-6.01033	0.31160	-0.24271
H	-6.36455	-0.65456	-0.59811
C	-4.88743	0.89166	-0.81518
C	-4.09809	0.22619	-1.87998
C	-4.10761	-1.14954	-2.13253
C	-4.59129	-2.18902	-1.17514
C	-4.08671	-2.22928	0.12851
H	-3.39772	-1.44979	0.46439
C	-4.44113	-3.26024	0.99271
H	-4.02893	-3.27881	2.00638
C	-5.30287	-4.27979	0.58146
C	-5.61854	-5.42092	1.50843
H	-5.22757	-5.21891	2.51651
H	-6.70549	-5.57759	1.60236
S	-5.00998	-7.06117	0.94162
C	-5.81689	-4.23356	-0.71686
H	-6.48147	-5.02990	-1.06292

C	-5.46403	-3.20488	-1.58458
H	-5.87059	-3.19108	-2.59948
C	-3.53817	-1.63717	-3.33594
H	-3.56086	-2.70708	-3.55453
C	-2.95254	-0.79844	-4.24910
C	-2.42156	-1.35420	-5.52223
O	-2.51046	-2.53144	-5.80947
N	-1.80575	-0.45946	-6.39840
C	-1.30175	-1.02252	-7.64771
H	-0.85654	-0.20742	-8.22511
H	-0.55415	-1.79790	-7.43325
H	-2.12527	-1.48708	-8.20619
C	-1.63781	0.90836	-6.16005
O	-1.08984	1.63022	-6.96977
C	-2.16076	1.43112	-4.86846
C	-2.01848	2.76633	-4.57081
H	-1.54223	3.42089	-5.30265
C	-2.45053	3.26365	-3.32903
H	-2.29175	4.31861	-3.11306
C	-3.05325	2.44488	-2.38459
C	-3.45856	2.93427	-1.04495
C	-2.93877	4.07758	-0.42916
C	-1.66693	4.74636	-0.83581

C	-0.48243	3.99927	-0.90003
H	-0.51260	2.92632	-0.69434
C	0.72311	4.60953	-1.21077
H	1.64247	4.01749	-1.23014
C	0.78516	5.98419	-1.47437
C	2.10939	6.62899	-1.79442
H	2.65622	6.04010	-2.54577
H	1.97980	7.65088	-2.17660
S	3.11325	6.66780	-0.25866
C	-0.38981	6.73151	-1.39393
H	-0.36028	7.80814	-1.58227
C	-1.60360	6.12112	-1.07421
H	-2.51453	6.72347	-1.02063
C	-3.58773	4.60537	0.71453
H	-3.20523	5.51231	1.18804
C	-2.81392	0.57634	-3.95102
C	-3.32803	1.08330	-2.73346
C	-4.49897	2.20168	-0.38544
C	-5.15868	2.77787	0.72650
C	-4.69843	4.00673	1.25266

Optimized Geometry of L_2 + 1,4-dimethoxybenzene

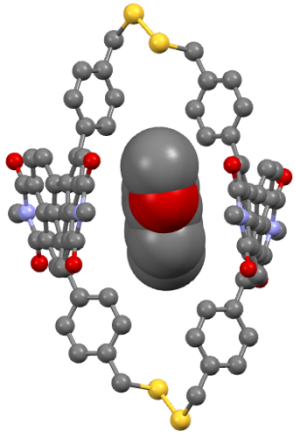

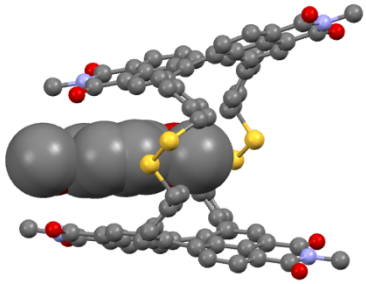

Atom, angstroms (x, y, z)

C	3.61037	0.83071	3.88113
C	2.70729	0.46131	4.84417
C	1.95302	-0.72269	4.68069
C	3.88408	0.01150	2.75669
C	3.22194	-1.21508	2.62505
C	2.15859	-1.53153	3.53613
C	1.00443	-1.08878	5.66360
C	0.27640	-2.24515	5.50852
C	1.29327	-2.65477	3.32788
C	0.41537	-3.01450	4.34096
C	3.57575	-2.25880	1.63120
C	2.61224	-3.27312	1.31907

C	1.39055	-3.40821	2.05539
C	4.81217	-2.30841	1.00395
C	5.08583	-3.22689	-0.02485
C	4.11676	-4.10949	-0.43747
C	2.87993	-4.15622	0.24499
C	1.90077	-5.09241	-0.15271
C	0.39582	-4.26525	1.57086
C	0.68478	-5.11743	0.47896
C	2.50574	1.33135	6.03300
N	1.56609	0.91205	6.97565
C	0.79673	-0.25129	6.87611
O	3.12206	2.36525	6.19967
O	-0.00280	-0.55798	7.73869
C	1.39285	1.77309	8.14187
H	0.63581	1.31575	8.78505
H	1.07567	2.77485	7.82247
H	2.34655	1.87168	8.67737
C	4.37681	-4.98916	-1.60841
N	3.35605	-5.87348	-1.97210
C	2.13983	-5.99519	-1.30896
H	6.05144	-3.22730	-0.53316
H	5.59396	-1.60595	1.28428
H	-0.08084	-5.80055	0.10523

O	5.41967	-4.93857	-2.23075
O	1.30833	-6.80284	-1.68440
C	3.53127	-6.69099	-3.16940
H	3.26416	-7.73066	-2.94528
H	4.57711	-6.61193	-3.47944
H	2.86874	-6.31386	-3.96224
H	-0.42410	-2.53594	6.29309
H	-0.19714	-3.90811	4.23752
H	4.13342	1.78221	3.99949
C	4.84181	0.58614	1.76325
C	4.47049	0.74139	0.42362
C	5.34236	1.34437	-0.47753
C	6.58984	1.82437	-0.07061
C	6.95866	1.66684	1.26702
C	6.09639	1.05503	2.17203
H	6.40313	0.93921	3.21515
H	7.92406	2.04819	1.61088
H	3.49009	0.39386	0.08378
H	5.03739	1.46027	-1.52270
C	7.47393	2.54798	-1.04662
S	7.65921	4.35035	-0.72030
H	7.11291	2.40483	-2.07579
H	8.51196	2.18038	-1.00629

C	-1.02609	-4.27234	2.02923
C	-1.77034	-3.08489	1.99177
C	-1.67919	-5.45616	2.38048
C	-3.12381	-3.08700	2.28963
C	-3.04086	-5.45426	2.68808
C	-3.78018	-4.27240	2.64321
H	-1.27697	-2.15083	1.71081
H	-3.69549	-2.15837	2.21892
H	-1.11844	-6.39416	2.41326
H	-3.53526	-6.39245	2.95474
C	-5.26807	-4.26137	2.87647
S	-6.07283	-4.27844	1.22463
H	-5.57791	-3.34592	3.40060
H	-5.59923	-5.13224	3.45888
C	-3.29789	7.16628	0.62912
O	-2.61607	8.10556	0.98906
N	-4.66060	7.12990	0.92675
C	-5.19017	8.27058	1.66846
H	-4.67460	8.36010	2.63402
H	-5.01813	9.19562	1.10222
H	-6.26063	8.10395	1.81764
C	-5.53075	6.09415	0.57179
O	-6.71062	6.13061	0.86052

C	-4.93884	4.94915	-0.17254
C	-5.74172	3.89666	-0.54543
H	-6.80560	3.93509	-0.30566
C	-5.18644	2.77930	-1.19284
H	-5.84522	1.95020	-1.44417
C	-3.83458	2.70896	-1.49825
C	-3.21493	1.50988	-2.11368
C	-3.77028	0.22565	-2.08034
C	-4.85028	-0.20810	-1.14362
C	-4.69882	-0.02896	0.23463
H	-3.81525	0.48980	0.61699
C	-5.65753	-0.51010	1.12099
H	-5.51782	-0.36397	2.19664
C	-6.78863	-1.18766	0.66021
C	-7.77730	-1.75554	1.64133
H	-7.51309	-1.45751	2.66650
H	-8.79796	-1.38914	1.44439
S	-7.97213	-3.58592	1.57961
C	-6.94540	-1.35876	-0.71778
H	-7.81587	-1.90006	-1.09845
C	-5.98873	-0.87975	-1.60701
H	-6.12739	-1.02873	-2.68127
C	-3.24459	-0.78038	-2.92968

H	-3.69182	-1.77689	-2.93287
C	-2.18261	-0.53848	-3.76322
C	-1.70929	-1.60994	-4.68083
O	-2.25234	-2.70009	-4.73220
N	-0.61935	-1.31684	-5.49310
C	-0.16644	-2.35993	-6.41179
H	0.44345	-1.88494	-7.18603
H	0.43747	-3.10869	-5.87766
H	-1.04390	-2.85253	-6.84649
C	0.09976	-0.11667	-5.45841
O	1.07087	0.05373	-6.16773
C	-0.39576	0.93793	-4.53410
C	0.23280	2.15992	-4.50158
H	1.07750	2.33559	-5.16961
C	-0.19243	3.14978	-3.59866
H	0.34424	4.09622	-3.58451
C	-1.25086	2.93819	-2.72693
C	-1.65911	3.93334	-1.70464
C	-0.83627	4.95691	-1.22140
C	0.64377	5.00796	-1.40885
C	1.43847	3.91319	-1.04236
H	0.96737	3.00585	-0.65606
C	2.81599	3.96039	-1.18364

H	3.41770	3.10239	-0.87691
C	3.44802	5.09942	-1.70143
C	4.94562	5.11801	-1.88303
H	5.26694	4.26420	-2.49861
H	5.27739	6.04261	-2.37546
S	5.75734	4.96351	-0.24500
C	2.66106	6.19907	-2.04129
H	3.13384	7.10335	-2.43405
C	1.27346	6.15623	-1.89417
H	0.67337	7.02461	-2.17926
C	-1.40458	5.99648	-0.44379
H	-0.77374	6.80979	-0.07845
C	-1.52343	0.71039	-3.71336
C	-1.99951	1.72199	-2.84435
C	-3.01466	3.85566	-1.24332
C	-3.56775	4.93859	-0.51785
C	-2.74102	6.02044	-0.13795
C	2.25251	-1.50192	-2.33796
C	1.20387	-1.18224	-1.46396
C	0.06702	-1.98357	-1.44465
C	2.16071	-2.60460	-3.16965
C	1.01716	-3.41913	-3.15037
C	-0.02703	-3.09998	-2.28796

H	-0.93369	-3.70471	-2.25797
H	-0.77258	-1.76300	-0.78314
H	2.97542	-2.86019	-3.85127
H	3.14222	-0.86796	-2.34902
O	1.39318	-0.07546	-0.67685
O	1.02501	-4.48292	-4.00557
C	-0.14722	-5.29053	-4.05669
H	-0.31616	-5.79516	-3.09224
H	0.05112	-6.05200	-4.82147
H	-1.02427	-4.68903	-4.34679
C	0.41152	0.20459	0.29592
H	0.28875	-0.63976	0.99921
H	-0.56515	0.44057	-0.16694
H	0.76951	1.08058	0.85405

Optimized Geometry of L'$_2$

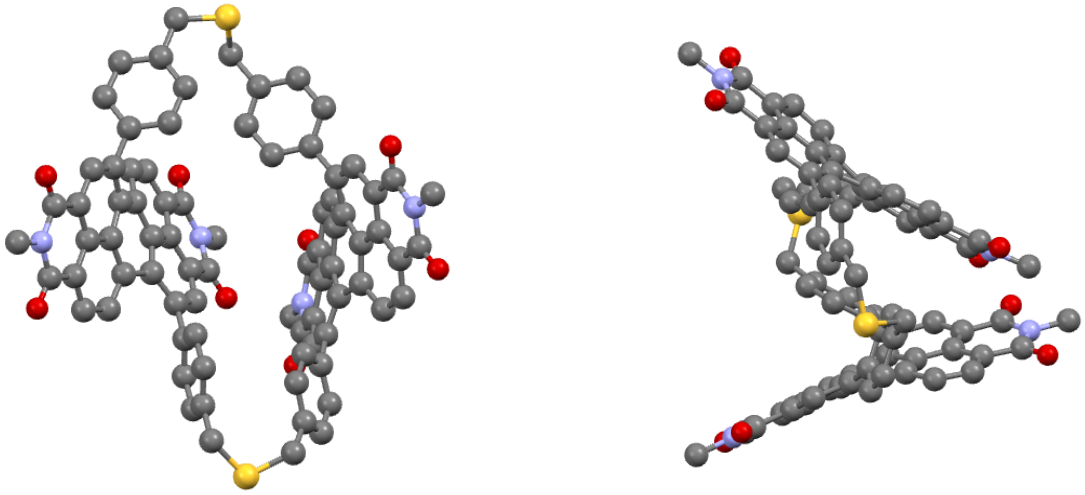

Atom, angstroms (x, y, z)

C	1.24565	3.03492	3.68863
C	2.02651	2.23564	4.47049
C	2.97154	1.38279	3.87010
C	1.42376	3.12042	2.28981
C	2.44184	2.38572	1.69287
C	3.13133	1.40560	2.47060
C	3.74451	0.51463	4.66397
C	4.65287	-0.31955	4.06855
C	3.97633	0.43282	1.86486
C	4.75475	-0.36799	2.67472
C	2.93774	2.59073	0.31480
C	3.67968	1.54560	-0.30900
C	4.02539	0.35373	0.39253

C	2.75390	3.77065	-0.37616
C	3.22789	3.93844	-1.68345
C	3.85159	2.90536	-2.33031
C	4.06229	1.68879	-1.65570
C	4.64487	0.59932	-2.32880
C	4.43891	-0.75998	-0.33079
C	4.75853	-0.60294	-1.69763
C	1.83696	2.23048	5.94080
N	2.64407	1.37142	6.67944
C	3.59654	0.50600	6.14001
O	1.02463	2.93502	6.49750
O	4.26344	-0.21437	6.84818
C	2.45360	1.39312	8.12552
H	3.14985	0.68834	8.56488
H	1.42895	1.11807	8.36735
H	2.63511	2.39621	8.50575
C	4.31906	3.08252	-3.72811
N	4.90514	1.98003	-4.33801
C	5.06358	0.72964	-3.74441
H	3.09237	4.87802	-2.20239
H	2.23512	4.59418	0.09045
H	5.10667	-1.45215	-2.27124
O	4.19339	4.13686	-4.31417

O	5.54999	-0.18447	-4.36903
C	5.33165	2.08786	-5.72763
H	6.37416	1.79110	-5.81568
H	5.19975	3.11688	-6.04158
H	4.73524	1.42001	-6.34827
H	5.26589	-0.95727	4.69121
H	5.44879	-1.06609	2.23089
H	0.47142	3.62304	4.16484
C	0.41188	3.94358	1.56935
C	-0.36126	3.38601	0.55471
C	-1.42246	4.08776	0.00571
C	-1.74371	5.36447	0.45320
C	-0.94212	5.93851	1.43429
C	0.11431	5.23781	1.98980
H	0.70785	5.69663	2.77160
H	-1.16558	6.93631	1.79459
H	-0.15006	2.37930	0.21155
H	-2.02983	3.61806	-0.76004
C	-2.95127	6.09814	-0.06974
S	-4.16319	6.48351	1.24780
H	-3.45487	5.51347	-0.83843
H	-2.65697	7.04695	-0.51710
C	4.46947	-2.14661	0.20699

C	3.41484	-2.61735	0.98646
C	5.48453	-3.03776	-0.13264
C	3.38470	-3.92821	1.41867
C	5.43252	-4.36112	0.27461
C	4.37574	-4.82833	1.04598
H	2.60522	-1.94911	1.25280
H	2.55947	-4.26519	2.03297
H	6.32403	-2.69636	-0.72604
H	6.22209	-5.04209	-0.02177
C	4.27796	-6.27721	1.42980
S	3.55274	-7.36122	0.16160
H	3.70936	-6.40341	2.35195
H	5.26952	-6.69719	1.59918
C	-7.25538	-3.24227	1.01675
O	-8.21731	-2.80206	1.60510
N	-7.10023	-4.61517	0.85364
C	-8.15279	-5.45355	1.41749
H	-8.22617	-5.28175	2.48935
H	-9.10903	-5.19826	0.96557
H	-7.90123	-6.48794	1.21443
C	-6.03010	-5.22770	0.20208
O	-5.96546	-6.43104	0.09143
C	-4.98034	-4.33071	-0.34290

C	-3.90208	-4.86676	-0.99326
H	-3.84626	-5.93971	-1.11910
C	-2.87019	-4.03920	-1.45165
H	-2.01498	-4.49963	-1.92216
C	-2.91584	-2.67010	-1.29228
C	-1.80595	-1.77814	-1.69634
C	-0.47673	-2.16852	-1.83608
C	0.09235	-3.43092	-1.28617
C	-0.16522	-3.81806	0.02630
H	-0.80348	-3.20474	0.65060
C	0.37497	-4.98404	0.53806
H	0.15158	-5.26813	1.56062
C	1.21481	-5.78519	-0.22839
C	1.77461	-7.06398	0.34582
C	1.49260	-5.38802	-1.53003
H	2.16108	-5.98439	-2.13917
C	0.93757	-4.23096	-2.05230
H	1.15701	-3.95283	-3.07622
C	0.42245	-1.30882	-2.50867
H	1.45122	-1.61705	-2.64994
C	0.02758	-0.10564	-3.01944
C	0.97373	0.70348	-3.83091
O	2.10754	0.33442	-4.05218

N	0.49092	1.89969	-4.35067
C	1.34755	2.68734	-5.23291
H	0.77023	2.99850	-6.09936
H	1.71324	3.57807	-4.72530
H	2.18511	2.06734	-5.53337
C	-0.76128	2.43965	-4.07097
O	-1.07489	3.52175	-4.51304
C	-1.67562	1.62504	-3.23942
C	-2.93640	2.08267	-2.97265
H	-3.24637	3.03523	-3.38215
C	-3.79725	1.33775	-2.16162
H	-4.76968	1.74791	-1.94438
C	-3.42955	0.11132	-1.64552
C	-4.31126	-0.67833	-0.75925
C	-5.35273	-0.14746	-0.00605
C	-5.49119	1.31009	0.26304
C	-4.49651	1.97127	0.97201
H	-3.65601	1.40971	1.36250
C	-4.54749	3.34272	1.15976
H	-3.75965	3.83821	1.71126
C	-5.58137	4.09322	0.61862
C	-5.64721	5.60210	0.71572
C	-6.60749	3.42160	-0.04400

H	-7.43693	3.98601	-0.45589
C	-6.57733	2.04623	-0.20173
H	-7.37509	1.54719	-0.73958
C	-6.29617	-1.01427	0.58045
H	-7.12380	-0.60346	1.14522
C	-1.27469	0.36451	-2.76055
C	-2.17122	-0.43825	-2.02762
C	-4.10232	-2.08835	-0.75707
C	-5.09323	-2.93274	-0.21774
C	-6.20372	-2.36953	0.44015
H	-6.39488	5.89550	1.45600
H	-5.98388	6.01086	-0.23810
H	1.32092	-7.92020	-0.15696
H	1.51498	-7.15033	1.40199

Geometry Optimization of L'$_2$ + 1,4-dimethoxybenzene

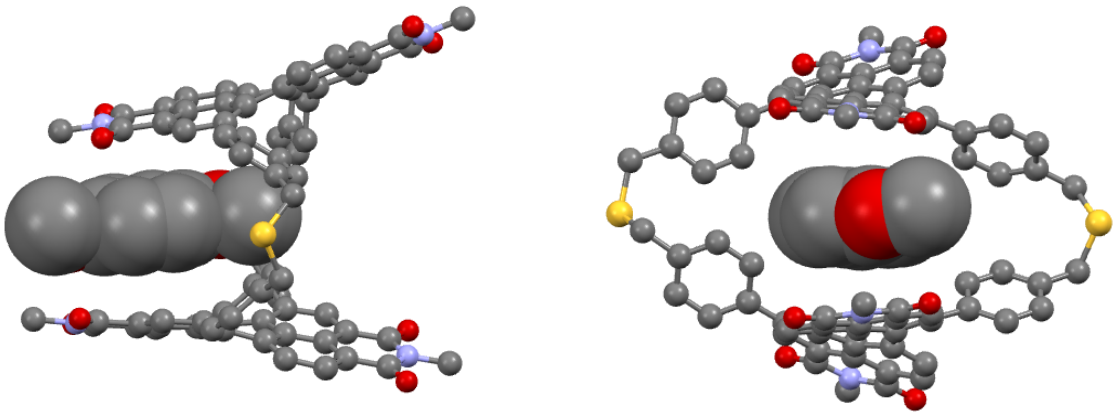

Atom, angstroms (x, y, z)

C	0.15450	2.92388	4.30694
C	0.47866	1.93962	5.20456
C	1.49227	1.00786	4.88591
C	0.87272	3.10689	3.09681
C	1.95743	2.26756	2.81678
C	2.18809	1.12779	3.65890
C	1.80135	-0.03198	5.79261
C	2.78842	-0.93829	5.47916
C	3.11078	0.09583	3.29424
C	3.42896	-0.87814	4.23027
C	2.95448	2.50320	1.74343
C	3.77296	1.41076	1.30671
C	3.72921	0.13214	1.94941
C	3.15374	3.74943	1.16772

C	4.06014	3.93990	0.10926
C	4.76518	2.87423	-0.39781
C	4.63041	1.60012	0.19732
C	5.34227	0.49992	-0.32984
C	4.31202	-0.97225	1.31464
C	5.14314	-0.75383	0.18919
C	-0.27174	1.83394	6.48333
N	0.09030	0.80031	7.34839
C	1.08601	-0.14826	7.09197
O	-1.16337	2.60253	6.78577
O	1.34802	-1.02350	7.89372
C	-0.64719	0.72302	8.60592
H	-0.24469	-0.11781	9.17773
H	-1.71681	0.57620	8.40412
H	-0.53092	1.66159	9.16397
C	5.64754	3.07009	-1.57823
N	6.34108	1.94805	-2.04480
C	6.21966	0.66600	-1.51863
H	4.19327	4.92340	-0.34447
H	2.58941	4.60934	1.52427
H	5.62756	-1.59865	-0.30489
O	5.76633	4.14955	-2.12369
O	6.80552	-0.27578	-2.02494

C	7.15739	2.10481	-3.24596
H	8.01707	1.42979	-3.17765
H	7.47496	3.14984	-3.31123
H	6.55963	1.84336	-4.13191
H	3.04155	-1.71298	6.20485
H	4.18212	-1.62916	3.99505
H	-0.68193	3.58407	4.54631
C	0.32005	4.15226	2.18122
C	-0.02192	3.82915	0.86296
C	-0.68649	4.75085	0.05954
C	-1.04091	6.01207	0.54713
C	-0.66096	6.34671	1.85004
C	0.00536	5.43039	2.65849
H	0.27399	5.70974	3.68094
H	-0.91825	7.33031	2.25378
H	0.21214	2.84083	0.45981
H	-0.97514	4.46044	-0.95557
C	-1.86946	6.96979	-0.27338
S	-3.55946	7.23209	0.39693
H	-1.95799	6.62854	-1.31527
H	-1.39736	7.96360	-0.29373
C	4.01660	-2.39475	1.66287
C	2.69144	-2.80299	1.86935

C	5.01671	-3.37179	1.69920
C	2.38510	-4.13013	2.12902
C	4.70130	-4.70894	1.94147
C	3.38178	-5.10982	2.15932
H	1.88783	-2.06347	1.83680
H	1.34567	-4.41207	2.30402
H	6.06077	-3.08525	1.54700
H	5.50339	-5.45207	1.96649
C	3.03846	-6.55148	2.43849
S	2.54481	-7.57320	1.00527
H	2.24086	-6.62564	3.19406
H	3.91584	-7.07280	2.84948
C	-7.70467	-1.74137	0.68788
O	-8.51474	-0.98188	1.18158
N	-7.88349	-3.12155	0.78427
C	-9.07965	-3.57071	1.49046
H	-9.06609	-3.19680	2.52301
H	-9.97591	-3.17386	0.99528
H	-9.08473	-4.66421	1.47692
C	-7.01014	-4.07905	0.25976
O	-7.23102	-5.26868	0.37514
C	-5.80070	-3.56948	-0.44244
C	-4.90963	-4.46698	-0.98349

H	-5.12216	-5.53425	-0.90267
C	-3.73776	-4.00532	-1.60362
H	-3.03771	-4.73762	-2.00381
C	-3.44872	-2.65161	-1.70291
C	-2.19245	-2.16792	-2.31654
C	-1.03021	-2.94062	-2.45331
C	-0.68552	-4.12685	-1.61145
C	-0.92232	-4.11323	-0.23108
H	-1.45630	-3.27173	0.21812
C	-0.49037	-5.15900	0.57830
H	-0.71046	-5.13016	1.64994
C	0.23098	-6.23195	0.04927
C	0.73328	-7.35120	0.92960
C	0.45982	-6.25190	-1.32909
H	1.01720	-7.08240	-1.77114
C	0.00285	-5.22405	-2.14704
H	0.19019	-5.27476	-3.22262
C	-0.03762	-2.51777	-3.37159
H	0.85120	-3.12874	-3.53994
C	-0.14340	-1.33656	-4.05807
C	0.90001	-0.97285	-5.05350
O	1.80141	-1.73547	-5.35521
N	0.80641	0.28197	-5.64495

C	1.83978	0.63057	-6.61761
H	1.54174	1.56614	-7.09947
H	2.80881	0.75852	-6.11318
H	1.92943	-0.17813	-7.35371
C	-0.15963	1.24114	-5.32333
O	-0.14677	2.34555	-5.82987
C	-1.21298	0.83414	-4.35417
C	-2.22117	1.71148	-4.03939
H	-2.23278	2.69392	-4.51434
C	-3.21345	1.35028	-3.11074
H	-3.98357	2.08285	-2.89039
C	-3.23180	0.10752	-2.49195
C	-4.27743	-0.29080	-1.50996
C	-5.16557	0.59201	-0.88375
C	-5.03202	2.08274	-0.85944
C	-4.06569	2.68245	-0.05203
H	-3.39055	2.05794	0.53920
C	-3.95198	4.07059	0.01513
H	-3.21382	4.51696	0.68186
C	-4.77056	4.89264	-0.75603
C	-4.63077	6.40300	-0.80796
C	-5.76158	4.28961	-1.54234
H	-6.43555	4.91442	-2.13657

C	-5.90772	2.90695	-1.57730
H	-6.69072	2.45732	-2.19437
C	-6.26940	0.08213	-0.15731
H	-6.97210	0.77436	0.31161
C	-1.19818	-0.44657	-3.75869
C	-2.21655	-0.84096	-2.85602
C	-4.42478	-1.70002	-1.26456
C	-5.56949	-2.18079	-0.58047
C	-6.49769	-1.26405	-0.03731
C	1.79192	1.86558	-2.28584
C	1.42677	0.76650	-1.49582
C	2.10516	-0.43811	-1.64595
C	2.80628	1.74901	-3.22110
C	3.47601	0.52779	-3.39471
C	3.12356	-0.55864	-2.60037
H	3.62694	-1.51915	-2.71265
H	1.85143	-1.31131	-1.04153
H	3.09404	2.60021	-3.84282
H	1.25977	2.81079	-2.15362
O	0.39175	0.97493	-0.62414
O	4.43874	0.50267	-4.36284
C	4.98869	-0.76673	-4.70006
H	5.57585	-1.17563	-3.86211

H	5.66062	-0.58306	-5.54824
H	4.18939	-1.46280	-5.00336
C	0.03245	-0.08485	0.23274
H	0.87327	-0.37133	0.89059
H	-0.30420	-0.97109	-0.33533
H	-0.79597	0.28636	0.85102
H	-5.61693	6.86688	-0.64686
H	-4.31646	6.70998	-1.81927
H	0.36218	-8.31584	0.54946
H	0.34983	-7.24858	1.95646

REFERENCES

Chapter I

[1] E. Fischer, *Berichte der deutschen chemischen Gesellschaft* **1894**, *27*, 2985.

[2] The Nobel Prize in Chemistry **1987**, nobelprize.org.

[3] H.-J. Schneider, *Journal of Physical Organic Chemistry* **2022**, *35*, e4340.

[4] D. Bardhan, D. K. Chand, *Chemistry – A European Journal* **2019**, *25*, 12241.

[5] V. Balzani, A. Credi, F. M. Raymo, J. F. Stoddart, *Angew. Chem., Int. Ed.* **2000**, *39*, 3348.

[6] L. Cademartiri, K. J. M. Bishop, *Nature Mater.* **2015**, *14*, 2.

[7] The Nobel Prize in Chemistry **2016**, nobelprize.org.

[8] P. Mukhopadhyay, A. Wu, L. Isaacs, *J. Org. Chem.* **2004**, *69*, 6157.

[9] A. Wu, L. Isaacs, *J. Am. Chem. Soc.* **2003**, *125*, 4831.

[10] M. M. Safont-Sempere, G. Fernández, F. Würthner, *Chem. Rev.* **2011**, *111*, 5784.

[11] K. Makabe, D. McElheny, V. Tereshko, A. Hilyard, G. Gawlak, S. Yan, A. Koide, S. Koide, *Proc. Natl. Acad. Sci.* **2006**, *103*, 17753.

[12] R. E. Franklin, R. G. Gosling, *Nature* **1953**, *171*, 740.

[13] E. N. Nikolova, H. Zhou, F. L. Gottardo, H. S. Alvey, I. J. Kimsey, H. M. Al-Hashimi, *Biopolymers* **2013**, *99*, 955.

[14] P. R. Ashton, T. T. Goodnow, A. E. Kaifer, M. V. Reddington, A. M. Z. Slawin, N. Spencer, J. F. Stoddart, C. Vicent, D. J. Williams, *Angew. Chem., Int. Ed.* **1989**, *28*, 1396.

[15] P. Politzer, J. S. Murray, T. Clark, *Phys. Chem. Chem. Phys.* **2013**, *15*, 11178.

[16] Y.-J. Zhu, Y. Gao, M.-M. Tang, J. Rebek, Y. Yu, *Chem. Commun.* **2021**.

[17] M. Fujita, O. Sasaki, T. Mitsuhashi, T. Fujita, J. Yazaki, K. Yamaguchi, K. Ogura, *Chem. Commun.* **1996**, 1535.

[18] Q. Wang, D. Astruc, *Chem. Rev.* **2020**, *120*, 1438.

[19] A. U. Czaja, N. Trukhan, Ulrich. Muller, *Chem. Soc. Rev.* **2009**, *38*, 1284.

[20] J. Liu, L. Chen, H. Cui, J. Zhang, L. Zhang, C.-Yong. Su, *Chem. Soc. Rev.* **2014**, *43*, 6011.

[21] J. Y. Lee, H. Koh, D.-N. Kim, *Nat. Commun.* **2023**, *14*, 7079.

[22] M. Thomas, R. Schwartz, *Phys. Biol.* **2017**, *14*, 035003.

[23] X.-H. Hu, S. Xiong, *front. nanotechnol.* **2022**, *4*.

[24] D. Bhatia, C. Wunder, L. Johannes, *ChemBioChem* **2021**, *22*, 763.

[25] S. Huang, X. Kong, Y. Xiong, X. Zhang, H. Chen, W. Jiang, Y. Niu, W. Xu, C. Ren, *Eur. Polym. J.* **2020**, *141*, 110094.

[26] Y. Jin, C. Yu, R. J. Denman, W. Zhang, *Chem. Soc. Rev.* **2013**, *42*, 6634.

[27] Y. Jin, Q. Wang, P. Taynton, W. Zhang, *Acc. Chem. Res.* **2014**, *47*, 1575.

[28] K. Wu, T. K. Ronson, L. Goh, W. Xue, A. W. Heard, P. Su, X. Li, M. Vinković, J. R. Nitschke, *J. Am. Chem. Soc.* **2023**, *145*, 11356.

[29] Shoichi Tanaka, Hisako Iimura, Toyoki Sugiyama, *Japan Society of Cosmetic Chemists* **1992**, *25*, 232.

[30] D. M. Beaupre, R. G. Weiss, *Molecules* **2021**, *26*, 3332.

[31] R. Ikura, J. Park, M. Osaki, H. Yamaguchi, A. Harada, Y. Takashima, *NPG Asia Mater* **2022**, *14*, 1.

[32] N. Zheng, Y. Xu, Q. Zhao, T. Xie, *Chem. Rev.* **2021**, *121*, 1716.

[33] F. Lu, H. Zhang, W. Pan, N. Li, B. Tang, *Chem. Commun.* **2021**, *57*, 7067.

[34] M. A. Pitt, D. W. Johnson, *Chem. Soc. Rev.* **2007**, *36*, 1441.

[35] V. M. Cangelosi, L. N. Zakharov, J. L. Crossland, B. C. Franklin, D. W. Johnson, *Cryst. Growth Des.* **2010**, *10*, 1471.

[36] T. G. Carter, W. J. Vickaryous, V. M. Cangelosi, D. W. Johnson, *Inorg. Chem.* **2007**, *28*, 97.

[37] S. C. Grund, K. Hanusch, H. U. Wolf, In *Ullmann's Encyclopedia of Industrial Chemistry*, John Wiley & Sons, Ltd, 2008.

[38] W. J. Vickaryous, R. Herges, D. W. Johnson, *Angew. Chem., Int. Ed.* **2004**, *43*, 5831.

[39] V. M. Cangelosi, A. C. Sather, L. N. Zakharov, O. B. Berryman, D. W. Johnson, *Inorg. Chem.* **2007**, *46*, 9278.

[40] V. M. Cangelosi, T. G. Carter, J. L. Crossland, L. N. Zakharov, D. W. Johnson, *Inorg. Chem.* **2010**, *49*, 9985.

[41] T. G. Carter, E. R. Healey, M. A. Pitt, D. W. Johnson, *Inorg. Chem.* **2005**, *44*, 9634.

[42] M. S. Collins, M. E. Carnes, B. P. Nell, L. N. Zakharov, D. W. Johnson, *Nat. Commun.* **2016**, *7*, 11052.

[43] M. S. Collins, M. E. Carnes, A. C. Sather, O. B. Berryman, L. N. Zakharov, S. J. Teat, D. W. Johnson, *Chem. Commun.* **2013**, *49*, 6599.

[44] M. S. Collins, N.-M. Phan, L. N. Zakharov, D. W. Johnson, *Inorg. Chem.* **2018**, *57*, 3486.

[45] M. Montanari, A. Bugana, A. K. Sharma, D. Pasini, *Org. Biomol. Chem.* **2011**, *9*, 5018.

[46] J. Bruhin, W. Jenny, *Tetrahedron Lett.* **1973**, *14*, 1215.

[47] D. J. Cram, H. Steinberg, *J. Am. Chem. Soc.* **1951**, *73*, 5691.

[48] N.-M. Phan, L. N. Zakharov, D. W. Johnson, *Chem. Commun.* **2018**, *54*, 13419.

[49] T. A. Shear, F. Lin, L. N. Zakharov, D. W. Johnson, *Angew. Chem., Int. Ed.* **2020**, *59*, 1496.

[50] M. S. Collins, T. A. Shear, E. K. Smith, S. M. Strain, L. N. Zakharov, D. W. Johnson, *Chem. - Eur. J.* **2019**, *25*, 13290.

[51] N.-M. Phan, E. P. K. L. Choy, L. N. Zakharov, D. W. Johnson, *Chem. Commun.* **2019**, *55*, 11840.

Chapter II

[1] M. C. T. Fyfe, J. F. Stoddart, *Acc. Chem. Res.* **1997**, *30*, 393-401.

[2] P. T. Corbett, J. Leclaire, L. Vial, K. R. West, J.-L. Wietor, J. K. M. Sanders, S. Otto, *Chem. Rev.* **2006**, *106*, 3652-3711.

[3] L. Hu, F. Schaufelberger, B. J. J. Timmer, M. A. Flos, O. Ramström, in *Kirk-Othmer Encyclopedia of Chemical Technology*, pp. 1-25.

[4] Y. Jin, Q. Wang, P. Taynton, W. Zhang, *Acc. Chem. Res.* **2014**, *47*, 1575-1586.

[5] S. J. Rowan, S. J. Cantrill, G. R. L. Cousins, J. K. M. Sanders, J. F. Stoddart, *Angew. Chem. Int. Ed.* **2002**, *41*, 898-952.

[6] W. F. Gorham, *J. Poly. Sci. Part A-1: Poly. Chem.* **1966**, *4*, 3027-3039.

[7] D. H. Leung, D. Fiedler, R. G. Bergman, K. N. Raymond, *Angew. Chem. Int. Ed.* **2004**, *116*, 981-984.

[8] M. Zhang, D. Xu, X. Yan, J. Chen, S. Dong, B. Zheng, F. Huang, *Angew. Chem. Int. Ed.* **2012**, *124*, 7117-7121.

[9] C.-Y. Yu, M. L. Turner, *Angew. Chem. Int. Ed.* **2006**, *118*, 7961-7964.

[10] D. Beaudoin, F. Rominger, M. Mastalerz, *Angew. Chem. Int. Ed.* **2017**, *56*, 1244-1248.

[11] R.-C. Brachvogel, F. Hampel, M. von Delius, *Nature Comm.* **2015**, *6*, 7129.

[12] R.-C. Brachvogel, M. von Delius, *Eur. J. Org. Chem.* **2016**, 3662-3670.

[13] C.-W. Hsu, O. Š. Miljanić, *Angew. Chem. Int. Ed.* **2015**, *54*, 2219-2222.

[14] M. Mastalerz, *Angew. Chem. Int. Ed.* **2010**, *49*, 5042-5053.

[15] O. Š. Miljanić, *Nature. Chem.* **2011**, *3*, 909-910.

[16] O. Š. Miljanić, *Chem* **2017**, *2*, 502-524.

[17] M. S. Collins, M. E. Carnes, B. P. Nell, L. N. Zakharov, D. W. Johnson, *Nature. Comm.* **2016**, 7, 11052.

[18] M. S. Collins, N.-M. Phan, L. N. Zakharov, D. W. Johnson, *Inorg. Chem.* **2018**, *57*, 3486-3496.

[19] M. S. Collins, T. A. Shear, E. K. Smith, S. M. Strain, L. N. Zakharov, D. W. Johnson, *Chem. Eur. J.* **2019**, *25*, 13290-13293.

[20] For representative examples, see: (I) P. Black, J. K. M. Sanders and A. R. Stefankiewicz, *Chem. Soc. Rev.* **2014**, *43*, 1861–1872. (II) Y. Au-Yeung, G. D. Pantos and J. K. M. Sanders, *Angew. Chem., Int. Ed.* **2010**, *49*, 5331–5334. (III) A. Little, J. Donkin, J. Fisher, M. A. Halcrow, J. Loder and M. J. Hardie, *Angew. Chemie., Int. Ed.* **2012**, *51*, 764–766. (IV) Konopka and A. R. Stefankiewicz, *Sci Rep.* **2022**, *12*, 38.

[21] N.-M. Phan, L. N. Zakharov, D. W. Johnson, *Chem. Commun.* **2018**, *54*, 13419-13422.

[22] T. A. Shear, F. Lin, L. N. Zakharov, D. W. Johnson, *Angew. Chem. Int. Ed.* **2020**, *59*, 1496-1500.

[23] D. C. Montgomery, *Design and Analysis of Experiments*, John Wiley & Sons, Inc., **2017**.

[24] N.-M. Phan, T. A. Shear, L. N. Zakharov, D. W. Johnson, *Eur. J. Org. Chem.* **2020**, 6795-6800.

[25] C. A. Allen, V. M. Cangelosi, L. N. Zakharov, D. W. Johnson, *Cryst. Growth Des.* **2009**, *9*, 3011-3013.

[26] V. M. Cangelosi, M. A. Pitt, W. J. Vickaryous, C. A. Allen, L. N. Zakharov, D. W. Johnson, *Cryst. Growth Des.* **2010**, *10*, 3531-3536.

[27] T. G. Carter, W. J. Vickaryous, V. M. Cangelosi, D. W. Johnson, *Comm. Inorgn. Chem.* **2007**, *28*, 97-122.

[28] D. Fiedler, R. G. Bergman, K. N. Raymond, *Angew. Chem. Int. Ed.* **2006**, *45*, 745-748.

[29] Y. H. Ko, K. Kim, J.-K. Kang, H. Chun, J. W. Lee, S. Sakamoto, K. Yamaguchi, J. C. Fettinger, K. Kim, *J. Am. Chem. Soc.* **2004**, *126*, 1932-1933.

[30] M. Ziegler, J. L. Brumaghim, K. N. Raymond, *Angew. Chem. Int. Ed.* **2000**, *39*, 4119-4121.

[31] T. S. Bailey, H. A. Henthorn, M. D. Pluth, *Inorg. Chem.* **2016**, *55*, 12618-12625.

[32] R. D. Adams, J. L. Perrin, *J. Am. Chem. Soc.* **1999**, *121*, 3984-3991.

[33] Houk and G. M. Whitesides, *J. Am. Chem. Soc.,* **1987**, *109*, 6825–6836.

[34] Houk and G. M. Whitesides, *Tetrahedron*, **1989**, *45*, 91–102.

[35] G. Capozzi, V. Lucchini, G. Modena, *Reviews of Chemical Intermediates* **1979**, *2*, 347-375.

[36] G. Capozzi, S. Menichetti, C. Nativi, *Encyclopedia of Reagents for Organic Synthesis* **2001**.

[37] G. Eglinton, I. A. Lardy, R. A. Raphael, G. A. Sim, *J. Chem. Soc.* **1964**, 1154-1158.

[38] R. Gleiter, S. Rittinger, H. Irngartinger, *Chem. Ber.* **1991**, *124*, 365-369.

[39] V. M. Cangelosi, M. A. Pitt, W. J. Vickaryous, C. A. Allen, L. N. Zakharov, D. W. Johnson, *Crystal growth & design* **2010**, *10*, 3531-3536.

[40] M. Montanari, A. Bugana, A. K. Sharma, D. Pasini, *Organic & Biomolecular Chemistry* **2011**, *9*, 5018-5020.

[41] J. Houk, G. M. Whitesides, *Journal of the American Chemical Society* **1987**, *109*, 6825-6836.

[42] K. Wutticharoenwong, M. D. Soucek, *Macromolecular Materials and Engineering* **2008**, *293*, 45-56.

[43] B. Hendriks, O. van den Berg, F. E. Du Prez, *Progress in Organic Coatings* **2019**, *136*, 105215.

[44] L. Y. Sun, N. Sinha, T. Yan, Y. S. Wang, T. T. Tan, L. Yu, Y. F. Han, F. E. Hahn, *Angewandte Chemie International Edition* **2018**, *57*, 5161-5165.

Chapter III

[1] W. F. Gorham, J. Polym. Sci., *Part A-1: Polym. Chem.* **1966**, *4*, 3027.

[2] B. J. Lidster, D. R. Kumar, A. M. Spring, C.-Y. Yu, M. Helliwell, J. Raftery, M. L. Turner, Org. Biomol. Chem. **2016**, 14, 6079.

[3] Z. Hassan, D. Varadharajan, C. Zippel, S. Begum, J. Lahann, S. Bräse, *Adv. Mater.* **2022**, *34*, 2201761.

[4] G. S. Papaefstathiou, T. Friščić, L. R. MacGillivray, *J. Am. Chem. Soc.* **2005**, *127*, 14160.

[5] E. Elacqua, T. Friščić, L. R. MacGillivray, *Isr. J. Chem.* **2012**, *52*, 53.

[6] T. Iwamoto, Y. Watanabe, T. Sadahiro, T. Haino, S. Yamago, *Angew. Chem. Int. Ed.* **2011**, *50*, 8342.

[7] B. Zhang, R. Hernández Sánchez, Y. Zhong, M. Ball, M. W. Terban, D. Paley, S. J. L. Billinge, F. Ng, M. L. Steigerwald, C. Nuckolls, *Nat. Commun.* **2018**, *9*, 1957.

[8] H. T. Nicolai, M. Kuik, G. a. H. Wetzelaer, B. de Boer, C. Campbell, C. Risko, J. L. Brédas, P. W. M. Blom, *Nat. Mater.* **2012**, *11*, 882.

[9] L. Dou, J. You, Z. Hong, Z. Xu, G. Li, R. A. Street, Y. Yang, *Adv. Mater.* **2013**, *25*, 6642.

[10] G. J. Hedley, A. Ruseckas, I. D. W. Samuel, *Chem. Rev.* **2017**, *117*, 796.

[11] M. L. Ball, B. Zhang, T. Fu, A. M. Schattman, D. W. Paley, F. Ng, L. Venkataraman, C. Nuckolls, M. L. Steigerwald, *Chem. Sci.* **2019**, *10*, 9339.

[12] J. E. Anthony, A. Facchetti, M. Heeney, S. R. Marder, X. Zhan, *Adv. Mater.* **2010**, *22*, 3876.

[13] M. Ball, Y. Zhong, B. Fowler, B. Zhang, P. Li, G. Etkin, D. W. Paley, J. Decatur, A. K. Dalsania, H. Li, S. Xiao, F. Ng, M. L. Steigerwald, C. Nuckolls, *J. Am. Chem. Soc.* **2016**, *138*, 12861.

[14] Y. Jin, Q. Wang, P. Taynton, W. Zhang, *Acc. Chem. Res.* **2014**, *47*, 1575.

[15] Y. Jin, C. Yu, R. J. Denman, W. Zhang, *Chem. Soc. Rev.* **2013**, *42*, 6634.

[16] S. Huang, X. Kong, Y. Xiong, X. Zhang, H. Chen, W. Jiang, Y. Niu, W. Xu, C. Ren, *Eur. Polym. J.* **2020**, *141*, 110094.

[17] N. Zheng, Y. Xu, Q. Zhao, T. Xie, *Chem. Rev.* **2021**, *121*, 1716.

[18] S. Ulrich, *Acc. Chem. Res.* **2019**, *52*, 510.

[19] M. S. Collins, M. E. Carnes, B. P. Nell, L. N. Zakharov, D. W. Johnson, *Nat. Commun.* **2016**, 7, 11052.

[20] M. S. Collins, M. E. Carnes, A. C. Sather, O. B. Berryman, L. N. Zakharov, S. J. Teat, D. W. Johnson, *Chem. Commun.* **2013**, *49*, 6599.

[21] T. A. Shear, J. T. Mayhugh, L. J. Zocchi, I. S. Demachkie, H. J. Trubenstein, L. N. Zakharov, D. W. Johnson, *Eur. J. Org. Chem.* **2022**, *2022*, e202200056.

[22] H. M. Bergman, G. R. Kiel, R. J. Witzke, D. P. Nenon, A. M. Schwartzberg, Y. Liu, T. D. Tilley, *J. Am. Chem. Soc.* **2020**, *142*, 19850.

[23] S. Izumi, H. F. Higginbotham, A. Nyga, P. Stachelek, N. Tohnai, P. de Silva, P. Data, Y. Takeda, S. Minakata, *J. Am. Chem. Soc.* **2020**, *142*, 1482.

[24] T. A. Shear, F. Lin, L. N. Zakharov, D. W. Johnson, *Angew. Chem. Int. Ed.* **2020**, *59*, 1496.

[25] C. Schaack, A. M. Evans, F. Ng, M. L. Steigerwald, C. Nuckolls, *J. Am. Chem. Soc.* **2022**, *144*, 42.

[26] T. Liu, J. Yang, F. Geyer, F. S. Conrad-Burton, R. Hernández Sánchez, H. Li, X. Zhu, C. P. Nuckolls, M. L. Steigerwald, S. Xiao, *Angew. Chem. Int. Ed.* **2020**, *59*, 14303.

[27] F. Würthner, C. R. Saha-Möller, B. Fimmel, S. Ogi, P. Leowanawat, D. Schmidt, *Chem. Rev.* **2016**, *116*, 962.

[28] Y. Wang, H. Wu, J. F. Stoddart, *Acc. Chem. Res.* **2021**, *54*, 2027.

[29] S. E. Penty, M. A. Zwijnenburg, G. R. F. Orton, P. Stachelek, R. Pal, Y. Xie, S. L. Griffin, T. A. Barendt, *J. Am. Chem. Soc.* **2022**, *144*, 12290.

[30] C. Zeng, Y. Liu, N. Xue, W. Jiang, S. Yan, Z. Wang, *Angew. Chem. Int. Ed.* **2021**, *60*, 19018.

[31] A. Sugie, W. Han, N. Shioya, T. Hasegawa, H. Yoshida, *J. Phys. Chem. C* **2020**, *124*, 9765.

[32] M. Konopka, A. R. Stefankiewicz, *Sci. Rep.* **2022**, *12*, 38.

[33] F. B. L. Cougnon, N. A. Jenkins, G. D. Pantoş, J. K. M. Sanders, *Angew. Chem. Int. Ed.* **2012**, *51*, 1443.

[34] N. Ponnuswamy, F. B. L. Cougnon, J. M. Clough, G. D. Pantoş, J. K. M. Sanders, *Science* **2012**, *338*, 783.

[35] K. Khokhlov, N. J. Schuster, F. Ng, C. Nuckolls, *Org. Lett.* **2018**, *20*, 1991.

[36] A. R. Zanatta, *Sci. Rep.* **2019**, *9*, 11225.

[37] D. J. cram, J. M. Cram, *Acc. Chem. Res.* **1971**, *4*, 204.

[38] W. Wang, J. J. Han, L.-Q. Wang, L.-S. Li, W. J. Shaw, A. D. Q. Li, *Nano Lett.* **2003**, *3*, 455.

[39] Y. Takashima, Y. Fukui, M. Otsubo, N. Hamada, H. Yamaguchi, H. Yamamoto, A. Harada, *Polym. J.* **2012**, *44*, 278.

[40] H. Langhals, R. Ismael, *Eur. J. Org. Chem.* **1998**, *1998*, 1915.

[41] J. You, L. Dou, K. Yoshimura, T. Kato, K. Ohya, T. Moriarty, K. Emery, C.-C. Chen, J. Gao, G. Li, Y. Yang, *Nat. Commun.* **2013**, *4*, 1446.

[42] H. Yao, Y. Cui, D. Qian, J. Carlito S. Ponseca, A. Honarfar, Y. Xu, J. Xin, Z. Chen, L. Hong, B. Gao, R. Yu, Y. Zu, W. Ma, P. Chabera, T. Pullerits, A. Yartsev, F. Gao, J. Hou, *J. Am. Chem. Soc.* **2019**. *141*, 19, 7743

[43] W. Li, K. H. Hendriks, A. Furlan, M. M. Wienk, R. A. J. Janssen, *J. Am. Chem. Soc.* **2015**, *137*, 2231.

[44] K. Khokhlov, N. J. Schuster, F. Ng, C. Nuckolls, *Org. Lett.* **2018**, *20*, 1991.

[45] J. L. Howard, C. Schotten, S. T. Alston, D. L. Browne, *Chem. Commun.* **2016**, *52*, 8448.

Chapter IV

[1] D. B. Amabilino, P. R. Ashton, M. Belohradsky, F. M. Raymo, J. Fraser. Stoddart, *J. Chem. Soc., Chem. Commun.* **1995**, 747–50.

[2] D. B. Amabilino, P. R. Ashton, J. Fraser. Stoddart, *Supramol. Chem.* **1995**, *5*, 5–8.

[3] P. R. Ashton, C. G. Claessens, W. Hayes, S. Menzer, J. F. Stoddart, A. J. P. White, D. J. Williams, *Angew. Chem., Int. Ed. Engl.* **1995**, *34*, 1862–5.

[4] M. Fujita, D. Oguro, M. Miyazawa, H. Oka, K. Yamaguchi, K. Ogura, *Nature* **1995**, *378*, 469–471.

[5] O. Kocian, N. Spencer, J. F. Stoddart, I. Cragg-Hine, M. Davidson, F. S. Mair, P. Raithby, R. Snaith, T. Kottke, al. et, *Tetrahedron* **1995**, *51*, 579–90.

[6] S. J. Langford, L. Perez-Garcia, J. Fraser. Stoddart, *Supramol. Chem.* **1995**, *6*, 11–27.

[7] L. R. MacGillivray, J. L. Atwood, *Nature* **1997**, *389*, 469–472.

[8] S.-W. Tam-Chang, J. S. Stehouwer, J. Hao, *J. Org. Chem.* **1999**, *64*, 334–335.

[9] M. Yoshizawa, Y. Takeyama, T. Kusukawa, M. Fujita, *Angewandte Chemie International Edition* **2002**, *41*, 1347–1349.

[10] W. Wang, J. J. Han, L.-Q. Wang, L.-S. Li, W. J. Shaw, A. D. Q. Li, *Nano Lett.* **2003**, *3*, 455–458.

[11] Z. Wu, Q. Chen, S. Xiong, B. Xin, Z. Zhao, L. Jiang, J. S. Ma, *Angewandte Chemie International Edition* **2003**, *42*, 3271–3274.

[12] Z. Wu, Q. Chen, S. Xiong, B. Xin, Z. Zhao, L. Jiang, J. S. Ma, *Angewandte Chemie International Edition* **2003**, *42*, 3271–3274.

[13] S. Höger, *Chemistry – A European Journal* **2004**, *10*, 1320–1329.

[14] L. Yang, Q. Chen, Y. Li, S. Xiong, G. Li, J. S. Ma, *European Journal of Inorganic Chemistry* **2004**, *2004*, 1478–1487.

[15] W. J. Vickaryous, E. Rather Healey, O. B. Berryman, D. W. Johnson, *Inorg. Chem.* **2005**, *44*, 9247–9252.

[16] V. M. Cangelosi, A. C. Sather, L. N. Zakharov, O. B. Berryman, D. W. Johnson, *Inorg. Chem.* **2007**, *46*, 9278–9284.

[17] M. A. Pitt, D. W. Johnson, *Chem. Soc. Rev.* **2007**, *36*, 1441–1453.

[18] K. Wu, T. K. Ronson, L. Goh, W. Xue, A. W. Heard, P. Su, X. Li, M. Vinković, J. R. Nitschke, *J. Am. Chem. Soc.* **2023**, *145*, 11356–11363.

[19] Y.-J. Zhu, Y. Gao, M.-M. Tang, J. Rebek, Y. Yu, *Chem. Commun.* **2021**, DOI 10.1039/D0CC07784D.

[20] Y. Wang, H. Wu, J. F. Stoddart, *Acc. Chem. Res.* **2021**, *54*, 2027–2039.

[21] S. Datta, Y. Kato, S. Higashiharaguchi, K. Aratsu, A. Isobe, T. Saito, D. D. Prabhu, Y. Kitamoto, M. J. Hollamby, A. J. Smith, R. Dalgliesh, N. Mahmoudi, L. Pesce, C. Perego, G. M. Pavan, S. Yagai, *Nature* **2020**, *583*, 400–405.

[22] D. Armspach, P. R. Ashton, R. Ballardini, V. Balzani, A. Godi, C. P. Moore, L. Prodi, N. Spencer, J. F. Stoddart, al. et, *Chem. - Eur. J.* **1995**, *1*, 33–55.

[23] J. F. Stoddart, D. J. Williams, D. B. Amabilino, P.-L. Anelli, P. R. Ashton, G. R. Brown, E. Cordova, L. A. Godinez, W. Hayes, al. et, *J. Am. Chem. Soc.* **1995**, *117*, 11142–70.

[24] M. Mastalerz, *Angewandte Chemie International Edition* **2010**, *49*, 5042–5053.

[25] R. Nishiyabu, Y. Kubo, T. D. James, J. S. Fossey, *Chem. Commun.* **2011**, *47*, 1124–1150.

[26] N. Ponnuswamy, F. B. L. Cougnon, J. M. Clough, G. D. Pantoş, J. K. M. Sanders, *Science* **2012**, *338*, 783–785.

[27] S. P. Black, J. K. M. Sanders, A. R. Stefankiewicz, *Chem. Soc. Rev.* **2014**, *43*, 1861–1872.

[28] K.-L. Tong, C.-C. Yee, Y. C. Tse, H. Y. Au-Yeung, *Inorg. Chem. Front.* **2016**, *3*, 348–353.

[29] T. A. Barendt, W. K. Myers, S. P. Cornes, M. A. Lebedeva, K. Porfyrakis, I. Marques, V. Félix, P. D. Beer, *J. Am. Chem. Soc.* **2020**, *142*, 349–364.

[30] F. B. L. Cougnon, N. A. Jenkins, G. D. Pantoş, J. K. M. Sanders, *Angewandte Chemie International Edition* **2012**, *51*, 1443–1447.

[31] Z. Rodriguez-Docampo, S. Otto, *Chem. Commun.* **2008**, 5301–5303.

[32] A. Wu, L. Isaacs, *J. Am. Chem. Soc.* **2003**, *125*, 4831–4835.

[33] P. Mukhopadhyay, A. Wu, L. Isaacs, *J. Org. Chem.* **2004**, *69*, 6157–6164.

[34] M. M. Safont-Sempere, G. Fernández, F. Würthner, *Chem. Rev.* **2011**, *111*, 5784–5814.

[35] Y. Rudzevich, V. Rudzevich, F. Klautzsch, C. A. Schalley, V. Böhmer, *Angewandte Chemie International Edition* **2009**, *48*, 3867–3871.

[36] W. Jiang, A. Schäfer, P. C. Mohr, C. A. Schalley, *J. Am. Chem. Soc.* **2010**, *132*, 2309–2320.

[37] L. Zhao, B. H. Northrop, Y.-R. Zheng, H.-B. Yang, H. J. Lee, Y. M. Lee, J. Y. Park, K.-W. Chi, P. J. Stang, *J. Org. Chem.* **2008**, *73*, 6580–6586.

[38] Y. Ma, S. V. Kolotuchin, S. C. Zimmerman, *J. Am. Chem. Soc.* **2002**, *124*, 13757–13769.

[39] H. V. Schröder, Y. Zhang, A. J. Link, *Nat. Chem.* **2021**, *13*, 850–857.

[40] F. Esteve, B. Altava, E. García-Verdugo, S. V. Luis, J.-M. Lehn, *Chem* **2022**, *8*, 2023–2042.

[41] H. Jędrzejewska, A. Szumna, *Chem. Rev.* **2017**, *117*, 4863–4899.

[42] M. S. Collins, M. E. Carnes, B. P. Nell, L. N. Zakharov, D. W. Johnson, *Nature Communications* **2016**, *7*, 11052.

[43] M. S. Collins, M. E. Carnes, A. C. Sather, O. B. Berryman, L. N. Zakharov, S. J. Teat, D. W. Johnson, *Chem. Commun. (Cambridge, U. K.)* **2013**, *49*, 6599–6601.

[44] M. S. Collins, N.-M. Phan, L. N. Zakharov, D. W. Johnson, *Inorg. Chem.* **2018**, *57*, 3486–3496.

[45] T. A. Shear, F. Lin, L. N. Zakharov, D. W. Johnson, *Angewandte Chemie International Edition* **2020**, *59*, 1496–1500.

[46] N.-M. Phan, E. P. K. L. Choy, L. N. Zakharov, D. W. Johnson, *Chem. Commun. (Cambridge, U. K.)* **2019**, *55*, 11840–11843.

[47] N.-M. Phan, E. P. K. L. Choy, L. N. Zakharov, D. W. Johnson, *Chem. Commun. (Cambridge, U. K.)* **2019**, *55*, 11840.

[48] M. S. Collins, M. E. Carnes, B. P. Nell, L. N. Zakharov, D. W. Johnson, *Nat. Commun.* **2016**, *7*, 11052.

[49] A. W. Van der Made, R. H. Van der Made, *J. Org. Chem.* **1993**, *58*, 1262.

Chapter V

[1] P. R. Ashton, T. T. Goodnow, A. E. Kaifer, M. V. Reddington, A. M. Z. Slawin, N. Spencer, J. F. Stoddart, C. Vicent, D. J. Williams, *Angew. Chem., Int. Ed.* **1989**, *28*, 1396.

[2] Y. Segawa, M. Kuwayama, Y. Hijikata, M. Fushimi, T. Nishihara, J. Pirillo, J. Shirasaki, N. Kubota, K. Itami, *Science* **2019**, *365*, 272.

[3] X. Zhou, H. Kwon, R. R. Thompson, R. J. Herman, F. R. Fronczek, C. J. Bruns, S. Lee, *Chem. Commun.* **2021**, *57*, 10887.

[4] O. B. Berryman, D. W. Johnson, *Chem. Commun.* **2009**, 3143.

[5] Y. Fu, N. S. Finney, *RSC Adv.* **2018**, *8*, 29051.

[6] C. Chen, K. Wang, L. Gu, H. Li, *RSC Adv.* **2017**, *7*, 42685.

[7] J. Zhang, L. Shen, X. Li, W. Song, Y. Liu, L. Huang, *ACS Nano* **2019**, *13*, 12511.

[8] Y. Wang, Z. Zhang, X. Zhao, L. Xu, Y. Zheng, H.-B. Li, D.-S. Guo, L. Shi, Y. Liu, *Theranostics* **2022**, *12*, 3747.

[9] N.-M. Phan, E. P. K. L. Choy, L. N. Zakharov, D. W. Johnson, *Chem. Commun.* **2019**, *55*, 11840.

[10] J. Cornforth, R. H. Cornforth, R. T. Gray, *J. Chem. Soc., Perkin Trans. 1* **1982**, 2289.